

Universitätsklinikum Hamburg-Eppendorf  
Universitäres Herzzentrum  
Abteilung für Herz- und Gefäßchirurgie

# **Generation of fully immune evasive cell therapeutics**

**Cumulative dissertation**

to obtain the Doctoral degree in Natural Sciences (Dr. rer. nat.) at the  
faculty of Mathematics, Informatics, and Natural Sciences  
Department of Biology of the University Hamburg

presented by

**Alessia Gravina**

Hamburg 2023

1. Examiner:

Prof. Dr. Sonja Schrepfer

2. Examiner:

Prof. Dr. Dr. Andreas H. Guse

Date of disputation:

18 January 2024

This PhD Thesis was conducted from July 2018 to March 2023 at University of California San Francisco in the Department of Surgery under the supervision of Prof. Dr. Sonja Schrepfer.

## Table of Contents

<b>Table of Contents</b> .....	2
<b>List of Abbreviations</b> .....	4
<b>List of Figures</b> .....	7
<b>Abstract</b> .....	8
<b>Zusammenfassung</b> .....	10
<b>1 Introduction</b> .....	12
1.1 The immune system .....	12
1.1.1 Natural Killer cells (NK cells).....	13
1.1.2 T and B cells .....	13
1.2 The Major Histocompatibility Complex (MHC).....	14
1.3 The immune system in transplantation .....	16
1.3.1 Immunomodulatory function of MHC.....	16
1.3.2 Antibody-mediated rejection .....	17
1.3.2.1 Complement-dependent cytotoxicity.....	18
1.3.2.2 Antibody-dependent cellular cytotoxicity .....	18
1.4 Autoimmune diseases .....	19
1.5 Transplantation and cell therapy.....	20
1.5.1 Role of ESCs in transplantation.....	20
1.5.2 Role of iPSCs in transplantation.....	21
1.6 Gene editing.....	22
1.6.1 CRISPR/Cas9 .....	22
1.6.2 Lentiviral overexpression .....	24
1.7 Thesis goal .....	25
<b>2 Publications</b> .....	26
2.1 Hypoimmunogenic derivatives of induced pluripotent stem cells evade immune rejection in fully immunocompetent allogeneic recipients.....	26
2.2 Hypoimmune induced pluripotent stem cell–derived cell therapeutics treat cardiovascular and pulmonary diseases in immunocompetent allogeneic mice.....	61
2.3 Protection of cell therapeutics from antibody-mediated killing by CD64 overexpression .....	81
<b>3 Discussion</b> .....	119
<b>4 References</b> .....	141

<b>Authorship contributions</b> .....	151
<b>Declaration on oath</b> .....	156
<b>Acknowledgements</b> .....	157

## List of Abbreviations

A1AT	Alpha-1 antitrypsin
ADCC	Antibody-Dependent Cellular Cytotoxicity
AMR	Antibody-Mediated Rejection
AP20187	B/B Homodimerizer (C <sub>82</sub> H <sub>107</sub> N <sub>5</sub> O <sub>20</sub> )
APC	Antigen Presenting Cell
B2M	Beta-2-Microglobulin
BALB/c	Bagg Albino mice
BCR	B Cell Receptor
BLT	Bone Marrow-Liver-Thymic
C	Celsius
C1q	Complement Component 1q
C57BL/6	C57 Black 6 mice
CAR	Chimeric Antigen Receptors
Cas9	CRISPR Associated Protein 9
CCL21	CC-Chemokine Ligand 21
CD/Cd	Cluster of Differentiation
CDC	Complement-Dependent Cytotoxicity
CIITA	Class II Major Histocompatibility Complex Transactivator
CM	Cardiomyocytes
C-MYC	Cellular Myelocytomatosis Oncogene
CLI	Critical Limb Ischemia
CRISPR	Clustered Regularly Interspaced Short Palindromic Repeats
crRNA	CRISPR-RNA
CTLA4	Cytotoxic T-Lymphocyte-Associated Protein 4
DNA	Deoxyribonucleic Acid
DSA	Donor-Specific Antibodies
DSB	Double-Strand Break
EC	Endothelial Cell
ER	Endoplasmatic Reticulum
ESC	Embryonic Stem Cell
F <sub>ab</sub>	Fragment Antigen-Binding
FasL	Fas Ligand
F <sub>c</sub>	Fragment Crystallizable Region
FcγR	Fc-gamma Receptors
FK506	Tacrolimus
FLuc	Firefly Luciferase
GAD65	Glutamate Decarboxylase 65
GCV	Ganciclovir
GFP	Green Fluorescent Protein
H2 complex	Histocompatibility 2 complex
H2-M3	Histocompatibility 2, M Region Locus 3
HDR	Homology-Directed Repair
HLA	Human Leukocyte Antigen

HSV-TK	Herpes Simplex Virus Thymidine Kinase
iC9	Inducible Caspase 9
IdeS	Immunoglobulin G-degrading Enzyme of Streptococcus Pyogenes
IgG	Immunoglobulin G
IgH	Immunoglobulin Heavy Chain
IgL	Immunoglobulin Light Chain
iPSC	Induced Pluripotent Stem Cell
ITAM	Immunoreceptor Tyrosine-based Activation Motif
kb	Kilobases
KIR	Killer Ig-Like Receptors
KIR2DL1	Killer cell immunoglobulin-like receptor two Ig domains and long cytoplasmic tail 1
KLF4	Krüppel-like factor 4
KO	Knockout
MAC	Membrane Attack Complex
MFGE8	Milk Fat Globule EGF And Factor V/VIII Domain Containing
MHC	Major Histocompatibility Complex
MICA	MHC Class I Polypeptide-Related Sequence A
NANOG	Homeobox Transcription Factor Nanog
NCAM1/CD56	Neural Cell Adhesion Molecule 1
NE	Neutrophil Elastase
NHEJ	Non-Homologous End Joining
NK	Natural Killer
NKG2D	Natural Killer Group 2D
NRG	NOD Rag Gamma mice
p53	Cellular Tumor Antigen p53
PAM	Protospacer Adjacent Motif
PBMC	Peripheral Blood Mononuclear Cell
PD-L1	Programmed Death-Ligand 1
PID	Primary Immunodeficiency
POU5F1/ OCT4	POU Class 5 Homeobox 1
pre-crRNA	pre-CRISPR-RNA
PSC	Pluripotent Stem Cell
RFX5	Regulatory Factor X5
RFXANK	Regulatory Factor X Associated Ankyrin Containing Protein
RFXAP	Regulatory Factor X Associated Protein
RNA	Ribonucleic Acid
SERPINB9	Serpin Family B Member 9
sgRNA	Single Guide RNA
SIRPa	Signal Regulatory Protein Alpha
SMC	Smooth Muscle Cell
SOX2	SRY-Box Transcription Factor 2
SRC	SRC Proto-Oncogene, Non-Receptor Tyrosine Kinase
SYK	Spleen Associated Tyrosine Kinase
T1D	Type 1 Diabetes
TAP	Transporter Associated with Antigen Processing

TCR	T Cell Receptor
Tg	Transgene
TG	Thyroglobulin
TP53	Tumor Protein p53
TPO	Thyroid Peroxidase
tracrRNA	Trans-activating crRNA
TSP-1	Thrombospondin 1
UPR	Unfolded Protein Response
WT	Wild Type



## List of Figures

Figure 1: Structural representation of MHC class I and class II molecules. ....	15
Figure 2: Structure of the Cas9-sgRNA complex.....	23
Figure 3: Schematic representation of the gene editing strategies to generate hypimmunogenic cells. .	127

## Abstract

End-stage organ failure is affecting millions of people every year. In Europe and in the United States the number of transplants performed yearly represent less than half of the transplantations needed. One of the main issues is immunological incompatibility between donor and recipient which leads to an unsuccessful transplantation due to the rejection of grafted cells, tissues or organs.

To address this problem, we aimed to generate universal “off-the-shelf” iPSCs and their derivatives which can be allogeneically transplanted without the use of immunosuppressive drugs.

Mouse and human iPSCs were engineered by CRISPR-Cas9 knock out of *B2m/B2M*, a gene encoding for an essential component of Major Histocompatibility Complex (MHC) molecules and *Ciita/CIITA*, a gene regulating the expression of MHC molecules, and lentivirally overexpressing the surface protein Cd47/CD47. The generated hypoimmunogenic iPSCs and their derivatives show both in *in vivo* and *in vitro* immunological assays immune evasion in allogeneic settings. Long-term allogeneic survival of *in vivo* engrafted hypoimmunogenic cells without the administration of immunosuppressive drugs was achieved.

The generated hypoimmunogenic cell therapeutics evade immune rejection in allogeneic recipients, however are susceptible to antibody-mediated killing.

To generate fully immune evasive cell therapeutics, we engineered the IgG receptor CD64 on human and mouse hypoimmune iPSC-derived iECs. CD64 binds the free F<sub>c</sub> region of IgGs while the F<sub>ab</sub> region binds its antigen, rendering the F<sub>c</sub> region not available to immune cells for binding and therefore making the cells fully protected from antibody-mediated cellular cytotoxicity (ADCC) and complement-dependent cytotoxicity (CDC).

We subsequently engineered disease-relevant cells such as human thyroid epithelial cells, pancreatic beta cells and CAR T cells to overexpress CD64t, a truncated form of CD64. The transgenic cells were able to fully evade disease-specific antibody-mediated killing.

This work demonstrates a new strategy for the generation of hypoimmunogenic cell therapeutics which evade all cellular-mediated and antibody-mediated killing. These results could potentially address the major hurdles in transplantation and regenerative medicine.

## Zusammenfassung

Organversagen im Endstadium betrifft jedes Jahr Millionen von Menschen. In Europa und den Vereinigten Staaten ist die Zahl der jährlich durchgeführten Transplantationen weniger als die Hälfte der benötigten Transplantationen. Eines der Hauptprobleme ist die immunologische Inkompatibilität zwischen Spender und Empfänger, die zu einer erfolglosen Transplantation aufgrund der Abstoßung von transplantierten Zellen, Geweben oder Organen führt.

Um dieses Problem anzugehen, wollten wir universelle iPSCs „off-the-shelf“ und ihre Derivate herstellen, die ohne den Einsatz von immunsuppressiven Medikamenten allogene transplantiert werden können.

Universelle murine und humane iPSCs wurden durch CRISPR-Cas9-Knockout von *B2m/B2M*, einem Gen, das für eine wesentliche Komponente von Molekülen des Major Histocompatibility Complex (MHC) kodiert, und *Ciita/CIITA*, einem Gen, das die Expression von MHC-Molekülen reguliert, und lentiviraler Überexpression des Oberflächenproteins Cd47/CD47 generiert. Die kreierte hypoimmunogenen iPSCs und ihre Derivate zeigen sowohl in *in vivo* als auch in *in vitro* immunologischen Assays Immunevasion unter allogenen Konditionen. Es wurde ein langfristiges allogenes Überleben von *in vivo* transplantierte hypoimmunogenen Zellen ohne die Verabreichung von Immunsuppressiva erreicht.

Die generierten hypoimmunogenen Zelltherapeutika entziehen sich der Immunabstoßung in allogenen Empfängern, sind jedoch anfällig für eine Antikörper-vermittelte Tötung.

Um vollständig immunevasive Zelltherapeutika zu entwickeln, haben wir den IgG-Rezeptor CD64 auf murinen und humanen hypoimmunogenen iPSC-derivierten Endothelzellen generiert. CD64 bindet die frei zugängliche F<sub>c</sub>-Region von IgGs, während die F<sub>ab</sub>-Region ihr Antigen bindet, wodurch die F<sub>c</sub>-Region Immunzellen nicht zur Bindung zur Verfügung steht und die Zellen daher vollständig vor Antikörper-vermittelter zellulärer Zytotoxizität (ADCC) und Komplement-abhängiger Zytotoxizität (CDC) geschützt sind.

Anschließend haben wir krankheitsrelevante Zellen wie menschliche Schilddrüsenepithelzellen, Betazellen der Bauchspeicheldrüse und CAR-T-Zellen so manipuliert, dass sie CD64t, eine

trunkierte Form von CD64, überexprimieren. Die transgenen Zellen konnten sich der krankheitsspezifischen Antikörper-vermittelten Tötung vollständig entziehen.

Diese Arbeit demonstriert eine neue Strategie für die Generierung von hypoimmunogenen Zelltherapeutika, die jegliche zellvermittelte und Antikörper-vermittelte Tötung umgehen. Diese Ergebnisse bieten somit eine Basis für mögliche Anwendungen in der Transplantation und regenerativen Medizin.

# 1 Introduction

End-stage organ failure is a major cause of death worldwide and patients can be treated by organ transplantation. One of the main challenges of organ transplantation is the unmet demand of organs. According to the Organ Procurement and Transplant Network database in the USA by the end of 2019, there were 112,568 patients waiting and 39,718 solid organ transplants performed (Edgar et al. 2020). Alongside with the worldwide shortage of organs, immune activation following transplant threatens long-term transplantation outcomes and leads to graft rejection.

## 1.1 The immune system

The immune system has the role of protecting the host from the continuous exposure to pathogens and hostile environment while simultaneously maintaining the ability to remain tolerant to its own. In vertebrates, the immune system consists of two different types of responses which are characterized by the speed and the specificity of the reaction. One type of response is mediated by the innate immune system and the other one is mediated by the adaptive immune system. Both of these immune systems are constantly interacting (Fearon and Locksley 1996). The innate immune system is responsible for the immediate non-specific immune response after a foreign organism encounter. Foreign organisms are recognized by the innate immune system through receptors binding to peptides or carbohydrates. The major components of the innate immune system are granulocytes, macrophages, dendritic cells, natural killer cells and complement system. The adaptive immune system consists of the slower antigen-specific reactions carried out by T cells and B cells. The rejection of donor's organs and tissues in the recipient is mediated by both innate and adaptive immune cells system.

### 1.1.1 Natural Killer cells (NK cells)

Natural killer (NK) cells are lymphocytes originating from bone marrow precursors and account for 2-18% of the total lymphoid population when analyzing human peripheral blood mononuclear cells (PBMCs). NK cells have cytotoxic and cytokine-producing effector functions (Raulet 2004). Circulating NK cells can recognize and kill both tumor and virally infected cells. They are also able to regulate other immune cells (Waggoner et al. 2011; Cooper, Fehniger, and Caligiuri 2001). The effector functions of NK cells are tightly controlled by the extensive repertoire of stimulatory, co-stimulatory and inhibitory receptors. The overall immune response results from the combination of inhibiting and activating signals that the NK cell receives at the time of antigen encounter (Vivier et al. 2008). The balance of these signals ensures that the NK cells discriminate between healthy self-cells and non self-cells. Self-cells present a surface protein called Major Histocompatibility Antigen (MHC) class I, which binds to Killer Cell Immunoglobulin-like Receptors (KIRs) on the surface of NK cells suppressing cytotoxicity (Karre et al. 1980). This ensures that self-cells are not eliminated, and it is called the “missing-self” theory. NK cell subsets can be distinguished by the expression levels of the phenotypic markers F<sub>c</sub> Gamma Receptor IIIa (also known as CD16) and Neural Cell Adhesion Molecule 1 (also known as CD56). The CD56<sup>dim</sup> NK cells represent a highly cytotoxic NK cell population. CD56<sup>dim</sup> NK cells can lyse the target cells by secreting granules containing granzyme B and perforin (Cooper, Fehniger, and Caligiuri 2001).

### 1.1.2 T and B cells

T and B cells originate from the bone marrow and as they mature, they move to the circulation and to secondary lymphoid organs. On their cell surface, T and B cells express receptors recognizing specific antigens. B cells bind antigens through the cell surface localized B cell receptor (BCR) (Reth 1992). The antigen-binding subunit consists of two identical transmembrane immunoglobulin heavy chain (IgH) and two identical light chains (IgL). These are arranged so that there are two antigen-binding (F<sub>ab</sub>) regions linked to a fragment crystallizable (F<sub>c</sub>). The heavy chain is non-covalently associated with a heterodimer consisting of Ig $\alpha$  and Ig $\beta$  signaling proteins.

T cells express the T cell receptor (TCR) which consists of two variable chains responsible for antigen binding and a protein complex called Cluster of Differentiation 3 (CD3). Antigen recognition by T cells occurs when the TCR interacts with Major Histocompatibility Complex (MHC) which are surface molecules able to bind antigens. To ensure a stable interaction between TCR and the antigen-MHC complex, the T cell co-receptor molecules CD4 or CD8 additionally bind to the MHC. During T cell maturation in the thymus, only T cells expressing TCR with a weak affinity to self-peptide bound to MHC complexes are chosen to be released into the circulation. This results in a set of T cells that remain tolerant to self-cells and are only activated by non-self antigens. Once B and T cells express their cell specific receptors, they are released into the circulation and interact with each other as well as with antigens resulting in the first antigen-specific immune responses (Weih and Caamano 2003). After a first encounter, subpopulations of B and T cells recognizing the antigen differentiate and clonally expand into long-lived antigen-specific memory B cells, plasma cells and T cells (Klein and Dalla-Favera 2008). Those subpopulations remain in the circulation and enable the host to mount a more rapid immune response upon second encounter with the same antigen (Huston 1997).

## **1.2 The Major Histocompatibility Complex (MHC)**

The MHC consists of surface proteins which are encoded by a set of genes found in a defined genetic region. MHC molecules are polymorphic and each individual carries a unique combination of molecules which are necessary for cell self-recognition and prevention of the immune system to target its own. Each MHC subunit gene is highly polymorphic and therefore the MHC molecules are able to bind a large repertoire of different antigen fragments (Wieczorek et al. 2017).

Gorer and Snell discovered the MHC in 1936 as skin transplantation experiments between various mouse strains revealed that the survival of the grafts was dependent on the genetic background of the mice (Snell 1948). Successful grafts performed between mice of the same genetic background are termed syngeneic. Unsuccessful grafts performed between mice of a different genetic background are termed allogeneic. There are two classes of MHC proteins: class I and class II. In mice the MHC is also known as H2 complex. MHC class I consists of three subclasses H-2D, H-2K and H-2L, whereas the MHC class II consists of H2-A and H2-E molecules.



The MHC class I molecules are heterodimers of a large transmembrane  $\alpha$  chain (encoded by the MHC genes) and non-polymorphic molecule called  $\beta$ 2-microglobulin ( $\beta$ 2m) which is not encoded by MHC genes. On the cell surface,  $\beta$ 2m is located extracellularly with the  $\alpha$  chain and stabilizes the structure of MHC class I. The MHC class II molecule is composed of a heterodimer of a transmembrane  $\alpha$  chain and  $\beta$  chain, both encoded by the MHC genes (**Figure 1**).

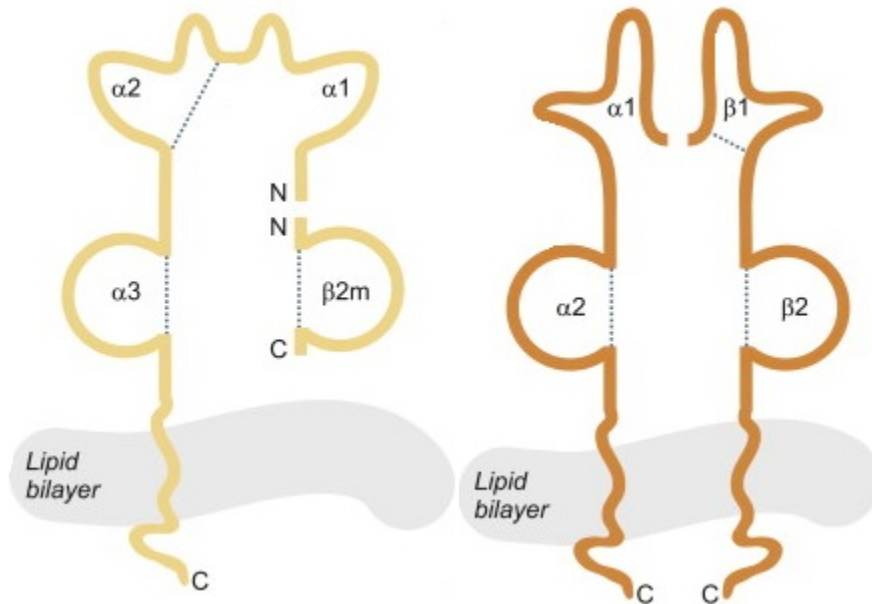


**Figure 1:** Structural representation of MHC class I and class II molecules.

(Left) HLA class I molecule consisting of  $\alpha$ -chain transmembrane protein and  $\beta$ 2-microglobulin molecule. (Right) The HLA class II molecule is made of a transmembrane  $\alpha$  chain and a transmembrane  $\beta$  chain, both encoded by the HLA region. The HLA class I molecule has two peptide-binding domains ( $\alpha$ 1 and  $\alpha$ 2) as well as an immunoglobulin-like domain  $\alpha$ 3. The HLA class II molecule has a peptide-binding domain consisting of  $\alpha$ 1 and  $\beta$ 1 chains and it has two immunoglobulin-like domains  $\alpha$ 2 and  $\beta$ 2. (Mak, Saunders, Jett 2014).

After the discovery of the mouse MHC, the first histocompatibility antigen was discovered in humans (Dausset 1958; Marchal, Dausset, and Colombani 1962) by observing the development of antibodies in the serum of patients that received various blood transfusions. These antibodies were directed against the blood cells of another person and were termed histocompatibility antigen or Human Leukocyte Antigen (HLA).

HLA class I molecules are present on all nucleated cells and mainly present peptides originating from endogenous and foreign cytoplasmic antigens which have been degraded by proteasomes in the cytosol (Gabriel et al. 2014). In humans, the HLA class I molecules can be further divided into

classical and non-classical groups. The classical group consists of molecules presenting antigens to T cells, whereas the molecules of the non-classical group are not as polymorphic and are not involved in antigen presentation. The classical HLA class I molecules are encoded by the HLA-A, HLA-B and HLA-C loci, whereas the non-classical HLA class I proteins are encoded by the HLA-E, HLA-F, HLA-G and MHC class I polypeptide-related sequence A (MICA) loci. The HLA class II is encoded by the HLA-DR, HLA-DQ and HLA-DP loci and their constitutive expression is restricted to specific antigen-presenting cells (APC), such as dendritic cells, macrophages and B cells.

### **1.3 The immune system in transplantation**

The immune system protects the host from foreign antigens by mounting a strong immune response against them. Due to the enormous polymorphism of HLA molecules, the immune system of the recipient might recognize as foreign the graft non-self antigens. This immune response is mediated mainly by T cells and leads to the rejection of the donor allograft (Hall 1991). Besides T cell activation, the presence of antibodies directed against graft HLA and other antigens might result in graft damage and rejection in a process called antibody-mediated rejection (AMR). AMR is mainly mediated by NK cells, neutrophils and macrophages. HLA matching of organ donor and recipient as well as immunosuppressive therapies can help mitigate the strong activation of the recipient's immune system upon transplantation.

#### **1.3.1 Immunomodulatory function of MHC**

The MHC molecules play an essential role in the activation of the immune system, as they allow the recognition of foreign peptide fragments by T cells. MHC class I proteins display the processed antigen to T cells through interaction with the TCR. T cells expressing a specific TCR for a particular MHC-non-self antigen complex will be activated upon binding, only when co-stimulation and cytokine binding occur. T cells not only recognize foreign antigens in combination to self MHC molecules, but also recognize foreign antigens in combination with non-self MHC

molecules. Both lead to the lysis of the target cell in a process called alloreactivity. Cytotoxic T cells express the co-stimulatory molecule CD8 and mediate the lysis of the target cells by releasing perforin or granzymes.

MHC class II molecules typically present peptides originating from exogenous antigens (Sadegh-Nasseri and Kim 2015). When an antigen is presented by the cells through MHC class II molecules, the MHC class II:non-self antigen complex is recognized by CD4<sup>+</sup> T cells via the TCR. Upon activation, CD4<sup>+</sup> T cells release a variety of cytokines which trigger CD8<sup>+</sup> T cells and NK cells. CD4<sup>+</sup> T cells can also activate B cells which produce antibodies against the antigen on the target cells, a process called opsonization. Opsonization results in the target cells getting tagged by antibodies for elimination.

### **1.3.2 Antibody-mediated rejection**

Antibody-mediated rejection (AMR) is a well-known post-transplantation consequence, recognized as a clinicopathological entity for the first time in 1997 (Colvin et al. 1997). In general, AMR is characterized by the presence of anti-HLA donor specific antibodies (DSAs) or antibodies directed against graft antigens in the recipient. The presence of DSAs is correlated with long term poor graft survival (Lachmann et al. 2009; Campos et al. 2006). By ten years after kidney transplant, approximately 25% of the transplant recipients have developed antibodies against the graft (Everly 2013). DSAs can be found in the serum of recipients before transplantation due to a previous transplant, pregnancy, blood transfusion or insufficient immunosuppression (Wiebe et al. 2012), but can also develop later (Wiebe et al. 2012). After transplantation, new or already present DSAs bind their epitopes on the endothelium of the graft which is the first exposed surface of the graft to the recipient immune system (Chen et al. 2018). DSAs can bind allogeneic HLA or non-HLA molecules on the graft's endothelial cells (Farkash and Colvin 2012) triggering an immune reaction via complement-dependent cytotoxicity (CDC) or antibody dependent cellular cytotoxicity (ADCC) (Zwirner et al. 2000; Mizutani et al. 2005; Zou et al. 2002).

### **1.3.2.1 Complement-dependent cytotoxicity**

The complement is part of the innate immune system (Walport 2001) and consists of various membrane receptors and non-membrane bound proteins mainly originating from the liver and released into the circulatory system. The initial reaction that triggers CDC is the binding of the complement molecule C1q to the target cell. In solid organ transplantation the majority of the DSAs consist of the IgG1 antibody subclass (Lefaucheur et al. 2016). When DSAs or antibodies directed against donor's antigens bind to the endothelium of the graft, the exposed F<sub>c</sub> region of the antibody allows for the binding of the complement molecule C1q. This leads to the recruitment of a series of complement proteins such as C3 convertase. C3 convertase promotes a series of chain reactions, inducing the assembly of the Membrane Attack Complex (MAC) which causes cell membrane perforation and injury. One of the criteria of pathological diagnosis for antibody-mediated rejection is the deposition of the molecule C4d in the endothelium of renal grafts (Bohmig et al. 2002; Feucht et al. 1993; Lederer et al. 2001; Gaston et al. 2010; Mauiyyedi et al. 2001). C4d is a typical degradation product of the activation of the complement cascade that remains bound to the endothelium of the graft.

### **1.3.2.2 Antibody-dependent cellular cytotoxicity**

ADCC was described in 1965 by Erna Moeller, as an immune system mechanism where target cells become opsonized by antibodies which leads to the recruitment of effector cells inducing cell death (Moeller 1965). In transplantation, DSAs and antibodies against the donor's antigens create "bridges" between the antigen on the target cell bound via the F<sub>ab</sub> region and the effector cells bound to the free F<sub>c</sub> region of the IgG. The effector cells bind the free F<sub>c</sub> region via the F<sub>c</sub> gamma receptors (FcγRs). FcγRs are expressed on the surface of NK cells, macrophages and neutrophils. In humans there are activating FcγRs (FcγRI, FcγRIIA/C, FcγRIII) or inhibitory FcγR (FcγRIIB). Human NK cells express only activating FcγR (FcγRIIIa alternatively known as CD16a or FcγRIIc or CD32c) and no inhibitory FcγR to counteract their activity. When NK cells encounter free IgG-F<sub>c</sub> the binding triggers the activation of the NK cells leading to cytokine production and lysis of the target cell. The activating receptor Killer Cell Lectin Like Receptor K1 (also known as

NKG2D) is found on the surface of NK cells and promotes the CD16a signaling. In transplantation, the graft endothelial cells maintain a low level of cell surface NKG2D ligands expression such as MICA, a protein part of the non-classical MHC class I. Host antibodies directed against MICA can trigger ADCC and subsequently graft damage. MICA is associated with increased kidney allograft rejection rates and poor graft survival (Zou et al. 2007).

In humans there are several different types of Fc $\gamma$ Rs that differ in their expression and binding affinity to different classes of IgG. Typically, the majority of DSAs consist of IgG1 antibodies and the Fc $\gamma$ R with the highest affinity for this antibody class is Fc $\gamma$ RI or CD64. CD64 is prevalently found on the surface of macrophages and neutrophils and has high affinity for IgG1, IgG3 and IgG4 but has no affinity to IgG2. The therapeutic anti-tumorigenic potential of many antibodies such as anti-CD20 (Rituximab) and anti-HER2 (Trastuzumab) has been studied in mouse models to demonstrate that ADCC activity was essential to the reduction of the tumors (Clynes et al. 2000). In humans, clinical trials have shown that administered antibodies are able to reduce or eliminate the tumorigenic cells, partly by triggering ADCC. The polymorphisms of FcRIIa and FcRIIIa having a higher affinity for IgG1 showed a stronger ADCC activity (Bibeau et al. 2009). Significant improvements have been observed in patients with B cell lymphoma carrying activating Fc $\gamma$ R alleles with a higher affinity to Rituximab IgG1 antibodies when administered (Weng et al. 2004; Cartron et al. 2002).

#### **1.4 Autoimmune diseases**

Autoimmune diseases are caused by the failure of tolerance mechanisms in the body thus the immune system cannot discern self-antigens from foreign. Hallmarks of autoimmune disorders are autoreactive CD8<sup>+</sup> and CD4<sup>+</sup> T cells attacking tissues and organs and producing cytokines to trigger autoantibody production in plasma cells (Sinha, Lopez, and McDevitt 1990). This leads to the destruction or dysfunction of the tissue itself (Xiao, Miller, and Zheng 2021).

Hashimoto's thyroiditis is an example of an autoimmune disorder targeting thyroid cells with an incidence estimated at 80 cases per 100000 per year. Although its etiology is unclear, this disease is characterized by the presence of self-reactive CD4<sup>+</sup> T cells which by cytokine release recruit B

cells and CD8<sup>+</sup> T cells to the thyroid tissue. Plasma cells produce autoantibodies against thyroid cell surface proteins such as anti-thyroid peroxidase (TPO) antibodies and anti-thyroglobulin (TG) antibodies. These autoantibodies are found in the serum of patients (Roitt et al. 1956). Mice models show that the immunization of susceptible mice with thyroglobulin leads to the breakdown of tolerance (Tomazic and Rose 1976; Kong 2007) .

Type 1 diabetes (T1D) is another autoimmune disease targeting  $\beta$  cells which are insulin producing cells found within the pancreatic islets of Langerhans in the pancreas (Ke et al. 2020). T1D is caused by the tolerance breakdown to  $\beta$  cell antigens a few examples being proinsulin, insulin, and glutamic acid decarboxylase (GAD65) and the consequent destruction of the  $\beta$  cells. The etiology is not quite understood however fragments of autoantigens are displayed to T cells and this leads to the activation and differentiation to T effector cells initiating the  $\beta$  cell damage.

## **1.5 Transplantation and cell therapy**

Worldwide organ shortage is the main cause of death of patients with end-stage organ failure. The transplantation field has been profoundly impacted by the advances in cell therapies. These therapies are dedicated to the regenerative use of stem cells and their derivatives to replace and/or repair tissues and organs to restore their functionality. Pluripotent stem cells are unspecialized cells which are able to differentiate into any cell type of the organism have the ability of self-renewal *in vitro* indefinitely. Their regenerative potential might offer a solution to the organ shortage. In regenerative medicine two main sources of stem cells are employed: embryonic stem cells (ESCs) and induced pluripotent stem cells (iPSCs).

### **1.5.1 Role of ESCs in transplantation**

In 1981 Evans, Kaufman and Martin first described the isolation and culture of mouse ESCs (mESCs) derived from mouse early embryos (Evans and Kaufman 1981; Martin 1981). Later in 1998 Thomson described the first isolation of human blastocyst-derived pluripotent stem cells (Thomson et al. 1998). The potential for tissue regeneration of human ESCs (hESCs) allowed the

establishment of hESC-based therapies for various diseases such as macular degeneration (Liu, Xu, et al. 2018), ischemic heart disease (Menasche et al. 2018), and diabetes mellitus (Schulz 2015). A concern for the clinical use of ESCs is their survival post-transplant which is limited as ESCs express MHC class I proteins on their cell surface and ESCs derivatives have an even increased expression of MHC class I (Drukker et al. 2002). MHC class I molecules on the surface of the grafted cells can be recognized by the recipient's immune system as non-self and trigger a strong T cell response, the vigorous immune response leads to their rapid depletion. The tumorigenic nature of ESCs (Nussbaum et al. 2007), and the ethical concerns regarding the research on human embryos make them a non-ideal source of stem cells for transplantation.

### **1.5.2 Role of iPSCs in transplantation**

In 2006, Yamanaka and Takahashi reported the generation of mouse induced pluripotent stem cells (miPSCs) from adult murine fibroblasts. iPSCs were artificially generated from mouse somatic cells by introduction of four factors *Pou5f1* (or *Oct3/4*), *Sox2*, *Klf4*, and *c-Myc* (Takahashi and Yamanaka 2006). miPSCs and mESCs have similar morphology, developmental patterns and gene expression profiles (Takahashi and Yamanaka 2006).

Shortly after, in 2007, Yamanaka and colleagues described the generation of human iPSCs (hiPSCs) from adult somatic cells with a similar approach to the generation of miPSCs (Takahashi et al. 2007). The introduction of *POU5F1* (or *OCT3/4*), *SOX2*, *KLF4*, and *C-MYC* by retroviral transduction of somatic cells resulted in the formation of ESC-like colonies. hiPSCs have been shown to maintain a similar gene expression profile and developmental potential compared to the ESCs (Liang and Zhang 2013). In clinical settings, an immune activation due to the immunogenicity of the iPSCs might lead to the rejection of these cells/tissues. Some studies found little to no signs of immune rejection of the miPSC grafts and of miPSC-derived cells grafts (de Almeida et al. 2014; Guha et al. 2013; Araki et al. 2013), as well as minimal immune response in the brain after iPSC-derived neurons were transplanted in nonhuman primates (Morizane et al. 2013). These studies reported contrasting results compared the findings of others, which showed rejection of miPSCs upon syngeneic transplantation (Zhao et al. 2011). An immune activation should however not occur when transplanting hiPSC derivatives generated from patient-specific

hiPSCs which are immune matched to the patient. Retinal cells derived from such autologous hiPSC have been used already for the treatment of patients with macular degeneration (Mandai, Kurimoto, and Takahashi 2017). However, even autologous hiPSC derivatives could trigger an immune response leading to their rejection, i.e. *de novo* mutations developed during reprogramming of the somatic cells into iPSCs and their expansion in culture and/or differentiation may contribute to the generation of gene mutations in the mitochondrial DNA. The corresponding proteins might act as neoantigens which lead to rejection of the cells after autologous transplantation when presented to the immune system (Deuse, Hu, Agbor-Enoh, et al. 2019).

Another consideration regarding the use of hiPSC derivatives for clinical applications and their long-term survival is AMR. DSAs are directed against but not limited to MHC molecules of the grafted cells/tissues derived from hiPSCs therefore antigens might trigger CDC and ADCC generating damage and cell rejection.

Despite the potential of iPSCs to treat major diseases their immunogenic potential barrier needs to be overcome. Targeted gene editing could potentially offer a solution to reduce the immunogenicity of iPSCs.

## **1.6 Gene editing**

Gene editing is the process through which DNA or RNA are manipulated to add, delete, or replace nucleotides in the genome. Two of the most frequently used techniques are the Clustered Regularly Interspaced Short Palindromic Repeats (CRISPR)/CRISPR-associated system (Cas) or CRISPR/Cas9 and lentiviral overexpression.

### **1.6.1 CRISPR/Cas9**

The Clustered Regularly Interspaced Short Palindromic Repeats were discovered in 1987 in the bacterium *E.Coli* (Ishino et al. 1987; Mojica et al. 2000). These sequences are part of an adaptive, prokaryotic immune defense mechanism against foreign DNA and RNA of phages/viruses and they induce RNA-guided DNA cleavage (Li et al. 2020; Jinek et al. 2012). There are different



types of nucleases and the most frequently used for gene editing is the Cas9 from the bacteria *Streptococcus pyogenes* system. The CRISPR locus is composed of a Cas9 nuclease gene, two noncoding CRISPR RNAs (crRNAs): trans-activating crRNA (tracrRNA) and a precursor crRNA (pre-crRNA) which is a short nucleotide sequence complementary to the target genomic DNA sequence. The single guide RNA (sgRNA) consists of the crRNA and the tracrRNA. The sgRNA has a sequence complementing the DNA targeted and binds adjacent to a short sequence called “protospacer adjacent motif” (PAM). The endonuclease Cas9-sgRNA complex is able to precisely cleave the DNA to generate a double strand break (DSB) which is then repaired by the endogenous DNA repair machinery through non-homologous end joining (NHEJ) or homology-directed repair (HDR). This leads to targeted deletions or insertions in the genome (**Figure 2**).

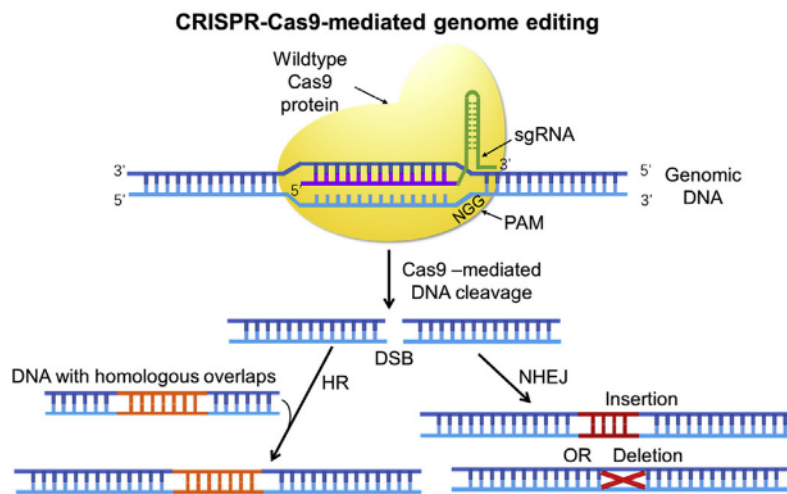


**Figure 2:** Structure of the Cas9-sgRNA complex.

The sgRNA binds to the DNA target site, the Cas9 protein cleaves the DNA creating a DSB near the PAM sequence. Upon generation of DSB either Random insertion-deletions (INDELs) or precise modifications are inserted into the DNA by NHEJ or HDR pathway (Tian et al. 2017).

Active Cas9 enzyme introduces a double-stranded break (DSB). The cell repairs through two methods, one of which is the error-prone non-homologous end joining (NHEJ) that creates InDels. Alternatively, if a double stranded DNA donor template is provided, the DSB is repaired through homology-directed repair (HDR) resulting in a targeted insertion. Cong et al. demonstrated for the first time in 2013 the targeted cleavage of mammalian chromosomes (Cong et al. 2013).

## **1.6.2 Lentiviral overexpression**

Lentiviruses are part of the family of retroviruses and carry two copies of sense strand viral RNA. Retroviruses have, among others, genes encoding reverse transcriptase, integrase and protease as well as viral envelope proteins. Following infection of the cell, the viral reverse transcriptase and integrase perform reverse transcription and random integration of the virus encoded gene into the host cellular DNA (Cockrell and Kafri 2007) allowing for long-term expression. One of the advantages of using lentiviruses to modify gene expression in comparison to other retroviruses is their efficacy into infecting non-proliferating cells.

## 1.7 Thesis goal

The goal of this PhD Thesis was to engineer cell therapeutics that can be universally transplanted and can be used as a therapy option in clinical settings. To achieve this, the immunogenicity of stem cells needed to be investigated. Human and mouse induced pluripotent stem cells were engineered using CRISPR/Cas9 technology to generate MHC class I and class II null cells and to induce exogenous expression of the non-immunogenic molecule CD47. These hypoimmunogenic cells were differentiated in various mesodermal lineages and their immunogenicity was investigated *in vitro* and *in vivo*. Hypoimmunogenic stem cell derivatives were subsequently modified by forced overexpression of non-immunogenic CD64 or CD64t (the truncated version of CD64) to protect them against humoral responses. Similarly, various disease-relevant cell types were engineered to evade antibody-mediated killing. Their protection was assessed by *in vitro* and *in vivo* experiments.

## 2 Publications

### 2.1 Hypoimmunogenic derivatives of induced pluripotent stem cells evade immune rejection in fully immunocompetent allogeneic recipients

In Chapter 2 is presented the publication ‘Hypoimmunogenic derivatives of induced pluripotent stem cells evade immune rejection in fully immunocompetent allogeneic recipients’. The paper has been published in Nature Biotechnology in 2019. My contribution to this paper includes performing imaging studies and analysis of the data. This contribution resulted in a second authorship on the paper.

**Title:** Hypoimmunogenic derivatives of induced pluripotent stem cells evade immune rejection in fully immunocompetent allogeneic recipients

**Authors:** Tobias Deuse\*, Xiaomeng Hu\*, Alessia Gravina, Dong Wang, Grigol Tediashvili, Chandrav De, William O. Thayer, Angela Wahl, J. Victor Garcia, Hermann Reichenspurner, Mark M. Davis, Lewis L. Lanier & Sonja Schrepfer

\*share co-authorship

**Journal:** Nature Biotechnology

**DOI:** 10.1038/s41587-019-0016-3

# Hypoimmunogenic derivatives of induced pluripotent stem cells evade immune rejection in fully immunocompetent allogeneic recipients

Tobias Deuse<sup>1,7</sup>, Xiaomeng Hu<sup>1,2,3,7</sup>, Alessia Gravina<sup>1</sup>, Dong Wang<sup>1,2</sup>, Grigol Tediashvili<sup>1,2,3</sup>, Chandrav De<sup>4</sup>, William O. Thayer<sup>4</sup>, Angela Wahl<sup>4</sup>, J. Victor Garcia<sup>4</sup>, Hermann Reichenspurner<sup>2,3</sup>, Mark M. Davis<sup>5</sup>, Lewis L. Lanier<sup>6</sup> and Sonja Schrepfer<sup>1\*</sup>

**Autologous induced pluripotent stem cells (iPSCs) constitute an unlimited cell source for patient-specific cell-based organ repair strategies. However, their generation and subsequent differentiation into specific cells or tissues entail cell line-specific manufacturing challenges and form a lengthy process that precludes acute treatment modalities. These shortcomings could be overcome by using prefabricated allogeneic cell or tissue products, but the vigorous immune response against histoincompatible cells has prevented the successful implementation of this approach. Here we show that both mouse and human iPSCs lose their immunogenicity when major histocompatibility complex (MHC) class I and II genes are inactivated and CD47 is over-expressed. These hypoimmunogenic iPSCs retain their pluripotent stem cell potential and differentiation capacity. Endothelial cells, smooth muscle cells, and cardiomyocytes derived from hypoimmunogenic mouse or human iPSCs reliably evade immune rejection in fully MHC-mismatched allogeneic recipients and survive long-term without the use of immunosuppression. These findings suggest that hypoimmunogenic cell grafts can be engineered for universal transplantation.**

Treatment of heart disease with adult multipotent, bone marrow-derived stem cells has shown marginal efficacy in patients with acute myocardial infarction<sup>1</sup> or chronic ischemic cardiomyopathy<sup>2,3</sup>. This has been attributed to the limited plasticity of adult hematopoietic stem cells, which do not differentiate into cardiomyocytes and thus cannot replace contractile elements<sup>4</sup>. Pluripotent stem cells are more promising cell sources for regenerative strategies as they can produce an unlimited amount of progeny cells that can be differentiated into functional tissue cells. Although reprogramming technology allows the generation of autologous iPSCs for patient-specific treatments, this is laborious, costly, associated with uncertain quality and efficacy of individual cell products and is only practical for chronic diseases<sup>5–7</sup>. Thus, most regenerative approaches relying on autologous iPSC generation have been abandoned. Allogeneic cell therapies targeting large patient populations could be more economically feasible<sup>8,9</sup>, but are subject to forceful immune rejection<sup>10</sup>.

The use of allogeneic iPSC- or embryonic stem cell (ESC)-based products would require strong immunosuppression.

We envisioned engineering hypoimmunogenic pluripotent stem cells as a source for universally compatible cell or tissue grafts not requiring any immunosuppression. During pregnancy, the maternal immune system is tolerant of allogeneic paternal antigens although it would reject cells from the baby later in life<sup>11</sup>. We examined syncytiotrophoblast cells, which form the interface between maternal blood and fetal tissue, and found low MHC class I and II expression (Supplementary Fig. 1) as well as strong expression of CD47, a ubiquitous membrane protein that can interact with several cell surface receptors to inhibit phagocytosis<sup>12</sup>. We used this knowledge to design hypoimmunogenic mouse iPSCs (miPSCs).

C57BL/6 wild type (WT) miPSCs<sup>13</sup> give rise to classical teratomas with ectodermal, mesodermal and endodermal features in SCID-beige mice (Supplementary Fig. 2). To achieve hypoimmunogenicity, these miPSCs underwent a three-step gene-editing process (Supplementary Fig. 3a). First, CRISPR guide RNAs targeting the coding sequence of the mouse  $\beta 2$ -microglobulin (*B2m*) gene were ligated into vectors containing the Cas9 expression cassette and subsequently transfected into miPSCs. *B2m* is a structural component of MHC class I. Second, *B2m*<sup>-/-</sup> miPSCs were transfected with a CRISPR-Cas9 vector targeting *Ciita*, the master regulator of MHC class II molecules<sup>14</sup>. Third, the *Cd47* gene sequence was synthesized and cloned into a lentivirus with blasticidin resistance, which was used to transduce *B2m*<sup>-/-</sup>*Ciita*<sup>-/-</sup> miPSC clones followed by a antibiotic selection and expansion of *B2m*<sup>-/-</sup>*Ciita*<sup>-/-</sup> *Cd47* transgene (tg)-expressing miPSCs. WT miPSCs had no interferon- $\gamma$  (IFN- $\gamma$ )-inducible MHC class I surface expression, low but detectable MHC class II expression and negligible *Cd47* expression (Supplementary Fig. 3b–d). We confirmed that the miPSC lines we generated lacked MHC class I and II expression, and over-expressed *Cd47* roughly 4.5-fold in flow cytometry. All three lines maintained their expression of pluripotency genes (Supplementary Fig. 3e–h).

Next, we transplanted WT miPSCs or engineered miPSCs into syngeneic C57BL/6 (H2<sup>b</sup>) and allogeneic (H2<sup>d</sup>) BALB/c recipients without immunosuppression. As expected, WT miPSCs showed

<sup>1</sup>Department of Surgery, Division of Cardiothoracic Surgery, Transplant and Stem Cell Immunobiology-Lab, University of California San Francisco, San Francisco, CA, USA. <sup>2</sup>Department of Cardiovascular Surgery, University Heart Center Hamburg, Hamburg, Germany. <sup>3</sup>Cardiovascular Research Center Hamburg and DZHK (German Center for Cardiovascular Research), Partner Site Hamburg/Kiel/Luebeck, Hamburg, Germany. <sup>4</sup>Division of Infectious Diseases, UNC Center for AIDS Research, University of North Carolina School of Medicine, Chapel Hill, NC, USA. <sup>5</sup>Howard Hughes Medical Institute, Institute for Immunity, Transplantation and Infection, and Department of Microbiology and Immunology, Stanford University School of Medicine, Stanford, CA, USA. <sup>6</sup>Department of Microbiology and Immunology and the Parker Institute for Cancer Immunotherapy, University of California San Francisco, San Francisco, California, USA. <sup>7</sup>These authors contributed equally: Tobias Deuse, Xiaomeng Hu. \*e-mail: Sonja.Schrepfer@ucsf.edu

100% teratoma growth in syngeneic recipients, but all cell grafts were rejected in allogeneic BALB/c mice (Fig. 1a,b). After 5 days, splenocytes from allogeneic BALB/c recipients showed a strong IFN- $\gamma$  and a moderate IL-4 response relative to baseline responder cell activity (not shown); syngeneic mice showed no responsiveness (Fig. 1c). Only allogeneic BALB/c recipients mounted a strong IgM antibody response against the WT miPSCs relative to baseline MFI (not shown) (Fig. 1d). Engineered miPSCs developed comparable teratomas to WT miPSCs in syngeneic recipients, with enhanced survival in allogeneic recipients that depended on their level of hypoimmunogenicity and increased with every engineering step (Supplementary Fig. 4a–h). Our final  $B2m^{-/-}Ciita^{-/-}$  Cd47 tg miPSC line showed 100% teratoma formation and induced no IFN- $\gamma$  or antibody responses (Fig. 1e–h).

We further evaluated the contribution of Cd47 overexpression by comparing  $B2m^{-/-}Ciita^{-/-}$  miPSCs to  $B2m^{-/-}Ciita^{-/-}$  Cd47 tg miPSCs in natural killer (NK) cell toxicity assays. Gene editing did not enhance the expression of stimulatory ligands for the mouse NK cell NK G2D or NKp46 receptors (Supplementary Fig. 4i), which are constitutively expressed in the NK cell-sensitive target cell line YAC-1<sup>15</sup>.  $B2m^{-/-}Ciita^{-/-}$  miPSCs induced IFN- $\gamma$  release that was significantly elevated when compared to unchallenged NK cells, but lower than IFN- $\gamma$  release triggered by YAC-1 (Supplementary Fig. 4j). This suggested that Cd47 overexpression completely prevented any miPSC-induced NK cell IFN- $\gamma$  release *in vitro*. To further assess innate miPSC clearance *in vivo*, a 1:1 mixture of CFSE-labeled WT miPSCs and either  $B2m^{-/-}Ciita^{-/-}$  miPSCs or  $B2m^{-/-}Ciita^{-/-}$  Cd47 tg miPSCs were injected into the innate immune cell-rich peritoneum of syngeneic C57BL/6 mice (Supplementary Fig. 5a). Using a syngeneic host for this assay precluded relevant T cell-mediated cytotoxicity. After 48 h, the peritoneal fluid was aspirated and CFSE-labeled cells were analyzed by flow cytometry.  $B2m^{-/-}Ciita^{-/-}$  Cd47 tg miPSCs, but not  $B2m^{-/-}Ciita^{-/-}$  miPSCs, were resistant to innate immune clearance and the 1:1 ratio with WT miPSCs could be maintained. We observed the same pattern of cell clearance when mice were pretreated with clodronate to eliminate macrophages (Supplementary Fig. 5b). Notably, a blocking antibody against mouse Cd47 completely abolished the protective effect of Cd47 in macrophage-depleted mice and  $B2m^{-/-}Ciita^{-/-}$  Cd47 tg miPSCs were rapidly eliminated (Supplementary Fig. 5c). Collectively, these data suggest an inhibitory effect of Cd47 on NK cells *in vivo*.

To test whether hypoimmunogenic  $B2m^{-/-}Ciita^{-/-}$  Cd47 tg miPSCs could give rise to hypoimmunogenic cardiac tissue, they were differentiated into endothelial cells (miECs), smooth muscle cells (miSMCs) and cardiomyocytes (miCMs) with WT miPSC derivatives serving as controls (Supplementary Fig. 6). All derivatives showed the morphologic appearance, cell marker immunofluorescence and gene expression characteristic of their mature target tissue cell lines, and cultures achieved >90% purity of VE-Cadherin<sup>+</sup> miECs, Sma<sup>+</sup> miSMCs and troponin I<sup>+</sup> miCMs. The expression of MHC class I and II molecules in WT derivatives markedly varied by cell type (Supplementary Fig. 7a–c) but, as expected, miECs had by far the highest expression of IFN- $\gamma$  induced MHC class I and II, miSMCs had moderate MHC class I and II expression<sup>16</sup> and miCMs had moderate MHC class I but very low MHC class II expression<sup>17</sup>. All  $B2m^{-/-}Ciita^{-/-}$  Cd47 tg derivatives appropriately showed a complete lack of MHC class I and II and significantly elevated Cd47 compared to their WT counterparts. None of the  $B2m^{-/-}Ciita^{-/-}$  Cd47 tg derivatives showed upregulation of NK G2D or NKp46 ligands (Supplementary Fig. 7d,e).

We next assessed the *in vivo* immunogenicity of WT and hypoimmunogenic miPSC derivatives. miECs, miSMCs or miCMs derived from WT or  $B2m^{-/-}Ciita^{-/-}$  Cd47 tg were transplanted intramuscularly into syngeneic C57BL/6 or allogeneic BALB/c mice and adaptive immune responses were assessed after 5 days. All allogeneic recipients mounted a strong cellular IFN- $\gamma$  response, as well

as a strong IgM antibody response against all differentiated WT cell grafts (Supplementary Fig. 8a–c). In contrast, neither of the corresponding  $B2m^{-/-}Ciita^{-/-}$  Cd47 tg derivatives showed detectable increases in IFN- $\gamma$  Elispot frequencies or IgM antibody production (Supplementary Fig. 8d–f). To assess the efficacy of Cd47 to mitigate the susceptibility to innate immune killing, we performed NK cell Elispot assays with antibody-coated magnetic bead-enriched BALB/c NK cells and  $B2m^{-/-}Ciita^{-/-}$  or  $B2m^{-/-}Ciita^{-/-}$  Cd47 tg derivatives (Supplementary Fig. 8g–i). While  $B2m^{-/-}Ciita^{-/-}$  derivatives triggered NK cell IFN- $\gamma$  release, none of the  $B2m^{-/-}Ciita^{-/-}$  Cd47 tg derivatives produced IFN- $\gamma$  spot frequencies significantly exceeding those of unchallenged NK cells. Accordingly, *in vivo* innate immune assays showed rapid clearance of all  $B2m^{-/-}Ciita^{-/-}$  derivatives, but confirmed that none of the  $B2m^{-/-}Ciita^{-/-}$  Cd47 tg derivatives showed susceptibility to innate elimination (Supplementary Fig. 8j–l). To confirm an inhibitory effect of Cd47 on NK cells, we next performed real-time *in vitro* killing assays with confluent miECs and highly purified NK cells. Both allogeneic (BALB/c) and syngeneic (C57BL/6) NK cells rapidly killed  $B2m^{-/-}Ciita^{-/-}$  miECs, but not WT and  $B2m^{-/-}Ciita^{-/-}$  Cd47 tg miECs (Supplementary Fig. 5d,e). However, antibody blocking of mouse Cd47 resulted in the rapid killing of  $B2m^{-/-}Ciita^{-/-}$  Cd47 tg miECs (Supplementary Fig. 5f). The effect of Cd47 is species-specific as human NK cells rapidly killed both  $B2m^{-/-}Ciita^{-/-}$  and  $B2m^{-/-}Ciita^{-/-}$  Cd47 tg miECs (Supplementary Fig. 5g).

We next examined survival of WT and hypoimmunogenic miPSC derivatives *in vivo*. WT and  $B2m^{-/-}Ciita^{-/-}$  Cd47 tg derivatives were transduced to express firefly luciferase, and Matrigel plugs containing differentiated cells were transplanted into syngeneic C57BL/6 or allogeneic BALB/c mice. All three WT derivatives showed long-term (50 days) survival in syngeneic C57BL/6 recipients, but were rejected in allogeneic mice (Fig. 11–k). In contrast, all three  $B2m^{-/-}Ciita^{-/-}$  Cd47 tg derivatives showed 100% long-term survival in both syngeneic and allogeneic recipients (Fig. 11–n).

Matrigel plugs containing WT or  $B2m^{-/-}Ciita^{-/-}$  Cd47 tg miECs were transplanted into allogeneic BALB/c recipients (Supplementary Fig. 9a). ECs are the most immunogenic cardiac cell type due to their high expression of MHC class I and II, which allows them to function as antigen-presenting cells. We observed infiltrating immune cells containing mostly T and B lymphocytes, but also some NK cells and macrophages in WT miEC plugs.  $B2m^{-/-}Ciita^{-/-}$  Cd47 tg miEC-containing plugs had almost no immune cell infiltration (Supplementary Fig. 9b). In the WT plugs, cytokine arrays on day 10 revealed an inflammatory milieu that included upregulated T helper cell (T<sub>H</sub>)-1 cytokines (IFN- $\gamma$  and IL-2) and T<sub>H</sub>-2 cytokines (IL-4, IL-5, IL-10 and IL-13). In contrast, in plugs containing  $B2m^{-/-}Ciita^{-/-}$  Cd47 tg miECs, the cytokine milieu was very similar to that of cell-free plugs containing only Matrigel, with no indication of immune activation (Supplementary Fig. 9c). Over time, transplanted  $B2m^{-/-}Ciita^{-/-}$  Cd47 tg miECs organized in circular structures and formed primitive vessels that contained erythrocytes (Supplementary Fig. 10a). Similarly transplanted  $B2m^{-/-}Ciita^{-/-}$  Cd47 tg miSMCs (Supplementary Fig. 10b) or miCMs (Supplementary Fig. 10c) did not form three-dimensional structures, and their *in vivo* maturation and integration potential in cardiac tissue remains to be studied.

We next applied our engineering strategy to human iPSCs (hiPSCs) using a human episomal iPSC line derived from CD34<sup>+</sup> cord blood that showed a normal human XX karyotype and features of pluripotency (Supplementary Fig. 11a–c,g–h). The gene editing process included two steps (Fig. 2a). First, both the human *B2M* and human *CIITA* genes were simultaneously targeted for CRISPR/Cas9-mediated disruption. Second, these edited hiPSCs were transduced with a lentivirus carrying human CD47 complementary DNA using an EFS promoter and puromycin resistance. An antibiotic-resistant  $B2M^{-/-}CIITA^{-/-}$  CD47 tg hiPSC colonies maintained their normal

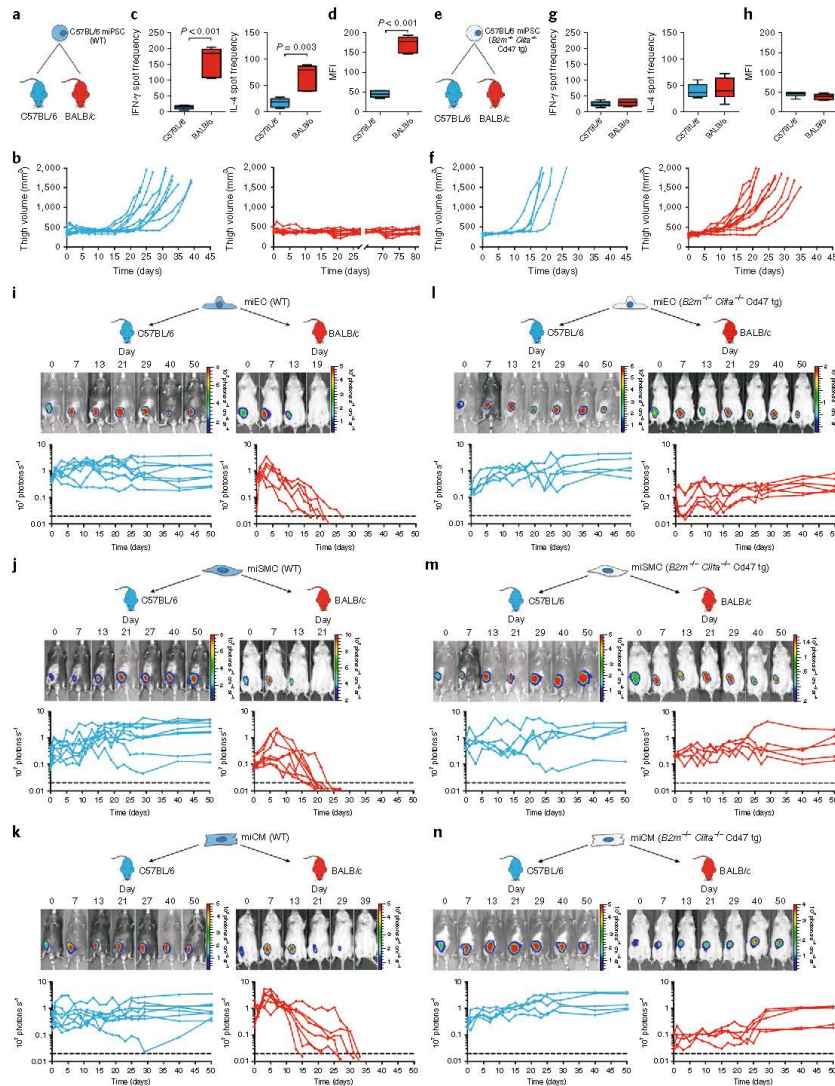


**Fig. 1 | Survival of miPSCs and miPSC derivatives.** **a**, WT C57BL/6 miPSCs were injected into the thigh muscle of syngeneic C57BL/6 or allogeneic BALB/c mice. **b**, Teratoma formation was observed by measuring the thigh muscle ( $n=10$  per group). **c**, IFN- $\gamma$  and IL-4 enzyme-linked immunospots (Elispots) with splenocytes recovered 5 days after the transplantation (box 25th to 75th percentile with median, whiskers min-max, five animals per group, two-tailed Student's *t*-test). **d**, Mean fluorescence imaging (MFI) of IgM binding to WT miPSCs incubated with recipient serum after 5 days (box 25th to 75th percentile with median, whiskers min-max, six animals per group, two-tailed Student's *t*-test). **e**,  $B2m^{-/-} Ciita^{-/-} Cd47$  tg C57BL/6 miPSCs were transplanted into syngeneic C57BL/6 or allogeneic BALB/c recipients. **f**, Thigh volume C57BL/6 ( $n=5$ ) and BALB/c ( $n=11$ ) animals. The overall percentage of cell grafts that survived and formed teratomas in BALB/c was 100%. **g**, IFN- $\gamma$  and IL-4 Elispots with splenocytes recovered 5 days after the transplantation and  $B2m^{-/-} Ciita^{-/-} Cd47$  tg miPSCs stimulator cells (box 25th to 75th percentile with median, whiskers min-max,  $n=6$  per group, two-tailed Student's *t*-test). **h**, MFI of IgM binding to  $B2m^{-/-} Ciita^{-/-} Cd47$  tg miPSCs incubated with recipient serum after 5 days (box 25th to 75th percentile with median, whiskers min-max, six animals per group, two-tailed Student's *t*-test). **i-n**, Grafts of Fluc $^{+}$  C57BL/6 miPSC derivatives in C57BL/6 or BALB/c recipients were longitudinally followed by bioluminescent imaging (BLI). One representative animal is depicted per group and the BLI values of all animals are plotted. All WT miPSC-derived miECs (**i**, eight animals in C57BL/6 and six animals in BALB/c), miSMCs (**j**, nine animals in C57BL/6 and eight animals in BALB/c) and miCMs (**k**, eight animals in C57BL/6 and seven animals in BALB/c) showed long-term survival in syngeneic C57BL/6 recipients but were rejected in allogeneic BALB/c animals. In contrast, all  $B2m^{-/-} Ciita^{-/-} Cd47$  tg miPSC-derived miECs (**l**, five animals in C57BL/6 and six animals in BALB/c), miSMCs (**m**, five animals in C57BL/6 and five animals in BALB/c) and miCMs (**n**, five animals in C57BL/6 and five animals in BALB/c) showed long-term survival in both syngeneic C57BL/6 and allogeneic BALB/c recipients.

human karyotype and pluripotency (Supplementary Fig. 11d–f, i–j) and successful depletion of HLA I and II surface expression, along with overexpression of CD47, was confirmed by flow cytometry (Fig. 2b). Both WT hiPSCs and  $B2M^{-/-}CIITA^{-/-}$  CD47 tg hiPSCs were differentiated into endothelial-like cells (hiECs) and cardiomyocyte-like cells (hiCMs) (Fig. 2c). All derivatives showed the morphologic features and protein expression of the differentiated target cells and lost their pluripotency genes (Supplementary Fig. 12a,b). Cultures showed >95% purity for VE-Cadherin<sup>+</sup> hiECs and troponin I<sup>+</sup> hiCMs. There were no alterations in the expression of stimulatory NK cell ligands with gene engineering (Supplementary Fig. 12c–i). WT hiECs and hiCMs upregulated IFN- $\gamma$  induced HLA I expression roughly three- and two-fold, respectively, compared to WT hiPSCs and hiECs also showed roughly 11-fold elevated HLA II (Fig. 2d–e).  $B2M^{-/-}CIITA^{-/-}$  CD47 tg hiECs and hiCMs exhibited HLA I and II depletion and significant CD47 upregulation compared to their WT counterparts.

We next performed transplant studies in humanized CD34<sup>+</sup> hematopoietic stem cell-engrafted NSG-SGM3 mice<sup>18</sup>, which were allogeneic to the hiPSC, hiEC and hiCM grafts. Since no syngeneic controls are available in this humanized mouse model, background measurements were collected in naïve mice. After 5 days, recipients of WT hiPSCs (Fig. 2f) showed a high splenocyte IFN- $\gamma$  spot frequency (Fig. 2g) and elevated IgM levels (Fig. 2h). Recipients of  $B2M^{-/-}CIITA^{-/-}$  CD47 tg hiPSCs did not mount any detectable cellular IFN- $\gamma$  response or antibody response. NK cell activation was assessed using *in vitro* incubation with human enriched CD56<sup>+</sup> NK cells.  $B2M^{-/-}CIITA^{-/-}$  hiPSCs resulted in an IFN- $\gamma$  release reaching roughly one-third of the spot frequency of the highly NK cell susceptible K562 line, whereas  $B2M^{-/-}CIITA^{-/-}$  CD47 tg hiPSCs did not provoke any measurable response (Fig. 2i). The allogeneic transplantation of WT hiECs (Fig. 2j) and WT hiCMs (Fig. 2n) resulted in strong systemic IFN- $\gamma$  reactions (Fig. 2k,o) and IgM antibody increases (Fig. 2l,p) of similar intensity as WT hiPSCs, whereas hypoinnogenic hiECs and hiCMs did not induce any cellular or humoral immune response. Moreover, *in vitro*, hypoinnogenic derivatives did not trigger NK cell activation (Fig. 2m, q) or NK cell killing (Supplementary Fig. 5h). As with the miPSCs, a blocking antibody specific for human CD47 completely abolished NK cell protection of  $B2M^{-/-}CIITA^{-/-}$  CD47 tg hiPSCs (Supplementary Fig. 5i).

We also assessed the survival of hiPSCs, as well as their derivatives in an allogeneic humanized NSG-SGM3 mice. All cell lines

were transduced to express Fluc to enable tracking by BLI. There was no significant difference in HLA-A mismatch between groups (Supplementary Fig. 12j). As expected, all WT hiPSC grafts in Matrigel plugs underwent rejection (Fig. 3a) and all  $B2M^{-/-}CIITA^{-/-}$  CD47 tg hiPSCs formed teratomas. Similarly, WT hiECs (Fig. 3b) and WT hiCMs (Fig. 3c) were rejected, although at slightly slower rate than in the corresponding miPSC derivative experiments. This difference may be based on the reduced number, diversity and function of human immune cells in mouse recipients<sup>19</sup>, although the triple transgenic NSG-SGM3 mice specifically express human cytokines<sup>20</sup> to minimize these limitations. All  $B2M^{-/-}CIITA^{-/-}$  CD47 tg hiEC and hiCM grafts showed long-term survival (50 days) and stable BLI signal levels over time. The hiECs gradually organized into structures resembling primitive vascular structures, which occasionally contained erythrocytes, and the hiCMs acquired a limited polarized architecture (Fig. 3d,e).

hiECs, the most immunogenic derivatives, were further tested in the humanized BLT mouse model. BLT humanized mice are bioengineered by implantation of human fetal liver and thymic tissue under the kidney capsule followed by intravenous transplantation with autologous CD34<sup>+</sup> HSCs<sup>21</sup> (Fig. 3f). This allows for T cell maturation in human thymic tissue and permits HLA restricted T cell responses. WT hiEC grafts in Matrigel plugs triggered a roughly 40% stronger IFN- $\gamma$  response but 40% weaker IgM antibody response than in the previous NSG-SGM3 mice. No measurable immune activation was detected in recipients of  $B2M^{-/-}CIITA^{-/-}$  CD47 tg hiEC grafts (Fig. 3g,h). All WT hiEC grafts underwent rapid rejection while four out of five  $B2M^{-/-}CIITA^{-/-}$  CD47 tg hiEC grafts achieved survival (Fig. 3i). We assume a non-immune-related reason for the failure of the fifth graft since no immune activation could be detected in this specific recipient. We thus demonstrated that the combination of MHC class I and II depletion and CD47 overexpression renders both mouse and human stem cells, as well as their differentiated derivatives, hypoinnogenic. In the models studied here, engineered differentiated derivatives achieved long-term survival in fully allogeneic hosts without any immunosuppression and retained basic cell-specific features after transplantation.

The initial concept of hypoinnogenic pluripotent stem cells was based on a MHC class I knockdown and showed encouraging early results<sup>22</sup>. However, according to the ‘missing-self theory’, MHC class I-deficient mouse and human PSCs become susceptible to NK

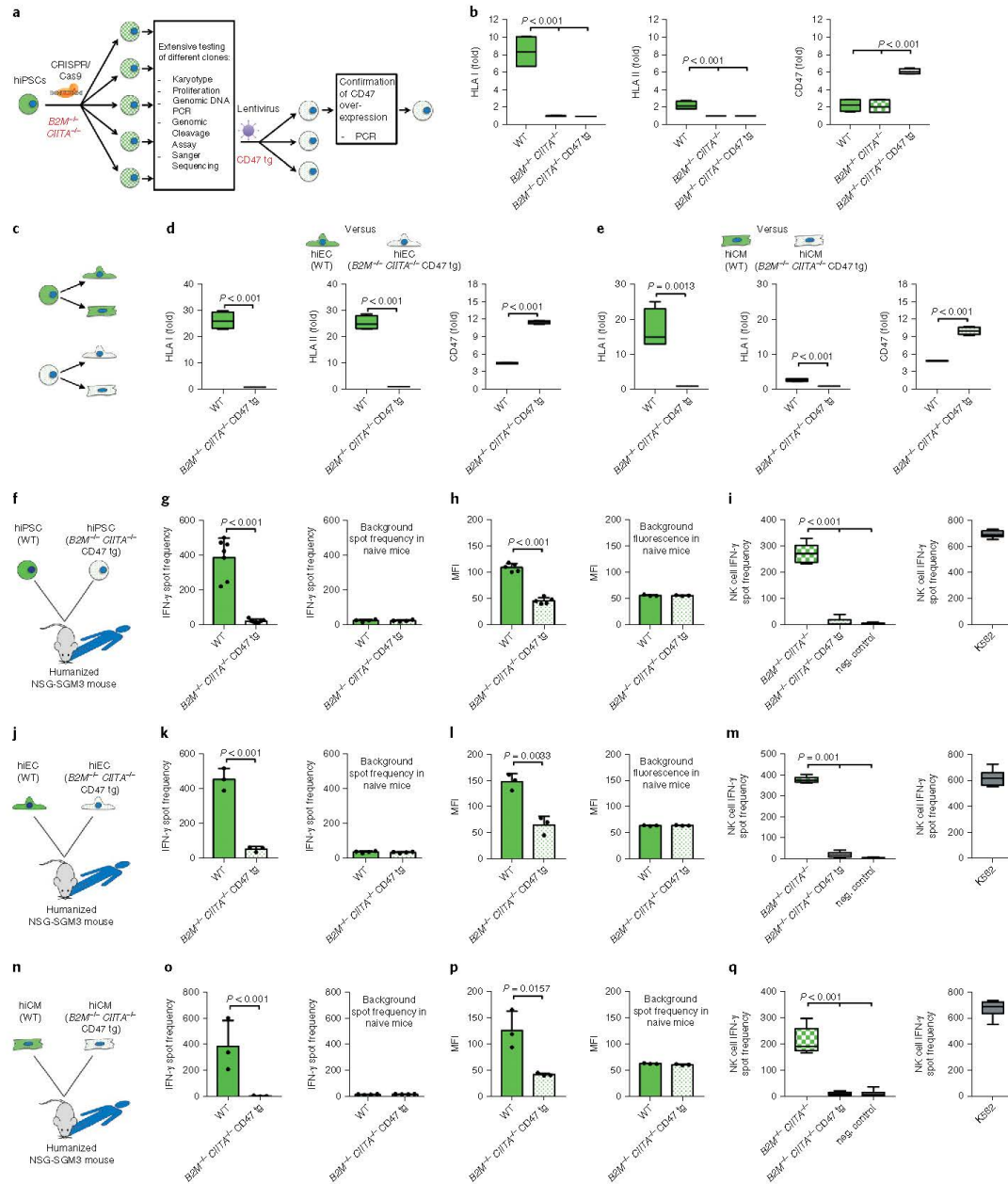
**Fig. 2 | Immune response against hiPSC derivatives.** **a**, WT hiPSCs first underwent  $B2M$  and  $CIITA$  gene disruption and then CD47 transgene overexpression **b**. Gene editing of hiPSCs was confirmed by flow cytometry (box 25th to 75th percentile with median, whiskers min–max, four independent experiments per graph, analysis of variance (ANOVA) with Bonferroni’s post-hoc test). **c**, WT and  $B2M^{-/-}CIITA^{-/-}$  CD47 tg hiPSCs were differentiated into both hiECs and hiCMs. **d–e**, The immune phenotype of WT and  $B2M^{-/-}CIITA^{-/-}$  CD47 tg hiECs (**d**) and hiCMs (**e**) is shown (box 25th to 75th percentile with median, whiskers min–max, four independent experiments per graph, two-tailed Student’s *t*-test). **f**, WT or  $B2M^{-/-}CIITA^{-/-}$  CD47 tg hiPSC grafts were injected into allogeneic humanized NSG-SGM3 mice. **g**, IFN- $\gamma$  Elispots were performed after 5 days (mean  $\pm$  s.d.,  $n=7$  per group, two-tailed Student’s *t*-test), the background spot frequency in naïve mice is shown (mean  $\pm$  s.d., four animals per group, two-tailed Student’s *t*-test). **h**, MFI of IgM binding to either hiPSC incubated with recipient serum after 5 days (mean  $\pm$  s.d., five animals per group, two-tailed Student’s *t*-test), the background fluorescence in naïve mice is shown (mean  $\pm$  s.d., three animals per group, Student’s *t*-test). **i**, IFN- $\gamma$  Elispots with human NK cells were performed with  $B2M^{-/-}CIITA^{-/-}$  hiPSC or  $B2M^{-/-}CIITA^{-/-}$  CD47 tg hiPSC (box 25th to 75th percentile with median, whiskers min–max, six independent experiments, ANOVA with Bonferroni’s post-hoc test). **j**, WT or  $B2M^{-/-}CIITA^{-/-}$  CD47 tg hiEC grafts were injected into allogeneic humanized NSG-SGM3 mice. **k**, IFN- $\gamma$  Elispots were performed after 5 days (mean  $\pm$  s.d., three animals per group, two-tailed Student’s *t*-test), the background spot frequency in naïve mice is shown (mean  $\pm$  s.d., four animals per group, two-tailed Student’s *t*-test). **l**, MFI of IgM binding to either hiEC incubated with recipient serum after 5 days (mean  $\pm$  s.d., three animals per group, two-tailed Student’s *t*-test), the background fluorescence in naïve mice is shown (mean  $\pm$  s.d., three animals per group, Student’s *t*-test). **m**, IFN- $\gamma$  Elispots with human NK cells were performed with  $B2M^{-/-}CIITA^{-/-}$  hiECs or  $B2M^{-/-}CIITA^{-/-}$  CD47 tg hiECs (box 25th to 75th percentile with median, whiskers min–max, six independent experiments, ANOVA with Bonferroni’s post-hoc test). **n**, WT or  $B2M^{-/-}CIITA^{-/-}$  CD47 tg hiCM grafts were injected into allogeneic humanized NSG-SGM3 mice. **o**, IFN- $\gamma$  Elispots were performed after 5 days (mean  $\pm$  s.d., three animals per group, two-tailed Student’s *t*-test), the background spot frequency in naïve mice is shown (mean  $\pm$  s.d., four animals per group, two-tailed Student’s *t*-test). **p**, MFI of IgM binding to either hiCM incubated with recipient serum after 5 days (mean  $\pm$  s.d., three animals per group, two-tailed Student’s *t*-test), the background fluorescence in naïve mice is shown (mean  $\pm$  s.d., three animals per group, Student’s *t*-test). **q**, IFN- $\gamma$  Elispots with human NK cells were performed with  $B2M^{-/-}CIITA^{-/-}$  hiCMs or  $B2M^{-/-}CIITA^{-/-}$  CD47 tg hiCMs (box 25th to 75th percentile with median, whiskers min–max, six independent experiments, ANOVA with Bonferroni’s post-hoc test).



cell killing<sup>23–25</sup>. Although isolated expression of HLA-E<sup>26</sup> or HLA-G<sup>27</sup> in human pluripotent stem cells has been used to mitigate NK cell cytotoxicity, we observed that CD47 is a very effective non-MHC ligand to silence all innate immune responses. However, cells eluding immune monitoring may pose the long-term risks of uncontrolled malignant transformation or rimpaired virus clearance,

although for the latter alternative mechanisms have been shown<sup>28</sup>. Inducible kill switches could enhance their overall safety.

The ability to generate substantial amounts of cardiac tissue from a allogeneic iPSC-derived CMs has been well demonstrated in macaques<sup>29</sup>. However, the amounts of toxic immunosuppressive drugs required to achieve allogeneic cell survival pose a major



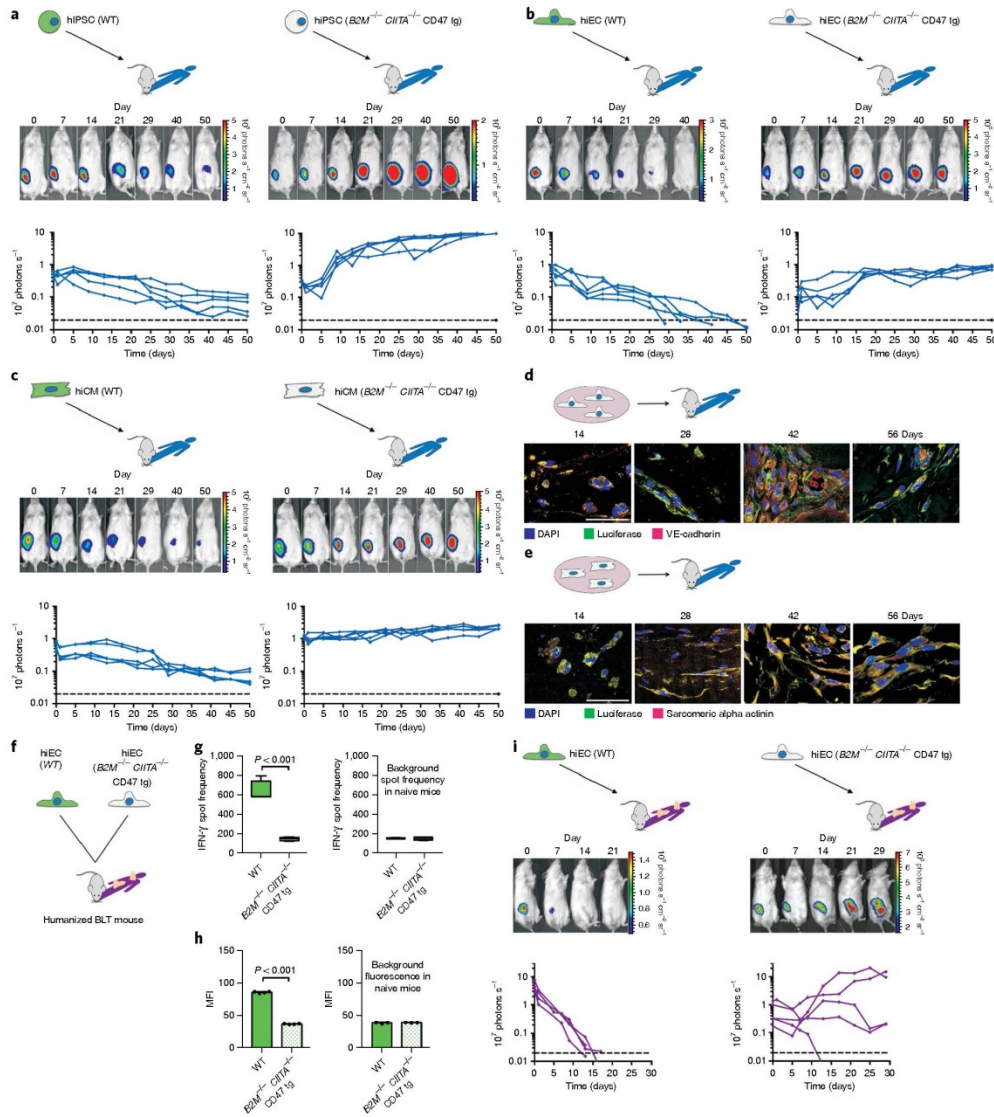


**Fig. 3 | Survival of hiPSCs and hiPSC derivatives in allogeneic hosts.** Grafts of Fluc<sup>+</sup> WT or *B2M*<sup>-/-</sup>*CIITA*<sup>-/-</sup> CD47 tg hiPSCs, hiECs and hiCMs were transplanted into allogeneic humanized mice (NSG-SGM3 mice in **a–e**, BLT mice in **f–i**) and were longitudinally followed by BLI. One representative animal is depicted per group and the BLI values of all animals are plotted. **a**, BLI signals over time of WT and *B2M*<sup>-/-</sup>*CIITA*<sup>-/-</sup> CD47 tg hiPSC grafts (*n* = 5 per group). **b**, WT and *B2M*<sup>-/-</sup>*CIITA*<sup>-/-</sup> CD47 tg hiECs were transplanted as in **a** (*n* = 5 per group). **c**, WT and *B2M*<sup>-/-</sup>*CIITA*<sup>-/-</sup> CD47 tg hiCMs (*n* = 5). **d**, *B2M*<sup>-/-</sup>*CIITA*<sup>-/-</sup> CD47 tg hiECs started to organize into a more complex structure, which included primitive vascular structures (representative pictures of three independent experiments). Scale bar, 50  $\mu$ m. **e**, The *B2M*<sup>-/-</sup>*CIITA*<sup>-/-</sup> CD47 tg hiCMs began to organize into a more polarized framework and maintained their sarcomeric  $\alpha$ -actinin cytoskeletal structure typical of cardiomyocytes (representative pictures of three independent experiments). Scale bar, 50  $\mu$ m. **f**, WT or *B2M*<sup>-/-</sup>*CIITA*<sup>-/-</sup> CD47 tg hiECs were transplanted into allogeneic humanized BLT mice. **g**, IFN- $\gamma$  Elispots were performed after 5 days (box 25th to 75th percentile with median, whiskers min-max, four animals per group, two-tailed Student's *t*-test), the background spot frequency in naïve mice is shown (mean  $\pm$  s.d., three animals per group, two-tailed Student's *t*-test), the background fluorescence in naïve mice is shown (mean  $\pm$  s.d., four animals per group, two-tailed Student's *t*-test). **h**, MFI of IgM binding to either hiEC incubated with recipient serum after 5 days (mean  $\pm$  s.d., four animals per group, two-tailed Student's *t*-test), the background fluorescence in naïve mice is shown (mean  $\pm$  s.d., three animals per group, two-tailed Student's *t*-test). **i**, Grafts of Fluc<sup>+</sup> WT or *B2M*<sup>-/-</sup>*CIITA*<sup>-/-</sup> CD47 tg hiECs were transplanted into allogeneic humanized BLT mice and were longitudinally followed by BLI. All WT hiEC grafts were rejected within roughly 14 days (four animals). Four of the five *B2M*<sup>-/-</sup>*CIITA*<sup>-/-</sup> CD47 tg hiEC grafts permanently survived, the one failure is believed not to be immune-mediated (five animals).

hurdle for clinical use. Even with fully MHC class I- and II-matched allogeneic iPSC-derived CM grafts, macaque recipients required substantial and highly toxic immunosuppression to prevent cell rejection<sup>29,30</sup>. Thus, the generation of universal hypoimmunogenic iPSCs that can be differentiated into the main components of cardiac tissue and achieve long-term survival in a fully allogeneic recipient without any immunosuppression may help to develop universal cell products to treat heart failure.

### Online content

Any methods, additional references, Nature Research reporting summaries, source data, statements of data availability and associated accession codes are available at <https://doi.org/10.1038/s41587-019-0016-3>.

Received: 23 April 2018; Accepted: 28 December 2018;  
Published online: 18 February 2019

### References

- Gyongyosi, M. et al. Meta-analysis of cell-based Cardiac stem cells (ACCURE) in patients with acute myocardial infarction based on individual patient data. *Circ. Res.* **116**, 1346–1360 (2015).
- Fisher, S. A., Doree, C., Mathur, A. & Martin-Rendon, E. Meta-analysis of cell therapy trials for patients with heart failure. *Circ. Res.* **116**, 1361–1377 (2015).
- Kandala, J. et al. Meta-analysis of stem cell therapy in chronic ischemic cardiomyopathy. *Am. J. Cardiol.* **112**, 217–225 (2013).
- Fernandez-Aviles, F. et al. Global position paper on cardiovascular regenerative medicine. *Eur. Heart J.* **38**, 2532–2546 (2017).
- Lipsitz, Y. Y., Timmins, N. E. & Zandstra, P. W. Quality cell therapy manufacturing by design. *Nat. Biotechnol.* **34**, 393–400 (2016).
- Blair, N. F. & Barker, R. A. Making it personal: the prospects for autologous pluripotent stem cell-derived therapies. *Regen. Med.* **11**, 423–425 (2016).
- Chakradhar, S. A. A new eye to the future: researchers debate best path for stem cell-derived therapies. *Nat. Med.* **22**, 116–119 (2016).
- Smith, D. M. Assessing commercial opportunities for autologous and allogeneic cell-based products. *Regen. Med.* **7**, 721–732 (2012).
- Lipsitz, Y. Y., Bedford, P., Davies, A. H., Timmins, N. E. & Zandstra, P. W. Achieving efficient manufacturing and quality assurance through synthetic cell therapy design. *Cell. Stem. Cell.* **20**, 13–17 (2017).
- van Berlo, J. H. & Molkentin, J. D. An emerging consensus on cardiac regeneration. *Nat. Med.* **20**, 1386–1393 (2014).
- Arck, P. C. & Hecher, K. Fetomaternal immune cross-talk and its consequences for maternal and offspring's health. *Nat. Med.* **19**, 548–556 (2013).
- Jaiswal, S. et al. CD47 is upregulated on circulating hematopoietic stem cells and leukemia cells to avoid phagocytosis. *Cell* **138**, 271–285 (2009).
- Diecke, S. et al. Novel codon-optimized mini-intronic plasmid for efficient, inexpensive, and xeno-free induction of pluripotency. *Sci. Rep.* **5**, 8081 (2015).
- Chang, C. H., Fontes, J. D., Peterlin, M. & Flavell, R. A. Class II transactivator (CIITA) is a switch for the inducible expression of major histocompatibility complex class II genes. *J. Exp. Med.* **180**, 1367–1374 (1994).
- Elsner, L. et al. The heat shock protein HSP70 promotes mouse NK cell activity against tumors that express inducible NKG2D ligands. *J. Immunol.* **179**, 5523–5533 (2007).
- Maddaluno, M. et al. Murine aortic smooth muscle cells acquire, though fail to present exogenous protein antigens on major histocompatibility complex class II molecules. *Biomed. Res. Int.* **2014**, 949845 (2014).
- Didie, M., Galla, S., Muppala, V., Dressel, R. & Zimmermann, W. H. Immunological properties of murine parthenogenetic stem cell-derived cardiomyocytes and engineered heart muscle. *Front. Immunol.* **8**, 955 (2017).
- Wunderlich, M. et al. AML xenograft efficiency is significantly improved in NOD/SCID-IL2RG mice constitutively expressing human SCF, GM-CSF and IL-3. *Leukemia* **24**, 1785–1788 (2010).
- Shultz, L. D., Ishikawa, F. & Greiner, D. L. Humanized mice in translational biomedical research. *Nat. Rev. Immunol.* **7**, 118–130 (2007).
- Billerbeck, E. et al. Development of human CD4+ FoxP3+ regulatory T cells in human stem cell factor-, granulocyte-macrophage colony-stimulating factor-, and interleukin-3-expressing NOD-SCID IL2Rgamma(null) humanized mice. *Blood* **117**, 3076–3086 (2011).
- Melkus, M. W. et al. Humanized mice mount specific adaptive and innate immune responses to EBV and TSST-1. *Nat. Med.* **12**, 1316–1322 (2006).
- Deuse, T. et al. Human leukocyte antigen I knockdown human embryonic stem cells induce host ignorance and achieve prolonged xenogeneic survival. *Circulation* **124**, S3–S9 (2011).
- Wang, D., Quan, Y., Yan, Q., Morales, J. E. & Wetzel, R. A. Targeted disruption of the beta2-microglobulin gene minimizes the immunogenicity of human embryonic stem cells. *Stem Cells Transl. Med.* **4**, 1234–1245 (2015).
- Dressel, R. et al. Pluripotent stem cells are highly susceptible targets for syngeneic, allogeneic, and xenogeneic natural killer cells. *FASEB J.* **24**, 2164–2177 (2010).
- Kruse, V. et al. Human induced pluripotent stem cells are targets for allogeneic and autologous natural killer (NK) cells and killing is partly mediated by the activating NK receptor DNAM-1. *PLoS ONE* **10**, e0125544 (2015).
- Gornalusse, G. G. et al. HLA-E-expressing pluripotent stem cells escape allogeneic responses and lysis by NK cells. *Nat. Biotechnol.* **35**, 765–772 (2017).
- Zhao, L., Teklemariam, T. & Hantash, B. M. Heterologous expression of mutated HLA-G decreases immunogenicity of human embryonic stem cells and their epidermal derivatives. *Stem Cell Res.* **13**, 342–354 (2014).
- Hou, S., Doherty, P. C., Zijlstra, M., Jaenisch, R. & Katz, I. M. Delayed clearance of Sendai virus in mice lacking class I MHC-restricted CD8+ T cells. *J. Immunol.* **149**, 1319–1325 (1992).
- Shiba, Y. et al. Allogeneic transplantation of iPSC cell-derived cardiomyocytes regenerates primate hearts. *Nature* **538**, 388–391 (2016).
- Kawamura, T. et al. Cardiomyocytes derived from MHC-homozygous induced pluripotent stem cells exhibit reduced allogeneic immunogenicity in MHC-matched non-human primates. *Stem Cell Rep.* **6**, 312–320 (2016).

### Acknowledgements

We thank C. Pahrman for cell culture work, imaging experiments and overall assistance and L. Li for his assistance. The in vivo BLT experiments were performed at the UCSF Pre-clinical Therapeutics Core (A. Fries, with special thanks to B.C. Hann). Special thanks go to J. Wu (Stanford Cardiovascular Institute, Stanford University School of Medicine) for providing the miPSCs and the help of his laboratory with developing the protocol for hiPSC differentiation into cardiomyocytes. We thank J.-E. Garcia-Gomez (City of Hope, Duarte) for the HLA typing of humanized BLT mice. We also thank E. Maltepe and H. Pektas for providing the syncytiotrophoblast cells. D.W. was supported by the Max Kade Foundation. A.W. received funding from the National Institutes of Health (grant AI123010). J.V.G. received funding from the National Institutes of Health (AI111899 and MH108179). The cardiomyocyte research was partly made possible by a grant from the California Institute for Regenerative Medicine (Grant Number DISC1-09984). Research related to cardiomyocyte immunobiology reported in this publication was supported by National Heart, Lung, and Blood Institute of the National Institutes of Health under award number R01HL140236. L.L.L. is an American Cancer Society Professor funded by NIH AI068129 and in part by the Parker Institute for Cancer Immunotherapy. S.S. and T.D. received funding for the cardiomyocyte research from the California Institute for Regenerative Medicine (Grant Number DISC1-09984) and for the immunobiology work from the National Heart, Lung, and Blood Institute of the National Institutes of Health under award number R01HL140236. The contents of this publication are solely the responsibility of the authors and do not necessarily represent the official views of the NIH, CRM and other agencies of the State of California.

### Author contributions

T.D. and S.S. designed the experiments, supervised the project, and wrote the manuscript. X.H. performed the adaptive and innate immunobiology experiments, molecular biology and imaging studies and cell culture work and analyzed the data. A.G. performed imaging studies and analyzed the data. D.W. performed the in vivo and immunofluorescence imaging studies (confocal microscopy) and histopathology. G.T. performed imaging studies and cell injections. C.D. and W.O.T. generated BLT mice and performed the BLT imaging experiments. A.W. and J.V.G. designed and supervised the experiments using BLT mice. W.O.T. and C.D. performed the experiments using BLT mice. H.R., M.M.D. and L.L.L. gave technical support and conceptual advice. All authors contributed to editing the manuscript.

### Competing interests

The authors declare no competing interests.

### Additional information

Supplementary information is available for this paper at <https://doi.org/10.1038/s41587-019-0016-3>.

Reprints and permissions information is available at [www.nature.com/reprints](http://www.nature.com/reprints).

Correspondence and requests for materials should be addressed to S.S.

Publisher's note: Springer Nature remains neutral with regard to jurisdictional claims in published maps and institutional affiliations.

© The Author(s), under exclusive licence to Springer Nature America, Inc. 2019, corrected publication 2022

## Methods

**Syncytiotrophoblast cells of mouse placenta.** On isolated mouse syncytiotrophoblast cells, expression of MHC class I, MHC class II and Cd47 was performed using PCR. RNA was isolated with the RNeasy Plus Mini kit (Qiagen) according to the manufacturer's protocol. RT-PCR was performed to generate the cDNA (Applied Biosystems). The following primers were used: mouse MHC class I: 5'-AGTGGTCTGCAGAGCATTACAA-3', reverse: 5'-GGTGACTTACCTTTAGATCTGGG-3', MHC class II forward: 5'-GATGTGGAAGACCTGCG-3', reverse: 5'-TGCATCTTCTGAGGGGTTTC-3'; mouse Cd47 forward: 5'-GGCGCAAAGCACCGAAGAATGTT-3', reverse: 5'-CCATGGCATGGCGCTTATCCATT-3'. PCRs were performed on Mastercycler nexus (Eppendorf) and the amplification products were visualized by 2% agarose gel electrophoresis (Thermo Fisher).

**Derivation of mouse iPSCs.** Mouse tail tip fibroblasts of mice were dissociated and isolated with collagenase type IV (Life Technologies) and maintained with Dulbecco's modified Eagle medium (DMEM) containing 10% fetal bovine serum (FBS), 1% glutamine, 4.5 g l<sup>-1</sup> glucose, 100 U ml<sup>-1</sup> penicillin, and 100 µg ml<sup>-1</sup> streptomycin (pen-strep) at 37 °C, 20% O<sub>2</sub>, and 5% CO<sub>2</sub> in a humidified incubator. 1 × 10<sup>6</sup> mouse fibroblasts were then re-programmed using a mini-intronic plasmid carrying sequences of Oct4, Klf4, Sox2 and c-Myc as well as short hairpin RNA against p53 (10–12 µM of DNA) using the Neon Transfection system<sup>11</sup>. After transfection, fibroblasts were plated on mitomycin-inhibited CF1 mouse embryonic fibroblasts (MEF, Applied Stemcell) and kept in fibroblast media with the addition of sodium butyrate (0.2 mM) and 50 µg ml<sup>-1</sup> ascorbic acid. When ESC-like colonies appeared, media was changed to mouse iPSC media containing DMEM + GlutaMax 31966 (Gibco) with 10% heat-inactivated fetal calf sera (FCS hi), 1% MEM-NEAA and 1% pen-strep (all Gibco). With every passage, the iPSCs were sorted for the mouse pluripotency marker SSEA-1 using antibody-coated magnetic bead based cell sorting.

**Mouse iPSC culture.** After the MEF feeder cells attached and were 100% confluent, miPSCs were grown on MEF in knockout DMEM 10829 with 15% knockout Serum Replacement, 1% glutamine, 1% MEM-NEAA, 1% pen-strep (all Gibco), 0.2% beta-mercaptoethanol and 100 units LIF (both Millipore). Cells were maintained in 10 cm dishes, medium was changed daily and the cells were passaged every 2–3 days using 0.05% trypsin-EDTA (Gibco). miPSCs were cultured on gelatin (Millipore) without feeders before experiments using the standard media. Cell cultures were regularly screened for mycoplasma infections using the MycoAlert Kit (Lonza).

**Pluripotency analysis by RT-PCR and immunofluorescence.** miPSC were plated in confocal dishes (MatTek) for immunofluorescence analysis 48 h after plating using the miPSC Characterization kit (Applied Stemcell). Briefly, cells were fixed, permeabilized, and stained overnight at 4 °C with the primary antibodies for Sox2, SSEA-1 and Oct4. After several washes the cells were incubated with a secondary antibody and DNA staining solution. Alkaline phosphatase activity assay was performed (Applied Stemcell). Stained cells were imaged using a fluorescent microscope.

For RT-PCR, RNA was extracted using the RNeasy Plus Mini Kit (Qiagen). Genomic DNA contamination was removed using the gDNA spin column. cDNA was generated using Applied Biosystems High-Capacity cDNA Reverse Transcription kit. Gene-specific primers of the miPSC Characterization Kit (Applied Stemcell) were used to amplify target sequences. Actin was used as housekeeping gene, which encodes a cellular cytoskeleton protein. PCR reactions were performed on Mastercycler nexus (Eppendorf) and visualized on 2% agarose gels.

**Pluripotency analysis by in vivo teratoma assay.** Ten million miPSCs were injected intramuscular into the hind limb of immunodeficient SCID-beige mice and teratoma development was observed within 14 days. Teratomas were recovered and fixed in 4% paraformaldehyde in PBS, dehydrated, embedded in paraffin, and cut into sections of 5 µm thickness. For histopathology, sections were rehydrated and stained with hematoxylin and eosin (Carl Roth). Images were taken with an inverted light microscope.

Immunofluorescence staining demonstrated differentiation into ectodermal, mesodermal, and endodermal cells using antibodies against brachyury (ab20680, Abcam), cytokeratin 8 (ab 192467) and GEAP (GA5, Cell Signaling). For visualization, secondary antibodies conjugated with Alexa Fluor 555, 488 and 647 (all Invitrogen) were used, respectively. Cell nuclei were counterstained with 4,6-diamidino-2-phenylindole (DAPI) and imaging was performed with a Leica SP5 laser confocal microscope (Leica).

**Gene editing of mouse iPSCs.** miPSCs underwent three gene-modification steps. First, CRISPR guides targeting the coding sequence of mouse *B2m* gene were annealed and ligated into vectors containing the Cas9 expression cassette. Transfected miPSCs were dissociated to single cells, expanded to colonies, sequenced and tested for homogeneity. Second, these *B2m*<sup>-/-</sup> miPSCs were transfected with vectors containing CRISPR guides targeting *Ctita*. Expanded single cell colonies were sequenced and *B2m*<sup>-/-</sup>*Ctita*<sup>-/-</sup> clones were identified

through the presence of aberrant sequence from the CRISPR cleavage site. Third, the *Cd47* gene sequence was synthesized and the DNA was cloned into a lentiviral with blasticidin resistance. *B2m*<sup>-/-</sup>*Ctita*<sup>-/-</sup> miPSCs were transduced with the resulting lentivirus and grown in the presence of blasticidin. Antibiotic-selected pools were tested for Cd47 overexpression and *B2m*<sup>-/-</sup>*Ctita*<sup>-/-</sup> Cd47 tg miPSCs were expanded.

**Generation of *B2m*<sup>-/-</sup> miPSCs.** CRISPR technology was used for disruption of the *B2m* gene. For targeting the coding sequence of mouse *B2m* gene, the CRISPR sequence 5'-TTCGGCTTCCCATTCTCCGG(TGG)-3' was annealed and ligated into the All-In-One (AIO) vectors containing the Cas9 expression cassette as per the kit's instructions (GeneArt CRISPR Nuclease Vector Kit, Thermo Fisher). miPSC were transfected with the AIO vectors using Neon electroporation with two 1,200 V pulses of 20 ms duration. The transfected iPSC cultures were dissociated to single cells using 0.05% trypsin (Gibco) and then sorted with FACSAria cell sorter (BD Bioscience) for removing doublets and debris by selective gating on forward and side light scatter properties. Single cells were expanded to full-size colonies and tested for CRISPR editing by screening for the presence of the altered sequence from the CRISPR cleavage site. Briefly, the target sequence was amplified via PCR using AmpliTaq Gold Master Mix (Applied Biosystems) and the primers B2m gDNA forward: 5'-CTGGATCAGACATATGTGTGGGA-3', reverse: 5'-GCAAAGCAGTTTTAAGTCCACACAG-3'. After cleanup of the obtained PCR product (PureLink Pro 96 PCR Purification Kit, Thermo Fisher), Sanger sequencing was performed. The Ion Personal Genome Machine (PGM) Sequencing was used for the identification of the homogeneity, through sequencing of a PCR amplified 250 base pair region of the *B2m* gene using primers B2m gDNA PGM forward: 5'-TTTTCAAATGTGGGTAGACTTTGG-3' and reverse: 5'-GGATTTCAATGTGAGGCGGGT-3'. The PCR product was purified as described above and prepared using the Ion PGM Hi-Q Template Kit (Thermo Fisher). Experiments were performed on the Ion PGM System with the Ion 318 Chip Kit v2 (Thermo Fisher).

**Generation of *B2m*<sup>-/-</sup>*Ctita*<sup>-/-</sup> miPSCs.** CRISPR technology was used for the further disruption of the *Ctita* gene. For targeting the coding sequence of mouse *Ctita* gene, the CRISPR sequence 5'-GGTCCATCTGGTCATAGAG (CGG)-3' was annealed and ligated into the All-In-One (AIO) vectors containing the Cas9 expression cassette as per the kit's instructions (GeneArt CRISPR Nuclease Vector Kit, Thermo Fisher). miPSC were transfected with the AIO vectors using the same condition for *B2m* disruption. The transfected miPSC cultures were dissociated to single cells using 0.05% trypsin (Gibco) and then sorted with FACSAria cell sorter (BD Bioscience) for removing doublets and debris by selective gating on forward and side light scatter properties. Single cells were expanded to full-size colonies and tested for CRISPR editing by screening for the presence of an altered sequence from the CRISPR cleavage site. Briefly, the target sequence was amplified via PCR using AmpliTaq Gold Master Mix (Applied Biosystems) and the primers *Ctita* gDNA forward: 5'-CCCCAGAACGATGAGCTT-3', reverse: 5'-TGCAGAAGTCCCTGAGAAGGCC-3'. After cleanup of the obtained PCR product (PureLink Pro 96 PCR Purification Kit, Thermo Fisher), Sanger sequencing was performed. Using the DNA sequence chromatogram, edited clones were then identified through the presence of altered sequence from the CRISPR cleavage site. Indel size was calculated using the TIDE tool. PCR and ICC were performed again to verify the pluripotency status of the cells.

**Generation of *B2m*<sup>-/-</sup>*Ctita*<sup>-/-</sup> Cd47 tg miPSCs.** Cd47 transgene overexpression was generated using lentivirus-mediated delivery of a Cd47-expressing vector containing the antibiotic resistance cassette blasticidin. The Cd47 cDNA was synthesized and cloned into the lentiviral plasmid pLent6/V5 (Thermo Fisher) with a blasticidin resistance. Sanger sequencing was performed to verify that no mutation had occurred. Lentivirus generation was performed with a stock titer of 1 × 10<sup>7</sup> TU per ml. The transduction was performed into 2 × 10<sup>6</sup> *B2m*<sup>-/-</sup>*Ctita*<sup>-/-</sup> miPSCs, grown on blasticidin-resistant MEF cells for 72 h with a MOI ratio of 1:10 followed by antibiotic selection with 12.5 µg ml<sup>-1</sup> blasticidin for 7 days. Antibiotic-selected pools were tested by RT-quantitative PCR amplification of Cd47 mRNA and flow cytometry detection of Cd47 on the surface of the cells. After the confirmation of Cd47, cells were expanded and validated by running pluripotency assays.

**Transduction to express firefly luciferase.** iPSCs were transduced to express Fluc. One hundred thousand miPSCs were plated in one gelatin-coated six-well plates and incubated overnight at 37 °C at 5% CO<sub>2</sub>. The next day, media was changed and one vial of Fluc lentiviral particles expressing luciferase II gene under re-engineered EF1a promoter (GenTarget) was added to 1.5 ml media. After 36 h, 1 ml of cell media was added. After further 24 h, complete media change was performed. After 2 days, luciferase expression was confirmed by adding D-luciferin (Promega). Signals were quantified with IVIS 200 (Perkin Elmer) in maximum photons s<sup>-1</sup> cm<sup>-2</sup> sr<sup>-1</sup>.

**Karyotyping.** Cell collection, slide preparation and G-banded karyotyping were performed using standard cytogenetics protocols optimized for human pluripotent

cells. Cells were incubated with ethidium bromide and colcemid (Gibco) and then trypsinized to detach the cells from the plate. The cells were placed in hypotonic solution (0.075 M potassium chloride, 0.559 g KCl in 100 ml water, Millipore), followed by fixation. Metaphase cell preparations were stained with Leishman's stain. Karyotype analysis consisted of chromosomes counted in twenty cells with band-by-band analysis of eight cells.

**Mice.** BALB/c (BALB/cAnNCrI, H2<sup>d</sup>), C57BL/6 (C57BL/6J, H2<sup>b</sup>) and SCID-beige (CBySmn.CB17-Prkdcscid/J) (all 6–12 weeks) were used as recipients for different assays. The number of animals per experimental group is presented in each figure. Mice were purchased from Charles River Laboratories (Sulzfeld) and received humane care in compliance with the Guide for the Principles of Laboratory Animals. Animal experiments were approved by the Hamburg 'Amt für Gesundheit und Verbraucherschutz' or the University of California San Francisco (UCSF) Institutional Animal Care and Use Committee and performed according to local and EU guidelines.

**Teratoma assays to study miPSC survival in vivo.** Six- to eight-week-old syngeneic or allogeneic mice were used for transplantation of WT miPSCs or hypomutagenic miPSCs. Two million cells were injected in 60  $\mu$ l saline into the right thigh muscle of the mice. Tumor growth was measured with a caliper every other day until day 30 and from day 30 to day 80 every tenth day. They were killed after development of tumors larger than 1.5 cm<sup>3</sup> or following an observation period of 80 days.

**Derivation and characterization of miPSC-derived endothelial cells (miECs).** miPSC were plated on gelatin in six-well plates and maintained in mouse iPSC media. After the cells reached 60% confluency, the differentiation was started and media was changed to RPMI-1640 containing 2% B-27 minus Insulin (both Gibco) and 5  $\mu$ M CHIR-99021 (Selleckchem). On day 2, the media was changed to reduced media: RPMI-1640 containing 2% B-27 minus Insulin (both Gibco) and 2  $\mu$ M CHIR-99021 (Selleckchem). From day 4 to day 7, cells were exposed to RPMI-1640 EC media, RPMI-1640 containing 2% B-27 minus Insulin plus 50 ng ml<sup>-1</sup> mouse vascular endothelial growth factor (mVEGF; R&D Systems), 10 ng ml<sup>-1</sup> mouse fibroblast growth factor basic (mFGFb; R&D Systems), 10  $\mu$ M Y-27632 (Sigma-Aldrich) and 1  $\mu$ M SB 431542 (Sigma-Aldrich). Endothelial cell clusters were visible from day 7 and cells were maintained in EGM-2 SingleQuots media (Lonza) plus 10% FCS hi (Gibco), 25 ng ml<sup>-1</sup> mVEGF, 2 ng ml<sup>-1</sup> mFGFb, 10  $\mu$ M Y-27632 (Sigma-Aldrich) and 1  $\mu$ M SB 431542. The differentiation process was completed after 21 days and undifferentiated cells detached during the differentiation process. For purification, cells went through magnetic-activated cell separation (MACS) purification according to the manufacturer's protocol using anti-CD15 mAb-coated magnetic microbeads (Miltenyi) for negative selection.

The highly purified miECs in the flow-through were cultured in EGM-2 SingleQuots media plus supplements and 10% FCS hi. TrypLE was used for splitting the cells 1:3 every 3–4 days. Their phenotype was confirmed by immunofluorescence for CD31 (ab28364, Abcam) and VE-Cadherin (sc-6458, Santa Cruz Biotechnology). Briefly, cells were fixed with 4% paraformaldehyde in PBS for 15 min. Cell membranes were permeabilized with Permeabilization solution (ASB-0102, Applied StemCell), followed by Blocking solution (ASB-0103, Applied StemCell) and incubation with the primary antibodies. For visualization, cells were incubated with secondary antibody conjugated with AF488 or AF555 (Invitrogen). After nuclei staining with DAPI, images were obtained and analyzed with a Leica SP5 laser confocal microscope (Leica).

Tube formation assay was performed for miEC characterization: 2.5  $\times$  10<sup>5</sup> miECs were stained with 5  $\mu$ M CFSE and 0.1  $\mu$ g ml<sup>-1</sup> Hoechst (both Thermo Fisher) for 10 min at room temperature and plated on 10 mg ml<sup>-1</sup> undiluted Matrigel (356231, Corning) in 24-well plates. After 48 h, tube formations were visualized by immunofluorescence. PCR was performed as described above. The following primers were used: VE-Cadherin forward: 5'-GGATGCAGAGGCTCACAGAG-3', reverse: 5'-CTGGCGGTTACGTTGGACT-3'.

**Derivation and characterization of miPSC-derived smooth muscle cells (miSMCs).** The resuspended miPSCs were cultivated on six-well, 0.1% gelatin-coated plastic petri dishes (Falcon, Becton-Dickinson) at 2  $\times$  10<sup>6</sup> cells per well at 37 °C, 5% CO<sub>2</sub> in 2 ml of differentiation medium with the presence of 10  $\mu$ M all-trans-retinoic acid. The differentiation medium was made of DMEM, 15% FCS, 2 mM L-glutamine, 1 mM methyl thioylglycolate (MTG) (Sigma-Aldrich), 1% non-essential amino acids and pen-strep. The culture was continued for 10 days with daily media changes. Starting from the 11th day, the differentiation medium was replaced by serum-free culture medium, which was composed of knock-out DMEM, 15% knock-out serum replacement, 2 mM L-glutamine, 1 mM MTG, 1% non-essential amino acids and pen-strep. The cultures were continued for another 10 days with daily change of the serum-free medium. For purification, cells were enriched according to the manufacturer's protocol using anti-CD15 mAb-coated magnetic microbeads (Miltenyi) for negative selection. The flow-through containing enriched miSMCs were cultured in RPMI-1640 GlutaMax plus 20% FCS hi and 1% pen-strep (all Gibco). Their phenotype was confirmed by immunofluorescence and PCR for both Sma and Sm22.

Immunofluorescence staining was performed as described above. Primary antibodies were used against smooth muscle actin (ab21027, Abcam) and sm22 (ab14106, Abcam), followed by the corresponding secondary antibody conjugated with AF488 or AF555 (Invitrogen).

PCR was performed as described above. The following primers were used: SMA forward: 5'-CGGCTTCGGCTGGTGATGAT-3', reverse: 5'-CATTCCAACCACTACTCCCTGAT-3'; SM22 forward: 5'-AACAGCGCTGACCCCTGATGG-3', reverse: 5'-CGGTAGTGCACATCATTCTT-3'.

#### Derivation and characterization of miPSC-derived cardiomyocytes (miCMs).

Before differentiation, miPSCs were passed two times on gelatin-coated flasks to remove the feeder cells. At day 0, differentiation was started with 80,000 cells per ml in IMEM/Ham's F12 (3/1, both Corning) +0.5% N2-Supplement, 1% B27 retinoic acid, 0.05% BSA, 1% pen-strep, 1% glutamine (Gibco), 5 mg ml<sup>-1</sup> ascorbic acid and 40 ng ml<sup>-1</sup> MTG (both Sigma-Aldrich) for 2 days in uncoated 10 cm plates. At day 2, cells were transferred in IMEM/Ham's F12 (3/1, both Corning) with 0.5% N2-Supplement, 1% B27 retinoic acid, 0.05% BSA, 1% pen-strep, 1% glutamine (all Gibco), 5 mg ml<sup>-1</sup> ascorbic acid and 40 ng ml<sup>-1</sup> MTG (Sigma-Aldrich) for 2 days in uncoated 10 cm plates. On day 4, cells were plated in gelatin-coated six-well plates in SP34 media containing 1% glutamine, 50  $\mu$ g ml<sup>-1</sup> ascorbic acid, 5 ng ml<sup>-1</sup> VEGF, 500  $\mu$ g ml<sup>-1</sup> hPGFb and 25 ng ml<sup>-1</sup> hPGF10 (R&D Systems). Media was changed on day 7 to SP34 media containing 1% glutamine and 50  $\mu$ g ml<sup>-1</sup> ascorbic acid and was changed every other day. Beating of cells started around days 11–14 and demonstrated their function.

For enrichment, cells separated by MACS according to the manufacturer's protocol using anti-CD15 mAb-coated magnetic microbeads (Miltenyi) for negative selection. The flow-through containing enriched miCMs were replated and used for different assays.

Immunofluorescence staining was performed as described above to confirm their phenotype. Primary antibodies were used against  $\alpha$ -sarcomeric actinin (EA-53, Abcam) or troponin I (ab47003, Abcam) followed by the corresponding secondary antibody conjugated with AF488 or AF555 (Invitrogen).

PCR for Gata4 forward: 5'-CTGTCATCTCACTATGGGCA-3', reverse: 5'-CCAAGTCCGAGCAGGAATT-3' and Myh6 forward: 5'-ATCATTCCCAACGAGCGAAAG-3', reverse: 5'-AAGTCCCATAGAGAATGCGG-3' was performed as described above.

**Flow cytometry analysis.** For the detection of MHC class I and II surface molecules on miPSCs, miECs, miSMCs and miCMs, cells were plated on gelatin-coated six-well plates in medium containing 100 ng ml<sup>-1</sup> of IFN- $\gamma$ . After collection, cells were labeled with antibodies. For MHC class I: PerCP-eFlour710-labeled anti-MHC class I antibody (clone AF6-88.5.5.3, eBioscience) or PerCP-eFlour710-labeled mouse IgG2b isotype-matched control antibody (clone eB149/10H5, eBioscience). The anti-MHC class I antibody reacts with the H-2K<sup>b</sup> MHC class I alloantigen. For MHC class II: PerCP-eFlour710-labeled anti-MHC class II antibody (clone M5/114.15.2, eBioscience) or PerCP-eFlour710-labeled mouse IgG2a isotype-matched control antibody (clone eBM2a, eBioscience). The MHC class II antibody reacts with the mouse MHC class II, both I-A and I-E subregion-encoded glycoproteins. Cd47: Alexa Fluor 647-labeled anti-mouse Cd47 antibody (clone miap301, BD Biosciences) or Alexa Fluor 647-labeled mouse IgG2a isotype-matched control antibody (clone R35-95, BD Biosciences). The anti-Cd47 antibody specifically binds to the extracellular domain of mouse Cd47, also known as Integrin-Associated Protein. Cells were analyzed by flow cytometry (BD Bioscience) and results were expressed as fold change to isotype-matched control Ig staining.

For the assessment of purity of miPSC derivatives, antibodies against SSEA-1 (Thermo Fisher), VE-Cadherin (Sigma), SMA (Abcam) and Troponin I (Santa Cruz) were used. The miECs, miSMCs and miCMs were generated with a purity of >90%.

**Elispot assays.** For uni-directional Elispot assays, recipient splenocytes were isolated from spleen 5 days after cell injection and used as responder cells. Donor cells were mitomycin-treated (50  $\mu$ g ml<sup>-1</sup> for 30 min) and used as stimulator cells. One hundred thousand stimulator cells were incubated with 1  $\times$  10<sup>6</sup> recipient responder splenocytes for 24 h and IFN- $\gamma$  and IL-4 spot frequencies were enumerated using an Elispot plate reader.

**Donor-specific antibodies.** Sera from recipient mice were de-complemented by heating to 56 °C for 30 min. Equal amounts of sera and cell suspensions (5  $\times$  10<sup>6</sup> ml) were incubated for 45 min at 4 °C. Cells were labeled with FITC-conjugated goat anti-mouse IgM (Sigma-Aldrich) and analyzed by flow cytometry (BD Bioscience).

**Mouse NK cell Elispot assays in vitro.** NK cells were isolated from fresh BALB/c spleen 18 h after poly I:C injection (150 ng poly I:C in 200  $\mu$ l sterile saline, intraperitoneally, Sigma-Aldrich). After red cell lysis, cells were purified by anti-CD49b mAb-coated magnetic bead-sorting and were used as responder cells. This cell population was >99% CD3<sup>+</sup> and contains NK cells (>90%) and other cells including myeloid cells (<10%). Using the Elispot principle, NK cells were

co-cultured with  $B2m^{-/-}CITA^{-/-}$  or  $B2m^{-/-}CITA^{-/-}$  Cd47 tg miPSCs in the presence of IL-2 (1 ng ml<sup>-1</sup>, Peprotech) and their IFN- $\gamma$  release was measured. YAC-1 cells (Sigma-Aldrich) served as positive control. Mitomycin-treated (50  $\mu$ g ml<sup>-1</sup> for 30 min) stimulator cells were incubated with NK cells (1:1) for 24 h and IFN- $\gamma$  spot frequencies were enumerated using an Elispot plate reader.

**Mouse in vivo innate cytotoxicity assay.** Five million WT miPSCs and  $5 \times 10^6$   $B2m^{-/-}CITA^{-/-}$  miPSCs or  $5 \times 10^6$   $B2m^{-/-}CITA^{-/-}$  Cd47 tg miPSCs were mixed and stained with 5  $\mu$ M CFSE. Cells in saline with IL-2 (1 ng ml<sup>-1</sup>, Peprotech) were injected intraperitoneally into syngeneic C57BL/6 mice. After 48 h, cells were collected from the abdomen and stained with PerCP-eFlour710 labeled anti-MHC class I mAb for 45 min at 4°C. The CFSE-positive and MHC class I-negative population was analyzed by flow cytometry (BD Bioscience) and compared between the WT and the engineered miPSC group. The assay was performed with miPSCs, miECs, miSMCs and miCMs. Some animals were pretreated with clodronate (200  $\mu$ l intraperitoneally 3 days before the experiment; Liposoma) to eliminate macrophages and make the assay more specific for NK cells. Some animals were pretreated with in vivo Cd47 blocking antibody (BE0270, 100  $\mu$ g intraperitoneally, 7 days and 3 days before the experiment; BioXCell) to eliminate Cd47.

**NK cell stimulatory ligands.** For the detection of NK cell stimulatory ligands on miPSCs, miECs, miSMCs and miCMs, cells were blocked with mouse FcR blocking reagent (Miltenyi) according to manufacturer's protocol. WT cells,  $B2m^{-/-}CITA^{-/-}$  cells and  $B2m^{-/-}CITA^{-/-}$  Cd47 tg cells were then incubated with the recombinant mouse Nkp46 or NKG2D human Fc chimera protein or the recombinant control IgG1 Fc protein (R&D systems) for 45 min at 4°C. FITC-conjugated anti-human IgG1 antibody (Invitrogen) served as secondary antibody. YAC-1 cells were used as positive control. Data analysis was carried out using flow cytometry (BD Bioscience) and FlowJo software, and results were expressed as fold change to the isotype-matched control Fc fusion protein.

**Survival analysis of differentiated derivatives using BLI.** For BLI, D-luciferin firefly potassium salt (375 mg kg<sup>-1</sup>; Biosynth) was dissolved in PBS (pH 7.4) (Gibco, Invitrogen) and was injected intraperitoneally (250  $\mu$ l per mouse) into anesthetized mice. Animals were imaged using the IVIS 200 system (Xenogen). Region of interest (ROI) bioluminescence was quantified in units of maximum photons per second per centimeter square per steradian (ps<sup>-1</sup> cm<sup>-2</sup> sr<sup>-1</sup>). The maximum signal from an ROI was measured using Living Image software (MediaCybernetics). Mice were monitored on day 0, day 1 and every other day until day 30 and every 10 days afterwards.

**Matrigel plugs: cell morphology for miECs, miSMCs or miCMs.** Eight hundred thousand  $B2m^{-/-}CITA^{-/-}$  Cd47 tg miECs, miSMCs or miCMs in 1:1 diluted Matrigel (Corning) were injected into allogeneic BALB/c mice. Matrigel plugs were recovered after 1, 2, 3, 4, 5, 6 and 8 weeks and fixed in 4% paraformaldehyde in PBS with 1% glutaraldehyde for 24 h. Samples were dehydrated, embedded in paraffin and cut into sections of 5  $\mu$ m thickness. For histopathology, sections were stained with hematoxylin and eosin (Carl Roth) and images taken with an inverted light microscope. Origin of cells was demonstrated with immunofluorescence staining. Sections were rehydrated, and underwent antigen retrieval and blocking. Samples were incubated with antibodies against luciferase (ab21176), SMA (ab21027, Abcam), VE-Cadherin (SC-6458) or  $\alpha$ -sarcomeric actinin (EA-53, Abcam) and a corresponding secondary antibody conjugated with AF488 or AF555 (Invitrogen). Cell nuclei were counterstained with DAPI and images taken with a Leica SP5 laser confocal microscope (Leica).

For co-staining experiments of miECs and immune cells, primary antibodies were used against VE-Cadherin (SC-6458, Sigma) and CD3 (ab16669, Abcam), followed by the corresponding secondary antibody conjugated with AF488 or AF555 (Invitrogen).

**Generation of human iPSCs (hiPSCs).** The Human Episomal iPSC Line was derived from CD34<sup>+</sup> cord blood using a three-plasmid, seven-factor (SOKMNL1; SOX2, OCT4 (POU5F1), KLF4, MYC, NANOG, LIN28 and SV40L T antigen) EBNA-based episomal system by Thermo Scientific. This cell line has been shown to be free of all reprogramming genes. These hiPSCs have a normal XX karyotype and endogenous expression of pluripotent markers including Oct4, SOX2 and NANOG (as shown by RT-PCR) and OCT4, SSEA4, TRA-1-60 and TRA-1-81 (as shown by immunofluorescence).

**Gene editing of hiPSC.** hiPSC underwent two gene-modification steps. In the first step, CRISPR technology was used for a combined targeting of the coding sequence of human *B2M* gene with the CRISPR sequence 5'-CGTGAGTAAACCTGAAATCTT-3' and the coding sequence of human *CITA* gene with the CRISPR sequence 5'-GATATTGGCATAAGCCTCCC-3'. Linearized CRISPR sequence with T7 promoter were used to synthesize gRNA as per the kit's instructions (MEGashortscript T7 Transcription Kit, Thermo Fisher). The obtained in vitro transcription (IVT) gRNA was then purified via the MEGAclear Transcription Clean-Up Kit. For IVT gRNA delivery, cells were

electroporated with 300 ng IVT gRNA using a Neon electroporation system and the conditions 1,200 V, 30 ms, 1 pulse into hiPSC stably expressing Cas9. After electroporation, edited hiPSC were expanded for single cell seeding; hiPSC cultures were dissociated into single cells using TrypLE Express (Gibco) and stained with Alexa Fluor 488-conjugated anti-TRA-160 mAb and propidium iodide. A FACSAria II cell sorter (BD Biosciences) was used for the sorting and doublets and debris were excluded from seeding by selective gating on forward and side light scatter properties. Viable pluripotent cells were selected on the absence of propidium iodide and presence of Tra1-60 staining. Single cells were then expanded into full-size colonies, after which the colonies were tested for CRISPR editing by sequencing. CRISPR-mediated cleavage was assessed using the GeneArt Genomic Cleavage Detection Kit (Thermo Fisher) for testing of the initial edited pools. For screening of the isolated clones, genomic DNA was isolated from  $1 \times 10^6$  hiPSCs and the *B2M* and *CITA* genomic DNA regions were PCR amplified using AmpliTaq Gold 360 Master Mix and the primer sets forward: 5'-TGGGGCCAAATCATGTAGACTC-3' and reverse: 5'-TCAGTGGGGTGAATTTCAGTGT-3' for *B2M* as well as forward: 5'-CTTAACAGCGATGCTGACCC-3' and reverse: 5'-TGGGCTCCATCTCCCTCTCTT-3' for *CITA*. For TIDE analysis, the obtained PCR product was cleaned up (PureLink PCR Purification Kit, Thermo Fisher) and Sanger sequencing was performed for the prediction of indel frequency. After the confirmation of *B2M* and *CITA* disruption, cells were further characterized through karyotype analysis and the TaqMan hiPSC Scorecard Panel (Thermo Fisher). The hiPSCs were found to be pluripotent and maintained a normal (46,XX) karyotype during the genome editing process.

In the second step, the CD47 cDNA was synthesized and the DNA was cloned into a lentiviral plasmid with an EPS promoter and puromycin resistance cassette. Cells were transduced with lentiviral stocks and 8  $\mu$ g ml<sup>-1</sup> of Polybrene (Thermo Fisher). Media was changed daily after transduction. Three days after transduction, cells were expanded and selected with 0.5  $\mu$ g ml<sup>-1</sup> of puromycin. After 5 days of antibiotic selection, antibiotic-resistant colonies emerged and were further expanded to generate stable pools. The expression of CD47 transcripts was confirmed by quantitative PCR. Pluripotency assay (TaqMan hiPSC Scorecard Panel, Thermo Fisher) and karyotyping was performed again to verify the pluripotent status of the cells.

**Teratoma assays to study iPSC survival in vivo.** Six to eight week-old immunodeficient SCID-beige mice were used for transplantation of WT hiPSC or  $B2m^{-/-}CITA^{-/-}$  CD47 tg hiPSCs. Here  $1 \times 10^6$  cells were resuspended in 100  $\mu$ l saline solution and injected into the right thigh muscle of the mice. Teratomas were recovered, fixed in 4% paraformaldehyde, dehydrated, embedded in paraffin and cut into sections of 5  $\mu$ m thickness. For histopathology, sections were rehydrated and stained with hematoxylin and eosin. Images were taken with an inverted light microscope. For immunofluorescence, slides underwent heat-induced antigen retrieval in a steamer with Dako antigen-retrieval solution (Dako), followed by antigen blocking with Image-IT FX signal enhancer solution (Invitrogen). Tissue sections were incubated with a primary antibody against brachyury (Ab20680, Abcam), followed by a goat anti-rabbit IgG secondary antibody conjugated with Alexa Fluor 555 (Invitrogen). Subsequently, sections were incubated with primary antibodies against cytokeratin 8 (EP1628Y, Abcam) and GFAP (GA5, Cell Signaling) conjugated with AF488 or AF647, respectively. DAPI was used to counterstain cell nuclei and images were acquired with a Leica SP5 laser confocal microscope (Leica).

**Pluripotency analysis by RT-PCR and immunofluorescence.** hiPSCs were plated in confocal dishes (MatTek) for immunofluorescence analysis 48 h after plating using the hiPSC Characterization Kit (Applied Stem Cell). Briefly, cells were fixed, permeabilized and stained overnight at 4°C with the primary antibodies for OCT4, SOX2, SSEA4, TRA-1-60 and TRA-1-81 (Applied Stem Cell). After several washes, the cells were incubated with a secondary antibody and DNA staining solution. Alkaline phosphatase activity assay was performed (Applied Stem Cell). Stained cells were imaged using a fluorescent microscope.

For RT-PCR, RNA was extracted using the RNeasy Plus Mini Kit (Qiagen). Genomic DNA contamination was removed using the gDNA spin column. cDNA was generated using Applied Biosystems High-Capacity cDNA Reverse Transcription Kit. Gene-specific primers of the hiPSC Characterization Kit (Applied Stem Cell) were used to amplify target sequences. Actin was used as housekeeping gene. PCR reactions were performed on Mastercycler nexus (Eppendorf) and visualized on 2% agarose gels.

**Humanized mice.** Humanized NSG-SGM3 mice (18–30 weeks) were purchased from Jackson Laboratories. Human CD34<sup>+</sup> hematopoietic stem cell-engrafted NSG-SGM3 mice develop multi-lineage human immune cells, and demonstrate a functional human immune system displaying T cell-dependent immune responses with no donor cell immune reactivity towards the host. Animals were randomly assigned to experimental groups. The percentage of CD3<sup>+</sup> cells among the human CD45<sup>+</sup> cell population was assessed in every animal and CD3 percentages were never significantly different between WT and  $B2m^{-/-}CITA^{-/-}$  CD47 tg groups (Supplementary Fig. 13a). The number of animals per

experimental group is presented in each figure. All humanized NSG-SGM3 mice were HLA-A typed and the number of mismatches to the cell graft calculated (Supplementary Fig. 13b). In the Elispot assays with hiPSCs, there were  $1.6 \pm 0.5$  and  $1.7 \pm 0.5$  ( $P = 0.61$ ), with hiCMs  $1.3 \pm 0.6$  and  $1.3 \pm 0.6$  ( $P = 1$ ) mismatches for WT and  $B2M^{-/-}CIITA^{-/-}$  CD47 tg, respectively, and in the hiEC groups there were always two mismatches. The mismatches for the BLI experiments are shown in Supplementary Fig. 10j.

All BLT mice were approved by the University of North Carolina at Chapel Hill Institutional Animal Care and Use Committee and were generated with the same human tissue using NSG mice (NOD.Cg-Prkdc<sup>scid</sup> Il2rg<sup>tm1Wjl</sup>/SzJ, Jackson Laboratories) and there were five out of six HLA class I and 4 out of 4 class II mismatches to the transplanted hiPSCs or derivatives. The percentage of CD3<sup>+</sup> cells among the human CD45<sup>+</sup> cell population was never significantly different between WT and  $B2M^{-/-}CIITA^{-/-}$  CD47 tg groups (Supplementary Fig. 13c). The percentage of CD3<sup>+</sup> cells among the human CD45<sup>+</sup> cell population was typically in the 15–65% range.

**Human iPSC differentiation into hiECs.** hiPSC were plated on diluted Matrigel (356231, Corning) in six-well plates and maintained in Essential 8 Flex media (Thermo Fisher). The differentiation was started at 60% confluency and media was changed to RPMI-1640 containing 2% B-27 minus insulin (both Gibco) and 5  $\mu$ M CHIR-99021 (Selleckchem). On day 2, the media was changed to reduced media: RPMI-1640 containing 2% B-27 minus insulin (Gibco) and 2  $\mu$ M CHIR-99021 (Selleckchem). From day 4 to 7, cells were exposed to RPMI-1640 EC media, RPMI-1640 containing 2% B-27 minus insulin plus 50 ng ml<sup>-1</sup> human vascular endothelial growth factor (VEGF; R&D Systems), 10 ng ml<sup>-1</sup> human fibroblast growth factor basic (FGFb; R&D Systems), 10  $\mu$ M Y-27632 (Sigma-Aldrich), and 1  $\mu$ M SB 431542 (Sigma-Aldrich). Endothelial cell clusters were visible from day 7 and cells were maintained in EGM-2 SingleQuots media (Lonza) plus 10% FCS hi (Gibco), 25 ng ml<sup>-1</sup> VEGF, 2 ng ml<sup>-1</sup> FGFb, 10  $\mu$ M Y-27632 (Sigma-Aldrich) and 1  $\mu$ M SB 431542 (Sigma-Aldrich). The differentiation process was completed after 14 days and undifferentiated cells detached during the differentiation process. For purification, cells were treated with 20  $\mu$ M PluriSln-1 (StemCell Technologies) for 48 h. The highly purified ECs were cultured in EGM-2 SingleQuots media (Lonza) plus supplements and 10% FCS hi (Gibco). TrypLE Express was used for passaging the cells 1:3 every 3–4 days.

Immunofluorescence staining was performed as described above to confirm their phenotype. Primary antibodies were used against CD31 (ab28364, Abcam) and VE-Cadherin (sc-6458, Santa Cruz Biotechnology), followed by the corresponding secondary antibody conjugated with AF488 or AF555 (Invitrogen). Cell nuclei were stained with DAPI. Imaging was performed using a Leica SP5 laser confocal microscope (Leica).

PCR for VE-Cadherin (forward: 5'-AAGATGCAGAGGCTCATG-3', reverse: 5'-CATGAGCCTCTGCATCTT-3') was performed as described above.

**Human iPSC differentiation into hiCMs.** hiPSCs were plated on diluted Matrigel (356231, Corning) in six-well plates and maintained in Essential 8 Flex media (Thermo Fisher). Differentiation was started at 90% confluency, and media was changed to 5 ml of RPMI-1640 containing 2% B-27 minus Insulin (Gibco) and 6  $\mu$ M CHIR-99021 (Selleckchem). After 2 days, media was changed to RPMI-1640 containing 2% B-27 minus insulin without CHIR. On day 3, 5  $\mu$ l IWR1 was added to the media for two further days. At day 5, the media was changed back to RPMI-1640 containing 2% B-27 minus insulin medium and left for 48 h. At day 7, media was changed to RPMI-1640 containing B27 plus insulin (Gibco) and replaced every 3 days thereafter with the same media. Spontaneous beating of cardiomyocytes was first visible around day 10. Purification of cardiomyocytes was performed on day 10 post-differentiation. Briefly, media was changed to low glucose media and maintained for 3 days. At day 13, media was changed back to RPMI-1640 containing B27 plus insulin. This procedure was repeated on day 14.

Immunofluorescence staining was performed as described above to confirm their phenotype. Primary antibodies were used against  $\alpha$ -sarcomeric actinin (EA-53, Abcam) and troponin I (ab47003, Abcam), followed by the corresponding secondary antibody conjugated with AF488 or AF555 (Invitrogen). Cell nuclei were stained with DAPI. Imaging was performed using a Leica SP5 laser confocal microscope (Leica).

PCR for troponin (cTNT, forward: 5'-GAGGCACCAAGTTGGGCATGAACG A-3', reverse: 5'-GGCAGCGGAAGAGGATGCTGAA') was performed as described above.

**Flow cytometry analysis.** Human iPSCs, iCMs and iECs were plated in six-well plates in medium containing 100 ng ml<sup>-1</sup> of IFN- $\gamma$ . Cells were harvested and labeled with antibodies. APC-conjugated anti-HLA-A,B,C antibody (clone G46\_2.6, BD Biosciences) or APC-conjugated IgG1 isotype-matched control antibody (clone MOPC-21, BD Biosciences). Alexa-fluor647-labeled anti-HLA-DR, DRPQ antibody (clone Tu3a, BD Biosciences) or Alexa-fluor647-labeled IgG2a isotype-matched control antibody (clone G155-178, BD Biosciences). PerCP-Cy5-conjugated anti-CD47 (clone B6H12, BD Biosciences) or PerCP-Cy5-conjugated IgG1 isotype-matched control antibody (clone MOPC-21, BD Biosciences). Results were expressed as fold change to isotype-matched control Ig staining.

For the assessment of purity of hiPSC derivatives, antibodies against TRA-1-60 (Thermo Fisher), VE-Cadherin (Santa Cruz) and Troponin I (Santa Cruz) were used. The hiECs and hiCMs were generated with a purity of >95%.

**Human NK cell Elispot assays.** Human NK cells were co-cultured with  $B2M^{-/-}CIITA^{-/-}$  or  $B2M^{-/-}CIITA^{-/-}$  CD47 tg hiPSC and their IFN- $\gamma$  release was measured. Human NK cells were purchased from StemCell Technologies and were >99% CD3<sup>+</sup> and 95% CD56<sup>+</sup>. Flow cytometry revealed >95% NK cells and <5% other cells including myeloid cells. Donor cells were mitomycin-treated and used as stimulator cells. K562 cells (Sigma-Aldrich) served as positive control. Stimulator cells were incubated with NK cells (1:1) in RPMI-1640 containing 1% pen-strep and 1 ng ml<sup>-1</sup> human IL-2 (Peprotech) for 24 h and IFN- $\gamma$  spot frequencies were enumerated using an Elispot plate reader.

**T cell Elispot using humanized mice.** For uni-directional Elispot assays, recipient splenocytes were isolated from humanized mice 5 days after cell injection and used as responder cells. Cells were incubated for 24 h in vitro with 1  $\mu$ g ml<sup>-1</sup> anti-CD3 and 1  $\mu$ g ml<sup>-1</sup> anti-CD28 before plated for Elispot Assay. Donor cells were mitomycin-treated (50  $\mu$ g ml<sup>-1</sup> for 30 min) and used as stimulator cells. One hundred thousand stimulator cells were incubated with  $1 \times 10^6$  recipient responder splenocytes for 48 h and IFN- $\gamma$  and IL-5 spot frequencies were enumerated using an Elispot plate reader.

**DSA.** Sera from recipient mice were de-complemented by heating to 56 °C for 30 min. Equal amounts of sera and cell suspensions ( $5 \times 10^6$  per ml) were incubated for 45 min at 4 °C. Cells were labeled with FITC-conjugated goat anti-human IgM (BD Bioscience) and analyzed by flow cytometry (BD Bioscience).

**Matrigel plugs: cell morphology.** One million  $B2M^{-/-}CIITA^{-/-}$  CD47 tg hiECs or hiCMs in 1:1 pro survival scaffold, consisting of 50% (vol/vol) Matrigel (Corning), 100  $\mu$ M ZVAD (Millipore), 50 nM Bcl-XI BH4 (Millipore), 200 nM cyclosporine A (Sigma-Aldrich), 100 ng ml<sup>-1</sup> IGF-1 (Peprotech) and 50  $\mu$ M Pinacidil (Sigma-Aldrich) were injected into humanized NSG-SGM3 mice. Matrigel plugs were recovered after 2, 4, 6 and 8 weeks, fixed in 4% paraformaldehyde in PBS with 1% glutaraldehyde, dehydrated and embedded in paraffin. Sections of 5  $\mu$ m thickness were cut. For immunofluorescence, sections were rehydrated and underwent antigen retrieval, followed by antigen blocking. After incubation with a primary antibody against luciferase (ab21176), VE-Cadherin (SC-6458) or  $\alpha$ -sarcomeric actinin (EA-53, Abcam), sections were incubated with a corresponding secondary antibody conjugated with AF488 or AF555 (Invitrogen). DAPI was used to counterstain cell nuclei and images were obtained with a Leica SP5 laser confocal microscope (Leica).

**BLI.** For BLI, D-luciferin firefly potassium salt (375 mg kg<sup>-1</sup>) (Biosynth) dissolved in sterile PBS (pH 7.4) (Gibco, Invitrogen) was injected intraperitoneally (250  $\mu$ l per mouse) into anesthetized mice. Animals were imaged using the ami HT (Spectral Instruments Imaging) ROI bioluminescence was quantified in units of maximum photons per second per centimeter square per steradian ( $p s^{-1} cm^{-2} sr^{-1}$ ). The maximum signal from an ROI was measured using Living Image software (MediaCybernetics). Humanized mice were injected with  $5 \times 10^6$  or  $1 \times 10^6$  cells in pro survival scaffold as described above. Mice were monitored on day 0, day 1 and every 4 days until cells were rejected or up to 50 days.

**In vitro NK cell killing.** Mouse NK cells were isolated from fresh BALB/c or C57BL/6 spleens 18 h after poly I:C injection (100  $\mu$ g intraperitoneally). After red cell lysis, NK cells were purified with MagniSort Mouse NK cell Enrichment Kit (Invitrogen), followed by CD49b MACS-sorting (Miltenyi). This cell population was highly selected for NK cells with a purity of >9%. Human NK cells from PBMCs were purchased from StemCell Technologies containing >99% NK cells.

NK cell killing assays were performed on the XCelligence SP platform (ACEA BioSciences). 96-well E-plates (ACEA BioSciences) were coated with collagen (Sigma-Aldrich) and  $4 \times 10^5$  WT,  $B2M^{-/-}CIITA^{-/-}$ , or  $B2M^{-/-}CIITA^{-/-}$  CD47 tg hiECs or WT,  $B2M^{-/-}CIITA^{-/-}$  or  $B2M^{-/-}CIITA^{-/-}$  CD47 tg hiECs were plated in 100  $\mu$ l cell-specific media containing 1 ng ml<sup>-1</sup> mouse or human IL-2 (Peprotech). After the Cell Index value reached 0.7, NK cells were added with an effector cell / target cell (E/T) ratio of 0.5/1, 0.8/1 or 1/1. As a negative control, cell treated with 2% Triton X100 was used. Some wells were pretreated with mouse Cd47 or human CD47-blocking antibody (BioXCel) with 10  $\mu$ g ml<sup>-1</sup> media for 2 h. Data were standardized and analyzed with the RTCA software (ACEA).

**NK cell stimulatory ligands.** For the detection of NKG2D, Nkp80, Nkp46, Nkp44 and Nkp30 on hiPSCs, hiECs and hiCMs, cells were plated on gelatin-coated six-well plates. K562 cells were plated in six-well plates as suspension cells. After harvesting, cells were blocked with human FcR blocking reagent (Miltenyi) according to manufacturer's protocol. Cells were labeled with recombinant human NKG2D, Nkp80, Nkp46, Nkp44 or Nkp30 Fc chimera proteins or the recombinant control IgG1 Fc protein (all R&D Systems) for 45 min at 4 °C, followed by the secondary antibody IgG1 conjugated with FITC (Invitrogen). Data analysis was

carried out by Flow Cytometry (BD Bioscience) and results were expressed as fold change to isotype control.

**Statistics.** All data are expressed as mean  $\pm$  s.d. or in box blot graphs showing the median and the minimum to maximum range. Intergroup differences were appropriately assessed by either an unpaired Student's *t*-test or a one-way ANOVA with Bonferroni's post-hoc test. Further information on experimental design and reagents is available in the Nature Research Reporting Summary linked to this article.

**Reporting Summary.** Further information on research design is available in the Nature Research Reporting Summary linked to this article.

#### **Data availability**

All data supporting the findings of this study are available in the paper and its Supplementary Information files.

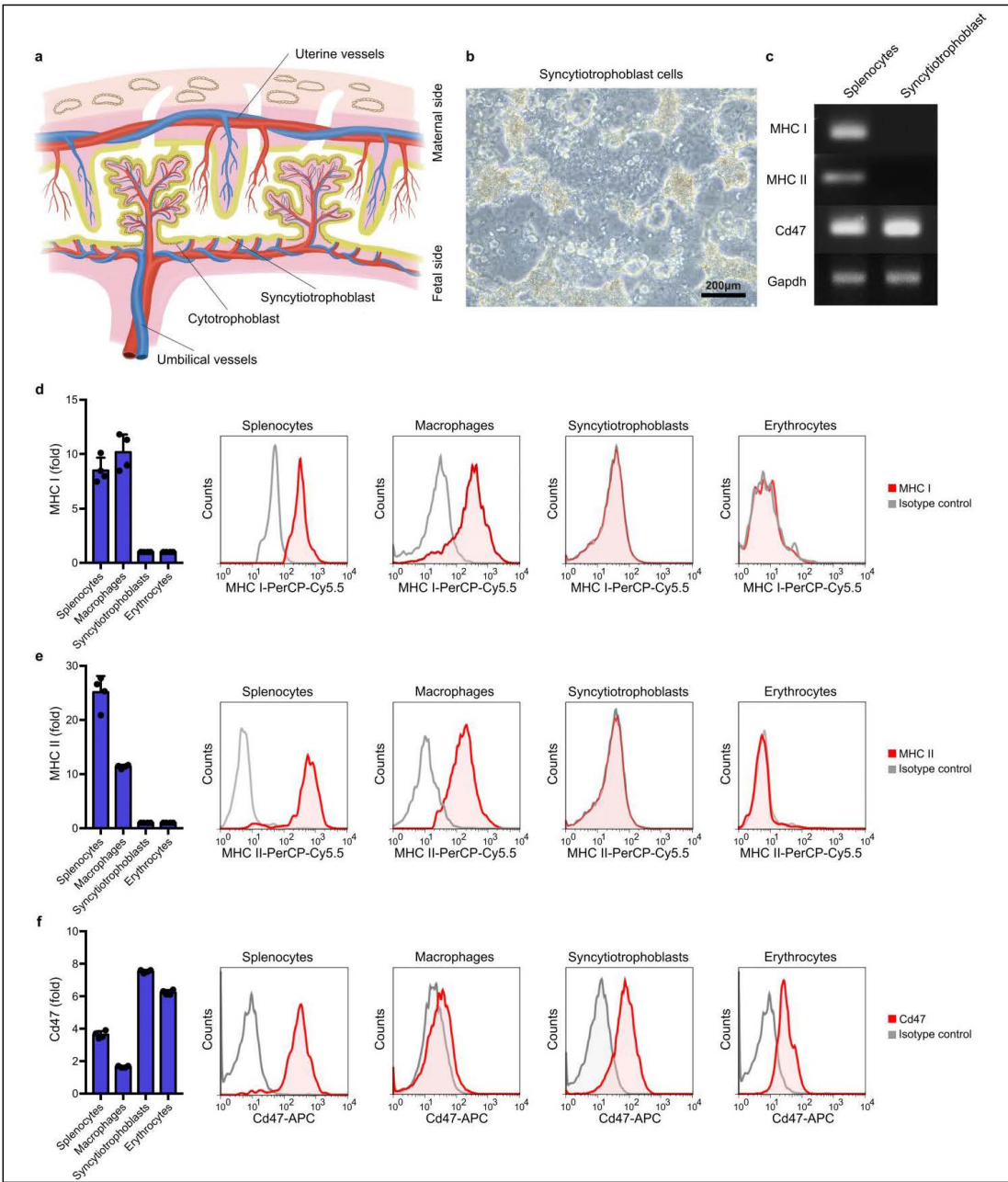


In the format provided by the authors and unedited.

# Hypoimmunogenic derivatives of induced pluripotent stem cells evade immune rejection in fully immunocompetent allogeneic recipients

Tobias Deuse<sup>1,7</sup>, Xiaomeng Hu<sup>1,2,3,7</sup>, Alessia Gravina<sup>1</sup>, Dong Wang<sup>1,2</sup>, Grigol Tediashvili<sup>1,2,3</sup>, Chandrav De<sup>4</sup>, William O. Thayer<sup>4</sup>, Angela Wahl<sup>4</sup>, J. Victor Garcia<sup>4</sup>, Hermann Reichenspurner<sup>2,3</sup>, Mark M. Davis<sup>5</sup>, Lewis L. Lanier<sup>6</sup> and Sonja Schrepfer<sup>1\*</sup>

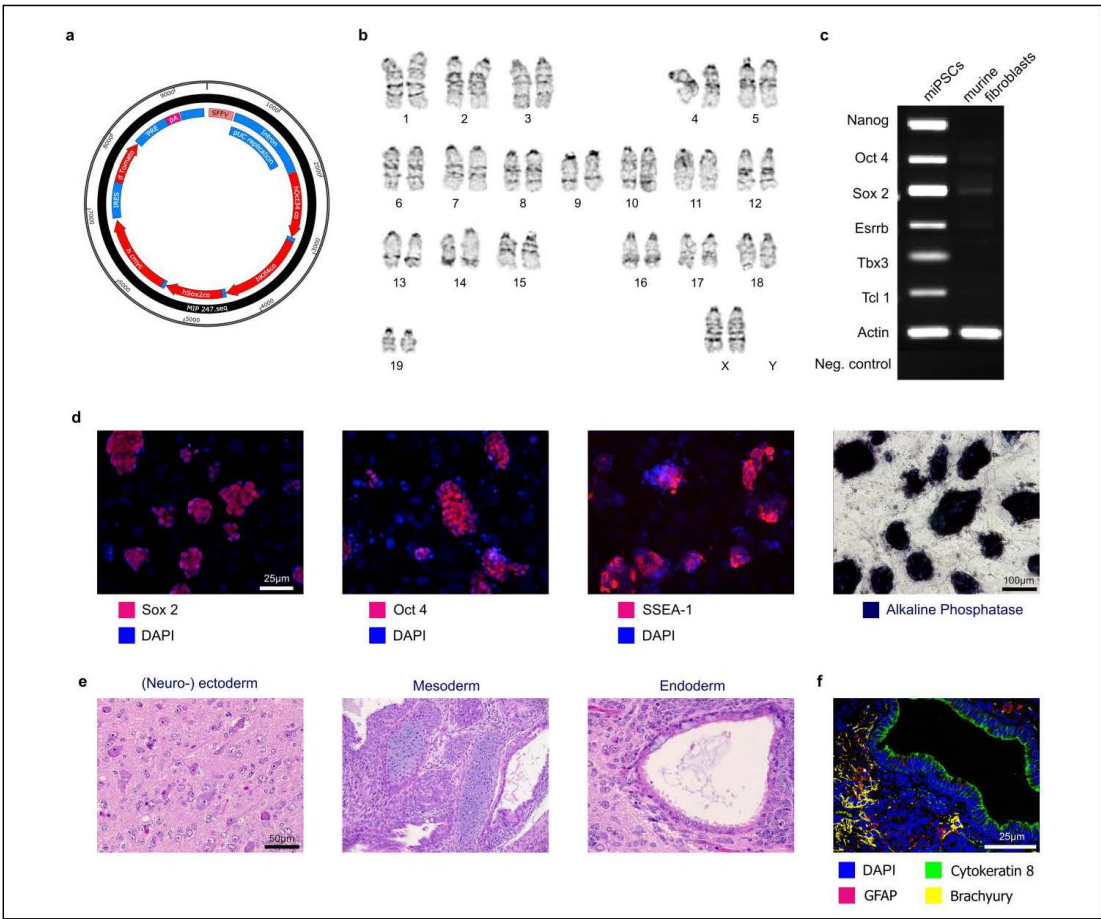
<sup>1</sup>Department of Surgery, Division of Cardiothoracic Surgery, Transplant and Stem Cell Immunobiology-Lab, University of California San Francisco, San Francisco, CA, USA. <sup>2</sup>Department of Cardiovascular Surgery, University Heart Center Hamburg, Hamburg, Germany. <sup>3</sup>Cardiovascular Research Center Hamburg and DZHK (German Center for Cardiovascular Research), Partner Site Hamburg/Kiel/Luebeck, Hamburg, Germany. <sup>4</sup>Division of Infectious Diseases, UNC Center for AIDS Research, University of North Carolina School of Medicine, Chapel Hill, NC, USA. <sup>5</sup>Howard Hughes Medical Institute, Institute for Immunity, Transplantation and Infection, and Department of Microbiology and Immunology, Stanford University School of Medicine, Stanford, CA, USA. <sup>6</sup>Department of Microbiology and Immunology and the Parker Institute for Cancer Immunotherapy, University of California San Francisco, San Francisco, California, USA. <sup>7</sup>These authors contributed equally: Tobias Deuse, Xiaomeng Hu. \*e-mail: [Sonja.Schrepfer@ucsf.edu](mailto:Sonja.Schrepfer@ucsf.edu)



**Supplementary Figure 1**

The immune phenotype of syncytiotrophoblast cells.

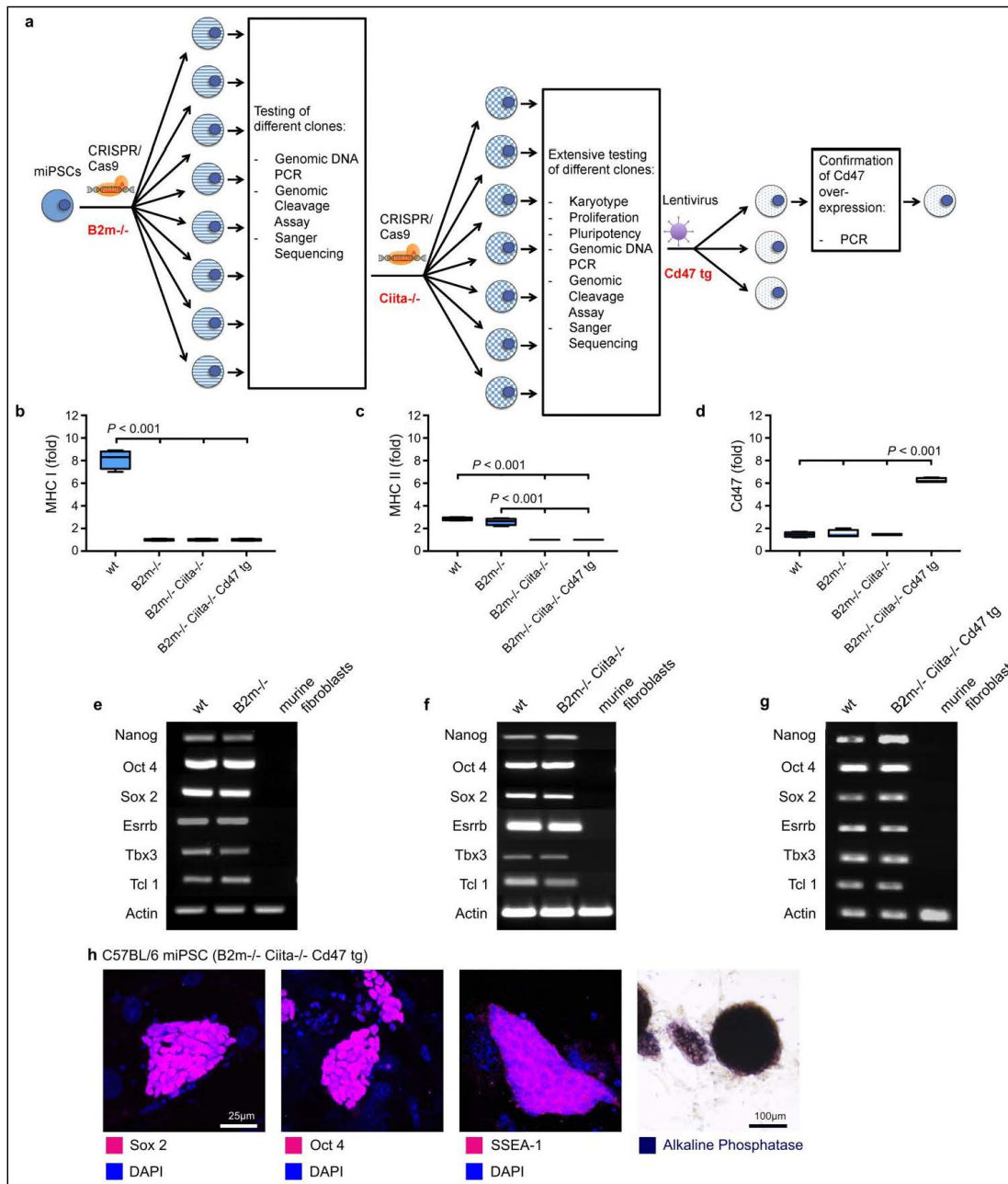
a, The syncytiotrophoblast is the immediate interface between maternal blood and the fetal side of the placenta. b, Mouse syncytiotrophoblast cells were isolated and cultured (representative picture of two independent experiments). c, RT-PCR showed depleted MHC class I and II expression, but positive Cd47 expression (representative gel of three independent experiments). d-f, The surface expression of MHC class I (d), MHC class II (e), and Cd47 (f) was assessed by flow cytometry (mean  $\pm$ s.d., 4 independent experiments per group). Representative histograms are shown.



**Supplementary Figure 2**

The generation of miPSCs.

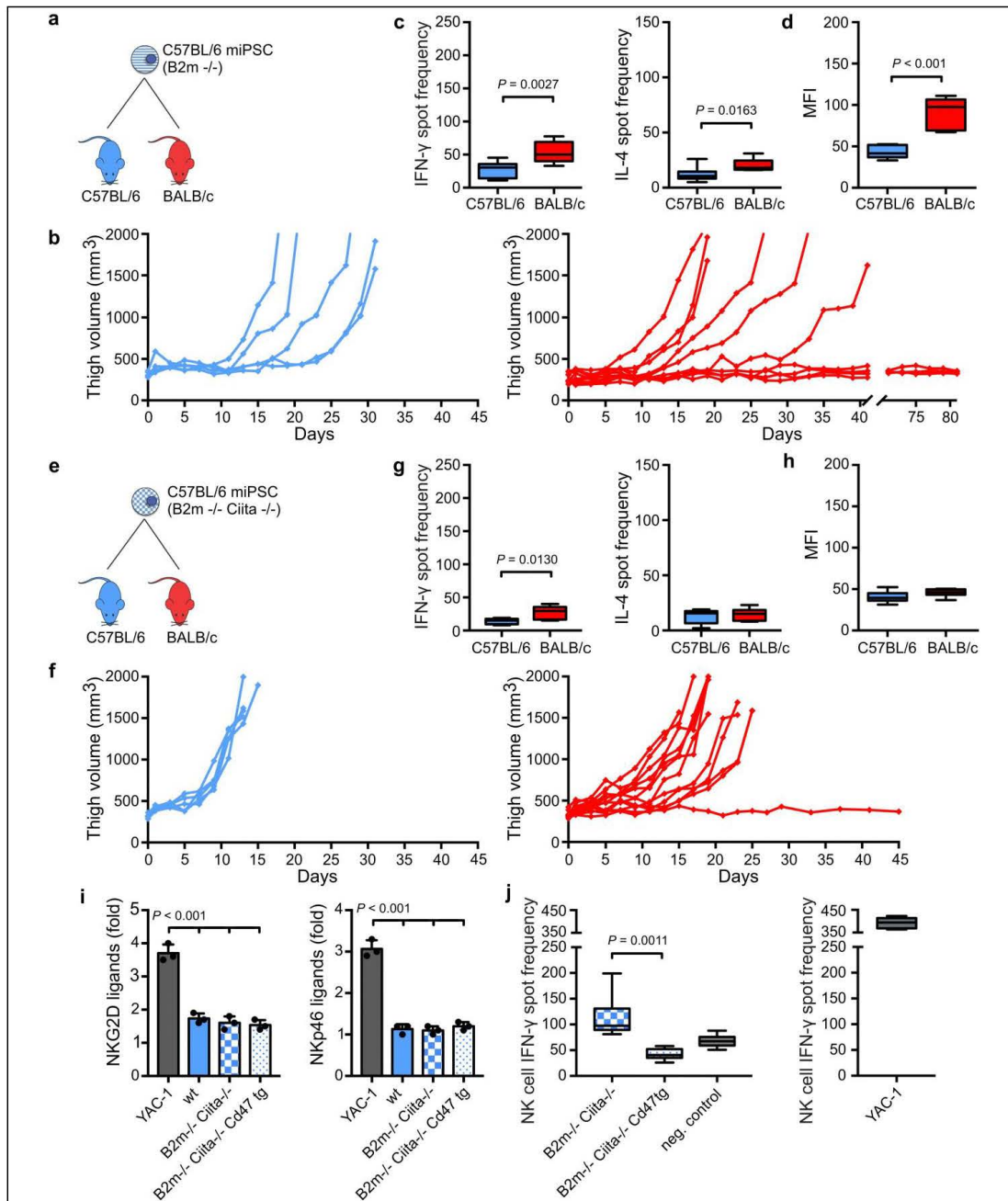
a, Mouse tail tip fibroblasts were re-programmed using a plasmid expressing the four re-programming factors Oct4, KLF4, Sox2, and c-Myc. b, The miPSCs showed a normal 40, XX mouse karyotype in one analysis. c, miPSCs showed the typical gene expression profile of pluripotent stem cells (representative gel of two independent experiments). d, In immunofluorescence, miPSC cultures were positive for Sox2, Oct4, SSEA-1, and alkaline phosphatase (representative pictures of three independent experiments). e, When transplanted into immunodeficient SCID-beige mice, they formed teratomas containing (neuro-) ectoderm, mesoderm, and endoderm (representative pictures of three independent experiments). f, Endodermal (cytokeratin 8), mesodermal (brachyury), and ectodermal (GFAP) lineages were demonstrated by confocal immunofluorescence microscopy (representative pictures of three independent experiments).



### Supplementary Figure 3

Immune phenotype and pluripotency of engineered miPSCs.

a, Mouse iPSCs underwent three editing steps to disrupt *B2m*, *Ciita*, and over-express Cd47 to achieve a hypo-immunogenic phenotype. Every step included rigorous testing for quality control. **b-d**, MHC class I (b), MHC class II (c), and Cd47 expression (d) by flow cytometry is shown for each engineering step, confirming successful gene editing (box 25th to 75th percentile with median, whiskers min-max, 4 independent experiments per graph, ANOVA with Bonferroni's post-hoc test). **e-g**, During the engineering process, all edited miPSCs maintained expression of the pluripotent gene expression signature (representative gel of two independent PCR experiments). **h**, *B2m<sup>-/-</sup>Ciita<sup>-/-</sup>* Cd47 tg miPSCs exhibited Sox2, Oct4, and SSEA-1 expression in confocal immunofluorescence stainings, as well as alkaline phosphatase in immunohistochemistry (representative pictures of three independent experiments).

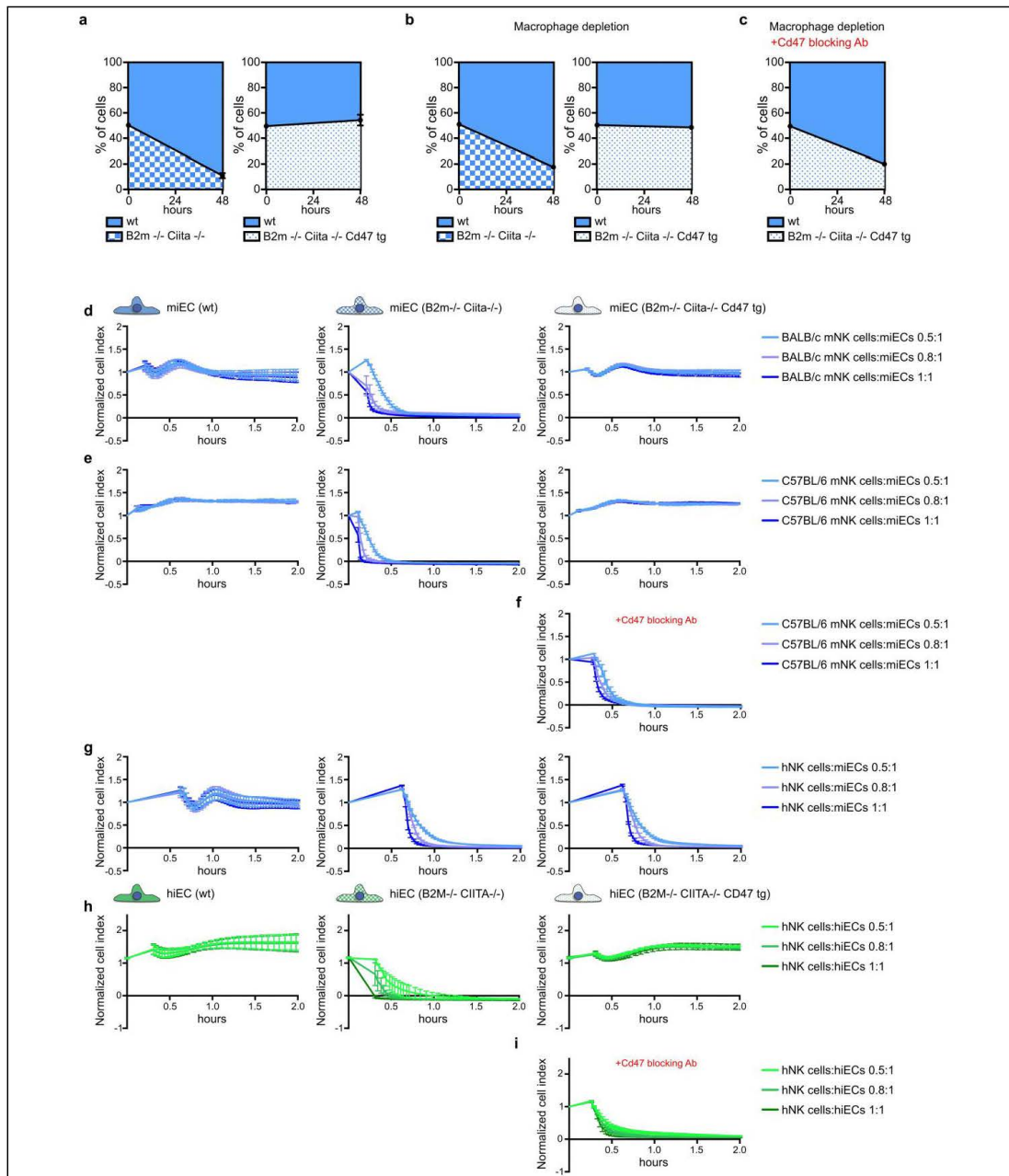


#### Supplementary Figure 4

##### Survival of gene-engineered miPSCs.

a, C57BL/6  $B2m^{-/-}$  miPSCs were transplanted into either syngeneic C57BL/6 (blue) mice or allogeneic (red) BALB/c mice. b, The thigh volume of all five C57BL/6 and ten BALB/c animals is shown over time. The overall percentage of cell grafts that survived and formed teratomas in BALB/c was 60%. c, IFN- $\gamma$  Elispots and IL-4 Elispots are shown with splenocytes recovered 5 days after the transplantation and  $B2m^{-/-}$  miPSCs stimulator cells (box 25th to 75th percentile with median, whiskers min-max, 8 animals per group, two-tailed Student's t-test). d, Mean fluorescence (MFI) of IgM binding to  $B2m^{-/-}$  miPSCs incubated with recipient serum after 5 days (box 25th to 75th percentile with median, whiskers min-max, 6 animals per group, two-tailed Student's t-test). e, C57BL/6  $B2m^{-/-}$   $Ciita^{-/-}$  miPSCs were transplanted into syngeneic C57BL/6 or allogeneic BALB/c mice. f, The thigh volume of all 5 C57BL/6 and 12 BALB/c animals is shown over time. The overall percentage of cell grafts that survived and formed teratomas in BALB/c was 91.7%. g, IFN- $\gamma$  Elispots and IL-4 Elispots are shown with splenocytes recovered 5 days after the transplantation and  $B2m^{-/-}$   $Ciita^{-/-}$  miPSCs stimulator cells (box 25th to 75th percentile with median, whiskers min-max, 6 animals per group, two-tailed Student's t-test). h, Mean fluorescence (MFI) of IgM binding to  $B2m^{-/-}$   $Ciita^{-/-}$  miPSCs incubated with recipient serum after 5 days (box 25th to 75th percentile with median, whiskers min-max, 6 animals per group, two-tailed Student's t-test). i, The expression of stimulatory NKG2D ligands and NKp46 ligands on miPSC lines and YAC-1 was assessed using receptor Fc chimera proteins in flow cytometry (mean  $\pm$  s.d., 3 independent experiments per group, ANOVA with Bonferroni's post-hoc test). j, IFN- $\gamma$  spot frequencies of miPSC lines and YAC-1 in Elispot assays with BALB/c NK cells (box 25th to 75th percentile with median, whiskers min-max, 6 independent experiments, ANOVA with Bonferroni's post-hoc test).

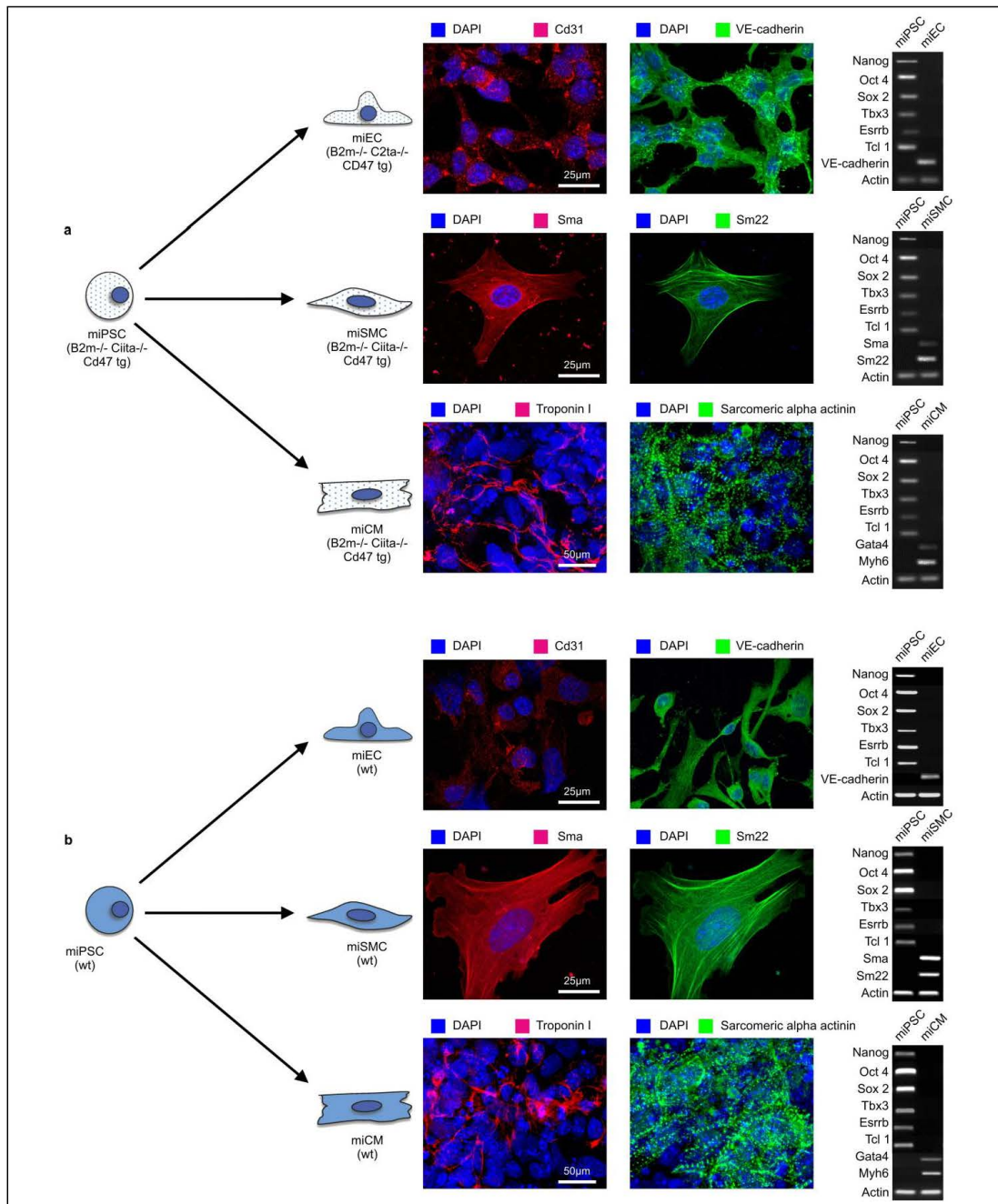




### Supplementary Figure 5

#### Interaction between CD47 and NK cells.

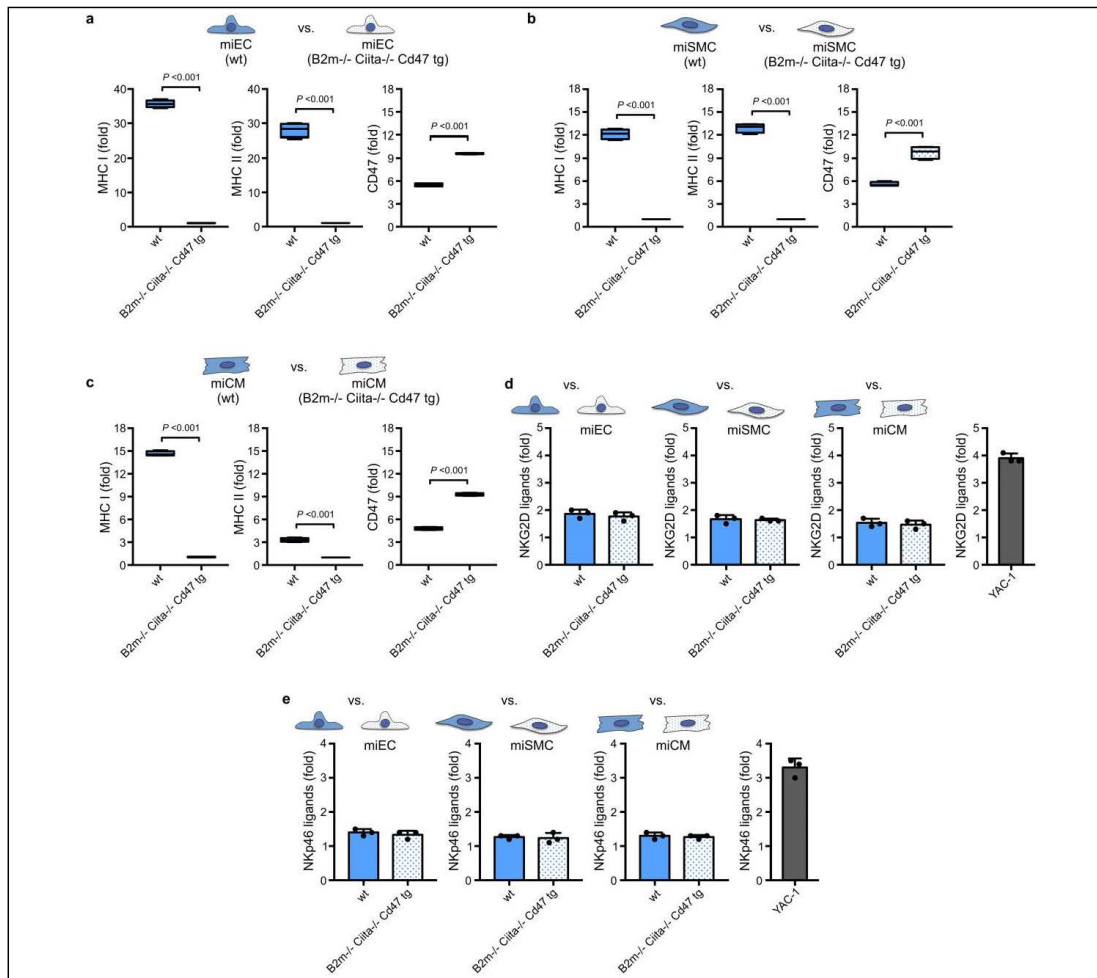
a, *In vivo* innate immune clearance was assessed by injecting a 1 : 1 mixture of CFSE-labeled wt miPSCs and either  $B2m^{+}Ciita^{+}$  or  $B2m^{+}Ciita^{-}$  Cd47 tg miPSCs into the peritoneum of syngeneic C57BL/6 mice. After 48 h, CFSE-labeled peritoneal miPSCs were recovered and the percentages of both fractions assessed by flow cytometry (mean  $\pm$  s.d., 4 animals per group). While  $B2m^{+}Ciita^{-}$  miPSCs were rapidly cleared,  $B2m^{+}Ciita^{+}$  Cd47 tg miPSCs were spared. b, Mice were pre-treated with clodronate to deplete macrophages, making this model more specific to NK cell killing and again only  $B2m^{+}Ciita^{-}$  Cd47 tg miPSCs were spared from NK cell killing (mean  $\pm$  s.d., 4 animals per group). c, When a Cd47 blocking antibody was co-injected into the peritoneum, the protection was abolished and  $B2m^{+}Ciita^{+}$  Cd47 tg miPSCs were killed (mean  $\pm$  s.d., 4 animals per group). d, *In vitro* real-time NK cell killing was assessed on confluent wt,  $B2m^{+}Ciita^{-}$ , and  $B2m^{+}Ciita^{+}$  Cd47 tg miECs in three different effector : target cell ratios. Using allogeneic BALB/c mouse NK (mNK) cells,  $B2m^{+}Ciita^{-}$  miECs were rapidly killed, and wt and  $B2m^{+}Ciita^{+}$  Cd47 tg miECs permanently survived (mean  $\pm$  s.d., 3 independent experiments per group). e, Similarly, using syngeneic C57BL/6 mNK cells,  $B2m^{+}Ciita^{-}$  miECs were rapidly killed, and wt and  $B2m^{+}Ciita^{+}$  Cd47 tg miECs permanently survived (mean  $\pm$  s.d., 3 independent experiments per group). f, When a Cd47 blocking antibody was added to syngeneic C57BL/6 mNK cells,  $B2m^{+}Ciita^{-}$  Cd47 tg miECs were swiftly killed (mean  $\pm$  s.d., 3 independent experiments per group). g, When human NK (hNK) cells were used, both  $B2m^{+}Ciita^{-}$  and  $B2m^{+}Ciita^{+}$  Cd47 tg miECs were rapidly killed (mean  $\pm$  s.d., 3 independent experiments per group). h, When hNK cells were used with human wt,  $B2M^{+}CIITA^{-}$ , and  $B2M^{+}CIITA^{+}$  CD47 tg hiECs, only  $B2M^{+}CIITA^{-}$  hiECs were rapidly killed and wt and  $B2M^{+}CIITA^{+}$  CD47 tg hiECs were spared (mean  $\pm$  s.d., 3 independent experiments per group). i, With a CD47 blocking antibody,  $B2M^{+}CIITA^{-}$  CD47 tg hiECs were then swiftly killed (mean  $\pm$  s.d., 3 independent experiments per group).



**Supplementary Figure 6**

Differentiation of miPSCs into miECs, miSMCs and miCMs.

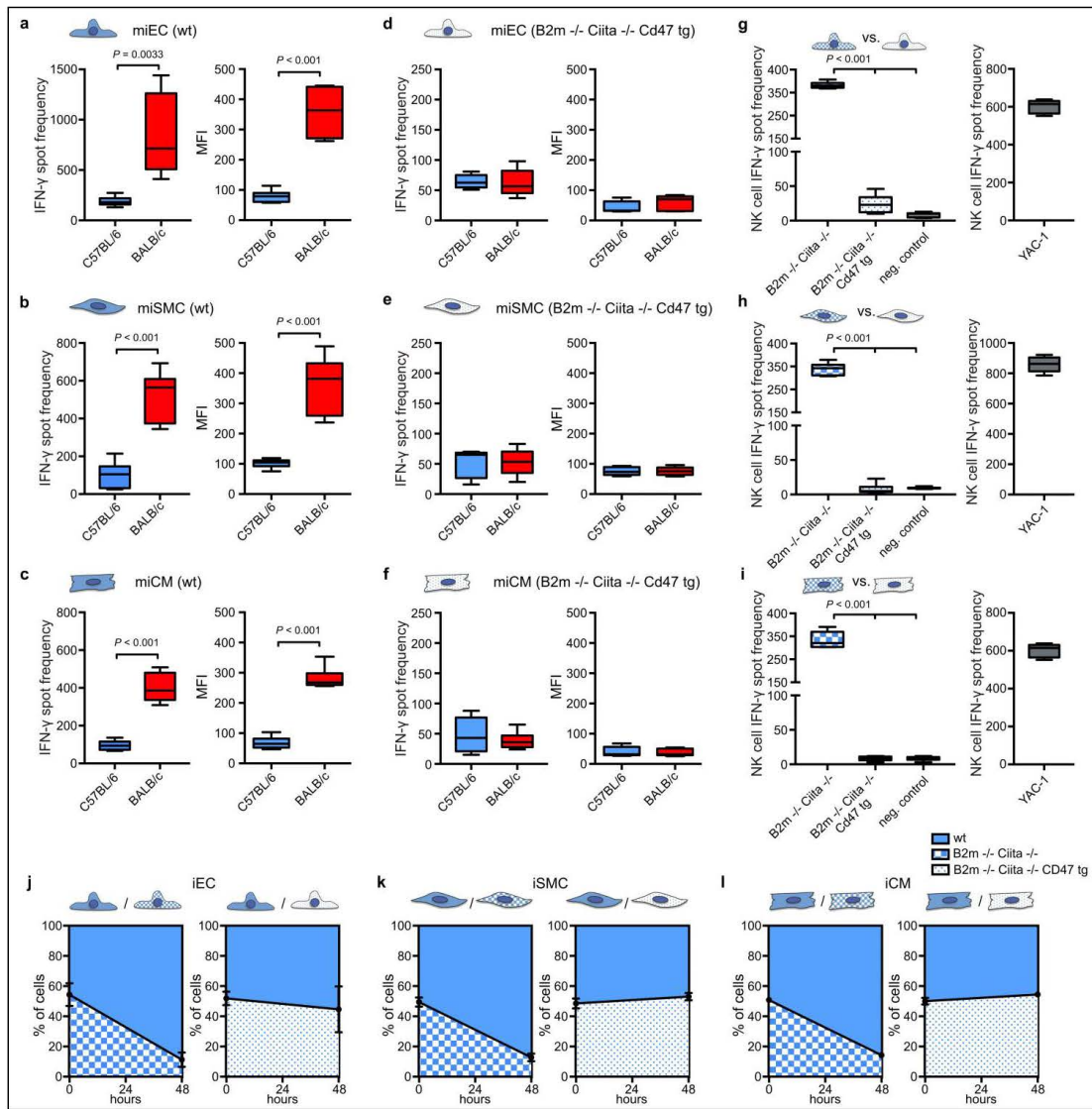
**a-b**,  $B2m^{-/-}Ciita^{-/-}$  Cd47 tg miPSCs (a) and wt miPSCs (b) were successfully differentiated into corresponding miEC, miSMC, and miCM derivatives (representative pictures of three independent experiments). miECs were positive for Cd31 and VE-cadherin, miSMCs were positive for Sma and Sm22, miCMs were positive for Troponin I and Sarcomeric alpha-actinin by confocal immunofluorescence. All derivatives lost their expression of pluripotency genes (representative pictures of two independent PCR experiments).



### Supplementary Figure 7

Immune phenotype of wt and engineered iPSC derivatives.

a, wt miECs showed high MHC class I and MHC class II expression, while *B2m<sup>-/-</sup>Ciita<sup>-/-</sup>Cd47 tg* miECs were MHC class I and MHC class II depleted and showed increased Cd47 expression (box 25th to 75th percentile with median, whiskers min-max, 4 independent experiments per graph, two-tailed Student's t-test). b, wt miSMCs showed moderate MHC class I and MHC class II expression, while *B2m<sup>-/-</sup>Ciita<sup>-/-</sup>Cd47 tg* miSMCs were MHC class I and MHC class II depleted and showed increased Cd47 expression (box 25th to 75th percentile with median, whiskers min-max, 4 independent experiments per graph, two-tailed Student's t-test). c, wt miCMs showed moderate MHC class I and low MHC class II expression; *B2m<sup>-/-</sup>Ciita<sup>-/-</sup>Cd47 tg* miCMs were MHC class I and MHC class II depleted and showed increased Cd47 expression (box 25th to 75th percentile with median, whiskers min-max, 4 independent experiments per graph, two-tailed Student's t-test). d-e, The expression of stimulatory NKG2D ligands (d) and NKp46 ligands (e) on wt and *B2m<sup>-/-</sup>Ciita<sup>-/-</sup>Cd47 tg* miECs, miSMCs, miCMs, and YAC-1 was assessed using receptor Fc chimera proteins in flow cytometry (mean ± s.d., 3 independent experiments per group, two-tailed Student's t-test).

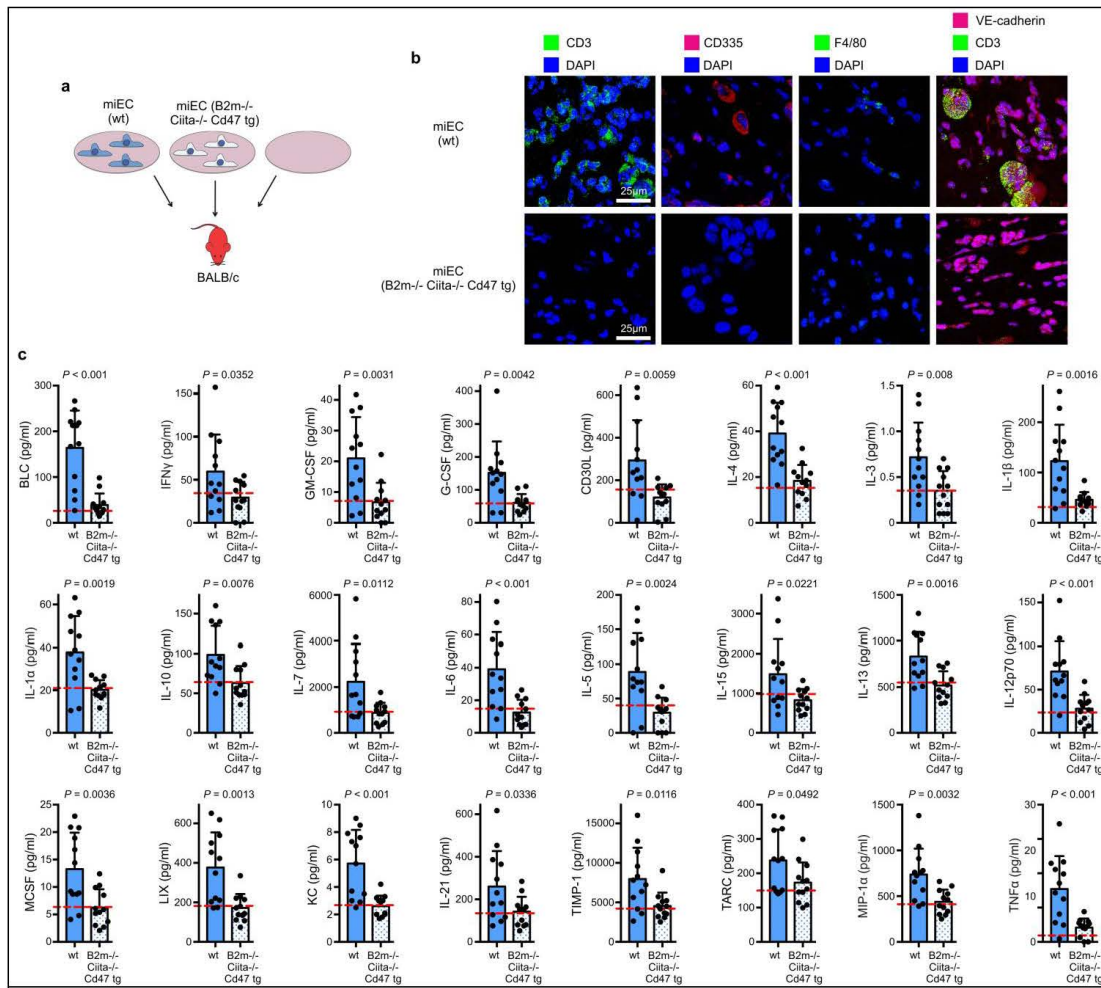


**Supplementary Figure 8**

Immune response against miPSC derivatives.

a-c, Five days after the injection of wt miPSC-derived miECs (a), miSMCs (b), or miCMs (c) into C57BL/6 or BALB/c recipients, splenocytes were recovered for IFN- $\gamma$  Elispot assays (box 25th to 75th percentile with median, whiskers min-max, 6 animals per group, two-tailed Student's t-test). The IFN- $\gamma$  response was vastly stronger in all allogeneic recipients. Mean fluorescence (MFI) of IgM binding to wt miPSC-derived miECs (a), miSMCs (b), and miCMs (c), incubated with recipient serum after 5 days (box 25th to 75th percentile

with median, whiskers min-max, 6 animals per group, two-tailed Student's t-test). There was a markedly stronger IgM response in all allogeneic recipients. **d-f**, Similarly,  $B2m^{+}Ciita^{-}$  Cd47 tg miPSC-derived miECs (d), miSMCs (e), or miCMs (f) were injected into C57BL/6 or BALB/c recipients and IFN- $\gamma$  Elispots were performed after 5 days (box 25th to 75th percentile with median, whiskers min-max, 6 animals per group, two-tailed Student's t-test). Mean fluorescence (MFI) of IgM binding to  $B2m^{+}Ciita^{-}$  Cd47 tg miPSC-derived miECs (d), miSMCs (e), and miCMs (f), incubated with recipient serum after 5 days (box 25th to 75th percentile with median, whiskers min-max, 6 animals per group, two-tailed Student's t-test). There was no measurable IFN- $\gamma$  response or IgM response in allogeneic recipients. **g-i**, To assess the inhibitory effect of Cd47 over-expression on NK cell killing, IFN- $\gamma$  Elispots with NK cells were performed with miECs (g), miSMCs (h), or miCMs (i) derived from  $B2m^{+}Ciita^{-}$  miPSC or  $B2m^{+}Ciita^{-}$  Cd47 tg miPSC (box 25th to 75th percentile with median, whiskers min-max, 6 independent experiments, ANOVA with Bonferroni's post-hoc test) Only derivatives from  $B2m^{+}Ciita^{-}$  miPSC were susceptible for NK cell killing. **j-l**, *In vivo* innate immune clearance was assessed by injecting a 1 : 1 mixture of wt derivative engineered derivative into the peritoneum of C57BL/6 mice. After 48 h, peritoneal miECs (j), miSMCs (k), and miCMs (l) were recovered and the percentage assessed by flow cytometry (mean  $\pm$  s.d., 4 animals per group).

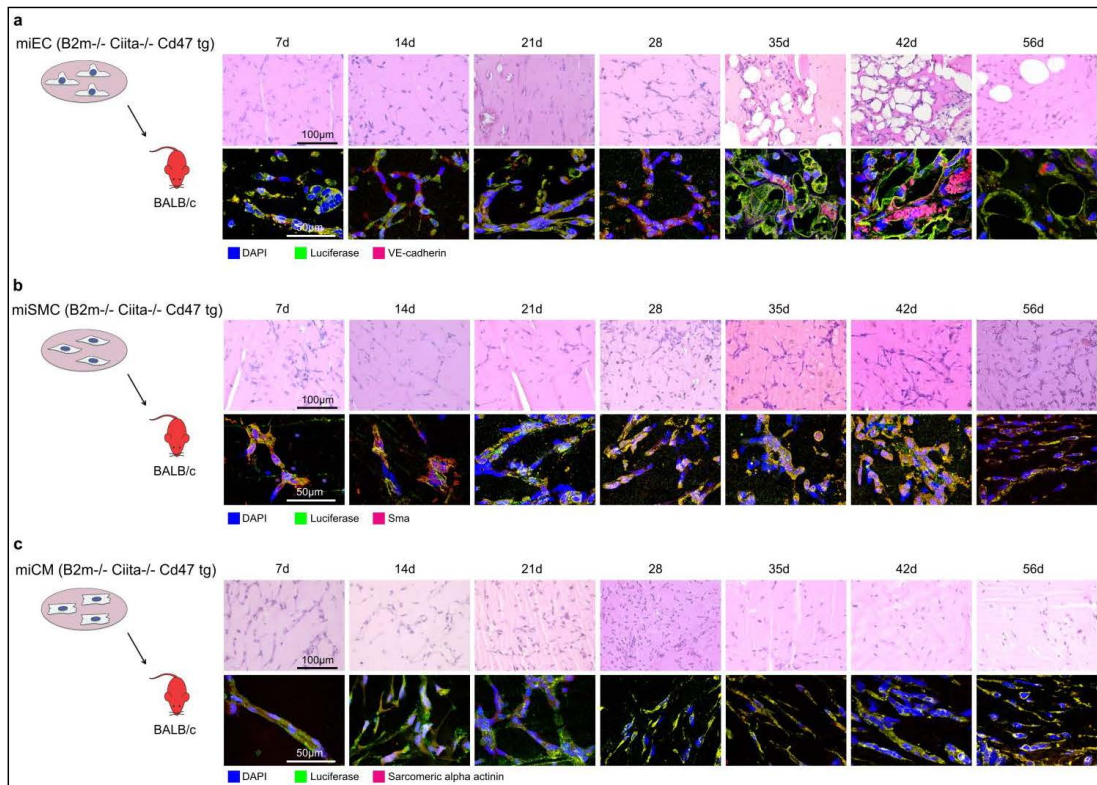


Supplementary Figure 9

Immune cell infiltration and cytokine expression in miEC grafts.

**a**, Matrigel plugs containing either wt miECs or *B2m*<sup>-/-</sup> *Ccl4a*<sup>-/-</sup> Cd47 tg miECs were implanted in allogeneic BALB/c recipients. Cell-free matrigel plugs served as controls. **b**, Immunofluorescence stainings detected immune cell infiltration in wt iEC-plaques containing CD3<sup>+</sup> T lymphocytes, CD335<sup>+</sup> NK cells, and sparse F4/80<sup>+</sup> macrophages. Co-staining of CD3 and VE-cadherin confirmed CD3<sup>+</sup> lymphocyte infiltration in EC grafts in the wt group. Practically no immune cells were found in plugs containing *B2m*<sup>-/-</sup> *Ccl4a*<sup>-/-</sup> Cd47 tg miECs (representative pictures of three independent experiments). **c**, The cytokine profile in wt miEC plugs was shifted towards a pro-inflammatory milieu. Multiple significantly up-regulated cytokines were typical of activated cytotoxic CD8<sup>+</sup> T cells, CD4<sup>+</sup> T helper-1 cells, and CD4<sup>+</sup> T helper-2 cells, as well as macrophages (mean  $\pm$  s.d., 12 animals per group, two-tailed Student's t-test; dashed red lines show levels of cell-free matrigel).

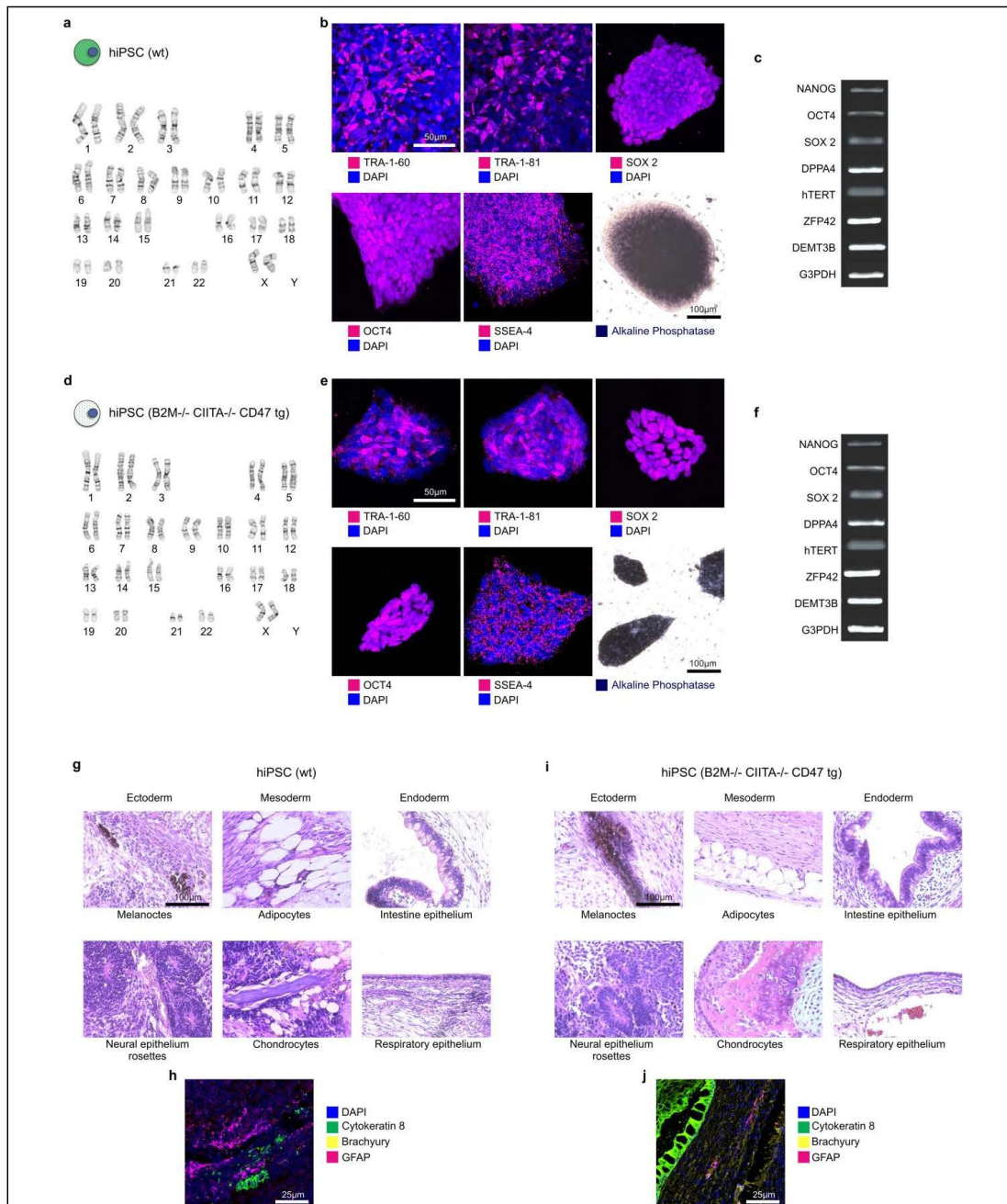




### Supplementary Figure 10

#### Morphology of transplanted $B2m^{-/-}$ $Ciita^{-/-}$ Cd47 tg miPSC derivatives in allogeneic hosts.

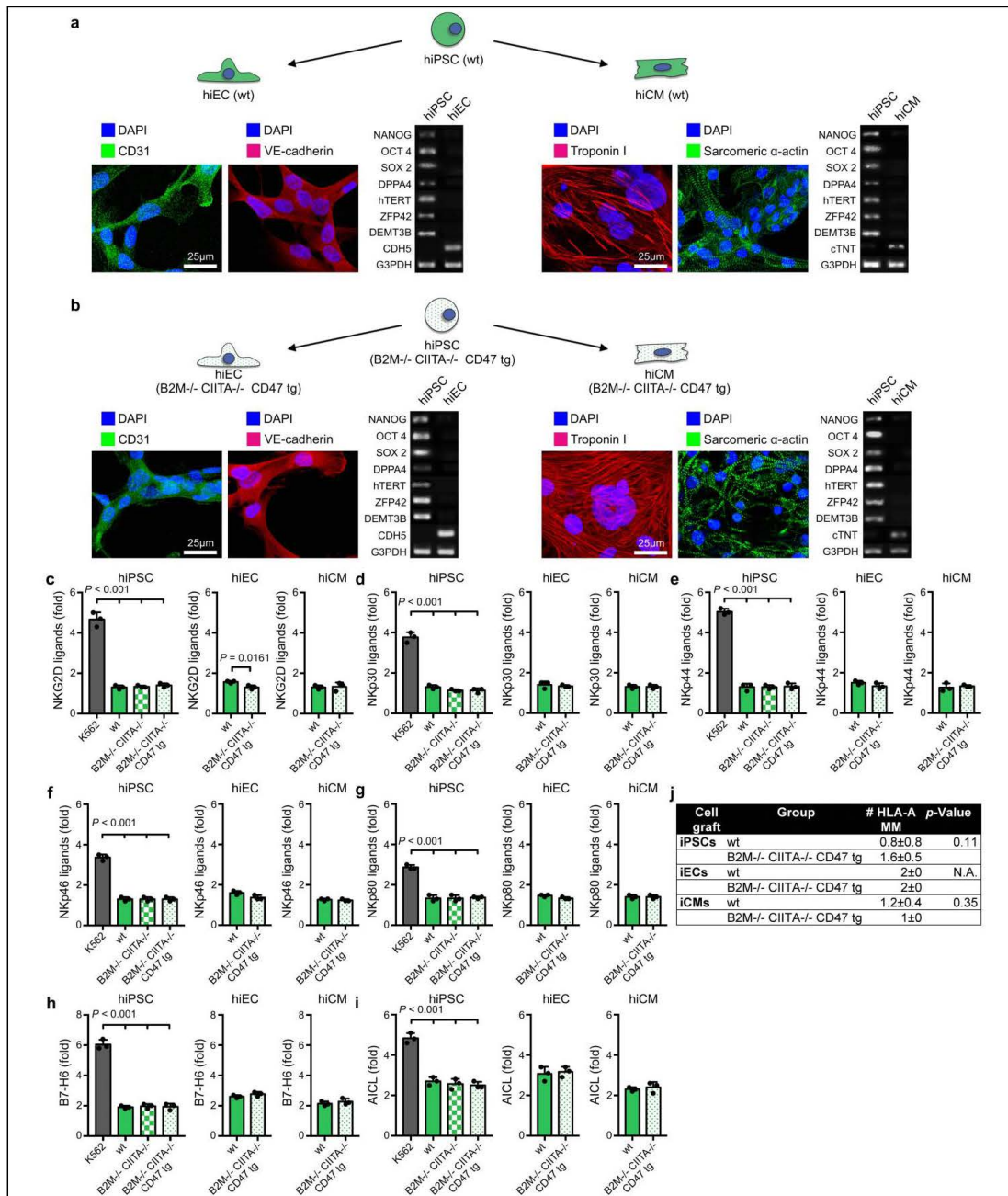
a-c,  $B2m^{-/-}$   $Ciita^{-/-}$  Cd47 tg miEC (a), miSMC (b), or miCM (c) grafts in matrigel were transplanted subcutaneously into allogeneic BALB/c mice to investigate whether these hypo-immunogenic derivatives further mature *in vivo* or change their morphology over time in allogeneic recipients. Matrigel plugs were recovered after different time points for hematoxylin and eosin and immunofluorescence stainings (representative pictures of two independent experiments). Transplanted miECs started to organize in circular structures around day 14 and formed primitive vessels that contained erythrocytes around day 35 (a). Transplanted miSMCs (b) maintained their typical spindle-shape appearance and loose arrangement, whereas miCMs retained their immature round progenitor morphology (c). Both latter cell types did not show a higher degree of three-dimensional organization, which may be attributed to the lack of mechanical stimulus necessary for maturation of any type of muscle cell.



**Supplementary Figure 11**

Pluripotency of wt and  $B2M^{+/-}CIITA^{+/-}$  CD47 tg hiPSCs.

**a**, wt hiPSCs showed a normal human 46, XX karyotype in one analysis. **b**, wt hiPSCs were positive for TRA-1-60, TRA-1-81, SOX 2, OCT4, and SSEA-4 in confocal immunofluorescence and positive for alkaline phosphatase in immunohistochemistry (representative pictures of three independent experiments). **c**, wt hiPSCs expressed typical pluripotency genes (representative gel of two independent PCR experiments). **d**,  $B2M^{+/-}CIITA^{+/-}CD47$  tg hiPSCs maintained the normal human 46, XX karyotype in one analysis. **e**,  $B2M^{+/-}CIITA^{+/-}CD47$  tg hiPSCs were also positive for TRA-1-60, TRA-1-81, SOX 2, OCT4, and SSEA-4 in confocal immunofluorescence and positive for alkaline phosphatase in immunohistochemistry (representative pictures of three independent experiments). **f**,  $B2M^{+/-}CIITA^{+/-}CD47$  tg hiPSCs continued to express the typical pluripotency genes (representative gel of two independent PCR experiments). **g-j**, wt hiPSCs (**g, h**) and  $B2M^{-/-}CIITA^{-/-}CD47$  tg hiPSCs (**i, j**) gave rise to cell types of all 3 germ layers after transplantation into SCID-beige mice. Endodermal (cytokeratin 8), mesodermal (brachyury), and ectodermal lineages (GFAP) were also demonstrated by confocal immunofluorescence microscopy (representative pictures of three independent experiments).



## Supplementary Figure 12

### Differentiation of hiPSCs into hiECs and hiCMs.

a-b, wt hiPSCs (a) and  $B2M^{fl}/CIITA^{fl}/CD47^{-/-}$  tg hiPSCs (b) were successfully differentiated into corresponding miEC and miCM derivatives (representative pictures of three independent experiments). miECs were positive for CD31 and VE-cadherin and miCMs were positive for Troponin I and Sarcomeric alpha-actinin by confocal immunofluorescence. All derivatives lost their expression of pluripotency genes (representative pictures of two independent experiments). c-g, The expression of stimulatory NK cell ligands was assessed on hiPSCs and their derivatives using receptor Fc chimera proteins in flow cytometry (mean  $\pm$  s.d., 3 independent experiments per group, ANOVA with Bonferroni's post-hoc test (hiPSCs) or two-tailed Student's t-test (hiECs and hiCMs)). Ligands for NKG2D (c), NKp30 (d), NKp44 (e), NKp46 (f), and NKp80 (g) were compared between wt and engineered hiPSCs, hiECs, hiCMs, and K562. h-i, The expression of specific human natural cytotoxicity receptor ligands was evaluated by flow cytometry (mean  $\pm$  s.d., 3 independent experiments per group, ANOVA with Bonferroni's post-hoc test (hiPSCs) or two-tailed Student's t-test (hiECs and hiCMs)). Surface expression of B7-H6 (h), and AIICL (i) was compared between wt and engineered hiPSCs and derivatives, and K562. j, The HLA-A mismatches in transplant experiments with wt and  $B2M^{fl}/CIITA^{fl}/CD47^{-/-}$  tg hiPSCs, hiECs, and hiCMs in allogeneic humanized NSG-HGM3 recipients (mean  $\pm$  s.d., 5 animals per group, two-tailed Student's t-test).

a				
Assay	Cell graft	Group	CD3% of hCD45	p-Value
Elispot	iPSCs	wt	38±35	0.31
		B2M-/- CIITA-/- CD47 tg	57±31	
	iECs	wt	22±13	0.22
		B2M-/- CIITA-/- CD47 tg	63±48	
	iCMs	wt	25±22	0.96
		B2M-/- CIITA-/- CD47 tg	26±29	
BLI	iPSCs	wt	17±10	0.19
		B2M-/- CIITA-/- CD47 tg	38±32	
	iECs	wt	52±28	0.25
		B2M-/- CIITA-/- CD47 tg	34±18	
	iCMs	wt	18±12	0.56
		B2M-/- CIITA-/- CD47 tg	15±3	

c				
Assay	Cell graft	Group	CD3% of hCD45	p-Value
Elispot	iECs	wt	48±18	0.70
		B2M-/- CIITA-/- CD47 tg	53±16	
BLI	iECs	wt	57±9	0.95
		B2M-/- CIITA-/- CD47 tg	58±8	

b					
Experiments with NSG-SGM3 mice					
Assay	Group	Recipient HLA-A		# HLA-A MM to cell graft	
Elispot iPSCs	wt	A*03:01	A*68:01	2	
	wt	A*03:01	A*68:01	2	
	wt	A*24:02	A*32:01	2	
	wt	A*24:02	A*32:01	2	
	wt	A*01:01	A*32:01	1	
	wt	A*01:01	A*32:01	1	
	B2M-/- CIITA-/- CD47 tg	A*03:01	A*68:01	2	
	B2M-/- CIITA-/- CD47 tg	A*02:01	A*29:02	2	
	B2M-/- CIITA-/- CD47 tg	A*24:02	A*32:01	2	
	B2M-/- CIITA-/- CD47 tg	A*01:01	A*32:01	2	
	B2M-/- CIITA-/- CD47 tg	A*01:01	A*30:02	1	
	B2M-/- CIITA-/- CD47 tg	A*01:01	A*30:02	1	
Elispot Ecs	wt	A*24:02	A*25:01	2	
	wt	A*24:02	A*25:01	2	
	wt	A*24:02	A*25:01	2	
	B2M-/- CIITA-/- CD47 tg	A*24:02	A*25:01	2	
	B2M-/- CIITA-/- CD47 tg	A*03:01	A*68:01	2	
	B2M-/- CIITA-/- CD47 tg	A*11:01	A*23:01	2	
	BLI iPSC	wt	A*01:01	A*02:01	0
		wt	A*01:01	A*02:01	0
		wt	A*02:01	A*24:02	1
		wt	A*02:01	A*24:02	1
		wt	A*30:01	A*30:02	2
		B2M-/- CIITA-/- CD47 tg	A*24:02	A*32:01	2
B2M-/- CIITA-/- CD47 tg		A*01:01	A*32:01	1	
B2M-/- CIITA-/- CD47 tg		A*01:01	A*32:01	1	
B2M-/- CIITA-/- CD47 tg		A*11:01	A*25:01	2	
B2M-/- CIITA-/- CD47 tg		A*11:01	A*25:01	2	
B2M-/- CIITA-/- CD47 tg		A*11:01	A*25:01	2	
BLI EC		wt	A*11:01	A*25:01	2
	wt	A*11:01	A*25:01	2	
	wt	A*11:01	A*25:01	2	
	wt	A*11:01	A*25:01	2	
	wt	A*11:01	A*25:01	2	
	B2M-/- CIITA-/- CD47 tg	A*11:01	A*25:01	2	
	B2M-/- CIITA-/- CD47 tg	A*11:01	A*25:01	2	
	B2M-/- CIITA-/- CD47 tg	A*11:01	A*25:01	2	
	B2M-/- CIITA-/- CD47 tg	A*11:01	A*25:01	2	
	B2M-/- CIITA-/- CD47 tg	A*11:01	A*25:01	2	
	B2M-/- CIITA-/- CD47 tg	A*11:01	A*25:01	2	
	BLI CM	wt	A*24:02	A*32:01	2
wt		A*01:01	A*32:01	1	
wt		A*01:01	A*03:01	1	
wt		A*01:01	A*03:01	1	
B2M-/- CIITA-/- CD47 tg		A*01:01	A*03:01	1	
B2M-/- CIITA-/- CD47 tg		A*01:01	A*03:01	1	
B2M-/- CIITA-/- CD47 tg		A*01:01	A*03:01	1	
B2M-/- CIITA-/- CD47 tg		A*01:01	A*03:01	1	
B2M-/- CIITA-/- CD47 tg		A*01:01	A*03:01	1	
B2M-/- CIITA-/- CD47 tg		A*01:01	A*03:01	1	
B2M-/- CIITA-/- CD47 tg		A*01:01	A*03:01	1	

Supplementary Figure 13

CD3 reconstitution and HLA matching in humanized mice.

a, Percentage of CD3<sup>+</sup> cells among the reconstituted human CD45<sup>+</sup> cell population in NSG-SGM3 mice receiving hiPSC grafts (n=7 per group), hiEC grafts (n=3 per group), or hiCM grafts (n=3 per group) in the Elispot groups or hiPSC grafts, hiEC grafts, or hiCM grafts (n=5 per group) in the BLI groups (mean ± s.d., two-tailed Student's t-test). b, All NSG-SGM3 mice were typed for HLA-A and the number of HLA-A mismatches (MM) was calculated for every single animal used in this study. 2 MM are coded in red, 1 MM in orange, and zero MM in green. c, Percentage of CD3<sup>+</sup> cells among the reconstituted human CD45<sup>+</sup> cell population in BLT mice receiving iEC grafts in the Elispot groups (n=4 per group) or BLI groups (n=5) (mean ± s.d., two-tailed Student's t-test).

## **2.2 Hypoimmune induced pluripotent stem cell–derived cell therapeutics treat cardiovascular and pulmonary diseases in immunocompetent allogeneic mice**

In Chapter 2 is presented the publication ‘Hypoimmune induced pluripotent stem cell–derived cell therapeutics treat cardiovascular and pulmonary diseases in immunocompetent allogeneic mice’. The paper has been published in Proceedings of the National Academy of Sciences of the United States of America in 2021. My contribution to this paper includes performing cell culture, flow cytometry experiments, lentiviral transductions, and analysis of the data. This contribution resulted in a second authorship on the paper.

**Title:** Hypoimmune induced pluripotent stem cell–derived cell therapeutics treat cardiovascular and pulmonary diseases in immunocompetent allogeneic mice

**Authors:** Tobias Deuse\*, Grigol Tediashvili\*, Xiaomeng Hu\*, Alessia Gravina, Annika Tamenang, Dong Wang, Andrew Connolly, Christian Mueller, Beñat Mallavia, Mark R. Looney, Malik Alawi, Lewis L. Lanier, and Sonja Schrepfer

\*sharing first authorship

**Journal:** in Proceedings of the National Academy of Sciences of the United States of America (PNAS)

**DOI:** 10.1073/pnas.2022091118



# Hypoimmune induced pluripotent stem cell–derived cell therapeutics treat cardiovascular and pulmonary diseases in immunocompetent allogeneic mice

Tobias Deuse<sup>a,1</sup>, Grigol Tediashvili<sup>a,b,1</sup>, Xiaomeng Hu<sup>a,b,c,d,1</sup>, Alessia Gravina<sup>a</sup>, Annika Tamenang<sup>a,b</sup>, Dong Wang<sup>a</sup>, Andrew Connolly<sup>e</sup>, Christian Mueller<sup>f,g</sup>, Beñat Mallavia<sup>h</sup>, Mark R. Looney<sup>h,i</sup>, Malik Alawi<sup>i</sup>, Lewis L. Lanier<sup>k,2,3</sup>, and Sonja Schrepfer<sup>a,d,2,3</sup>

<sup>a</sup>Division of Cardiothoracic Surgery, Department of Surgery, Transplant and Stem Cell Immunobiology Laboratory, University of California, San Francisco, CA 94143; <sup>b</sup>Department of Cardiovascular Surgery, University Heart Center Hamburg, 20246 Hamburg, Germany; <sup>c</sup>German Center for Cardiovascular Research (DZHK) partner site Hamburg/Kiel/Luebeck, 20246 Hamburg, Germany; <sup>d</sup>Sana Biotechnology Inc., South San Francisco, CA 94080; <sup>e</sup>Department of Pathology, University of California, San Francisco, CA 94143; <sup>f</sup>Horae Gene Therapy Center, University of Massachusetts, Worcester, MA 01605; <sup>g</sup>Department of Pediatrics, University of Massachusetts, Worcester, MA 01605; <sup>h</sup>Department of Medicine, University of California, San Francisco, CA 94143; <sup>i</sup>Department of Laboratory Medicine, University of California, San Francisco, CA 94143; <sup>j</sup>Bioinformatics Core, University Medical Center Hamburg-Eppendorf, 20246 Hamburg, Germany; and <sup>k</sup>Department of Microbiology and Immunology and the Parker Institute for Cancer Immunotherapy, University of California, San Francisco, CA 94143

Contributed by Lewis L. Lanier, May 25, 2021 (sent for review October 22, 2020); reviewed by John Cooke and Yuji Shiba

The emerging field of regenerative cell therapy is still limited by the few cell types that can reliably be differentiated from pluripotent stem cells and by the immune hurdle of commercially scalable allogeneic cell therapeutics. Here, we show that gene-edited, immune-evasive cell grafts can survive and successfully treat diseases in immunocompetent, fully allogeneic recipients. Transplanted endothelial cells improved perfusion and increased the likelihood of limb preservation in mice with critical limb ischemia. Endothelial cell grafts transduced to express a transgene for alpha1-antitrypsin (A1AT) successfully restored physiologic A1AT serum levels in mice with genetic A1AT deficiency. This cell therapy prevented both structural and functional changes of emphysematous lung disease. A mixture of endothelial cells and cardiomyocytes was injected into infarcted mouse hearts, and both cell types orthotopically engrafted in the ischemic areas. Cell therapy led to an improvement in invasive hemodynamic heart failure parameters. Our study supports the development of hypoimmune, universal regenerative cell therapeutics for cost-effective treatments of major diseases.

hypoimmune stem cells | immune evasion | cell therapy

Affordability will promote the development and commercialization of cell therapy products, and optimization of cost of goods should be addressed from the very beginning to facilitate broader adoption for patient treatment (1). From a population health standpoint, only allogeneic products will allow manufacturing at large scale and with rigorous quality standards necessary for the treatment of large patient populations (2). However, the need for immunosuppression is a major long-term concern and only acceptable for early proof-of-concept clinical studies. The emergence of immune engineering now offers a unique opportunity to develop universal off-the-shelf products for all patients and all tissue types. We (3) and others (4) have developed immune engineering concepts that allow cells to evade rejection in immunocompetent allogeneic recipients. We now present applications of this technology and report successful treatments of different diseases with hypoimmune (HIP) induced pluripotent stem cell (iPSC)–derived cells in allogeneic mice without the need for any immunosuppression.

## Results

### Generation of Universal, Hypoimmune Endothelial Cells and Cardiomyocytes.

To generate hypoimmune, universally compatible mouse cell products, we utilized a recently developed immune-editing strategy. Wild-type (WT) C57BL/6 (B6) mouse iPSCs underwent a three-step gene editing protocol (3). The *B2m* and *Ciita* genes were targeted for disruption with Cas9 nuclease and guides to deplete major histocompatibility complex (MHC) class I and class

II expression and Cd47 was overexpressed using lentiviral transduction. These B6HIP iPSCs as well as their parental B6 iPSCs were transduced to express firefly luciferase (FLuc) for subsequent bioluminescence imaging (BLI) studies to quantitatively assess their survival after transplantation. Both B6 and B6HIP iPSCs were differentiated into iPSC-derived endothelial cells (iECs) and cardiomyocytes (iCMs) (Fig. 1). The purity of the generated derivatives was >80% for iECs and >95% for iCMs and similar between B6 and B6HIP (SI Appendix, Fig. S1 A–D).

**HIP iECs for the Preservation of Critically Ischemic Hindlimbs.** First, the efficacy of transplanted B6HIP iECs to salvage hindlimbs in

## Significance

Precise gene editing allows engineering of immune receptors and ligands to reduce the immunogenicity of cells, and strategies for the generation of immune-evasive stem cell sources are currently being developed. This article describes the translational aspect of generating universally transplantable, disease-specific, therapeutic cell products. We provide proof of concept that immune-engineered cells can treat major cardiovascular and pulmonary diseases in fully allogeneic subjects without utilizing any immunosuppression. The translational aspect is emphasized by showing improvements in clinically relevant outcome measures, which are widely used in human trials. Depending on the feasibility of large-scale manufacturing of universal cell therapeutics, this approach could enable cost-effective cell therapy.

Author contributions: T.D., L.L.L., and S.S. designed research; G.T., X.H., A.G., A.T., D.W., B.M., and M.R.L. performed research; C.M. and M.R.L. contributed new reagents/analytic tools; T.D., G.T., X.H., A.G., A.T., D.W., A.C., B.M., M.R.L., M.A., and S.S. analyzed data; T.D. and S.S. wrote the paper; C.M. provided Serpina knockout mice; and L.L.L. edited the paper.

Reviewers: J.C., Houston Methodist; and Y.S., Shinshu University.

Competing interest statement: S.S. is scientific founder and senior vice president of Sana Biotechnology Inc. T.D., S.S., and X.H. own stock in Sana Biotechnology Inc. Neither a reagent nor any funding from Sana Biotechnology Inc. was used in this study. University of California, San Francisco has filed patent applications that cover these inventions.

This open access article is distributed under [Creative Commons Attribution License 4.0 \(CC BY\)](https://creativecommons.org/licenses/by/4.0/).

<sup>1</sup>T.D., G.T., and X.H. contributed equally to this work.

<sup>2</sup>L.L.L. and S.S. contributed equally to this work.

<sup>3</sup>To whom correspondence may be addressed. Email: sonja.schrepfer@ucsf.edu or lewis.lanier@ucsf.edu.

This article contains supporting information online at <https://www.pnas.org/lookup/suppl/doi:10.1073/pnas.2022091118/-DCSupplemental>.

Published July 9, 2021.

Downloaded from https://www.pnas.org by UCSF LIBRARY on March 24, 2023 from IP address 128.2.18.42.174.

IMMUNOLOGY AND INFLAMMATION



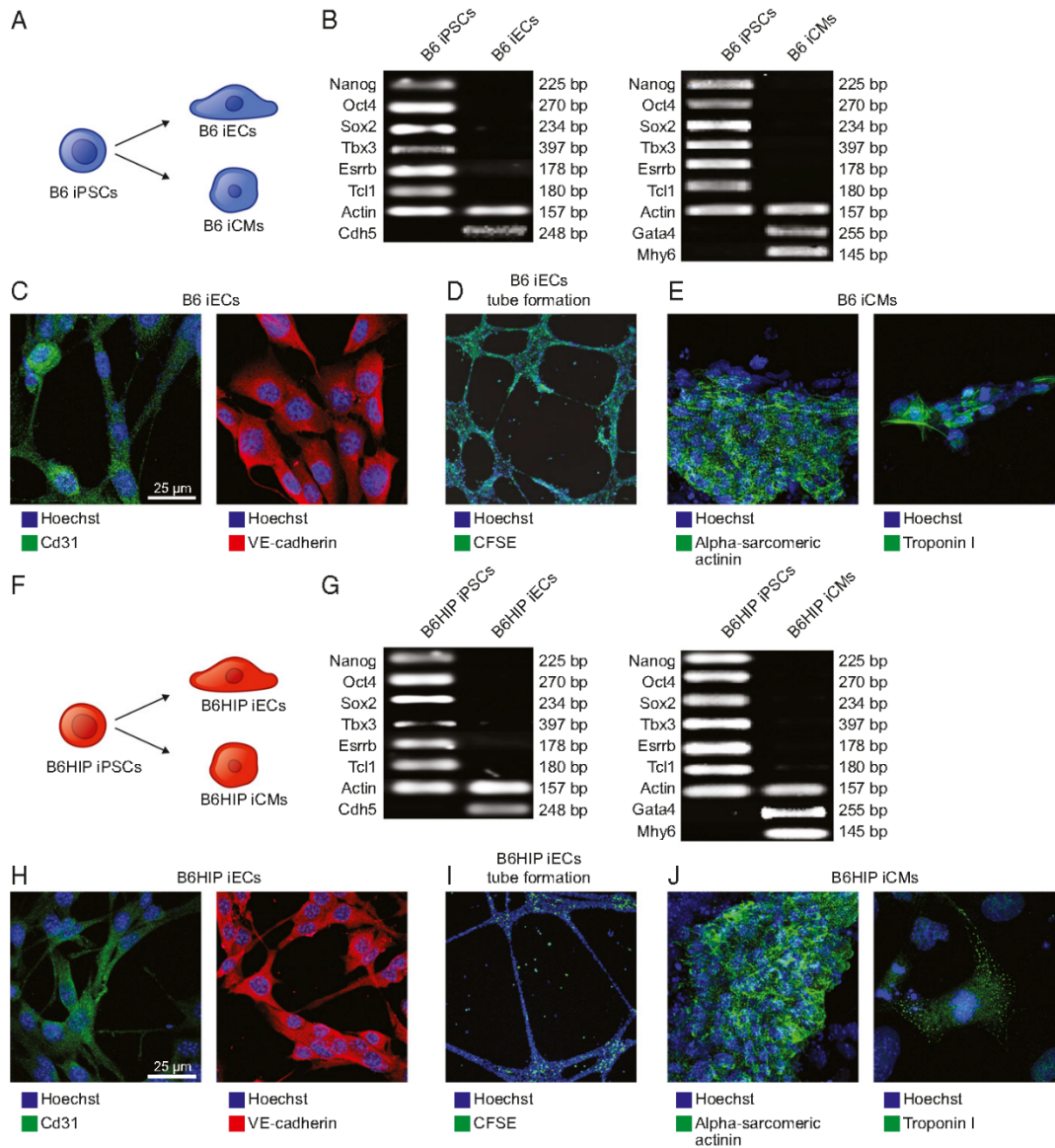


**Fig. 1.** Differentiation of B6 and B6HIP iPSCs into iECs and iCMs. (A) B6 iPSCs were differentiated into iECs and iCMs. (B) During the differentiation, the cells lost their typical pluripotent features of iPSCs and B6 iECs adopted genetic markers of endothelial cells and B6 iCMs of cardiomyocytes (representative gels of two independent experiments). (C and D) B6 iECs expressed Cd31 and VE-cadherin (C, representative pictures of five independent experiments) and formed tubular structures in vitro (D, representative pictures of five independent experiments). (E) B6 iCMs expressed alpha-sarcomeric actinin and troponin I (representative pictures of five independent experiments). (F) B6HIP iPSCs were differentiated into iECs and iCMs. (G) During the differentiation, the cells lost their typical pluripotent features of iPSCs and B6HIP iECs adopted genetic markers of endothelial cells and B6HIP iCMs of cardiomyocytes (representative gels of two independent experiments). (H and I) B6HIP iECs expressed Cd31 and VE-cadherin (H, representative pictures of five independent experiments) and formed tubular structures in vitro (I, representative pictures of five independent experiments). (J) B6HIP iCMs expressed alpha-sarcomeric actinin and troponin I (representative pictures of five independent experiments).

allogeneic BALB/c mice with critical limb ischemia (CLI) was evaluated. Previous studies with endothelial progenitor cells in CLI have used autologous settings (5) or immunocompromised

recipients (6, 7). BALB/c mice (H-2<sup>d</sup>), which are fully MHC mismatched to the B6 (H-2<sup>b</sup>) iECs, underwent ligation and excision of their left proximal superficial femoral artery (8)

(Fig. 2*A*). The animals were left untreated or received fan-shaped injections of allogeneic B6 (allo) or allogeneic B6HIP (alloHIP) iECs and followed for 28 d (Fig. 2*B* and *C*). Cell survival was assessed with BLI. All allo iEC grafts were rejected within 15 d (Fig. 2*D*), whereas all alloHIP iEC grafts survived and showed some proliferation with increasing BLI signals (Fig. 2*E*). Doppler imaging showed vastly reduced perfusion of the ischemic legs on the first day after the procedure in all groups (Fig. 2*F* and *SI Appendix*, Fig. S2). The perfusion index only increased in animals receiving alloHIP iECs and persistently showed better perfusion than in animals receiving allo iECs throughout the study period. The severity of ischemic sequelae was assessed using a standardized mouse limb ischemia grading scale (9). All animals receiving no cell therapy and the vast majority of animals receiving allo iEC grafts showed gangrenous lesions of different extents. Animals in the alloHIP iEC group, in contrast, showed less severe lesions, more than half of which were nongangrenous (Fig. 2*G* and *SI Appendix*, Fig. S3). The thighs were recovered and the area surrounding the excised femoral artery in which the cells were injected was sectioned (*SI Appendix*, Fig. S4). We found fatty replacement of muscle with endomyxial fat cells and occasional dystrophic calcifications. In alloHIP animals, we saw spindle cells of endothelial morphology, some outgrowing from Matrigel remnants. Some also showed small clusters of poorly differentiated cells. Using immunofluorescence imaging, we were able to detect FLuc<sup>+</sup> graft cells in many vascular structures, particularly small and larger arteries, in all alloHIP iEC recipients (Fig. 2*H*). The incorporated graft cells were VE-cadherin<sup>+</sup> and located along the endothelial cell layer in these vessels. We did not find any FLuc<sup>+</sup> allo iECs in any of the animals. These data show that alloHIP iECs survive and proliferate in allogeneic animals, incorporate into vascular structures, improve limb perfusion, and reduce the incidence of gangrenous limb complications.

**HIP iECs for the Treatment of A1AT.** Next, we aimed to use iEC grafts as factories to replace a crucial missing factor responsible for disease. We chose a mouse model of A1AT deficiency that quickly develops both structural and functional changes of lung disease (10). In B6 mice with quintuple *Serpina1a-e* knockout, a mild lipopolysaccharide (LPS) challenge that is well tolerated in WT B6 mice, leads to emphysema development due to the unabated activity of the secreted neutrophil elastase (NE) from recruited polymorphonuclear cells. To turn iECs into enzyme factories, both B6 and B6HIP iECs were engineered to secrete mouse A1AT. The mouse *Serpina1e* (S1e) cDNA sequence was synthesized and cloned into a lentiviral vector with zeocin resistance, B6 and B6HIP iECs were transduced, and antibiotic-selected pools of B6<sup>S1e</sup> and B6HIP<sup>S1e</sup> iECs were expanded. Since the *Serpina1e*<sup>-/-</sup> mice were bred on a B6 background and thus syngeneic to our iECs, we had to further engineer alloantigens into the iECs to make them allogeneic. We used two additional lentiviral particles carrying transgenes for H-2K<sup>d</sup>, a major allele of the BALB/c H-2<sup>d</sup> genotype, and the BALB/c-variant of *Co3*, an immunogenic minor antigen of the mitochondrial DNA (11). Such MHC-engineered <sup>c</sup>allo<sup>S1e</sup> and <sup>c</sup>alloHIP<sup>S1e</sup> iECs showed the classic EC phenotype (*SI Appendix*, Fig. S5*A* and *B*) and a similar purity (*SI Appendix*, Fig. S1*E* and *F*) as the parental B6 and B6HIP iECs. A total of  $1.5 \times 10^5$  <sup>c</sup>allo<sup>S1e</sup> and <sup>c</sup>alloHIP<sup>S1e</sup> iECs, as well as their parental and intermediary iEC populations, were plated for 24 h, and A1AT levels were measured (*SI Appendix*, Fig. S5*C* and *D*). The <sup>c</sup>allo<sup>S1e</sup> and <sup>c</sup>alloHIP<sup>S1e</sup> iECs produced ~50 ng A1AT in a day. With a half-life of A1AT in mice of approximately 4.5 d, we estimated that a cell number of  $1.5 \times 10^8$  A1AT-producing cells was necessary to restore and maintain physiologic A1AT serum levels, which are around 200 µg/mL. Seven days before induction of lung disease, *Serpina1e*<sup>-/-</sup> B6 mice received  $1.5 \times 10^8$  <sup>c</sup>allo<sup>S1e</sup> or <sup>c</sup>alloHIP<sup>S1e</sup> iECs in saline injected into the peritoneum and the subcutaneous tissue

in the lumbar area to equally split the cell load (Fig. 3*A*). *Serpina1e*<sup>-/-</sup> B6 mice without cell injection, as well as healthy WT B6 mice, served as controls (Fig. 3*B*). Lung disease was induced in all *Serpina1e*<sup>-/-</sup> B6 groups with LPS instillation on day 0 (7 d after cell injection) and repeated on day 11 (Fig. 3*C*). After 14 d, the established time period to assess lung disease in LPS-treated *Serpina1e*<sup>-/-</sup> B6 mice (10), all mice receiving the <sup>c</sup>allo<sup>S1e</sup> iECs and half of the animals receiving <sup>c</sup>alloHIP<sup>S1e</sup> iECs underwent FlexiVent evaluation. Five animals receiving <sup>c</sup>alloHIP<sup>S1e</sup> iECs were assessed on day 28 to have a consistent follow-up period with the other disease models in this study. Serum was drawn from animals after the FlexiVent. On day 14, A1AT was undetectable in both untreated *Serpina1e*<sup>-/-</sup> mice and those receiving <sup>c</sup>allo<sup>S1e</sup> iECs. Cell therapy with <sup>c</sup>alloHIP<sup>S1e</sup> iECs, in contrast, was able to restore A1AT levels and 14-d and 28-d levels were well in the physiologic range (Fig. 3*D*). Cell survival was assessed by BLI. All recipients of <sup>c</sup>allo<sup>S1e</sup> iECs (Fig. 3*E*) rapidly rejected their allogeneic, MHC-engineered grafts within 7 d, whereas all <sup>c</sup>alloHIP<sup>S1e</sup> iECs showed survival throughout the observation period (Fig. 3*F*). Two animals of the 28-d group missed their last imaging due to technical difficulties. Pulmonary mechanics were assessed using a computer-controlled piston ventilator for standardized measurements. On day 14 of the study, untreated *Serpina1e*<sup>-/-</sup> B6 mice showed ventilation patterns consistent with developing emphysema, including increased lung compliance and decreased elastance (Fig. 3*G–M*). The coefficients of tissue damping and tissue elasticity were both reduced and the total lung capacity was increased. As reported previously with this model, resistance did not change (10). Consistent with their rapid immune rejection, <sup>c</sup>allo<sup>S1e</sup> iECs did not provide any benefit against the development of emphysematous lung disease, and the lung function parameters were similar to *Serpina1e*<sup>-/-</sup> B6 mice not receiving any cell treatment. In contrast, <sup>c</sup>alloHIP<sup>S1e</sup> iEC therapy was effective in preventing emphysematous respiratory patterns as all lung function parameters remained within the range of healthy WT B6 animals. The lungs were then fixed for histology and serially cut for stereological assessment. We found morphometric criteria for emphysema in untreated *Serpina1e*<sup>-/-</sup> B6 mice, including distal airspace enlargement, loss of alveolar septa, and increase in mean linear intercept (chord) length, a parameter to describe the mean free distance in the air spaces (Fig. 3*N–Q*). Treatment with <sup>c</sup>alloHIP<sup>S1e</sup> iECs was successful in preventing all structural damages to the lung morphology. Overall, A1AT replacement via allogeneic cell therapy was able to prevent the development of emphysematous lung disease in *Serpina1e*<sup>-/-</sup> B6 mice.

**HIP iECs and iCMs for the Treatment of Ischemic Heart Failure.** In the first heart experiment, the ability of HIP iECs to treat cryoinjury-induced heart failure was evaluated. BALB/c mice underwent cryoinjury-induced myocardial infarction followed by injections of allo iECs or alloHIP iECs into the infarct border zone (Fig. 4*A* and *B*) and animals were followed for 28 d (Fig. 4*C*). As expected, allo iECs were rejected within 15 d, while alloHIP iECs survived and proliferated somewhat within the heart (Fig. 4*D* and *E*). Invasive pressure–volume loop measurements were performed to quantitatively assess hemodynamics during follow-up. The left ventricular ejection fraction markedly dropped with cryoinjury-induced myocardial infarction, and only hearts receiving the alloHIP iECs showed a subtle improvement in contractility over 28 d (Fig. 4*F*). The alloHIP iEC therapy significantly increased left ventricular stroke volume and stroke work, confirming a more physiologic inotropic state of the ventricle (Fig. 4*G* and *H*). Overall, alloHIP cell therapy led to a significant increase in cardiac output when compared to allo iEC therapy (Fig. 4*I*). The hearts were recovered, processed, and serially cut after 28 d, and immunofluorescence staining showed engrafted FLuc<sup>+</sup> alloHIP iECs within the injected areas, whereas no FLuc<sup>+</sup> allo iECs were detected in any hearts (Fig. 4*J*).

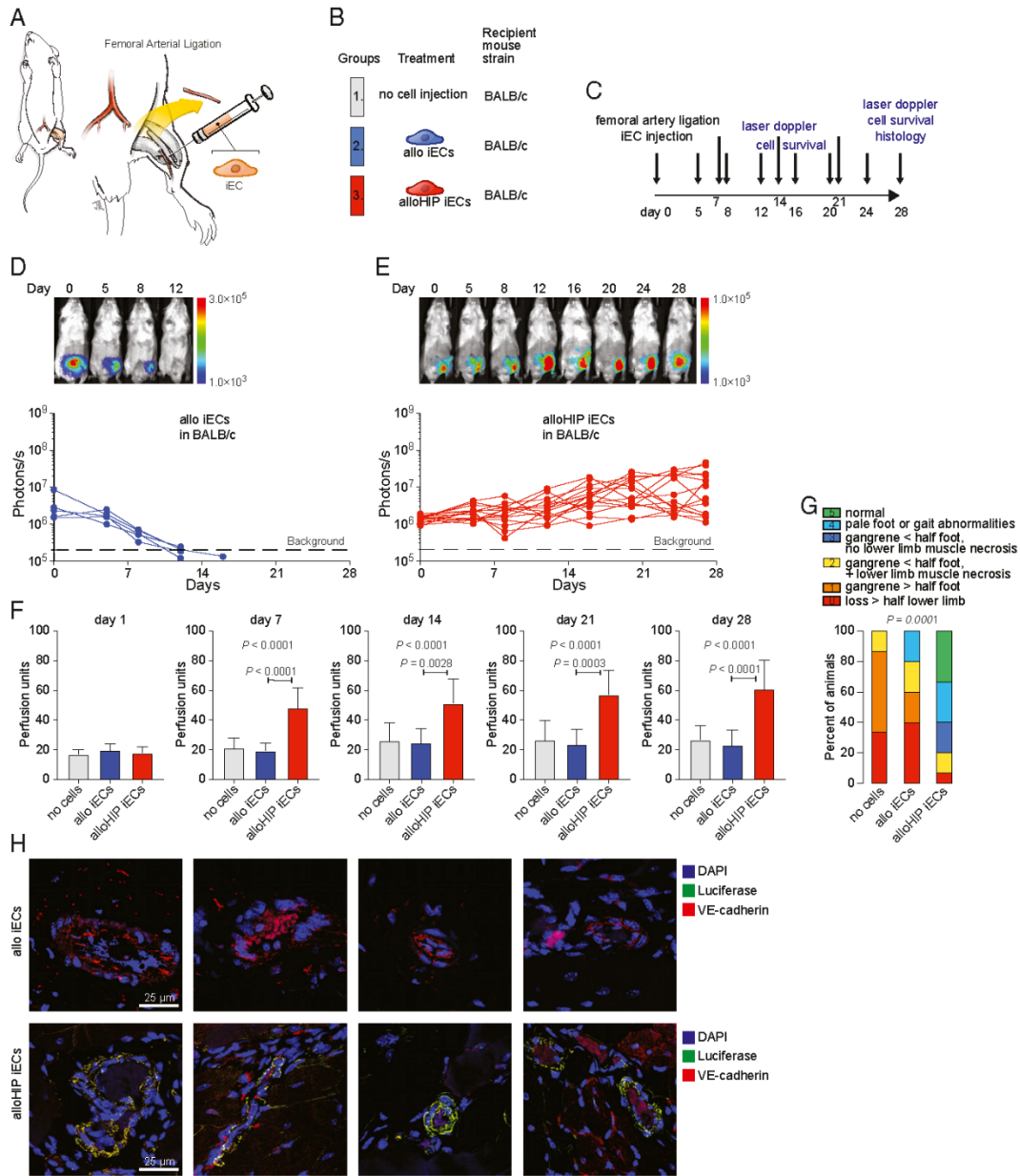
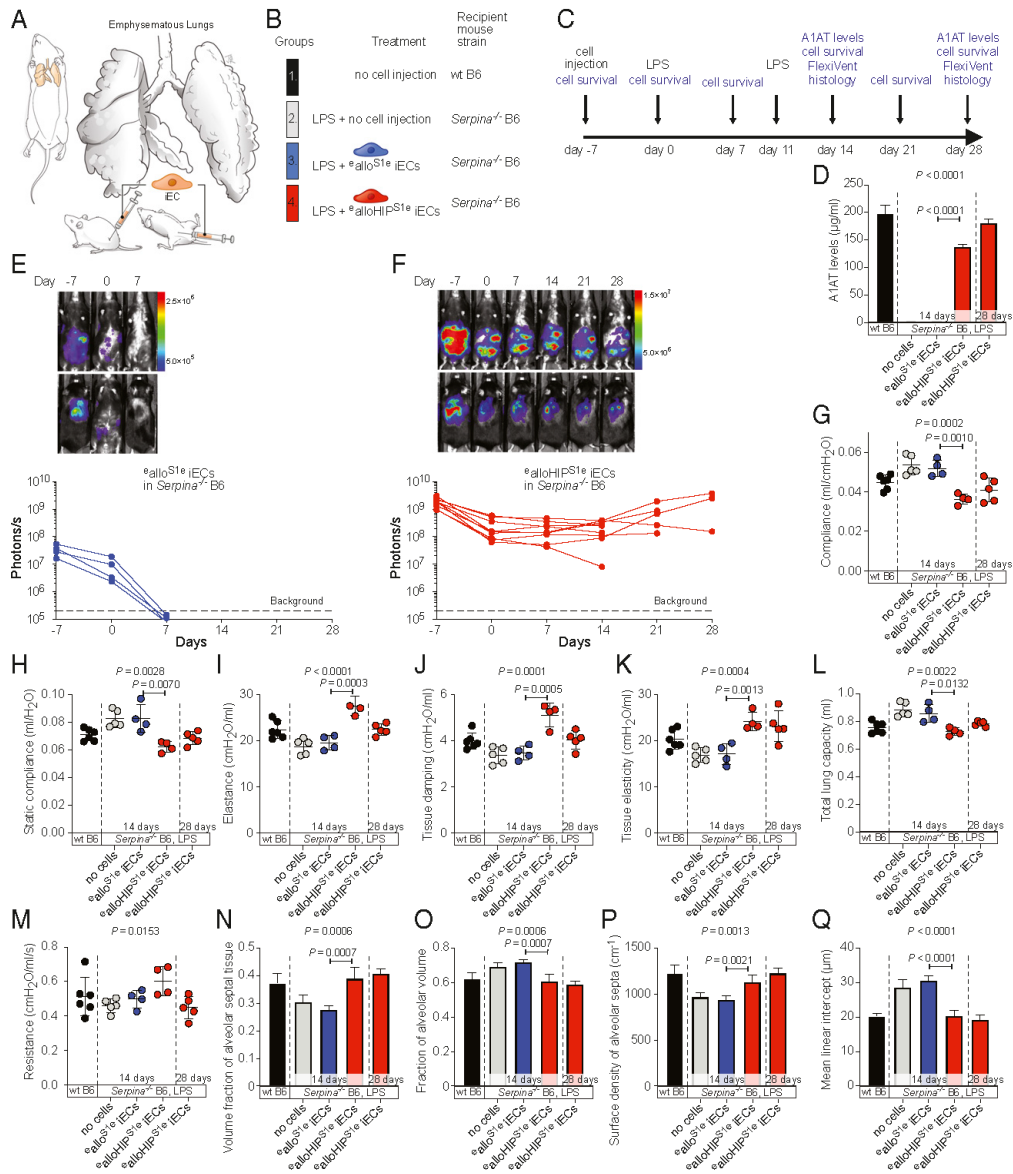


**Fig. 2.** Allogeneic HIP iECs facilitate ischemic limb preservation. (A) In BALB/c mice, the superficial femoral artery was ligated and partially resected to induce left lower limb ischemia. (B) Mice were left untreated or received fan-shaped injections of allo or alloHIP iECs into the surrounding tissue. (C) The study protocol included assessment of iEC survival and laser Doppler perfusion imaging and histology after 28 d. (D and E) The survival of FLuc<sup>+</sup> iEC grafts was longitudinally followed by BLI. All allo iEC grafts were rejected over 15 d (D, 5 animals), while all alloHIP iEC grafts survived and some grafts even showed proliferation (E, 15 animals). BLI signals of individual animals are plotted, representative pictures are shown. (F) Left lower extremity perfusion was serially assessed by laser Doppler imaging and showed an improvement over time only after transplantation of alloHIP iECs (mean  $\pm$  SD, 15 animals with no cell injection, 5 animals in the allo group, and 15 animals in the alloHIP group; ANOVA with Bonferroni post hoc test). (G) The sequelae of CLI after 28 d were graded according to a standardized scoring system and showed improved limb preservation with alloHIP iEC treatment (parts of whole graphs, 15 animals with no cell injection, 5 animals in the WT group, 15 animals in the HIP group; Kruskal–Wallis test). (H) Immunofluorescence staining showed no engrafted FLuc<sup>+</sup> allo iECs in allogeneic BALB/c recipients, but engraftment of FLuc<sup>+</sup> alloHIP iECs located along the endothelial layer of larger and smaller intramuscular vessels. Costaining showed that transplanted cells retained their VE-cadherin expression (representative pictures of five independent experiments).



IMMUNOLOGY AND INFLAMMATION

**Fig. 3.** A1AT-releasing allogeneic HIP iECs prevent emphysema development in *Serpina*<sup>-/-</sup> B6 mice. (A) *Serpina*<sup>-/-</sup> B6 mice were challenged with LPS via their airways to trigger emphysematous lung disease. (B) Some *Serpina*<sup>-/-</sup> B6 mice were treated with MHC-engineered A1AT-secreting allogeneic (\*allo<sup>S1E</sup>) or allogeneic HIP (\*alloHIP<sup>51E</sup>) iECs 7 d before the LPS challenge. Healthy WT B6 animals served as controls. (C) The study protocol included monitoring of graft survival, as well as functional and morphologic lung assessments. (D) Serum A1AT levels were quantified in all groups (mean ± SD, six animals in WT B6, five animals in *Serpina*<sup>-/-</sup> B6 LPS without cell injections at day 14, four animals in *Serpina*<sup>-/-</sup> B6 LPS \*allo<sup>S1E</sup> iECs at day 14, four animals in *Serpina*<sup>-/-</sup> B6 LPS \*alloHIP<sup>51E</sup> iECs at day 14, and five animals in *Serpina*<sup>-/-</sup> B6 LPS \*alloHIP<sup>51E</sup> iECs at day 28; ANOVA with Bonferroni post hoc test for 14-d groups). (E and F) The survival of Fluc<sup>+</sup> \*allo<sup>S1E</sup> iECs (E, four animals) and \*alloHIP<sup>51E</sup> iECs (F, nine animals) in *Serpina*<sup>-/-</sup> B6 recipients was longitudinally followed by BLI. BLI signals of individual animals are plotted, representative pictures are shown. (G–M) FlexiVent lung physiology assessments were done after 14 and 28 d (scatter dot plots, mean ± SD, six animals in WT B6, five animals in *Serpina*<sup>-/-</sup> B6 LPS without cell injections at day 14, four animals in *Serpina*<sup>-/-</sup> B6 LPS \*allo<sup>S1E</sup> iECs at day 14, four animals in *Serpina*<sup>-/-</sup> B6 LPS \*alloHIP<sup>51E</sup> iECs at day 14, and five animals in *Serpina*<sup>-/-</sup> B6 LPS \*alloHIP<sup>51E</sup> iECs at day 28; ANOVA with Bonferroni post hoc test for 14-d groups). (N–Q) Stereological lung assessments were done in all groups (mean ± SD, six animals in WT B6, five animals in *Serpina*<sup>-/-</sup> B6 LPS without cell injections at day 14, four animals in *Serpina*<sup>-/-</sup> B6 LPS \*allo<sup>S1E</sup> iECs at day 14, four animals in *Serpina*<sup>-/-</sup> B6 LPS \*alloHIP<sup>51E</sup> iECs at day 14, and five animals in *Serpina*<sup>-/-</sup> B6 LPS \*alloHIP<sup>51E</sup> iECs at day 28; ANOVA with Bonferroni post hoc test for 14-d groups).

Deuse et al.  
Hypimmune induced pluripotent stem cell-derived cell therapeutics treat cardiovascular and pulmonary diseases in immunocompetent allogeneic mice

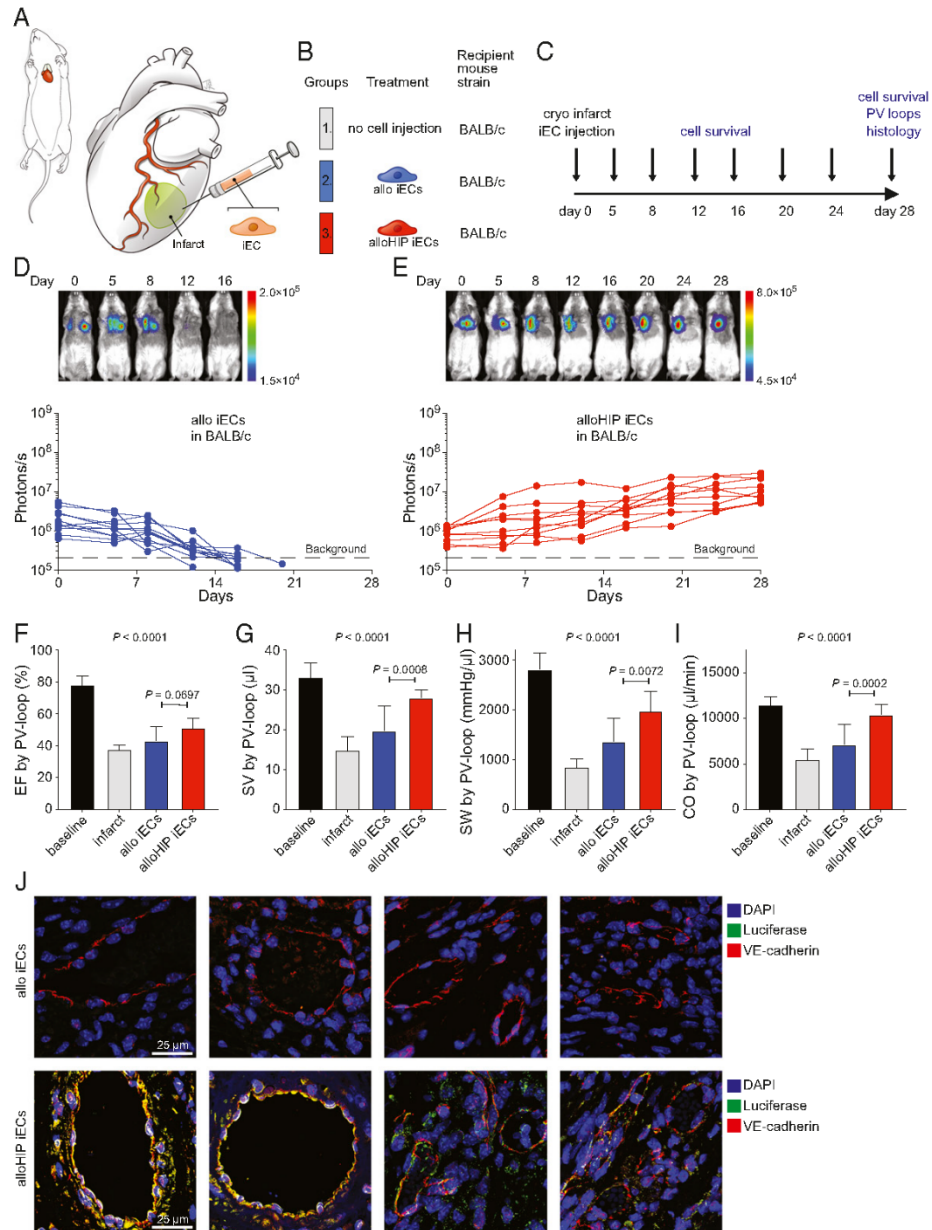


**Fig. 4.** Allogeneic HIP iECs alleviate heart failure in cryoinfarcted hearts. (A and B) BALB/c mice underwent cryoinfarction of their anterolateral left ventricle (A) and some subsequently received injections of allo iECs or alloHIP iECs (B) into the border zone. (C) Over a study period of 28 d, graft survival was monitored and iEC integration into host myocardium was assessed. (D and E) The survival of FLuc<sup>+</sup> allo iEC grafts (D, 11 animals) and alloHIP iEC grafts (E, 10 animals) was longitudinally followed by BLI. BLI signals of individual animals are plotted, representative pictures are shown. (F–I) Invasive PV loop analyses (mean  $\pm$  SD, 10 baseline animals, 4 infarct animals, 10 allo iEC animals, 10 alloHIP animals; ANOVA with Bonferroni post hoc test). Parameters included EF (F), SV (G), SW (H), and CO (I). (J) Immunofluorescence staining of the infarct border zone did not detect any FLuc<sup>+</sup> graft cells in recipients of allo iECs. However, all animals that received alloHIP iECs showed engraftment localized to the endothelial cell layers of larger and smaller intramyocardial vessels (representative pictures of 11 animals in the allo and 10 animals in the alloHIP group).

Next, a mixture of allo or alloHIP iECs and iCMs was used to improve remuscularization (Fig. 5 A–C). A more thorough assessment of the recipient immune response was conducted in this study. After 7 d, there was a vigorous immune cell and antibody response against the allo iEC and iCM grafts (Fig. 5 D–F) but no measurable immune response against the alloHIP cell mixture. All allo cell grafts were rejected within 14 d, but all alloHIP grafts survived and proliferated in the hearts of allogeneic BALB/c mice (Fig. 5 G and H). The survival of the alloHIP cell mixture in allogeneic recipients was not even inferior to their survival in severely immunodeficient SCID-beige mice, further supporting the absence of any relevant allo-immune responses in BALB/c (Fig. 5 I). Pressure–volume loop measurements again showed a nonsignificant improvement in the ejection fraction (EF) over 28 d (Fig. 5 J). The alloHIP cell mixture significantly increased left ventricular stroke volume (SV), stroke work (SW), and cardiac output (CO) when compared to allo cell therapy (Fig. 5 K–M). There was no difference between the hemodynamic parameters after alloHIP iEC therapy and alloHIP iEC and iCM therapy. The hearts were then cut into serial sections (SI Appendix, Fig. S6) and underwent histologic assessment. The cryoinjury resulted in very reproducible infarcts consisting of mostly fibrous replacement of the anterior and lateral left ventricular (LV) free wall, from the anterior septum to the posteromedial papillary muscle. There were a few chronic inflammatory cells, which appeared to be macrophages and lymphocytes, mostly at the edges of the fibrosis and without notable differences between groups. This response appeared typical for a reparative postinfarct inflammation. No undifferentiated cells, teratomas, or tumor formation were seen in any of the samples. In the alloHIP group, hearts had a thicker interventricular septum and posterior LV with a lack of dilatation. We could detect engraftment of transplanted FLuc<sup>+</sup> cells in the alloHIP-treated hearts (SI Appendix, Fig. S7). We could not detect any survival of allo graft cells in any of the hearts. Together our data show that alloHIP cell therapy was able to improve hemodynamics in allogeneic mice with myocardial infarction.

## Discussion

This study shows that HIP-derived cell therapeutics can successfully be employed in regenerative medicine to treat diseases for which there are no good treatment options available. We chose three major diseases affecting different organ systems to explore the versatility of HIP cell therapy. All three models, however, have sudden injury triggers, and a critical disease progression happens expeditiously after the initial event. This allows for standardized modeling of diseases in mice, although the progression in humans may be more chronic and protracted. It also allows for standardized assessment and comparison of the allo and alloHIP treatment groups in a convenient time period because any therapeutic effect will have to mainly mitigate the initial tissue injury in order to achieve a benefit. To underline the translational spirit of these studies, we aimed for subjective and clinically relevant endpoint measures used in clinical human trials.

Peripheral arterial disease has a prevalence of approximately 10% in individuals  $\geq 40$  y of age (12), and annually 11.2% of patients with peripheral arterial disease develop CLI, defined as chronic ischemic rest pain, ulcers, or gangrene (13). Clinically, CLI is associated with poor outcomes, since 30% of cases require amputation and 25% of patients will die within 1 y. Half of all patients with CLI are not candidates for surgical or percutaneous revascularization (14) and alternative cell-based therapies are desperately needed. So far, cell therapy trials have shown promising efficacy in patients with CLI when using peripheral blood or bone marrow mononuclear cells or more narrowly defined CD34<sup>+</sup> or CD133<sup>+</sup> stem cells (15). Clinically, the most relevant primary outcome endpoint used in randomized controlled trials is the amputation rate. Our data show that alloHIP iEC therapy markedly increased

limb preservation in an established mouse model for CLI. We could further correlate limb preservation with improved limb perfusion, a common secondary endpoint in clinical trials (16). Laser Doppler imaging is a very useful tool to noninvasively assess global blood perfusion in the mouse hindlimb without the use of tracer dyes (8, 17). BLI studies showed survival of transplanted alloHIP iECs in allogeneic recipients and histologically, we observed engraftment. FLuc<sup>+</sup> graft cells mainly localized along the endothelial layer of vascular structures, although we could not differentiate between the integration into existing host architecture and neovascularization. Prior animal studies showed that neovascularization occurs with transplanted endothelial progenitor cells (8). Clinical trials using cell therapy for CLI have so far only used autologous, patient-derived cells (15), which to a large extent have not even been well characterized or dedicated to the endothelial lineage. The prospect of developing universal, allogeneic off-the-shelf iEC therapeutics could advance cost-effective and widespread options to treat CLI.

Chronic obstructive pulmonary disease is the third leading cause of death worldwide (18), and it affects about 10% of the world population (19). Besides environmental risk factors, A1AT deficiency is the most common genetic mutation (20) located in the *SERPINA1* gene. Insufficient levels of the serum protease inhibitor A1AT (21) cause an imbalance in the alveolar interstitium with unopposed NE activity leading to a destruction of the alveolar walls and lung parenchyma. Patients with lung disease from A1AT deficiency are currently being treated with standard medical therapy (22), intravenous augmentation therapy, or require lung transplantation for respiratory failure (23). Although the infusion of pooled human A1AT is currently most efficient to elevate A1AT in the plasma and lung interstitium (24), it is very expensive and has not convincingly improved clinical endpoints in trials (25, 26). Specific mouse models for A1AT deficiency have long been missing and instillation of porcine pancreatic elastase or human NE have been used to create the protease/antiprotease imbalance (27). The quintuple *Serpina1-e* knockout B6 mouse used herein is the first animal model of A1AT deficiency that allows precise assessments of disease mechanisms linked to the underlying genetic mutations. Commonly used endpoints in clinical trials include measurements of lung function and lung density. We used various FlexiVent maneuvers to assess lung function in mice and were able to identify emphysematous disease in untreated *Serpina1-e* B6 mice. Transplantation of <sup>+</sup>alloHIP<sup>SLC</sup> iECs did not only normalize serum A1AT levels but also prevented deterioration of lung function. We used histology to assess lung structure and could correlate the preserved lung function in the treatment group with preserved alveolar septal tissue architecture. Our studies show that ectopic A1AT production by alloHIP iECs can restore plasma levels and prevent emphysema development.

Heart failure (HF) is a rising global epidemic (28) with more than 5.7 million patients in the United States, 870,000 new cases every year (29), and an increase in hospitalizations for HF (30). Clinical trials on cell therapy for heart failure have been conducted for almost two decades, so far with disappointing overall results (31). Objective clinical endpoints may include survival, number of events or hospitalizations, and subjective endpoints like symptom score and health-related quality of life (32, 33), but are difficult to use in mouse models. Instead, surrogate efficacy endpoints that correlate with clinical endpoints like hemodynamic improvement have been proposed (34). Invasive hemodynamic testing is best suited to assess cardiac output in mice and currently the gold standard tool (35–37). Our studies showed a significant treatment benefit for alloHIP iECs with improved hemodynamics. We observed survival and engraftment of alloHIP iECs in the areas of injection into ischemic myocardium. ECs promote cardiomyocyte survival and spatial reorganization via paracrine signaling (38), possibly involving the release of cytokines (39) or exosomes (40). While beneficial effects of endothelial progenitor

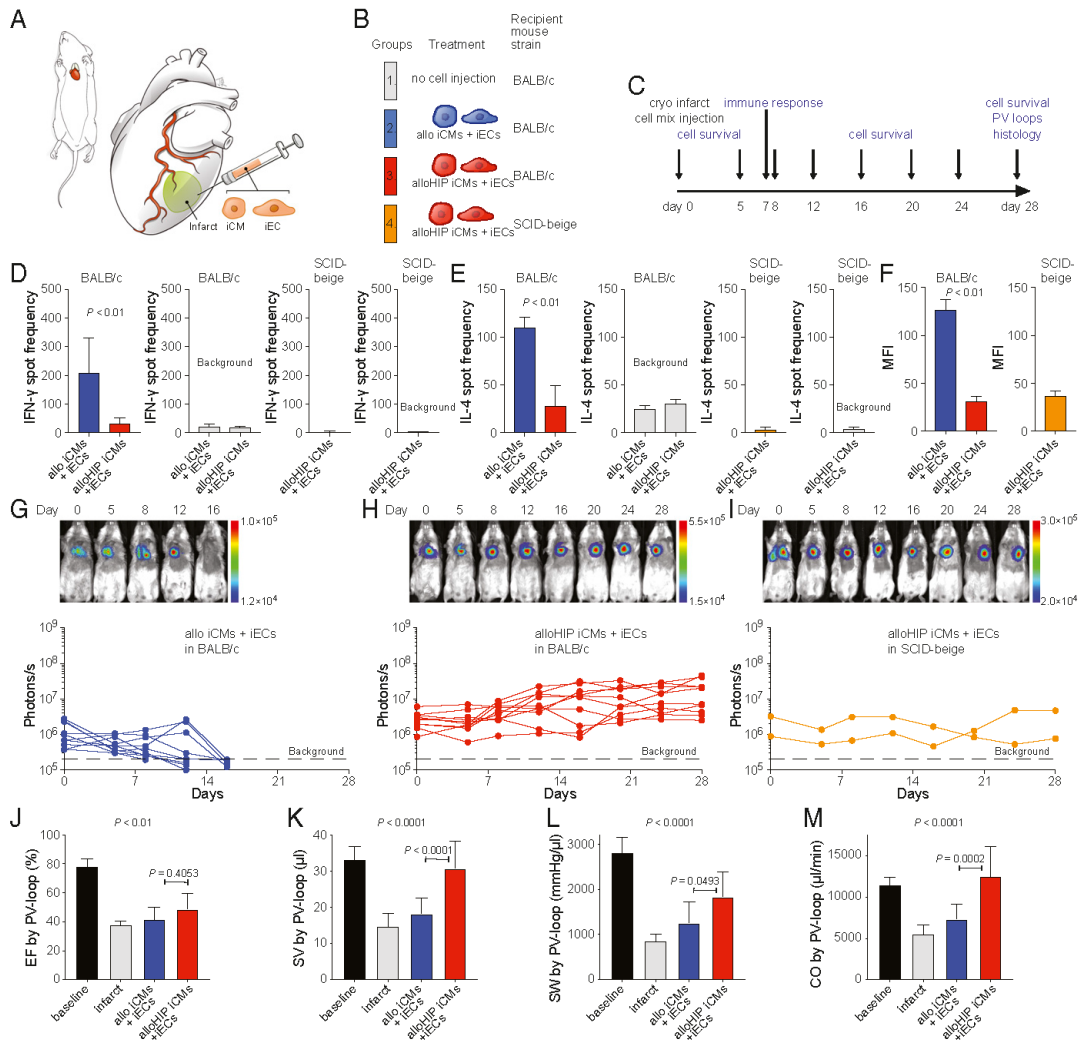


**Fig. 5.** Allogeneic cell mixture of HIP iECs and iCMs alleviates heart failure in infarcted hearts. (A and B) Mice underwent cryoinfarction of their heart (A) and some groups received a mixture of either allo or alloHIP iECs and iCMs (B). (C) The study protocol included early immune assays, longitudinal assessments of cell graft survival, invasive hemodynamic monitoring, and histology after 28 d. (D) After 6 d, the donor-specific IFN- $\gamma$  response of peripheral blood mononuclear cells (PBMCs) was assessed by Elispot assays (mean  $\pm$  SD, quadruplicates of 11 animals in the allo group and 10 animals in the alloHIP group; two-tailed Student's *t* test). Background spot frequencies were generated without stimulator cells. SCID-beige animals receiving alloHIP iECs and iCMs served as controls (mean  $\pm$  SD, quadruplicates of 10 animals). (E) Simultaneously, the donor-specific IL-4 response of peripheral PBMCs was assessed by Elispot assays (mean  $\pm$  SD, quadruplicates of 11 animals in the allo group and 10 animals in the alloHIP group; two-tailed Student's *t* test). Background spot frequencies were generated without stimulator cells. SCID-beige animals receiving alloHIP iECs and iCMs served as controls (mean  $\pm$  SD, quadruplicates of 10 animals). (F) Donor-specific IgM antibodies were assessed on day 6 (mean  $\pm$  SD, 10 animals per group; two-tailed Student's *t* test). SCID-beige animals receiving alloHIP iECs and iCMs served as controls (mean  $\pm$  SD, 5 animals). (G–I) The survival of FLuc<sup>+</sup> allo (G, 10 animals) and alloHIP iEC and iCM grafts (H, 9 animals) in allogeneic BALB/c mice was longitudinally followed by BLI. All alloHIP cell grafts also survived in SCID-beige mice (I, 2 animals). BLI signals of individual animals are plotted, representative pictures are shown. (J–M) Invasive PV loop analyses (mean  $\pm$  SD, 10 baseline animals, 4 infarct animals, 9 allo animals, 10 alloHIP animals; ANOVA with Bonferroni post hoc test). Parameters included EF (J), SV (K), SW (L), and CO (M).

cells have been described in immunodeficient mouse models (41) and in clinical trials using autologous cells (42), we herein show the use of universal cell products in immunocompetent allogeneic recipients.

In order to support cardiac remuscularization, we then added equal amounts of CMs to the EC injections and again observed improved hemodynamic parameters with alloHIP cells as compared to allo cells. The alloHIP cell grafts survived in allogeneic

recipients and engrafted in the cardiac wall. A recent study indicated the contribution of transplanted cardiomyocytes to improved vascularity in a preclinical model of myocardial infarction as a mechanism to enhance cardiac function (43). There was no obvious added benefit to hemodynamic recovery by the cotransplanted alloHIP CMs in our study, maybe because the cell amounts used were not sufficient to achieve relevant remuscularization. Alternatively, there might not be a linear correlation between cell amount and cardiac recovery as hinted by the similar results achieved across a wide range of cell doses reported by other groups (44, 45). Beneficial effects from transplantation of xenogeneic (43, 46, 47) or allogeneic (48, 49) iCMs had so far only been shown in animals treated with heavy immunosuppression. Here we report success with allogeneic cells in immunocompetent mice and show no measurable immune activation. Large-scale manufacturing of iCMs has been developed (50) and cell delivery to the heart is established (51). With the immunological barrier for immunosuppression-free allogeneic cell transplantation resolved, iCM engraftment issues, including avoidance of arrhythmogenic complications as described in pig and nonhuman primate studies, need to be overcome (47, 48).

Since the first description of HIP cells, many different derivatives and implant sites have been tested, and we have not yet encountered an allogeneic immune response. Universal off-the-shelf cell products can be a major factor in preventing spiraling of costs for regenerative medicine as has been encountered with novel cancer therapeutics (52). This study therefore provides a realistic outlook for advancements of affordable allogeneic cell therapies for large patient populations.

## Materials and Methods

**Mice.** BALB/c (BALB/cJ, H2<sup>b</sup>), C57BL/6 (C57BL/6J, H2<sup>b</sup>), and SCID-beige (CBySnm.CB17-Prkdcscid/J) (all 6 to 12 wk) were purchased from The Jackson Laboratory. *Serpina*<sup>-/-</sup> C57BL/6 mice were generated by C.M. as reported previously (10). The number of animals per experimental group is presented in each figure. Mice received humane care in compliance with the Guide for the Principles of Laboratory Animals. Animal experiments were approved by the University of California, San Francisco (UCSF) Institutional Animal Care and Use Committee and performed according to local guidelines.

**Mouse iPSC culture.** Mouse C57BL/6 iPSCs were generated from tail tip fibroblasts as reported previously (3). Briefly, iPSCs were grown in iPSC medium on confluent mouse embryonic fibroblast (MEF) feeder cells. Medium was changed daily, and cells were passaged every 2 to 3 d. Mouse iPSCs were cultured on gelatin (Millipore) without feeders prior to experiments. Cell cultures were regularly screened for mycoplasma infections using the MycoAlert Kit (Lonza). Gene editing was performed as described previously (3).

**Transduction to Express Firefly Luciferase.** A total of 100,000 iPSCs were plated in gelatin-coated six-well plates and incubated overnight at 37 °C at 5% CO<sub>2</sub>. Media were changed the next morning and 200  $\mu$ L of FLuc lentiviral particles (10<sup>7</sup> IFU/mL, GenTarget) was added. After 36 h, 1 mL of cell media was added and the next day, a complete media change was performed. After another 2 d, luciferase expression was confirmed by adding D-luciferin (Promega). Signals were quantified with the Ami HT system (Spectral Instruments Imaging) in maximum photons s<sup>-1</sup> cm<sup>-2</sup> per steradian.

**Derivation and Characterization of iECs.** Mouse iPSCs were plated on gelatin in 6-well plates and maintained in iPSC media until they reached 60% confluency. Differentiation into iECs was performed as described in detail previously (3). Cells after differentiation underwent magnetic-activated cell sorting (MACS) purification using negative selection with anti-CD15 mAb-coated magnetic microbeads (Miltenyi). The iEC phenotype was confirmed by immunofluorescence (IF) for expression of Cd31 (ab28364, Abcam), and VE-cadherin (sc-6458, Santa Cruz Biotechnology) with secondary antibodies conjugated with AF488 or AF555 (Invitrogen). For the tube formation assay, 2.5  $\times$  10<sup>5</sup> iECs were stained with 5  $\mu$ M carboxyfluorescein succinimidyl ester (CFSE) and 0.1  $\mu$ g/mL Hoechst (both Thermo Fisher) for 10 min at room temperature and plated on 10 mg/mL undiluted Matrigel (356231, Corning) in 24-well plates. After 48 h, tube formations were visualized by IF. PCR was performed using primers VE-cadherin (Cdh5): (forward) 5'-GGATGACAGAGGCTCACAGAG-3', (reverse) 5'-CTG

GCGGTTACCTGGACT-3'. All other primers were included in the Mouse ES/iPS Cell Pluripotency RT-PCR Kit (ASK-6001, Applied StemCell).

**Gene Editing to Generate A1AT-Secreting iECs.** The *Serpina1e* (NM\_009247.2) cDNA was synthesized and cloned into a lentivirus with zeocin resistance (Thermo Fisher Scientific), which was used to transduce B6 and B6HIP iECs followed by antibiotic selection and expansion of B6<sup>51e</sup> and B6HIP<sup>51e</sup> iECs. The cells were then transduced to express allogeneic major (H-2K<sup>d</sup>) and minor (BALB/c variant of Co3) histocompatibility antigens using lentiviral particles (both Gentarget). These MHC-engineered <sup>e</sup>allo<sup>51e</sup> and <sup>e</sup>alloHIP<sup>51e</sup> iECs were thus allogeneic to the *Serpina*<sup>-/-</sup> C57BL/6 recipient mice.

**Derivation and Characterization of iCMs.** Differentiation into iCMs was performed as described in detail previously (3). Beating cells developed around days 11 to 14. Cells then underwent MACS purification using negative selection with anti-CD15 mAb-coated magnetic microbeads (Miltenyi). IF staining was performed using primary antibodies against alpha-sarcomeric actinin (EA-53, Abcam) and Troponin I (ab47003, Abcam) followed by the corresponding secondary antibodies conjugated with AF488 or AF555 (Invitrogen). The following primers were Gata4: (forward) 5'-CTGTCATCTCACTATGGGCA-3', (reverse) 5'-CCAAGTCCGAGCAGGAATT-3'; Myh6: (forward) 5'-ATCATCCCAACGAGCGAAAG-3', (reverse) 5'-AAGTCCCATAGAGAAATGCGG-3'. All other primers were included in the Mouse ES/iPS Cell Pluripotency RT-PCR Kit (ASK-6001, Applied StemCell).

**Flow Cytometry.** Mouse iECs were labeled with a goat anti-mouse VE-cadherin primary antibody (sc-6458, Santa Cruz Biotechnology) and AF488 (A11055, Invitrogen) or AF555 (A21432, Invitrogen) conjugated donkey anti-goat IgG secondary antibodies (both Invitrogen). Mouse iCMs were treated with Fix/Perm solution (BD Bioscience) for 20 min at room temperature. The cells were subsequently washed twice and then labeled with fluorescein isothiocyanate (FITC)-conjugated anti-cardiac troponin T antibody (130-119-575, clone REA400, Miltenyi) or FITC-conjugated recombinant human IgG1 isotype control antibody (130-118-354, clone: REA293, Miltenyi). The expression of VE-cadherin and troponin T was assessed by flow cytometry (FACS Aria Fusion or FACS Calibur, BD Bioscience) and the analysis was performed using FlowJo software.

**Elispot assays.** For unidirectional Enzyme-Linked ImmunoSpot (Elispot) assays, recipient splenocytes were isolated from spleen 6 d after cell injection and used as responder cells (3). Donor cells were mitomycin-treated (50  $\mu$ g/mL for 30 min) and used as stimulator cells. A total of 100,000 stimulator cells were incubated with 1  $\times$  10<sup>6</sup> recipient responder splenocytes for 24 h and IFN- $\gamma$  and IL-4 spot frequencies were enumerated using an Elispot plate reader (AID GmbH).

**Donor-Specific Antibodies.** Sera from recipient mice were decanted by heating to 56 °C for 30 min as described previously (3). Equal amounts of sera and cell suspensions (5  $\times$  10<sup>6</sup> /mL) were incubated for 45 min at 4 °C. Cells were labeled with FITC-conjugated goat anti-mouse IgM (Sigma-Aldrich) and analyzed by flow cytometry (FACS Calibur, BD Bioscience).

**Graft Survival by BLI.** D-luciferin firefly potassium salt (375 mg/kg; Biosynth AG) was dissolved in phosphate-buffered saline (PBS) (pH 7.4, Gibco, Invitrogen) and injected intraperitoneally (i.p.) (250  $\mu$ L per mouse) into anesthetized mice. Animals were imaged using the Ami HT system (Spectral Instruments Imaging). Region of interest (ROI) bioluminescence was quantified in units of maximum photons s<sup>-1</sup> cm<sup>-2</sup> per steradian. The maximum signal from a ROI was measured using Aura Image software (Spectral Instruments Imaging).

**Histology.** Tissue was recovered and fixed in 4% paraformaldehyde in PBS for 24 h. Samples were dehydrated, embedded in paraffin, and cut into sections of 5  $\mu$ m thickness. For immunofluorescence, sections were rehydrated and underwent antigen retrieval and blocking. Samples were incubated with antibodies against luciferase (ab21176), VE-cadherin (sc-6458), or alpha-sarcomeric actinin (EA-53, Abcam) and a corresponding secondary antibody was conjugated with AF488 or AF555 (Invitrogen). Cell nuclei were counterstained with DAPI and images taken with a Leica SP5 laser confocal microscope (Leica).

**Mouse Hindlimb Ischemia Model.** BALB/c mice were anesthetized with isoflurane. One million iECs were resuspended in 100  $\mu$ L saline and mixed with 100  $\mu$ L Matrigel (Corning, 356231) prior to the injection. The femoral artery was exposed through a 2-cm skin incision. The femoral artery was ligated with 6-0 prolene (Ethicon) and excised from its proximal origin as a branch of the external iliac artery to the distal point where it bifurcates. Eight injections with



25  $\mu$ L cell suspension were made with a Hamilton 22-G syringe, intramuscularly around the removed artery. A laser Doppler perfusion imager (moorLDI2-IR, Moor Instruments) was used to sequentially measure the blood flow in the hindlimbs over time. Digital color-coded images were analyzed to quantify the blood flow in the region from the knee joint to the toe, and the mean perfusion units were calculated.

**Mouse Lung Emphysema Model.** WT or *Serpina<sup>1</sup>*<sup>-/-</sup> C57BL/6 mice received two sequential orotracheal doses of LPS to induce lung disease with 1  $\mu$ g in 30  $\mu$ L saline for the first dose and 0.5  $\mu$ g in 30  $\mu$ L for the second dose (serotype 055:B5 *Escherichia coli* LPS, L2880; Sigma-Aldrich). Mice were anesthetized with an i.p. dose of a ketamine/xylazine mixture (90 mg/kg of ketamine and 4.5 mg/kg of xylazine) and placed in dorsal recumbency on a rodent work stand (Bainbridge Scientific) and intubated. Following instillation, mice received three ventilations with 0.2 mL of air.

**Quantification of A1AT.** The mouse A1AT ELISA Kit (ab205088, Abcam) was used according to the manufacturer's protocol. Briefly, serum samples or cell culture supernatant were incubated with an AAT antibody, followed by incubation with a horseradish peroxidase (HRP)-conjugated secondary antibody and a peroxidase substrate. A microplate reader with an absorbance of OD450 nm (Molecular Devices) was used to measure the AAT level of the standards and study samples.

**FlexiVent.** Mice were anesthetized as outlined above. A tracheotomy was performed, and a precalibrated cannula was introduced into the trachea. The mouse was then placed on a computer-controlled piston-ventilator FlexiVent system (Scireq) and ventilated at a tidal volume of 10 mL/kg, at a rate of 150 breaths per minute, and a positive end expiratory pressure of 3 mmHg. Neuromuscular blockade with pancuronium bromide (2.5 mg/kg) was given to prevent spontaneous respiratory effort. Measurements were obtained as previously described (10).

**Lung Stereology.** Immediately following measurements of lung mechanics (FlexiVent), lungs were harvested for stereological analysis. The chest was opened and the pulmonary circulation flushed via right ventricular puncture with 10 mL cold PBS. The degassed lung was inflated with 1% ultra-low temperature gel agarose (Sigma-Aldrich) in neutral buffered paraformaldehyde (4%) to 25 cm pressure. Subsequently, lung tissues were oriented randomly in cassettes and embedded in paraffin, followed by sectioning started at random depth at a uniform thickness (5  $\mu$ m). Slides were stained with hematoxylin and eosin and 10 randomly oriented nonoverlapping fields from each section were photographed. Lung morphology was quantified using Stepanizer software (<https://www.stepanizer.com/>). Surrogate markers for lung morphology were calculated as follows (53, 54): Volume fraction of alveolar septal tissue:  $VV(\text{sept}/\text{par}) = \sum P(\text{sept}) / \sum P(\text{par})$ , fraction of alveolar volume:  $VV(\text{alv}/\text{par}) = \sum P(\text{alv}) / \sum P(\text{par})$ , surface density of alveolar septa:  $SV(\text{sept}/\text{par}) = (2 \times \sum \bar{N}(\sum P(\text{par}) \times l/p))$ , mean linear intercept:  $Lm = 2 \cdot k \cdot d \cdot P(\text{asp}) / l(A)$ .

**Mouse Myocardial Cryoinfarction Model.** A recently developed cryoinjury model was used (55). Briefly, after induction of analgesia and anesthesia, the mice

were intubated and a right thoracotomy was performed. A mini-Goldstein retractor (Fine Science Tools) was used to spread the ribs. With the blunt forceps, the pericardium was opened, and the heart was exposed. Cryoinfarction was produced by applying a cryoprobe of 3 mm in diameter (Cry-AC-3 B-800, Brymill Cryogenic Systems) to the anterolateral LV free wall followed by freezing for 10 s. The position of the probe was carefully chosen using the left anterior descending artery, the left atrium, and pulmonary artery as anatomic landmarks. Rinsing with saline at room temperature allowed nontraumatic detachment of the probe from the LV wall after the freezing. A total of 500,000 iECs and 500,000 iCMs were resuspended in 20  $\mu$ L saline, and 5  $\mu$ L Matrigel (356231, Corning) was added to the cells prior to the injection. Two injections were made with a Hamilton 30-G syringe both anterior and lateral to the infarction area.

**Pressure–Volume Loop (PV Loop).** PV loops of the LV were acquired and analyzed as previously described (56). Briefly, hemodynamic measurements were performed using a 1.2 Fr PV conductance catheter with the ADV500 PV measurement system (Transonic). Mice received buprenorphine (0.1 mg/kg) subcutaneously (s.c.) before initiating 5% (vol) isoflurane inhalation and were then mechanically ventilated and maintained at 0.5 to 1% (vol) isoflurane during the surgical procedure. An incision was performed above the xyphoid process, until the diaphragm became clearly visible from beneath. After cutting through the diaphragm to expose the heart, a stab wound near the apex was made using a 27-G needle. The PV catheter tip was inserted into the LV. After stabilization of the signal for 10 min, baseline PV loops at steady state or at varying preloads during the inferior vena cava occlusions were recorded. LabChart v.8 software (AdInstruments) was used for data analysis.

**Statistics.** All data are expressed as mean  $\pm$  SD or in box plot graphs showing the median and the minimum to maximum range. Intergroup differences were appropriately assessed by either unpaired Student's *t* test or one-way analysis of variance (ANOVA) with Bonferroni post hoc test.

**Data Availability.** All study data are included in the article and/or *SI Appendix*.

**ACKNOWLEDGMENTS.** We thank C. Pahrman for overall assistance with cell culture and experiments. Special thanks go to J. Wu (Stanford Cardiovascular Institute, Stanford University School of Medicine) for providing the mouse iPSCs. Special thanks also go to Keith Copeland and Bo Nelson (Spectral Instruments, Inc.) for their technical support. Medical illustrations were provided by Justin A. Klein, Mito Pop. We acknowledge the Parnassus Flow Cytometry Core, supported in part by Grant NIH P30 DK063720 and by NIH S10 Instrumentation Grant S10 15100D021822-01. D.W. was supported by the Max Kade Foundation. L.L.L. is an American Cancer Society Professor funded by NIH A1068129 and in part by the Parker Institute for Cancer Immunotherapy. The study was partially supported by the DZHK (German Centre for Cardiovascular Research), S.S. and T.D. received funding from the California Institute for Regenerative Medicine (Grant DISC1-09984) and from the National Heart, Lung, and Blood Institute of the NIH under Award R01HL140236. The contents of this publication are solely the responsibility of the authors and do not necessarily represent the official views of the NIH, California Institute for Regenerative Medicine, or other agencies of the state of California.

1. Y. Y. Lipsitz *et al.*, A roadmap for cost-of-goods planning to guide economic production of cell therapy products. *Cytotherapy* **19**, 1383–1391 (2017).
2. Y. Y. Lipsitz, P. Bedford, A. H. Davies, N. E. Timmins, P. W. Zandstra, Achieving efficient manufacturing and quality assurance through synthetic cell therapy design. *Cell Stem Cell* **20**, 13–17 (2017).
3. T. Deuse *et al.*, Hypoimmunogenic derivatives of induced pluripotent stem cells evade immune rejection in fully immunocompetent allogeneic recipients. *Nat. Biotechnol.* **37**, 252–258 (2019).
4. G. G. Gornaluse *et al.*, HLA-E-expressing pluripotent stem cells escape allogeneic responses and lysis by NK cells. *Nat. Biotechnol.* **35**, 765–772 (2017).
5. A. Aicher *et al.*, Essential role of endothelial nitric oxide synthase for mobilization of stem and progenitor cells. *Nat. Med.* **9**, 1370–1376 (2003).
6. T. M. Schwarz *et al.*, Vascular incorporation of endothelial colony-forming cells is essential for functional recovery of murine ischemic tissue following cell therapy. *Arterioscler. Thromb. Vasc. Biol.* **32**, e13–e21 (2012).
7. J. K. Park, T. W. Lee, E. K. Do, H. J. Moon, J. H. Kim, Role of Notch1 in the arterial specification and angiogenic potential of mouse embryonic stem cell-derived endothelial cells. *Stem Cell Res. Ther.* **9**, 197 (2018).
8. N. Prasain *et al.*, Differentiation of human pluripotent stem cells to cells similar to cord-blood endothelial colony-forming cells. *Nat. Biotechnol.* **32**, 1151–1157 (2014).
9. J. Yu *et al.*, Endothelial nitric oxide synthase is critical for ischemic remodeling, mural cell recruitment, and blood flow reserve. *Proc. Natl. Acad. Sci. U.S.A.* **102**, 10999–11004 (2005).
10. F. Borel *et al.*, Editing out five *Serpina1* paralogs to create a mouse model of genetic emphysema. *Proc. Natl. Acad. Sci. U.S.A.* **115**, 2788–2793 (2018).
11. T. Deuse *et al.*, De novo mutations in mitochondrial DNA of iPSCs produce immunogenic neoepitopes in mice and humans. *Nat. Biotechnol.* **37**, 1137–1144 (2019).
12. M. R. Nehler *et al.*, Epidemiology of peripheral arterial disease and critical limb ischemia in an insured national population. *J. Vasc. Surg.* **60**, 686–695.e2 (2014).
13. L. Norgren *et al.*, TASC II Working Group, Inter-society consensus for the management of peripheral arterial disease. *Int. Angiol.* **26**, 81–157 (2007).
14. H. Reinecke *et al.*, Peripheral arterial disease and critical limb ischaemia: Still poor outcomes and lack of guideline adherence. *Eur. Heart J.* **36**, 932–938 (2015).
15. M. Rigato, M. Monami, G. P. Fadini, Autologous cell therapy for peripheral arterial disease: Systematic review and meta-analysis of randomized, nonrandomized, and noncontrolled studies. *Circ. Res.* **120**, 1326–1340 (2017).
16. S. Misra *et al.*, American Heart Association Council on Peripheral Vascular Disease; Council on Clinical Cardiology; Council on Cardiovascular and Stroke Nursing. Perfusion assessment in critical limb ischemia: Principles for understanding and the development of evidence and evaluation of devices: A scientific statement from the American Heart Association. *Circulation* **140**, e657–e672 (2019).
17. F. Dick *et al.*, Basic control of reperfusion effectively protects against reperfusion injury in a realistic rodent model of acute limb ischemia. *Circulation* **118**, 1920–1928 (2008).
18. R. Lozano *et al.*, Global and regional mortality from 235 causes of death for 20 age groups in 1990 and 2010: A systematic analysis for the global burden of disease study 2010. *Lancet* **380**, 2095–2128 (2012).
19. A. S. Buist *et al.*, BOLD Collaborative Research Group, International variation in the prevalence of COPD (the BOLD Study): A population-based prevalence study. *Lancet* **370**, 741–750 (2007).

20. D. A. Lomas, E. K. Silverman, The genetics of chronic obstructive pulmonary disease. *Respir. Res.* **2**, 20–26 (2001).
21. C. M. Greene *et al.*,  $\alpha$ 1-Antitrypsin deficiency. *Nat. Rev. Dis. Primers* **2**, 16051 (2016).
22. M. Miravittles *et al.*, European respiratory society statement: Diagnosis and treatment of pulmonary disease in  $\alpha$ 1-antitrypsin deficiency. *Eur. Respir. J.* **50**, 1700610 (2017).
23. D. Weill *et al.*, A consensus document for the selection of lung transplant candidates: 2014—An update from the Pulmonary Transplantation Council of the International Society for Heart and Lung Transplantation. *J. Heart Lung Transplant.* **34**, 1–15 (2015).
24. M. D. Wevers *et al.*, Replacement therapy for alpha 1-antitrypsin deficiency associated with emphysema. *N. Engl. J. Med.* **316**, 1055–1062 (1987).
25. P. C. Getzschke, H. K. Johansen, Intravenous alpha-1 antitrypsin augmentation therapy for treating patients with alpha-1 antitrypsin deficiency and lung disease. *Cochrane Database Syst. Rev.* **9**, CD007851 (2016).
26. K. R. Chapman *et al.*, RAPID Trial Study Group, Intravenous augmentation treatment and lung density in severe  $\alpha$ 1 antitrypsin deficiency (RAPID): A randomised, double-blind, placebo-controlled trial. *Lancet* **386**, 360–368 (2015).
27. K. Ni, K. A. Serban, C. Batra, I. Petrache, Alpha-1 antitrypsin investigations using animal models of emphysema. *Ann. Am. Thorac. Soc.* **13** (suppl. 4), S311–S316 (2016).
28. T. Vos *et al.*, Years lived with disability (YLDs) for 1160 sequelae of 289 diseases and injuries 1990–2010: A systematic analysis for the global burden of disease study 2010. *Lancet* **380**, 2163–2196 (2012).
29. D. Mozaffarian *et al.*, Writing Group Members, American Heart Association Statistics Committee, Stroke Statistics Subcommittee, Heart disease and stroke statistics-2016 update: A report from the American Heart Association. *Circulation* **133**, e38–e360 (2016).
30. J. Fang, G. A. Mensah, J. B. Croft, N. L. Keenan, Heart failure-related hospitalization in the U.S., 1979 to 2004. *J. Am. Coll. Cardiol.* **52**, 428–434 (2008).
31. P. K. Nguyen, J. W. Rhee, J. C. Wu, Adult stem cell therapy and heart failure, 2000 to 2016: A systematic review. *JAMA Cardiol.* **1**, 831–841 (2016).
32. S. A. Fisher, C. Doree, A. Mathur, E. Martin-Rendon, Meta-analysis of cell therapy trials for patients with heart failure. *Circ. Res.* **116**, 1361–1377 (2015).
33. J. Kandala *et al.*, Meta-analysis of stem cell therapy in chronic ischemic cardiomyopathy. *Am. J. Cardiol.* **112**, 217–225 (2013).
34. F. Fernández-Avilés *et al.*, TACTICS (Transnational Alliance for Regenerative Therapies in Cardiovascular Syndromes) Writing Group, Authors/Task Force Members, Chairpersons, Basic Research Subcommittee, Translational Research Subcommittee, Challenges of Cardiovascular Regenerative Medicine Subcommittee, Tissue Engineering Subcommittee, Delivery, Navigation, Tracking and Assessment Subcommittee, Clinical Trials Subcommittee, Regulatory and funding strategies subcommittee, Delivery, Navigation, Tracking and Assessment Subcommittee, Global position paper on cardiovascular regenerative medicine. *Eur. Heart J.* **38**, 2532–2546 (2017).
35. D. Abraham, L. Mao, Cardiac pressure-volume loop analysis using conductance catheters in mice. *J. Vis. Exp.* ((103), 52942. (2015).
36. J. M. Nielsen *et al.*, Left ventricular volume measurement in mice by conductance catheter: Evaluation and optimization of calibration. *Am. J. Physiol. Heart Circ. Physiol.* **293**, H534–H540 (2007).
37. K. M. Shioura, D. L. Geenen, P. H. Goldspink, Assessment of cardiac function with the pressure-volume conductance system following myocardial infarction in mice. *Am. J. Physiol. Heart Circ. Physiol.* **293**, H2870–H2877 (2007).
38. D. A. Narmoneva, R. Vukmirovic, M. E. Davis, R. D. Kamm, R. T. Lee, Endothelial cells promote cardiac myocyte survival and spatial reorganization: Implications for cardiac regeneration. *Circulation* **110**, 962–968 (2004).
39. T. Deuse *et al.*, Hepatocyte growth factor or vascular endothelial growth factor gene transfer maximizes mesenchymal stem cell-based myocardial salvage after acute myocardial infarction. *Circulation* **120**(11 suppl.) S247–S254 (2009).
40. L. Gao *et al.*, Exosomes secreted by hiPSC-derived cardiac cells improve recovery from myocardial infarction in swine. *Sci. Transl. Med.* **12**, eaay1318 (2020).
41. J. Wang *et al.*, Human CD34+ cells in experimental myocardial infarction: Long-term survival, sustained functional improvement, and mechanism of action. *Circ. Res.* **106**, 1904–1911 (2010).
42. A. A. Quyyumi *et al.*, PreSERVE-AMI: A randomized, double-blind, placebo-controlled clinical trial of intracoronary administration of autologous CD34+ cells in patients with left ventricular dysfunction post STEMI. *Circ. Res.* **120**, 324–331 (2017).
43. L. W. van Laake *et al.*, Human embryonic stem cell-derived cardiomyocytes survive and mature in the mouse heart and transiently improve function after myocardial infarction. *Stem Cell Res. (Amst.)* **1**, 9–24 (2007).
44. M. A. Lafamme *et al.*, Cardiomyocytes derived from human embryonic stem cells in pro-survival factors enhance function of infarcted rat hearts. *Nat. Biotechnol.* **25**, 1015–1024 (2007).
45. O. Caspi *et al.*, Transplantation of human embryonic stem cell-derived cardiomyocytes improves myocardial performance in infarcted rat hearts. *J. Am. Coll. Cardiol.* **50**, 1884–1893 (2007).
46. Y. W. Liu *et al.*, Human embryonic stem cell-derived cardiomyocytes restore function in infarcted hearts of non-human primates. *Nat. Biotechnol.* **36**, 597–605 (2018).
47. R. Romagnuolo *et al.*, Human embryonic stem cell-derived cardiomyocytes regenerate the infarcted pig heart but induce ventricular tachyarrhythmias. *Stem Cell Rep.* **12**, 967–981 (2019).
48. Y. Shiba *et al.*, Allogeneic transplantation of iPSC cell-derived cardiomyocytes regenerates primate hearts. *Nature* **538**, 388–391 (2016).
49. C. Mauritz *et al.*, Induced pluripotent stem cell (iPSC)-derived Flk-1 progenitor cells engraft, differentiate, and improve heart function in a mouse model of acute myocardial infarction. *Eur. Heart J.* **32**, 2634–2641 (2011).
50. K. K. Dunn, S. P. Palecek, Engineering scalable manufacturing of high-quality stem cell-derived cardiomyocytes for cardiac tissue repair. *Front. Med. (Lausanne)* **5**, 110 (2018).
51. Y. Mitsutake *et al.*, Improvement of local cell delivery using Helix transcatheter delivery catheter in a porcine heart. *Int. Heart J.* **58**, 435–440 (2017).
52. P. Workman, G. F. Draetta, J. H. M. Schellens, R. Bernards, How much longer will we put up with \$100,000 cancer drugs? *Cell* **168**, 579–583 (2017).
53. C. Brandenberger, M. Ochs, C. Muhlfeld, Assessing particle and fiber toxicology in the respiratory system: The stereology toolbox. *Part. Fibre Toxicol.* **12**, 35 (2015).
54. L. Knudsen, E. R. Weibel, H. J. Gundersen, F. V. Weinstein, M. Ochs, Assessment of air space size characteristics by intercept (chord) measurement: An accurate and efficient stereological approach. *J. Appl. Physiol.* (1985) **108**, 412–421 (2010).
55. D. Wang *et al.*, A cryoinjury model to study myocardial infarction in the mouse. *J. Vis. Exp.* ((151), <https://doi.org/10.3791/59958>). (2019).
56. P. Pacher, T. Nagayama, P. Mukhopadhyay, S. Bátkai, D. A. Kass, Measurement of cardiac function using pressure-volume conductance catheter technique in mice and rats. *Nat. Protoc.* **3**, 1422–1434 (2008).

Supplementary Information for

## **Hypoimmune iPSC-derived cell products treat cardiovascular and pulmonary diseases in immunocompetent allogeneic mice**

Tobias Deuse<sup>1\*</sup>, Grigol Tediashvili<sup>1,2\*</sup>, Xiaomeng Hu<sup>1,2,3,4\*</sup>, Alessia Gravina<sup>1</sup>, Annika Tamenang<sup>1,2</sup>, Dong Wang<sup>1</sup>, Andrew Connolly<sup>5</sup>, Christian Mueller<sup>6,7</sup>, Beñat Mallavia<sup>8</sup>, Mark R. Looney<sup>8,9</sup>, Malik Alawi<sup>10</sup>, Lewis L. Lanier<sup>11#</sup>, Sonja Schrepfer<sup>1,4#</sup>

<sup>1</sup> Department of Surgery, Division of Cardiothoracic Surgery, Transplant and Stem Cell Immunobiology (TSI)-Lab, University of California San Francisco, San Francisco, California, USA;

<sup>2</sup> Department of Cardiovascular Surgery, University Heart Center Hamburg, Hamburg, Germany;

<sup>3</sup> German Center for Cardiovascular Research (DZHK), partner site Hamburg/Kiel/Luebeck, Hamburg, Germany;

<sup>4</sup> Sana Biotechnology Inc., 1 Tower Place, South San Francisco, CA, USA.

<sup>5</sup> Department of Pathology, University of California-San Francisco, San Francisco, California, USA.

<sup>6</sup> Horae Gene Therapy Center, University of Massachusetts, Worcester, Massachusetts, USA;

<sup>7</sup> Department of Pediatrics, University of Massachusetts, Worcester, Massachusetts, USA;

<sup>8</sup> Department of Medicine, University of California San Francisco, San Francisco, California, USA;

<sup>9</sup> Department of Laboratory Medicine, University of California San Francisco, San Francisco, California, USA;

<sup>10</sup> Bioinformatics Core, University Medical Center Hamburg-Eppendorf, Hamburg, Germany;

<sup>11</sup> Department of Microbiology and Immunology and the Parker Institute for Cancer Immunotherapy, University of California San Francisco, San Francisco, California, USA.

\*Authors share first authorship

#Authors share senior authorship

**Corresponding author:** Sonja Schrepfer

**Email:** Sonja.Schrepfer@ucsf.edu

**This PDF file includes:**

Figures S1 to S7

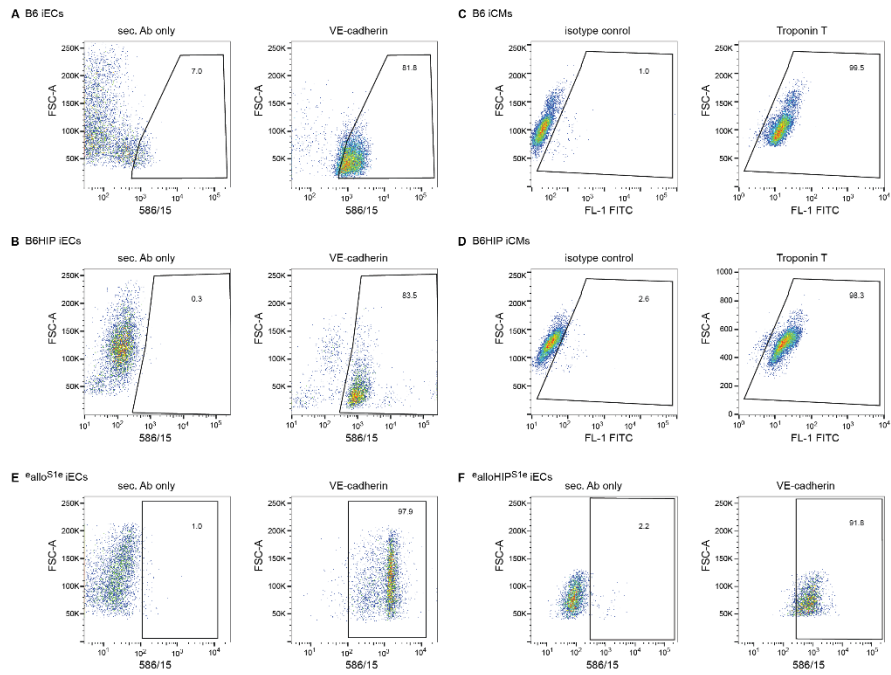


**Fig. S1: Purity of iECs and iCMs.** (A-F) B6 iECs (A) or B6HIP iECs (B), <sup>e</sup>allo<sup>S1e</sup> iECs (E) or <sup>e</sup>alloHIP<sup>S1e</sup> iECs (F) underwent quality control by flow cytometry. Successfully differentiated iECs were defined as being VE-cadherin+ (representative scatter blots from 3 independent experiments). Similarly, B6 iCMs (C) or B6HIP (D) iCMs were tested for their troponin T expression (representative scatter blots from 3 independent experiments).

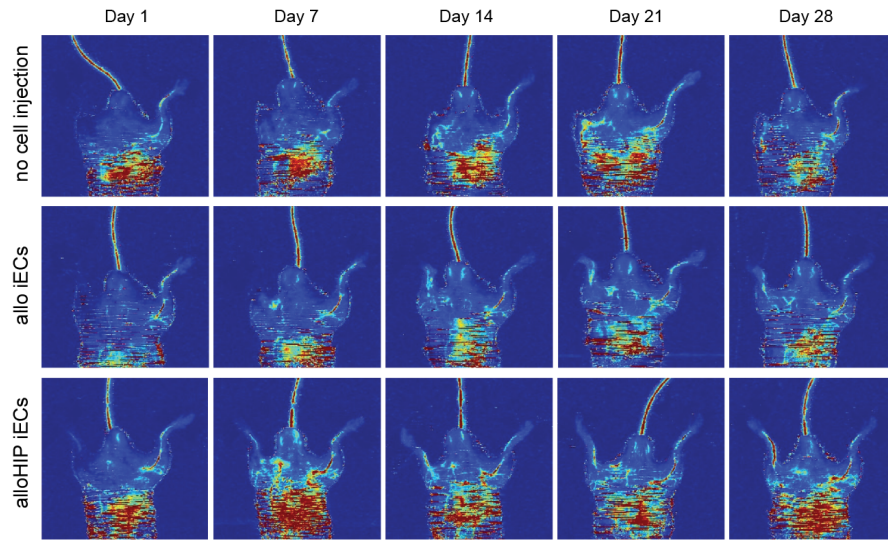


**Fig. S2: Hindlimb doppler.** Limb perfusion in mice with CLI was sequentially assessed by laser Doppler imaging. Five time points were picked after ligation and excision of the left proximal superficial femoral artery (representative pictures of 15 animals with no cell injection, 5 animals in the allo iEC group and 15 animals in the alloHIP iEC group).

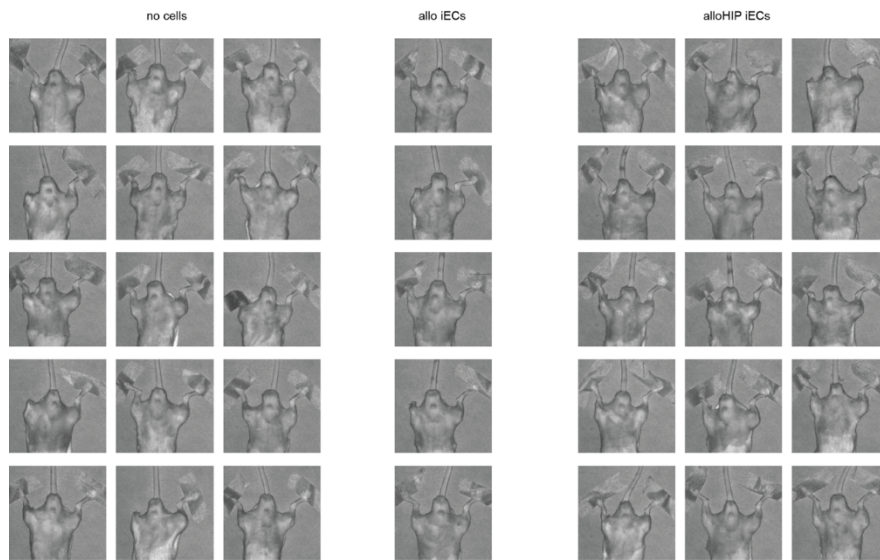


**Fig. S3:** *Hindlimb status.* After 28 days, the ischemic hindlimbs were assessed and photographed. All animals are shown.

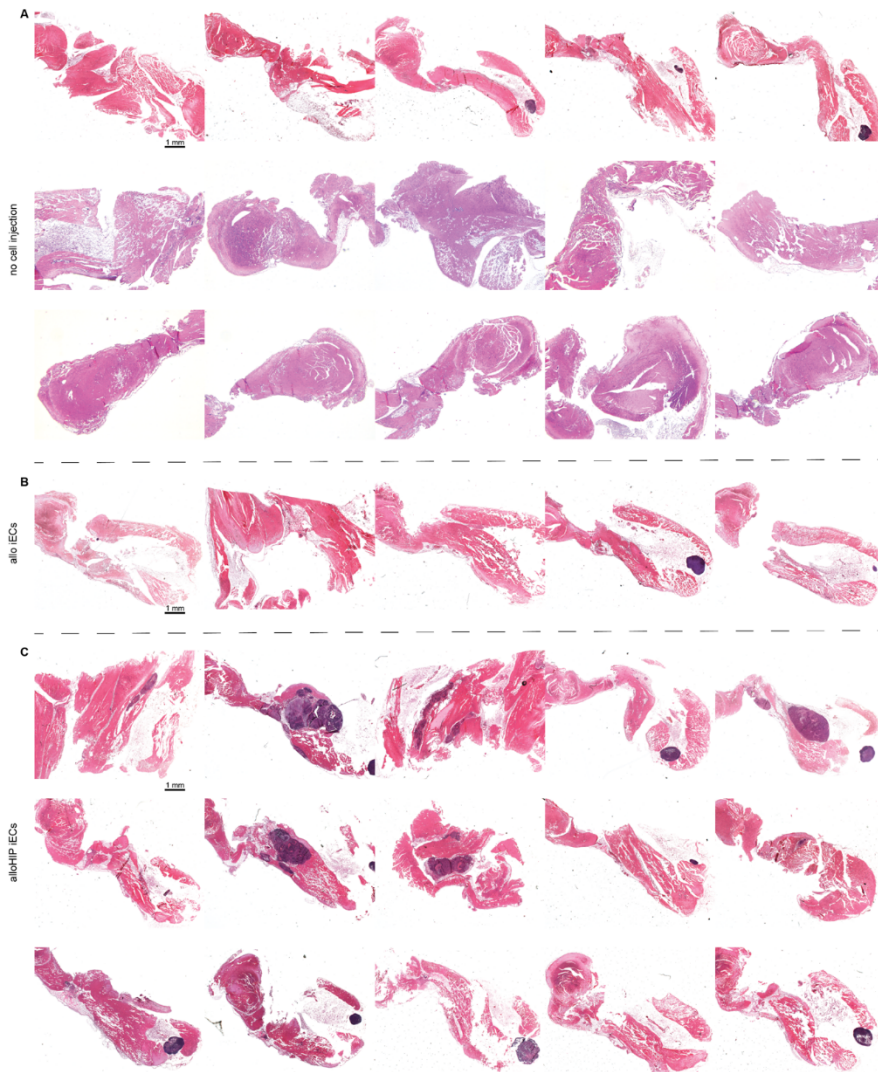


**Fig. S4:** *Hindlimb histology.* (A-C) The groin and thigh areas around the resected femoral artery, which contain the cell injections, were recovered, serially cut and stained with hematoxylin and eosin. Sections through the middle of this area at similar anatomic levels are shown for all animals in the no cell injection group (A), the allo iEC group (B) and the alloHIP iEC group (C).

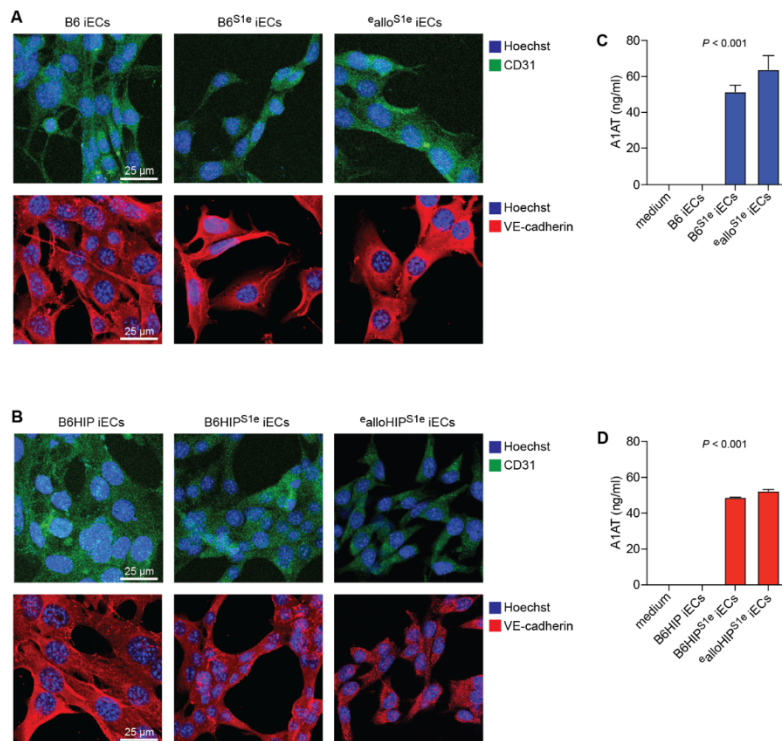


**Fig. S5:** A1AT-releasing <sup>e</sup>allo<sup>S1e</sup> and <sup>e</sup>alloHIP<sup>S1e</sup> iECs. (A and B) B6, B6<sup>S1e</sup>, and <sup>e</sup>allo<sup>S1e</sup> iECs (A) or B6HIP, B6HIP<sup>S1e</sup>, and <sup>e</sup>alloHIP<sup>S1e</sup> iECs (B) were grown in culture and shared typical endothelial cell features (representative pictures of 2 independent experiments). (C and D) A total of  $1.5 \times 10^5$  B6, B6<sup>S1e</sup>, and <sup>e</sup>allo<sup>S1e</sup> iECs (C) or B6HIP, B6HIP<sup>S1e</sup>, and <sup>e</sup>alloHIP<sup>S1e</sup> iECs (D) were cultured for 24 h in medium. The A1AT concentration was then assessed by Elisa (mean  $\pm$  s.d., 3 independent experiments, ANOVA).



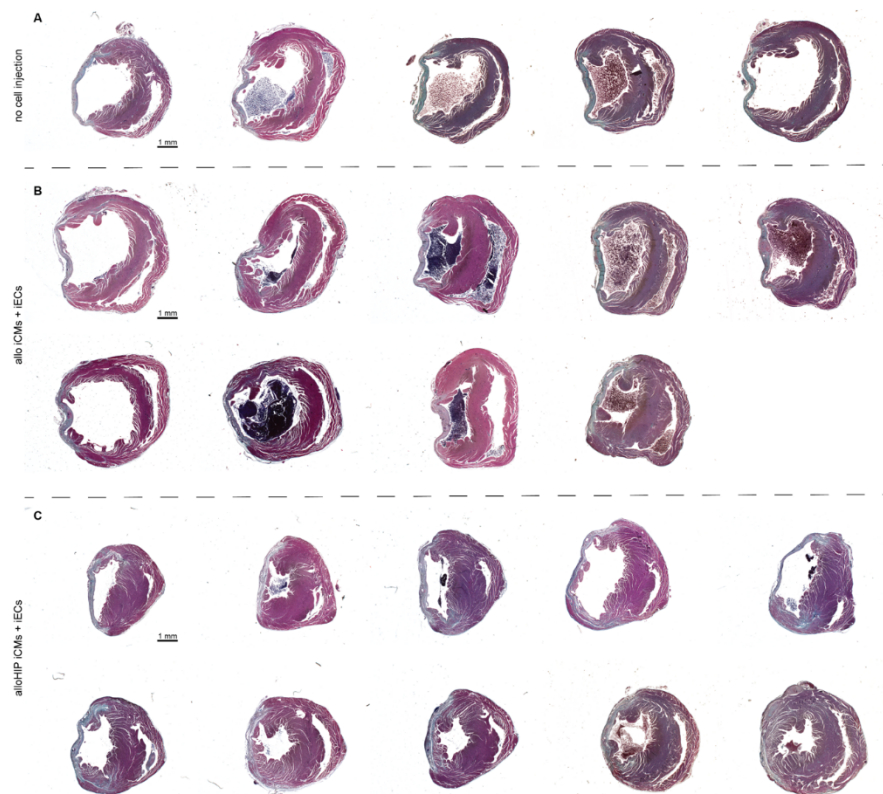


**Fig. S6:** *Histological evaluation of hearts.* (A-C) Explanted hearts were serially sectioned and stained with Masson's Trichrome. Sections through the mid cavity are shown for all animals in the no cell injection group (A), the allo iCM + iEC group (B) and the alloHIP iCM + iEC group (C).

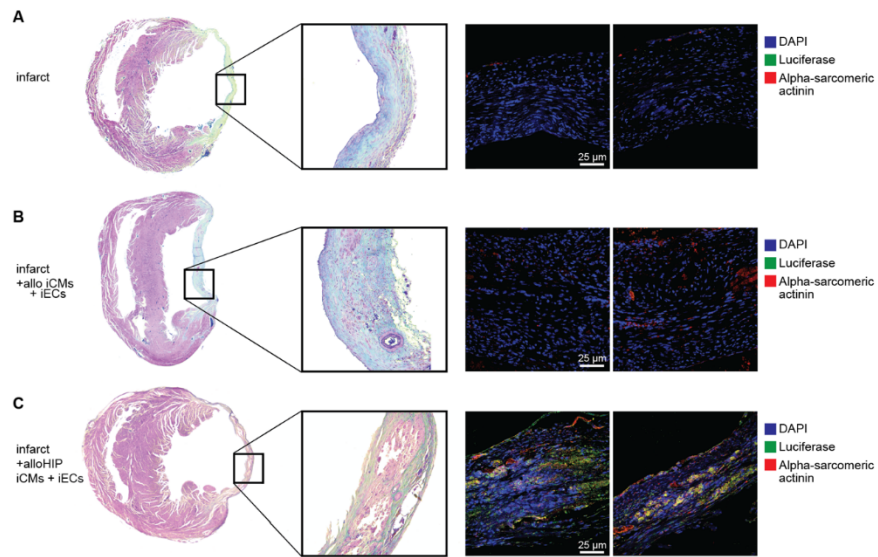


**Fig. S7:** *Histological evaluation of iCM engraftment.* (A-C) Sections of cryoinfarcted hearts without cell therapy (A) and infarcted heart that were injected with allo (B) or alloHIP iECs and iCMs (C) were stained for immunofluorescence. The scar areas were screened for transplanted cells. No FLuc<sup>+</sup> cells were found in hearts without cell injections or with injections of the allo cell mixture. In hearts injected with alloHIP cell mixture, we found several islands that stained positive for FLuc and alpha-sarcomeric actinin, suggesting engrafted alloHIP iCMs.

### **2.3 Protection of cell therapeutics from antibody-mediated killing by CD64 overexpression**

In Chapter 2 is presented the publication ‘Protection of cell therapeutics from antibody-mediated killing by CD64 overexpression’. The paper has been published in Nature Biotechnology in 2023. My contribution to this paper includes lentiviral transductions and cell sorting, immune killing assays, and imaging studies. This contribution resulted in a first authorship on the paper.

**Title:** Protection of cell therapeutics from antibody-mediated killing by CD64 overexpression

**Authors:** Alessia Gravina, Grigol Tediashvili, Raja Rajalingam, Zoe Quandt, Chad Deseinroth, Sonja Schrepfer, Tobias Deuse

**Journal:** Nature Biotechnology

**DOI:** 10.1038/s41587-022-01540-7



# Protection of cell therapeutics from antibody-mediated killing by CD64 overexpression

Received: 28 August 2021

Accepted: 3 October 2022

Published online: 02 January 2023

Check for updates

Alessia Gravina<sup>1</sup>, Grigol Tediashvili<sup>1</sup>, Raja Rajalingam<sup>2</sup>, Zoe Quandt<sup>3</sup>, Chad Deisenroth<sup>4</sup>, Sonja Schrepfer<sup>1</sup> & Tobias Deuse<sup>1</sup>✉

Allogeneic cell therapeutics for cancer therapy or regenerative medicine are susceptible to antibody-mediated killing, which diminishes their efficacy. Here we report a strategy to protect cells from antibody-mediated killing that relies on engineered overexpression of the IgG receptor CD64. We show that human and mouse iPSC-derived endothelial cells (iECs) overexpressing CD64 escape antibody-dependent cellular cytotoxicity (ADCC) and complement-dependent cytotoxicity from IgG antibodies in vitro and in ADCC-enabled mice. When CD64 expression was combined with hypimmune genetic modifications known to protect against cellular immunity, B2M<sup>-/-</sup>CIITA<sup>-/-</sup> CD47/CD64-transgenic iECs were resistant to both IgG antibody-mediated and cellular immune killing in vitro and in humanized mice. Mechanistic studies demonstrated that CD64 or its intracellularly truncated analog CD64t effectively capture monomeric IgG and occupy their F<sub>c</sub>, and the IgG bind and occupy their target antigens. In three applications of the approach, human CD64t-engineered thyroid epithelial cells, pancreatic beta cells and CAR T cells withstood clinically relevant levels of graft-directed antibodies and fully evaded antibody-mediated killing.

The concept of antibody-mediated rejection (AMR) after solid organ transplantation became a focus in transplant research in the 1990s, decades after the concept of cellular rejection had been widely accepted. A hallmark of AMR is the presence of graft-specific antibodies<sup>1</sup> in combination with graft damage. The emergence of such antibodies occurs despite the use of guideline-driven systemic immunosuppression. Outside of transplantation, some autoimmune diseases are characterized by autoantibodies that mediate the destruction of the target cells and persist even after the affected cell population has vanished. The emergence of antibodies against allogeneic cell therapeutics has been observed in clinical trials<sup>2-4</sup>. Cancer therapy with chimeric

antigen receptor (CAR) T cells induces antibodies, especially if tumor cell types other than B cells or plasma cells are targeted<sup>5</sup>. It is, therefore, likely that most allogeneic cellular grafts for long-term regenerative or oncology indications in immunocompetent patients will eventually experience some form of antibody-mediated killing. We, therefore, sought to develop a gene engineering approach that provides antibody protection for cell therapeutics.

For both antibody-mediated cellular cytotoxicity (ADCC) and complement-dependent cytotoxicity (CDC), antibodies of the IgG class mediate target cell killing by binding an epitope via their antigen-binding fragments (F<sub>ab</sub>) and activating effector cells or

<sup>1</sup>Transplant and Stem Cell Immunobiology (TSI) Laboratory, Department of Surgery, University of California, San Francisco, San Francisco, CA, USA.

<sup>2</sup>Immunogenetics and Transplantation Laboratory, Department of Surgery, University of California, San Francisco, San Francisco, CA, USA. <sup>3</sup>Department of Medicine, Division of Diabetes, Endocrinology and Metabolism, University of California, San Francisco, San Francisco, CA, USA. <sup>4</sup>United States

Environmental Protection Agency, Center for Computational Toxicology & Exposure, Durham, NC, USA. ✉e-mail: [tobias.deuse@ucsf.edu](mailto:tobias.deuse@ucsf.edu)

complement via their free fragment crystallizable domain (F<sub>c</sub>). We hypothesized that forced overexpression of the high-affinity receptor for IgG F<sub>c</sub> (CD64) on graft cells would capture monomeric IgG F<sub>c</sub> and make F<sub>c</sub> inaccessible for effector cells or complement. IgG against epitopes expressed on these cells could bind and occupy those. We found that the protection that CD64 overexpression reliably established was effective against ADCC and CDC, was agnostic to the specific type of cell and was applicable to three clinically relevant cell therapeutics.

## Results

### CD64-expressing mouse iECs are protected from antibody-mediated killing

Mouse C57BL/6 (B6) induced pluripotent stem cells (iPSCs) were differentiated into B6 iECs, and the cells were transduced with lentiviral particles to express the mouse Cd64 transgene. B6 iECs<sup>CD64</sup> were able to bind free mouse IgG2a F<sub>c</sub> in a concentration-dependent manner (Supplementary Fig. 1a,b). In mice, IgG2a and IgG2b are the main antibody isotypes mediating ADCC and CDC. For these F<sub>c</sub> binding assays, antibodies are used that are specific for an epitope that is not expressed on the cells to avoid any specific F<sub>ab</sub> binding. The flow cytometry signal then only measures antibodies captured via F<sub>c</sub>. For *in vitro* killing assays, B6 iECs and B6 iECs<sup>CD64</sup> were grown on electrode plates for real-time impedance cytotoxicity assays with B6 natural killer (NK) cells as effector cells (ADCC) or B6 serum (CDC). In this highly sensitive assay, target cell death leads to a disruption of the cell covering of electrodes with a decrease of impedance and drop of the plotted cell index curve.

We used a mouse IgG2a antibody against the B6 major histocompatibility complex (MHC) haplotype H-2<sup>b</sup> and found that it effectively mediates ADCC and CDC against B6 iECs. Engineered B6 iECs<sup>CD64</sup> were fully protected against ADCC and CDC (Supplementary Fig. 1c,d).

In a next step, we modified B6 *B2m*<sup>-/-</sup> *Ciita*<sup>-/-</sup> Cd47<sup>-/-</sup> hypoinnate (HIP; Supplementary Fig. 2a) iECs<sup>CD64</sup> to additionally express human CD64 (B6 HIP iECs<sup>CD64</sup>). HIP cells are protected from allogeneic innate and adaptive immune cell killing<sup>6,7</sup> but are potentially susceptible to antibody-mediated killing. To design a very stringent model, target cells were additionally transduced to express human CD52, the target for the highly cytotoxic anti-CD52 antibody alemtuzumab (Supplementary Fig. 2b). B6 HIP iECs<sup>CD64</sup> showed human IgG1 F<sub>c</sub> capture ability in a concentration-dependent manner (Supplementary Fig. 2c). In ADCC and CDC assays with anti-CD52, B6 HIP iECs<sup>CD52</sup> were killed by mouse NK cells and complement even at low antibody concentrations. This confirmed the high cytotoxic capacity of alemtuzumab and its functional compatibility with mouse NK cells and complement. B6 HIP iECs<sup>CD52,CD64</sup> were fully resistant against ADCC and CDC across the anti-CD52 concentration spectrum (Supplementary Fig. 2d,e).

Next, grafts of 1 million firefly luciferase-positive (Luc<sup>+</sup>) B6 HIP iECs<sup>CD52</sup> and B6 HIP iECs<sup>CD52,CD64</sup> were transplanted subcutaneously into Rag-1 deficient mice. This strain lacks mature B and T cells but has functional NK cells<sup>8</sup> and serves well as an ADCC *in vivo* model. Two alemtuzumab doses at 1 mg each were injected into the peritoneum on post-transplant days 0 and 3. Graft survival was followed by bioluminescence imaging (BLI) (Supplementary Fig. 2f). We saw the B6 HIP iECs<sup>CD52</sup> grafts vanish within approximately 1 week, whereas B6 HIP iECs<sup>CD52,CD64</sup> grafts survived and were protected from ADCC (Supplementary Fig. 2g,h). The ability of CD64 to capture F<sub>c</sub> was thus shown to add antibody protection to mouse HIP cells *in vivo* and *in vitro*.

### CD64-expressing human iECs are protected from antibody-mediated killing

Human iECs of the HLA-A\*02:01 genotype were transduced to overexpress human CD64 using lentiviral particles, and cells with high CD64 expression (iECs<sup>CD64</sup>) were enriched using cell sorting (Fig. 1a). Their ability to capture human IgG1 F<sub>c</sub> in a concentration-dependent manner was shown (Fig. 1b). *In vitro* killing assays were performed using

a recombinant human anti-HLA-A2 IgG1 antibody<sup>9</sup> with human NK cells as effector cells (ADCC) or human serum (CDC). Whereas iECs underwent increasingly rapid killing via NK cell ADCC (Fig. 1c) and CDC (Fig. 1d) with increasing anti-HLA-A2 concentrations, iECs<sup>CD64</sup> were fully protected, and no target cell killing was observed. The anti-HLA-A2 antibody in CDC assays was added to complete human serum containing 6–16 mg ml<sup>-1</sup> of total IgG, so that it had to compete with all serum IgG for target cell CD64. To assess whether this antibody protection would hold up in patients experiencing clinically relevant AMR, we identified two transplant recipients with anti-HLA-A2 mean fluorescence intensities (MFIs) >10,000 in single-antigen bead assays (Fig. 1e,f) and clinical signs of AMR of their grafts. Patient serum samples were incubated with iECs and iECs<sup>CD64</sup> (Fig. 1g,h). Whereas iECs were very rapidly killed in this CDC assay, iECs<sup>CD64</sup> again were completely protected without any signs of cell damage, as shown by the steady impedance for 90 hours. To next evaluate non-HLA antibody killing, we used a recombinant human IgG1 antibody against MHC class I-related sequence A (MICA)<sup>10,11</sup>, which is constitutively expressed on iECs<sup>12–14</sup> (Supplementary Fig. 3a,b). We again observed that iECs were very susceptible to NK cell ADCC and CDC, whereas iECs<sup>CD64</sup> were fully protected. These experiments show that high CD64 expression can protect target cells from HLA and non-HLA antibody-mediated killing.

### Generation of completely immune-evasive human cells

Human *B2M*<sup>-/-</sup> *CITA*<sup>-/-</sup> CD47<sup>-/-</sup> (HIP) iECs<sup>CD64</sup> (Fig. 2a) are naturally protected from HLA antibodies given their lack of HLA class I and II expression. To confirm that, human iECs and human HIP iECs (both HLA-A2\*02:01) were incubated with serum from two more transplant recipients with high anti-HLA-A2 MFIs and clinical signs of AMR (Fig. 2b). We saw CDC killing of iECs but not of HIP iECs. The killing was faster in the serum with higher anti-HLA-A2 MFI levels (Fig. 2c). The non-HLA epitope MICA is constitutively expressed on human HIP iECs (Fig. 2d), which leaves them susceptible to anti-MICA antibodies. We then generated CD64-expressing HIP iECs (HIP iECs<sup>CD64</sup>), which were able to capture human IgG1 F<sub>c</sub> *in vitro* (Fig. 2e,f). As expected, HIP iECs underwent increasingly rapid NK cell ADCC and CDC (Fig. 2g,h) with increasing concentrations of the humanized IgG1 anti-MICA antibody. Human HIP iECs<sup>CD64</sup> were completely resistant against anti-MICA ADCC and CDC. Because both HIP iECs and HIP iECs<sup>CD64</sup> were also positive for the rhesus D blood type antigen, ADCC and CDC assays were performed with a humanized IgG1 anti-Rh(D) antibody (Supplementary Fig. 4a,b). Whereas HIP iECs were killed in both assays, HIP iECs<sup>CD64</sup> were resistant against anti-Rh(D) cytotoxicity. We next tested the binding affinities of IgG isotypes and found that CD64 shows high affinity to monomeric IgG1, IgG3 and IgG4 (Supplementary Fig. 3c,d). Although IgG1 is the most relevant antibody isotype in solid organ AMR, other isotypes have been documented<sup>15</sup>. Kidney transplant patients with donor-specific antibodies experiencing AMR were shown to predominantly have complement-fixing IgG1 and IgG3 for HLA and non-HLA antibodies<sup>16–18</sup>. In a clinical setting, CD64 overexpression should thus protect from the vast majority of human IgG.

We next aimed to verify antibody evasiveness with the highly cytotoxic human anti-CD52 IgG1 alemtuzumab and generated HIP iECs<sup>CD52</sup> and HIP iECs<sup>CD52,CD64</sup> that express its CD52 target (Fig. 3a,b). *In vitro* ADCC and CDC assays with alemtuzumab and allogeneic human NK cells confirmed the high cytotoxicity of alemtuzumab, already killing human HIP iECs<sup>CD52</sup> at 0.0001 µg ml<sup>-1</sup> (Fig. 3c,d). Human HIP iECs<sup>CD52,CD64</sup> on the other side were resistant against ADCC and CDC, thus withstanding 100,000-times higher alemtuzumab concentrations. In an NSG mouse *in vivo* killing assay, 5 million HIP iECs<sup>CD52</sup> and HIP iECs<sup>CD52,CD64</sup> with different fluorescence labels were simultaneously injected intraperitoneally together with 100 million allogeneic human NK cells or macrophages and alemtuzumab (Supplementary Fig. 5a). After 48 hours, the peritoneal cells were recovered, and we saw that, with increasing alemtuzumab concentrations, we almost exclusively

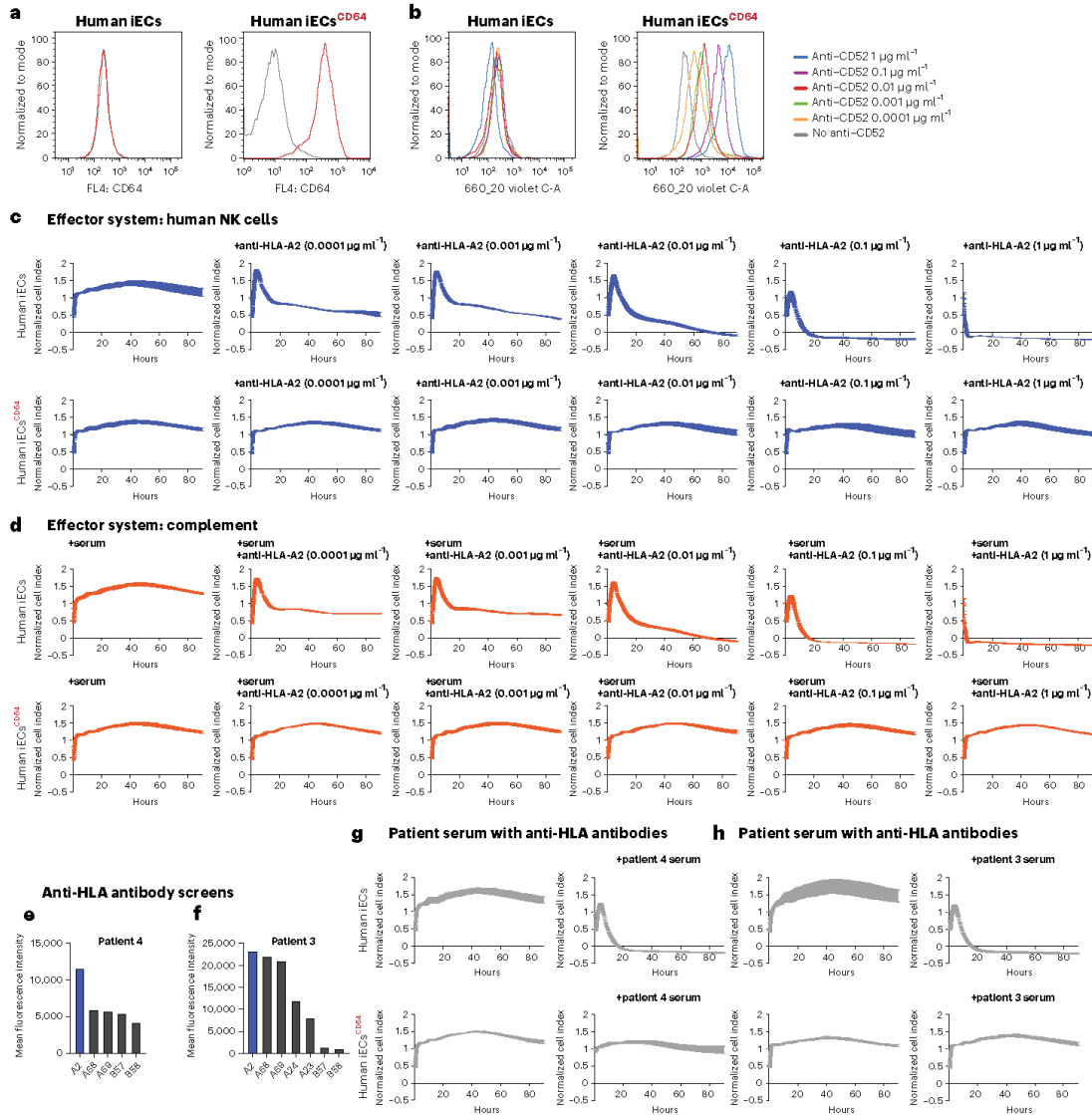


**Fig. 1 | Capturing of IgG<sub>Fc</sub> protects iECs from HLA antibody-mediated killing.** **a**, Flow cytometry histograms for CD64 expression on human iECs and iECs<sup>CD64</sup> (representative graph of two independent experiments). **b**, Flow cytometry histograms for the binding of free IgG1 Fc (anti-CD52, alemtuzumab; representative graph of two independent experiments). **c, d**, Human iECs and iECs<sup>CD64</sup> were challenged in impedance NK cell ADCC (**c**) and CDC (**d**) assays with

different concentrations of an anti-HLA-A2 IgG1 antibody (mean ± s.d.; three independent replicates per group and timepoint). **e, f**, Single antigen bead assay results for HLA class I and II antibodies in transplant recipients 4 (**e**) and 3 (**f**) experiencing AMR. **g, h**, Human iECs and iECs<sup>CD64</sup> were incubated with serum from patient 4 (**g**) and patient 3 (**h**) in impedance CDC assays (mean ± s.d.; three independent replicates per group and timepoint).

recovered HIP iECs<sup>CD52,CD64</sup>, whereas HIP iECs<sup>CD52</sup> had vanished (Supplementary Fig. 5b,c). We next assessed cell survival in an NSG mouse in vivo ADCC killing assay using BL1. A total of  $5 \times 10^4$  HIP iECs<sup>CD52</sup> or HIP iECs<sup>CD52,CD64</sup> were injected subcutaneously with 1 million human NK cells with or without alemtuzumab (Fig. 3e). Both cell populations showed consistent survival when no antibody was added. With

anti-CD52 administered at 1-mg doses on days 0, 1 and 2, HIP iECs<sup>CD52</sup> were expeditiously rejected (Fig. 3f). The survival of HIP iECs<sup>CD52,CD64</sup>, in contrast, remained completely unaffected (Fig. 3g). Together, these data show that CD64 expression is highly effective to prevent HIP iEC killing in vitro and in vivo by various non-HLA antibodies.

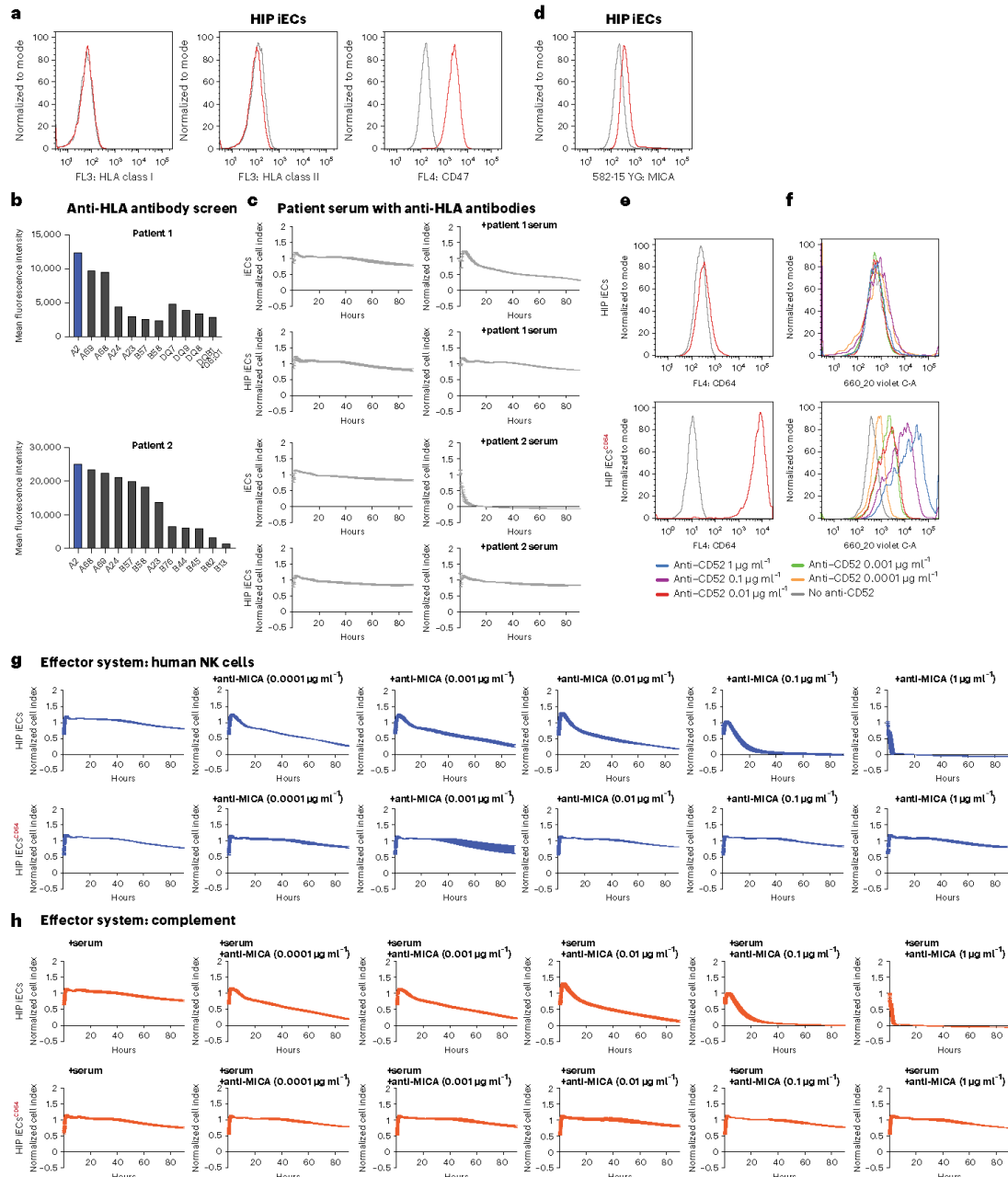


**Fig. 2 | Completely immune-evasive human HIP iECs<sup>CD64</sup>.** **a**, The HIP immune phenotype of HLA class I and II deficiency and CD47 overexpression was confirmed in flow cytometry (representative graph of two independent experiments). **b**, Single antigen bead assay results for HLA class I and II antibodies in transplant recipients 1 and 2 experiencing AMR. **c**, Human IECs and HIP iECs were incubated with serum from both patients in impedance CDC assays (mean  $\pm$  s.d.; three independent replicates per group and timepoint). **d**, Flow cytometry histogram for MICA expression on human HIP iECs (representative

graph of two independent experiments). **e**, Flow cytometry histograms for CD64 expression on human HIP iECs and HIP iECs<sup>CD64</sup> (representative graph of two independent experiments). **f**, Flow cytometry histograms for the binding of free IgG1F<sub>2</sub> (anti-CD52, alemtuzumab; representative graph of two independent experiments). **g, h**, Human HIP iECs and HIP iECs<sup>CD64</sup> were challenged in impedance NK cell ADCC (**g**) and CDC (**h**) assays with different concentrations of an anti-MICA IgG1 antibody (mean  $\pm$  s.d.; three independent replicates per group and timepoint).

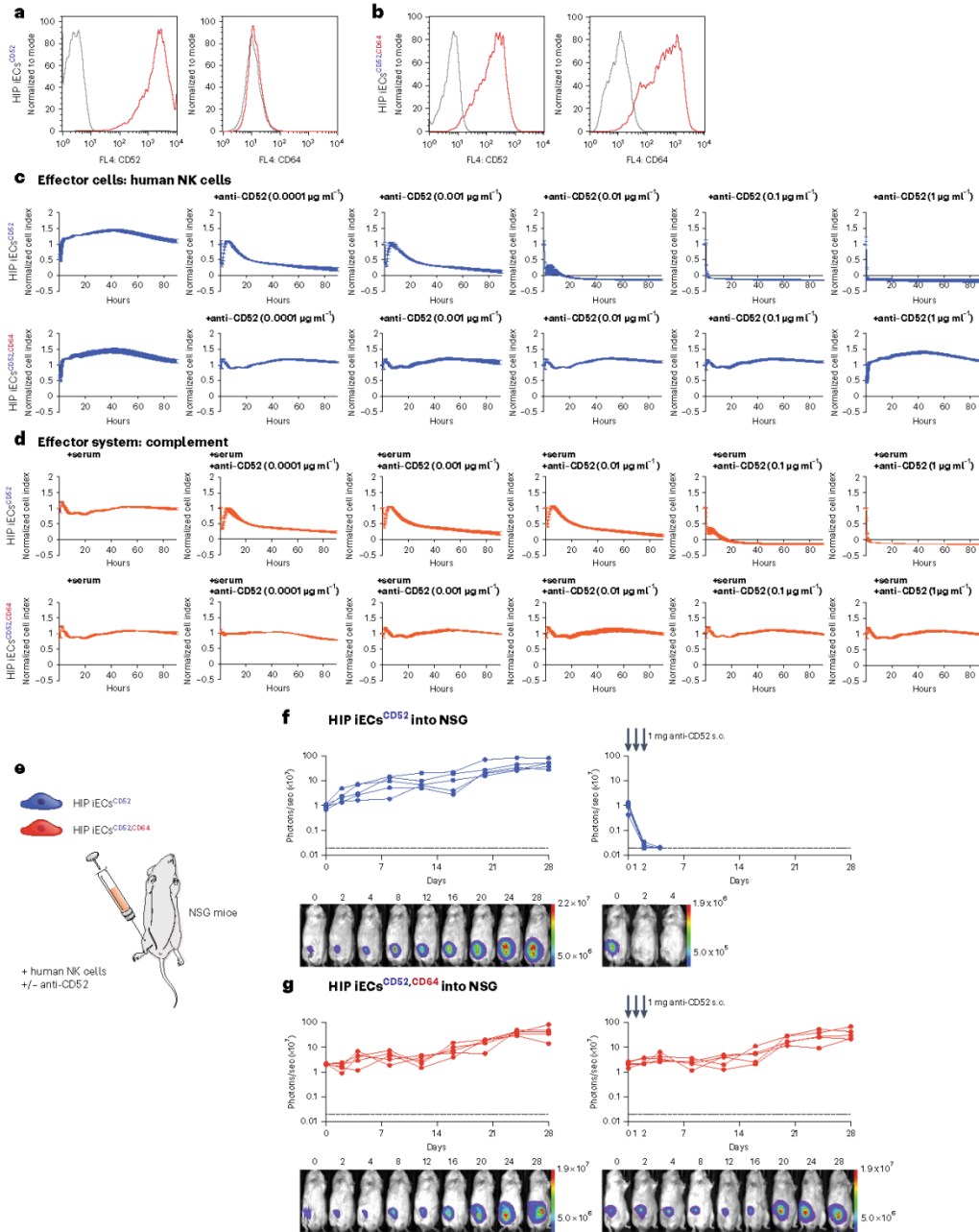


**Fig. 3 | CD64 expression protects human HIP IECs<sup>CD52, CD64</sup> from non-HLA antibody killing in vitro and in vivo. a,** Flow cytometry histograms for CD52 and CD64 expression on human HIP IECs<sup>CD52</sup> (representative graphs of two independent experiments). **b,** Flow cytometry histograms for CD52 and CD64 expression on human HIP IECs<sup>CD52, CD64</sup> (representative graphs of two independent experiments). **c, d,** Human HIP IECs<sup>CD52</sup> and HIP IECs<sup>CD52, CD64</sup> were challenged in impedance NK cell ADCC (c) and CDC (d) assays with different concentrations

of an anti-CD52 IgG1 antibody (mean  $\pm$  s.d.; three independent replicates per group and timepoint). **e,**  $5 \times 10^4$  HIP IECs<sup>CD52</sup> or HIP IECs<sup>CD52, CD64</sup> were injected subcutaneously into NSG mice with  $10^6$  human NK cells. Some groups received three subcutaneous doses of alemtuzumab 1 mg on days 0, 1 and 2. **f, g,** BLI signals of HIP IECs<sup>CD52</sup> (f) and HIP IECs<sup>CD52, CD64</sup> (g) were followed (all individual mice were plotted, and BLI pictures of one representative mouse per group are shown). s.c., subcutaneous.



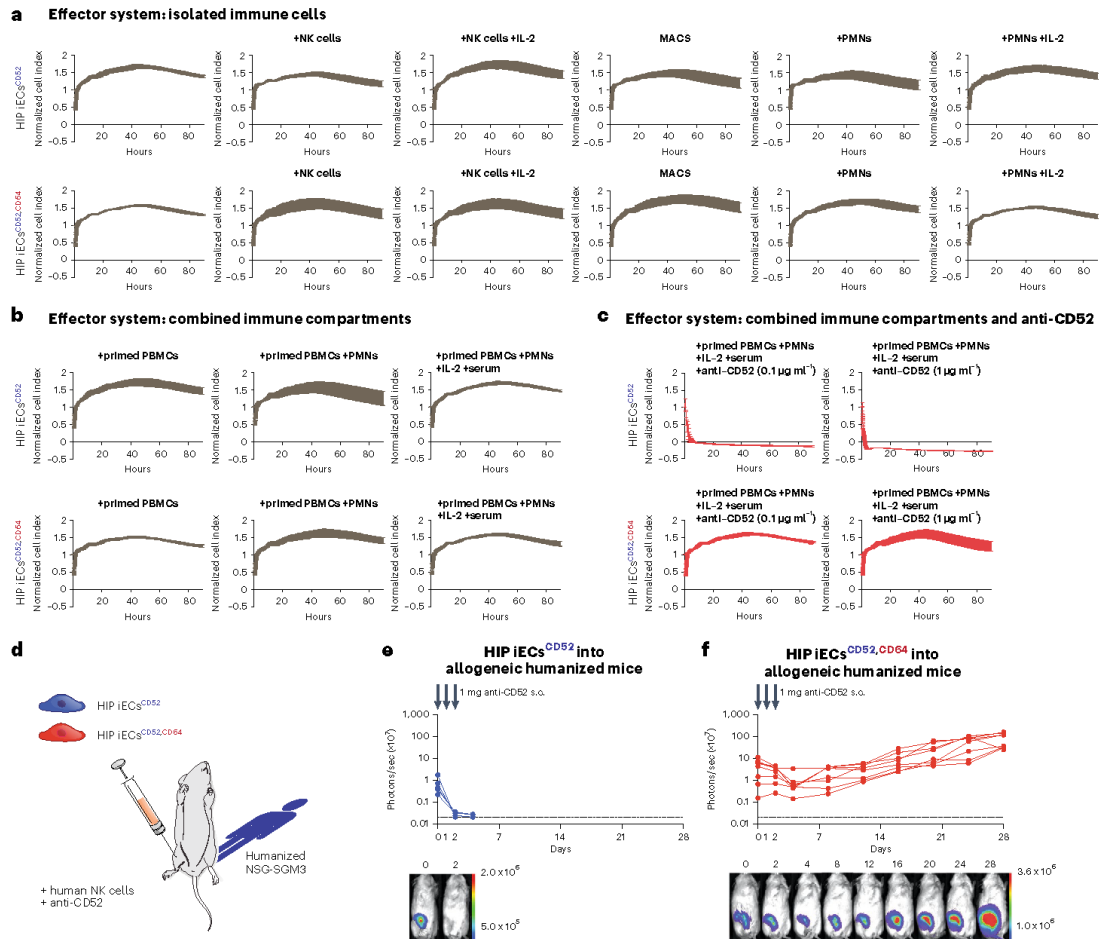


**Fig. 4 | Human HIP IECs<sup>CD52,CD64</sup> evade all cellular and antibody-mediated immune attacks. a**, Human HIP IECs<sup>CD52</sup> and HIP IECs<sup>CD52,CD64</sup> were challenged with isolated allogeneic innate immune cells. Allogeneic NK cells with or without IL-2, allogeneic macrophages or allogeneic PMN cells with or without IL-2 were used. **b**, Human HIP IECs<sup>CD52</sup> and HIP IECs<sup>CD52,CD64</sup> were challenged with primed allogeneic PBMCs after they underwent 10 days of in vitro stimulation with the target cells. Then, PMNs and serum were added to combine all immune compartments of the peripheral blood in this assay. **c**, Human HIP IECs<sup>CD52</sup> and HIP IECs<sup>CD52,CD64</sup>

were challenged with all immune compartments of the peripheral blood while adding anti-CD52 to enable ADCC and CDC. All graphs show mean  $\pm$  s.d. and three independent replicates per group and timepoint. **d**,  $5 \times 10^4$  HIP IECs<sup>CD52</sup> or HIP IECs<sup>CD52,CD64</sup> were injected subcutaneously into humanized mice with  $10^5$  human NK cells. Both groups received three subcutaneous doses of anti-CD52 IgG1 (alemtuzumab) 1 mg on days 0, 1 and 2. **e, f**, BLI signals of HIP IECs<sup>CD52</sup> (**e**) and HIP IECs<sup>CD52,CD64</sup> (**f**) were followed (all individual mice were plotted, and BLI pictures of one representative mouse per group are shown). s.c., subcutaneous.

Finally, HIP IECs<sup>CD52,CD64</sup> were exposed to increasingly harsh allogeneic immune environments to challenge their complete immune-evasiveness. Killing assays were first performed with only allogeneic NK cells, macrophages or polymorphonuclear (PMN) cells (Fig. 4a). Then, the whole cellular immune compartment of peripheral blood mononuclear cells (PBMCs) underwent 10 days of in vitro priming against the target cells to activate any possible adaptive immunity and was then used for the killing assay. We then added two more immune compartments, PMNs and complement-rich serum (Fig. 4b). The fact that the survival of both HIP IECs<sup>CD52</sup> and HIP IECs<sup>CD52,CD64</sup> remained unaffected confirms the reliability of the HIP technology to escape all cellular immunity. However, when anti-CD52

was added to enable ADCC and CDC, then HIP IECs<sup>CD52</sup> were rapidly killed (Fig. 4c). HIP IECs<sup>CD52,CD64</sup> were resistant against both allogeneic cellular and antibody-mediated killing.

For in vivo testing of complete immune-evasiveness,  $5 \times 10^4$  HIP IECs<sup>CD52</sup> or HIP IECs<sup>CD52,CD64</sup> were injected subcutaneously into humanized NSG-SGM3 mice reconstituted with allogeneic CD34<sup>+</sup> human hematopoietic stem cells. The cellular grafts were mixed with 1 million human NK cells before injection, and 1-mg doses of alemtuzumab were administered on days 0, 1 and 2 (Fig. 4d). All HIP IECs<sup>CD52</sup> grafts were quickly rejected (Fig. 4e), whereas all HIP IECs<sup>CD52,CD64</sup> grafts survived (Fig. 4f). Only HIP IECs<sup>CD52,CD64</sup> were completely resistant against all forms of allogeneic cellular and antibody-mediated immune attacks.

### Mechanistic features of $F_c$ capturing

Macrophages constitutively express CD64 and, thus, have some intrinsic protection against ADCC and CDC in the presence of anti-CD52 (Supplementary Fig. 6). When CD64 was knocked down using short hairpin RNA (shRNA), macrophages lost their protection. To test whether a second antibody would displace anti-CD52 IgG1 from CD64 and break the antibody-evasiveness of HIP IECs<sup>CD52,CD64</sup>, alemtuzumab had to compete with rituximab, a human IgG1 antibody against CD20, an epitope not expressed on IECs. (Supplementary Fig. 7). NK ADCC assays and CDC assays, however, confirmed the robustness of antibody protection, which could not be broken through competitive  $F_c$  displacement, even when alemtuzumab was given later. When FcγRIIB, the  $F_c$  receptor with the lowest IgG1 binding affinity, was used instead of CD64, the antibody protection was several orders of magnitudes lower than that for CD64 (Supplementary Fig. 8a–d). In further support of the notion that the protection against antibodies was dependent on the ability of CD64 to capture IgG  $F_c$ , we found that HIP IECs<sup>CD52,CD64</sup> were resistant against anti-CD52 human IgG1 but susceptible to an anti-CD52 mouse IgG2b, a subclass not binding to CD64<sup>19</sup> (Supplementary Fig. 8e,f). Antibody protection through CD64 was saturable, with low surface expression failing to protect against higher antibody concentrations (Supplementary Fig. 9a–d). Mechanistically, captured IgG1 bound to and occupied their target epitopes and made them unavailable for antibodies with lower  $F_c$  affinity to CD64 (Supplementary Fig. 9e), without affecting internalization of antibody-epitope complexes (Supplementary Fig. 9f–h). The next experiments were designed to reveal  $F_c$  and  $F_{ab}$  binding patterns of competitive antibodies. HIP cells were incubated with anti-CD20 IgG1 at fixed dose and increasing doses of anti-CD52 IgG1. When competing for CD64 on HIP IECs<sup>CD64</sup>, anti-CD52 binding increased in a concentration-dependent manner at the expense of anti-CD20 binding (Supplementary Fig. 10a,b). On HIP IECs<sup>CD52,CD64</sup>, the overall binding of anti-CD52 was enhanced and the reduction of anti-CD20 further facilitated with a significant interactive effect that was larger in magnitude (Supplementary Fig. 10c,d). Anti-CD20 showed negligible binding to HIP IECs<sup>CD52,FcγRIIB</sup> and remained unaffected by anti-CD52 binding (Supplementary Fig. 10e,f), and the interactive effect was not significant. In contrast, when competing with a human IgG1  $F_c$  fragment for CD64, the binding of anti-CD20 on HIP IECs<sup>CD64</sup> and HIP IECs<sup>CD52,CD64</sup> was qualitatively equivalent (Supplementary Fig. 11). Next, two anti-CD52 antibodies with cytotoxic properties in CDC assays (Supplementary Fig. 12a, Supplementary Fig. 8f and Fig. 3d) were competing for HIP IECs<sup>CD52,CD64</sup> binding in mouse serum. Only the human IgG1, but not the mouse IgG2b, could additionally ligate CD64. When mainly the mouse IgG2b was bound, we observed rapid target cell killing. When the mouse IgG2b was diminished with increasing concentrations of the human IgG1, the killing gradually slowed down and ceased at the high end (Supplementary Fig. 12b,c). Together, these results show how a favorable binding pattern of cytotoxic antibodies with high  $F_c$  affinity to CD64 establishes protection even in the presence of competing antibodies.

To assess whether antibody capturing also affects CD8<sup>+</sup> T cell cytotoxicity, we primed PBMCs from an HLA-A2<sup>+</sup> donor against HLA-A2<sup>+</sup> IECs in vitro (Supplementary Fig. 12d). Primed CD8<sup>+</sup> T cells killed both IECs and iECs<sup>CD64</sup> with similar kinetics (Supplementary Fig. 12e). However, when cytotoxic anti-HLA-A2 antibodies were added, only IECs were killed more quickly. IECs<sup>CD64</sup> were protected from CD8<sup>+</sup> T cell ADCC, even after the target cells were incubated with anti-CD20 for 30 minutes to saturate CD64. Overall, these results confirmed that  $F_c$  capturing also protects against CD8<sup>+</sup> T cell ADCC.

Next, applications of this technology were explored. Because CD64 downstream signaling after  $F_c$  ligation could alter the physiology of some engineered cell types, we used a truncated form of CD64 lacking its intracellular tail for all the following translational applications. Expression of truncated CD64 (CD64t) was found to be similarly effective in preventing NK cell and CD8<sup>+</sup> T cell ADCC and CDC as full-length CD64 (Supplementary Fig. 13).

### Engineered human thyroid cells evade autoimmune antibody killing

Hashimoto's thyroiditis is a prototypic disease in which cytotoxic autoantibodies lead to the destruction of thyroid tissue. Anti-thyroid peroxidase (TPO) antibodies, primarily of IgG1 subclass, are present at high concentrations in 90% of patients<sup>20,21</sup>, have been shown to mediate both ADCC<sup>22–24</sup> and CDC<sup>25,26</sup> and diminish the function of the thyroid gland<sup>27</sup>. Thyroid epithelial cells (epiCs) resistant to TPO antibodies would have a much better chance to survive and re-establish organ function if transplanted into hypothyroid patients. Functionally immortalized human thyroid epithelial cells were first transduced to enhance their expression of TPO, because cells in culture tend to downregulate its expression (Supplementary Fig. 14a). Then, epiCs were transduced to express CD64t, which was effective in binding free human IgG1  $F_c$  (Supplementary Fig. 14b). Both thyroid epiCs<sup>TPO</sup> and epiCs<sup>TPO,CD64t</sup> produced thyroxine irrespective of the presence of IgG1 antibodies (Supplementary Fig. 14c). A humanized anti-TPO IgG1 antibody was effective in killing thyroid epiCs<sup>TPO</sup> in ADCC and CDC assays, whereas thyroid epiCs<sup>TPO,CD64t</sup> were fully protected (Fig. 5a,b). Serum samples from three patients with Hashimoto's thyroiditis and anti-TPO antibody titers 21-fold, 26.3-fold and 29.6-fold the upper level of normal rapidly killed thyroid epiCs<sup>TPO</sup> in CDC assays (Fig. 5c–e). Thyroid epiCs<sup>TPO,CD64t</sup> were completely protected from killing in patient serum and, thus, withstood clinically relevant autoimmune conditions. NSG recipients were subcutaneously injected with  $5 \times 10^4$  epiCs<sup>TPO</sup> or epiCs<sup>TPO,CD64t</sup>, 1 million human NK cells and 1-mg doses of anti-TPO on days 0, 1 and 2 (Fig. 5f). All epiCs<sup>TPO</sup> grafts vanished quickly (Fig. 5g), whereas all epiCs<sup>TPO,CD64t</sup> grafts survived (Fig. 5h).

### Engineered human beta cells evade HLA antibody killing

Type 1 diabetes mellitus (T1DM) is another autoimmune disease, which is T cell mediated with an accompanying antibody response. We aimed to test whether CD64t expression can make them resistant against HLA antibody killing. Human iPSC-derived beta cells transduced to express CD64t (Supplementary Fig. 15a) were able to capture and bind free IgG  $F_c$  (Supplementary Fig. 15b). Both beta cells and beta cells<sup>CD64t</sup> showed intact glucose sensing and insulin production irrespective of the presence of antibodies (Supplementary Fig. 15c). HLA-A2-expressing beta cells were killed increasingly quickly with increasing anti-HLA-A2 IgG1 antibody concentrations in ADCC and CDC assays (Supplementary Fig. 15d,e). Beta cells<sup>CD64t</sup>, however, were completely resistant against HLA antibody-mediated killing. We then subcutaneously injected NSG mice with  $5 \times 10^4$  human beta cells or beta cells<sup>CD64t</sup> together with 1 million human NK cells. Three 1-mg doses of anti-HLA-A2 IgG1 were subcutaneously injected on days 0, 1 and 2 (Supplementary Fig. 15f). All beta cell grafts vanished within 2 days, whereas all beta cells<sup>CD64t</sup> grafts defied antibody-mediated killing and paralleled the survival of beta cells without antibody challenge (Supplementary Fig. 15g–i).

### Engineered human CAR T cells evade HLA and non-HLA antibody killing

Clinical CAR T cell therapy induces an antibody response, which is even more pronounced in patients with solid tumors. To test whether we can engineer antibody protection into CAR T cells, we transduced human T cells to express a CD19 scFv-4-1BB-CD3ζ construct with or without additional CD64t expression (Fig. 6a). CAR T<sup>CD64t</sup> cells were able to capture and bind free IgG1  $F_c$  (Fig. 6b). The killing efficacy of CAR T, CAR T<sup>CD64t</sup> and regular T cells was assessed against CD19<sup>+</sup> Nalm6 target cells. Whereas control T cells showed no killing, both CAR T and CAR T<sup>CD64t</sup> cells were equally effective killers across a wide range of effector cell-to-target cell ratios (Fig. 6c). Furthermore, the tumor killing capacity of CAR T<sup>CD64t</sup> cells was not affected by the presence of  $F_c$ -bound antibodies (Fig. 6d). ADCC and CDC assays with cytotoxic antibodies against an HLA epitope (HLA-A2), non-HLA epitopes (CD52

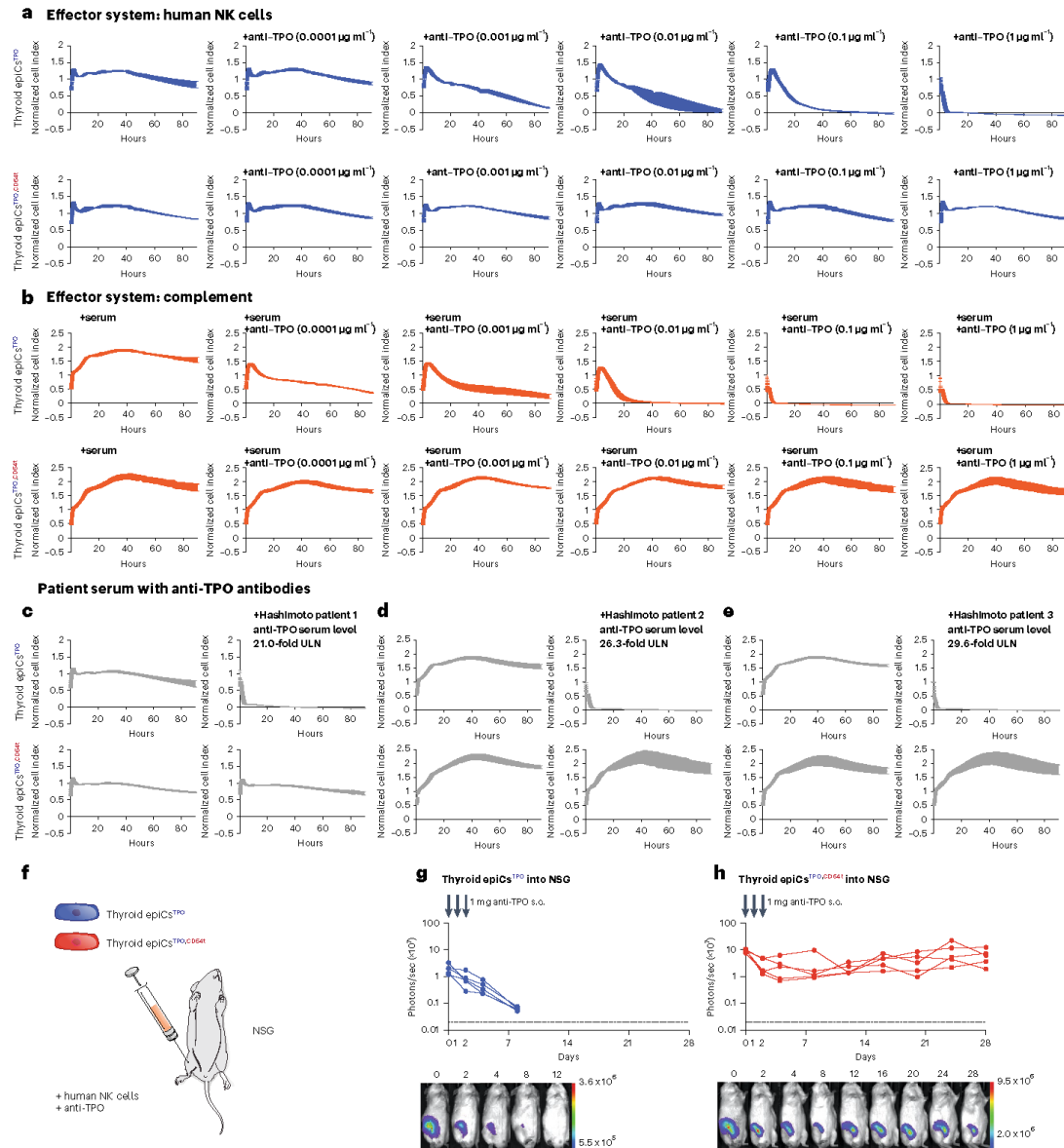


**Fig. 5 | Human thyroid epiCs<sup>TPO,CD64t</sup> are protected from antibody-mediated killing.** **a, b**, Human thyroid epiCs<sup>TPO</sup> and epiCs<sup>TPO,CD64t</sup> were challenged in impedance NK cell ADCC (**a**) and CDC (**b**) assays with different concentrations of an anti-TPO IgG1 antibody (mean ± s.d.; three independent replicates per group and timepoint). **c–e**, Human thyroid epiCs<sup>TPO</sup> and epiCs<sup>TPO,CD64t</sup> were incubated with serum from Hashimoto’s patients 1 (**c**), 2 (**d**) and 3 (**e**) in impedance CDC assays (mean ± s.d.; three independent replicates per group and timepoint).

ULN, upper limit of normal. **f**,  $5 \times 10^4$  human thyroid epiCs<sup>TPO</sup> or epiCs<sup>TPO,CD64t</sup> were injected subcutaneously into NSG mice with  $10^6$  human NK cells. Both groups received three subcutaneous doses of anti-TPO IgG1 mg on days 0, 1 and 2. **g, h**, BLI signals of thyroid epiCs<sup>TPO</sup> (**g**) and epiCs<sup>TPO,CD64t</sup> (**h**) were followed (all individual mice were plotted, and BLI pictures of one representative mouse per group are shown). s.c., subcutaneous.

and CD3), a blood type antigen (Rh(D)) and the CAR receptor (anti-CD19 scFv) were performed, and the CAR T cells were killed in all assays (Fig. 6e,f). CAR<sup>CD64t</sup> cells, however, were able to evade antibody-mediated

killing with all five antibodies in all assays. CD64t expression does not affect the cytotoxicity of human CAR T cells but makes them resistant against antibodies irrespective of their specificities.

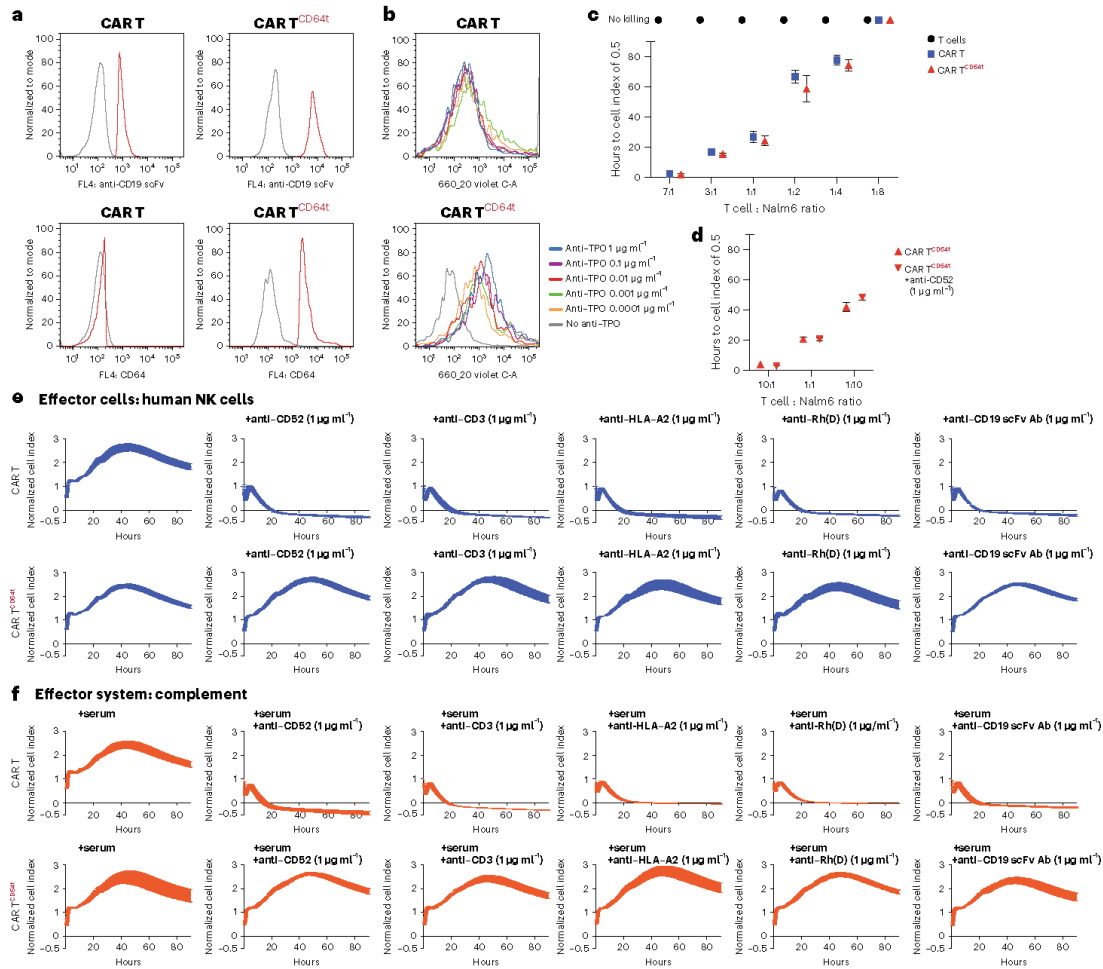


**Fig. 6 | Human CART<sup>CD64t</sup> cells are protected from antibody-mediated killing.** **a**, Flow cytometry histograms for anti-CD19 scFv and CD64t expression on human CART and CART<sup>CD64t</sup> cells (representative graphs of two independent experiments). **b**, Flow cytometry histograms for the binding of free IgG1Fc (anti-TPO IgG1); representative graph of two independent experiments). **c**, The kinetics of Nalm6 target cell killing by T cells, CART cells and CART<sup>CD64t</sup> cells is expressed as hours that it takes for the cell index to drop from 1 to 0.5. Different T cell-to-Nalm6 ratios are shown (mean ± s.d.; three independent replicates per group and timepoint). **d**, The kinetics of Nalm6 target cell killing by CART<sup>CD64t</sup> in

the presence and absence of 1 μg ml<sup>-1</sup> of anti-CD52 is expressed as hours that it takes for the cell index to drop from 1 to 0.5. Different CART cell-to-Nalm6 ratios are shown (mean ± s.d.; three independent replicates per group and timepoint). **e, f**, Human CART and CART<sup>CD64t</sup> cells were challenged in impedance NK cell ADCC (**e**) and CDC (**f**) assays with antibodies against HLA (HLA-A2), non-HLA (CD52 and CD3), rhesus blood type antigen D (Rh(D)) and the CAR (anti-CD19 scFv) at 1 μg ml<sup>-1</sup> (mean ± s.d.; three independent replicates per group and timepoint).

**Discussion**

Immune rejection presents the principal hurdle for the success of cell therapeutics, and much effort is currently devoted to developing universal allogeneic off-the-shelf cells that evade cellular rejection<sup>28–30</sup>. Such gene-edited HIP cells, however, remain susceptible to antibody killing directed against non-HLA epitopes, cell-type-specific autoantigens as well as xenogeneic<sup>31</sup> or synthetic constructs<sup>32</sup> in engineered cells and viral products from the transduction process<sup>33,34</sup>. Cytotoxic antibodies can be pre-existing or treatment induced<sup>35</sup> and jeopardize the persistence and efficacy of the cell therapeutics.

We aimed to expand the HIP concept to antibody resistance using non-immunogenic components. Microbial IgG-degrading enzymes have been administered systemically to deplete total IgG and HLA antibodies in highly sensitized patients before kidney transplantation<sup>36</sup>. More recently, these endopeptidases were shown to cleave IgG bound to target cells<sup>37</sup>. However, pre-existing antibodies against these bacterial enzymes are prevalent in the healthy population<sup>38</sup>, spike during streptococcal infections<sup>39,40</sup> and might themselves add unwanted immunogenicity. We have shown that human CD64 and its truncated form CD64t, which are non-immunogenic, have high affinity

for IgG<sup>41</sup> and protect very effectively against antibody killing in several translationally relevant cell types.

Applications for this technology include regenerative cell therapeutics, especially for diseases with an underlying autoimmune component in which antibodies are present that would destroy the transplanted cells<sup>42</sup>. Regenerative cell therapeutics would be destroyed similarly to the native cells if autoimmunity would not be circumvented<sup>43</sup>. Supporting this notion, we show that engineered epiCs<sup>TPO,CD64t</sup> were protected against clinically relevant anti-TPO killing. The most advanced stem-cell-derived pancreatic islet cells prepared for clinical trials in patients with T1DM are currently produced from embryonic stem cells (ESCs)<sup>45</sup> and, thus, are transplanted across an HLA mismatch. Currently, such ESC-derived beta cells are transplanted in immunoprotective encapsulation devices<sup>44</sup> or with immunosuppression<sup>45,46</sup>. We found that forced overexpression of CD64t on human beta cells was sufficient to protect them from anti-HLA ADCC and CDC.

Most success in CAR T cell therapy has been achieved with B cell neoplasms in which patients are treated with lymphocytotoxic drugs, and the CAR T cells directly target the B cell source of antibody production<sup>47</sup>, although antibody induction is still regularly observed<sup>48</sup>. An antibody response against a second infusion of CAR T cells has been documented in four out of 12 patients studied, and none of these patients showed expansion of CAR T cells in their blood<sup>37</sup>. The expression of CD64t on CAR T cells makes them resistant against anti-CAR T cell antibodies without affecting their specific killing capacity. Because early immune clearances are even more common in non-B cell cancer, CAR<sup>T</sup><sup>CD64t</sup> may be more efficient for these indications. The capturing of cytotoxic IgG<sub>Fc</sub> reliably builds protection against antibodies in several cell types and could further advance the immune-evasion concept for allogeneic regenerative and immune-oncology cell therapeutics.

### Online content

Any methods, additional references, Nature Research reporting summaries, source data, extended data, supplementary information, acknowledgements, peer review information; details of author contributions and competing interests; and statements of data and code availability are available at <https://doi.org/10.1038/s41587-022-01540-7>.

### References

- Loupy, A. & Lefaucheur, C. Antibody-mediated rejection of solid-organ allografts. *N. Engl. J. Med.* **379**, 1150–1160 (2018).
- Menasche, P. et al. Human embryonic stem cell-derived cardiac progenitors for severe heart failure treatment: first clinical case report. *Eur. Heart J.* **36**, 2011–2017 (2015).
- Panes, J. et al. Expanded allogeneic adipose-derived mesenchymal stem cells (Cx601) for complex perianal fistulas in Crohn's disease: a phase 3 randomised, double-blind controlled trial. *Lancet* **388**, 1281–1290 (2016).
- Skyler, J. S., Fonseca, V. A., Segal, K. R., Rosenstock, J. & Investigators, M.-D. Allogeneic mesenchymal precursor cells in type 2 diabetes: a randomized, placebo-controlled, dose-escalation safety and tolerability pilot study. *Diabetes Care* **38**, 1742–1749 (2015).
- Hege, K. M. et al. Safety, tumor trafficking and immunogenicity of chimeric antigen receptor (CAR)-T cells specific for TAG-72 in colorectal cancer. *J. Immunother. Cancer* **5**, 22 (2017).
- Deuse, T. et al. Hypoimmunogenic derivatives of induced pluripotent stem cells evade immune rejection in fully immunocompetent allogeneic recipients. *Nat. Biotechnol.* **37**, 252–258 (2019).
- Deuse, T. et al. The SIRPα-CD47 immune checkpoint in NK cells. *J. Exp. Med.* **218**, e20200839 (2021).
- Renard, V. et al. Normal development and function of natural killer cells in CD3 epsilon delta 5/delta 5 mutant mice. *Proc. Natl. Acad. Sci. USA* **92**, 7545–7549 (1995).
- Watkins, N. A., Brown, C., Hurd, C., Navarrete, C. & Ouwehand, W. H. The isolation and characterisation of human monoclonal HLA-A2 antibodies from an immune V gene phage display library. *Tissue Antigens* **55**, 219–228 (2000).
- Shiina, T., Hosomichi, K., Inoko, H. & Kulski, J. K. The HLA genomic loci map: expression, interaction, diversity and disease. *J. Hum. Genet.* **54**, 15–39 (2009).
- Leelayuwat, C., Townend, D. C., Degli-Esposti, M. A., Abraham, L. J. & Dawkins, R. L. A new polymorphic and multicopy MHC gene family related to nonmammalian class I. *Immunogenetics* **40**, 339–351 (1994).
- Zou, Y., Stastny, P., Susal, C., Dohler, B. & Opelz, G. Antibodies against MICA antigens and kidney-transplant rejection. *N. Engl. J. Med.* **357**, 1293–1300 (2007).
- Suarez-Alvarez, B. et al. The relationship of anti-MICA antibodies and MICA expression with heart allograft rejection. *Am. J. Transplant.* **7**, 1842–1848 (2007).
- Angaswamy, N. et al. Development of antibodies to human leukocyte antigen precedes development of antibodies to major histocompatibility class I-related chain A and are significantly associated with development of chronic rejection after human lung transplantation. *Hum. Immunol.* **71**, 560–565 (2010).
- Valenzuela, N. M. & Reed, E. F. Antibody-mediated rejection across solid organ transplants: manifestations, mechanisms, and therapies. *J. Clin. Invest.* **127**, 2492–2504 (2017).
- Honger, G. et al. Pretransplant IgG subclasses of donor-specific human leukocyte antigen antibodies and development of antibody-mediated rejection. *Transplantation* **92**, 41–47 (2011).
- Arnold, M. L. et al. Donor-specific HLA antibodies: evaluating the risk for graft loss in renal transplant recipients with isotype switch from complement fixing IgG1/IgG3 to noncomplement fixing IgG2/IgG4 anti-HLA alloantibodies. *Transpl. Int.* **27**, 253–261 (2014).
- Dragun, D. Agonistic antibody-triggered stimulation of angiotensin II type 1 receptor and renal allograft vascular pathology. *Nephrol. Dial. Transplant.* **22**, 1819–1822 (2007).
- Pfefferkorn, L. C., van de Winkel, J. G. & Swink, S. L. A novel role for IgG-Fc. Transductional potentiation for human high affinity Fcγ receptor (Fcγ R) signaling. *J. Biol. Chem.* **270**, 8164–8171 (1995).
- Rapoport, B. & McLachlan, S. M. Thyroid autoimmunity. *J. Clin. Invest.* **108**, 1253–1259 (2001).
- Doullay, F., Ruf, J., Codaccioni, J. L. & Carayon, P. Prevalence of autoantibodies to thyroperoxidase in patients with various thyroid and autoimmune diseases. *Autoimmunity* **9**, 237–244 (1991).
- Bogner, U., Schleusener, H. & Wall, J. R. Antibody-dependent cell mediated cytotoxicity against human thyroid cells in Hashimoto's thyroiditis but not Graves' disease. *J. Clin. Endocrinol. Metab.* **59**, 734–738 (1984).
- Stathatos, N. & Daniels, G. H. Autoimmune thyroid disease. *Curr. Opin. Rheumatol.* **24**, 70–75 (2012).
- Stassi, G. & De Maria, R. Autoimmune thyroid disease: new models of cell death in autoimmunity. *Nat. Rev. Immunol.* **2**, 195–204 (2002).
- Rebuffat, S. A., Nguyen, B., Robert, B., Castex, F. & Peraldi-Roux, S. Antithyroperoxidase antibody-dependent cytotoxicity in autoimmune thyroid disease. *J. Clin. Endocrinol. Metab.* **93**, 929–934 (2008).
- Chiovato, L. et al. Antibodies producing complement-mediated thyroid cytotoxicity in patients with atrophic or goitrous autoimmune thyroiditis. *J. Clin. Endocrinol. Metab.* **77**, 1700–1705 (1993).
- Pearce, E. N., Farwell, A. P. & Braverman, L. E. Thyroiditis. *N. Engl. J. Med.* **348**, 2646–2655 (2003).
- Yoshihara, E. et al. Immune-evasive human islet-like organoids ameliorate diabetes. *Nature* **586**, 606–611 (2020).

29. Wang, B. et al. Generation of hypoinmunogenic T cells from genetically engineered allogeneic human induced pluripotent stem cells. *Nat. Biomed. Eng.* **5**, 429–440 (2021).
30. Deuse, T. et al. Hypoimmune induced pluripotent stem cell-derived cell therapeutics treat cardiovascular and pulmonary diseases in immunocompetent allogeneic mice. *Proc. Natl Acad. Sci. USA* **118**, e2022091118 (2021).
31. Klee, G. G. Human anti-mouse antibodies. *Arch. Pathol. Lab. Med.* **124**, 921–923 (2000).
32. Choe, J. H. et al. SynNotch-CAR T cells overcome challenges of specificity, heterogeneity, and persistence in treating glioblastoma. *Sci. Transl. Med.* **13**, eabe7378 (2021).
33. Lamers, C. H. et al. Immune responses to transgene and retroviral vector in patients treated with ex vivo-engineered T cells. *Blood* **117**, 72–82 (2011).
34. Jensen, M. C. et al. Antitransgene rejection responses contribute to attenuated persistence of adoptively transferred CD20/CD19-specific chimeric antigen receptor redirected T cells in humans. *Biol. Blood Marrow Transplant.* **16**, 1245–1256 (2010).
35. Wagner, D. L. et al. Immunogenicity of CAR T cells in cancer therapy. *Nat. Rev. Clin. Oncol.* **18**, 379–393 (2021).
36. Jordan, S. C. et al. IgG endopeptidase in highly sensitized patients undergoing transplantation. *N. Engl. J. Med.* **377**, 442–453 (2017).
37. Peraro, L. et al. Incorporation of bacterial immunoevasins to protect cell therapies from host antibody-mediated immune rejection. *Mol. Ther.* **29**, 3398–3409 (2021).
38. Akesson, P. et al. Low antibody levels against cell wall-attached proteins of *Streptococcus pyogenes* predispose for severe invasive disease. *J. Infect. Dis.* **189**, 797–804 (2004).
39. Lei, B. et al. Evasion of human innate and acquired immunity by a bacterial homolog of CD11b that inhibits opsonophagocytosis. *Nat. Med.* **7**, 1298–1305 (2001).
40. Okamoto, S., Tamura, Y., Terao, Y., Hamada, S. & Kawabata, S. Systemic immunization with streptococcal immunoglobulin-binding protein Sib 35 induces protective immunity against group: a *Streptococcus* challenge in mice. *Vaccine* **23**, 4852–4859 (2005).
41. Bruhns, P. et al. Specificity and affinity of human Fcγ receptors and their polymorphic variants for human IgG subclasses. *Blood* **113**, 3716–3725 (2009).
42. Hollenberg, A. N., Choi, J., Serra, M. & Kotton, D. N. Regenerative therapy for hypothyroidism: mechanisms and possibilities. *Mol. Cell. Endocrinol.* **445**, 35–41 (2017).
43. Melton, D. The promise of stem cell-derived islet replacement therapy. *Diabetologia* **64**, 1030–1036 (2021).
44. Desai, T. & Shea, L. D. Advances in islet encapsulation technologies. *Nat. Rev. Drug Discov.* **16**, 338–350 (2017).
45. Ramzy, A. et al. Implanted pluripotent stem-cell-derived pancreatic endoderm cells secrete glucose-responsive C-peptide in patients with type 1 diabetes. *Cell Stem Cell* **28**, 2047–2061 (2021).
46. Shapiro, A. M. J. et al. Insulin expression and C-peptide in type 1 diabetes subjects implanted with stem cell-derived pancreatic endoderm cells in an encapsulation device. *Cell Rep. Med.* **2**, 100466 (2021).
47. Brudno, J. N. & Kochenderfer, J. N. Chimeric antigen receptor T-cell therapies for lymphoma. *Nat. Rev. Clin. Oncol.* **15**, 31–46 (2018).
48. Till, B. G. et al. Adoptive immunotherapy for indolent non-Hodgkin lymphoma and mantle cell lymphoma using genetically modified autologous CD20-specific T cells. *Blood* **112**, 2261–2271 (2008).

**Publisher's note** Springer Nature remains neutral with regard to jurisdictional claims in published maps and institutional affiliations.

**Open Access** This article is licensed under a Creative Commons Attribution 4.0 International License, which permits use, sharing, adaptation, distribution and reproduction in any medium or format, as long as you give appropriate credit to the original author(s) and the source, provide a link to the Creative Commons license, and indicate if changes were made. The images or other third party material in this article are included in the article's Creative Commons license, unless indicated otherwise in a credit line to the material. If material is not included in the article's Creative Commons license and your intended use is not permitted by statutory regulation or exceeds the permitted use, you will need to obtain permission directly from the copyright holder. To view a copy of this license, visit <http://creativecommons.org/licenses/by/4.0/>.

© The Author(s) 2023

## Methods

### Mice

C57BL/6 (C57BL/6J, B6, H2<sup>b</sup>, 000664), Rag-1 knockout (KO) (B6.129S7-Rag1<sup>tm1Mom</sup>/J, 002216) and NSG (NOD.Cg-Prkdc<sup>scid</sup>Il2rg<sup>tm1Wjl</sup>/SzJ, 005557) mice, 6–12 weeks old, and humanized NSG-SGM3 (NOD.Cg-Prkdc<sup>scid</sup>Il2rg<sup>tm1Wjl</sup>Tg(CMV-IL3,CSF2,KITLG)IEav/MloySzJ, 013062) reconstituted with human CD34<sup>+</sup> hematopoietic stem cells were purchased from The Jackson Laboratory. The number of animals used in the experiments is presented in each figure. Mice received humane care in compliance with the *Guide for the Principles of Laboratory Animals*. Animal experiments were approved by the University of California, San Francisco (UCSF) Institutional Animal Care and Use Committee and performed according to local guidelines.

### Methods for mouse cells

**Mouse iPSC culture.** All iPSCs were grown on mouse embryonic fibroblast (MEF) feeder cells in KO DMEM 10829 with 15% KO Serum Replacement, supplemented with 1% glutamine, 1% MEM-NEAA, 1% penicillin–streptomycin (all Gibco), 0.2% beta-mercaptoethanol and 100 U of leukemia inhibitory factor (LIF) (both Millipore). Medium was changed daily, and the cells were passaged every 2–3 days using 0.05% trypsin–EDTA (Gibco). Cell cultures were regularly screened for mycoplasma infections using the MycoAlert Kit (Lonza). B6 iPSCs were transduced to express Fluc. Then, 100,000 iPSCs were plated in one gelatin-coated six-well plate and incubated overnight at 37 °C in 5% CO<sub>2</sub>. Medium was changed the next day, and one vial of Fluc lentiviral particles expressing luciferase II gene under the re-engineered EF1a promoter (Gentarget) was added. One milliliter of cell medium was added after 36 hours. Then, 24 hours later, complete media change was performed, and, after another 2 days, luciferase expression was confirmed by adding D-luciferin (Promega). Signals were quantified with Spectral Imaging AMI (Spectral Instruments) in maximum photons per second per centimeter square per steradian (p/s/cm<sup>2</sup>/sr). B6 iPSC gene editing to engineer B6 HIP iPSCs was performed as described<sup>4</sup>.

**EC differentiation of iPSCs.** To initiate the differentiation of mouse iPSCs to ECs, medium was changed to RPMI-1640 containing 2% B-27 minus insulin (both Gibco) and 5 μM CHIR-99021 (Selleckchem). Starting on day 2, RPMI-1640 containing 2% B-27 minus insulin (both Gibco) and 2 μM CHIR-99021 (Selleckchem) was used. From day 4 to day 7, cells were exposed to RPMI-1640 EC medium containing 2% B-27 minus insulin plus 50 ng ml<sup>-1</sup> of mouse vascular endothelial growth factor (mVEGF, R&D Systems), 10 ng ml<sup>-1</sup> of mouse fibroblast growth factor basic (mFGFb, R&D Systems), 10 μM Y-27632 (Sigma-Aldrich) and 1 μM SB 431542 (Sigma-Aldrich). EC clusters were visible from day 7, and cells were maintained in Endothelial Cell Basal Medium 2 (PromoCell) plus supplements, 10% FCS heat-inactivated (HI) (Gibco), 1% penicillin–streptomycin, 25 ng ml<sup>-1</sup> of VEGF, 2 ng ml<sup>-1</sup> of FGFb, 10 μM Y-27632 (Sigma-Aldrich) and 1 μM SB 431542 (Sigma-Aldrich). The differentiation process was completed after 21 days, and undifferentiated cells were detached during the differentiation process. For purification, cells went through MACS purification using anti-CD15 mAb-coated magnetic microbeads (Miltenyi) for negative selection.

**Transduction and sorting of mouse iECs.** In a pre-coated 12-well plate, mouse iECs were plated at a density of 5 × 10<sup>4</sup> in EC media and then incubated overnight at 37 °C in 5% CO<sub>2</sub>. The next day, cells were incubated overnight at 37 °C in 5% CO<sub>2</sub> with lentiviral particles carrying a transgene for mouse Cd64 (NM\_010186, Gentarget, custom product), human CD64 (NM\_000566, Origene, RC207487L2V) or human CD52 (NM\_001803, Gentarget, custom product) at a multiplicity of infection (MOI) of 4. Polybrene (8 μg ml<sup>-1</sup>, Millipore) was added to the media, and the plate was centrifuged at 800g for 30 minutes before overnight incubation. Cell populations were sorted on a FACSAria (BD Biosciences) for high expression of Cd64, CD64 or CD52 using BV421-labeled

anti-mouse Cd64 (FcγRI) antibody (clone XS4-S/7.1, BioLegend, 139309, concentration 0.01 mg ml<sup>-1</sup>), BV421-labeled anti-human CD64 antibody (clone 10.1, BD Biosciences, 562872, concentration 0.01 mg ml<sup>-1</sup>) or APC-conjugated anti-human CD52 antibody (clone H1186, BioLegend, 316008, concentration 0.005 mg ml<sup>-1</sup>), respectively.

**Flow cytometry analysis.** For the detection of MHC class I and II surface expression on iECs, cells were stimulated with 100 ng ml<sup>-1</sup> of IFN-γ and 100 ng ml<sup>-1</sup> of TNFα (both PeproTech) for 48 hours. Cells were harvested and labeled with flow cytometry antibodies for MHC class I (clone AF6-88.5.5.3, eBioscience, 46-5958-82, concentration 0.01 mg ml<sup>-1</sup>) or mouse IgG2a isotype-matched control antibody (clone eBM2a, eBioscience, 46-4724-80, concentration 0.01 mg ml<sup>-1</sup>), MHC class II (clone M5/114.15.2, eBioscience, 46-5321-82, concentration 0.01 mg ml<sup>-1</sup>) or rat IgG2b isotype-matched control antibody (clone eB149/10H5, eBioscience, 46-4031-80, concentration 0.01 mg ml<sup>-1</sup>), Cd47 (clone m1ap301, BD Biosciences, 563584, concentration 0.01 mg ml<sup>-1</sup>) or rat IgG2a isotype-matched control antibody (clone R35-95, BD Biosciences, 557690, concentration 0.01 mg ml<sup>-1</sup>). Surface expression of Cd64, CD64 or CD52 was assessed using the antibodies listed above.

To assess mouse Cd64-Fc receptor binding, mouse iECs were incubated with different concentrations of mouse IgG2a anti-CD20 (clone rIGEL/773, Abcam, ab219329) and QDot655-labeled F(ab')<sub>2</sub>-goat anti-mouse IgG secondary antibody (Thermo Fisher Scientific, Q-1102IMP, concentration 0.002 mg ml<sup>-1</sup>). Similarly, human CD64-Fc receptor binding was assessed with a humanized IgG1 anti-CD52 (alemtuzumab, ichorbio, ICH4002) and QDot655-labeled F(ab')<sub>2</sub>-goat anti-human IgG secondary antibody (Thermo Fisher Scientific, Q-1122IMP, concentration 0.002 mg ml<sup>-1</sup>). Cells were analyzed on a LSRFortessa (BD Biosciences), and results were expressed as fold change to isotype-matched control Ig staining. FlowJo 10 was used to analyze flow cytometric data.

**Mouse NK cell isolation.** C57BL/6 mice were stimulated with poly I:C injections (100 μg intraperitoneally, Sigma-Aldrich) and, 18 hours later, NK cells were isolated from spleens. After red blood cell lysis, NK cells were purified using the MagniSort Mouse NK Cell Enrichment Kit (Invitrogen), followed by CD49b MACS-sorting (Miltenyi). This mouse NK cell population had a purity of >99%.

**XCelligence killing assays.** Real-time killing assays were performed on the XCelligence SP platform and MP platform (ACEA Biosciences). Special 96-well E-plates (ACEA Biosciences) coated with collagen (Sigma-Aldrich) were used. A total of 4 × 10<sup>4</sup> mouse iECs were plated in 100 μl of medium. After the cell index reached 0.7, we added 4 × 10<sup>4</sup> C57BL/6 NK cells to ADCC assays or 50 μl of C57BL/6 serum to CDC assays. The following antibodies were used and added after mixing with the NK cells in 50 μl of medium or in the serum as indicated: mouse IgG2a anti-H-2<sup>b</sup> (BioXCell, clone AF6-88.5.5.3, BE0121) and humanized anti-CD52 IgG1 (alemtuzumab, ichorbio, ICH4002). Different concentrations ranging from 0.0001 μg ml<sup>-1</sup> to 1 μg ml<sup>-1</sup> were used. As a negative control, cells were treated with 2% Triton X-100 in medium. Data were standardized and analyzed with RTCA Pro 2.3.2 software (ACEA Biosciences).

**Survival analysis of mouse iECs using BLI.** One million firefly Luc<sup>+</sup> B6 HIP iECs<sup>CD52</sup> and B6 HIP iECs<sup>CD52,CD64</sup> were transplanted subcutaneously, and 1 mg of alemtuzumab was injected into the peritoneum on post-transplant days 0 and 3. For imaging, D-luciferin firefly potassium salt (375 mg kg<sup>-1</sup>, Biosynth) was dissolved in PBS (pH 7.4, Gibco), and 250 μl was injected intraperitoneally in anesthetized mice. Animals were imaged in the AMIHT (Spectral Instruments). Region of interest (ROI) bioluminescence was quantified in units of maximum p/s/cm<sup>2</sup>/sr. The maximum signal from an ROI was measured using Aura Imaging software (Spectral Instruments).

### Methods for human cells

**Human iPSC culture.** Human iPSCs were cultured on diluted feeder-free Matrigel-coated 10-cm dishes (hESC qualified, BD Biosciences) in Essential 8 Flex Medium (Thermo Fisher Scientific). Medium was changed every 24 hours, and Versene (Gibco) was used for cell passaging at a ratio of 1:6. For luciferase transduction,  $1 \times 10^5$  iPSCs were plated in one six-well plate and grown overnight at  $37^\circ\text{C}$  in 5%  $\text{CO}_2$ . Medium was changed the next day, and 200  $\mu\text{l}$  of Fluc lentiviral particles expressing Luciferase II gene under re-engineered EF1a promoter (Gentarget) was added. After 36 hours, 1 ml of cell medium was added. After another 24 hours, complete medium change was performed. Then, 2 days later, luciferase expression was confirmed by adding D-luciferin (Promega). Signals were quantified in p/s/cm<sup>2</sup>/sr. **Human iPSC gene editing to engineer HIP iPSCs** was performed as described<sup>8</sup>.

**Endothelial cell differentiation from human iPSCs.** When the iPSC confluency reached 60%, the differentiation was initiated, and medium was changed to RPMI-1640 containing 2% B-27 minus insulin (both Gibco) and 5  $\mu\text{M}$  CHIR-99021 (Selleckchem). On day 2, the medium was changed to RPMI-1640 containing 2% B-27 minus insulin (Gibco) and 2  $\mu\text{M}$  CHIR-99021 (Selleckchem). From culture day 4 to day 7, cells were exposed to RPMI-1640 EC medium, RPMI-1640 containing 2% B-27 minus insulin plus 50 ng ml<sup>-1</sup> of VEGF (PeproTech), 10 ng ml<sup>-1</sup> of human FGFb (PeproTech), 10  $\mu\text{M}$  Y-27632 (Sigma-Aldrich) and 1  $\mu\text{M}$  SB 431542 (Sigma-Aldrich). EC clusters were visible from day 7, and cells were maintained in Endothelial Cell Basal Medium 2 (PromoCell) plus supplements, 10% FCS HI (Gibco), 1% penicillin–streptomycin, 25 ng ml<sup>-1</sup> of VEGF, 2 ng ml<sup>-1</sup> of FGFb, 10  $\mu\text{M}$  Y-27632 (Sigma-Aldrich) and 1  $\mu\text{M}$  SB 431542 (Sigma-Aldrich). The differentiation protocol was completed after 14 days, and undifferentiated cells were detached during the differentiation process. TrypLE (Gibco) was used for passaging the cells 1:3 every 3–4 days.

**NK cell culture.** Human primary NK cells were purchased from STEMCELL Technologies (70036) and cultured in RPMI-1640 plus 10% FCS HI and 1% penicillin–streptomycin before performing the assays.

**Macrophage differentiation from PBMCs.** PBMCs were isolated by Ficoll separation from fresh blood and re-suspended in RPMI-1640 with 10% FCS HI and 1% penicillin–streptomycin (all Gibco). Cells were plated in 24-well plates at a concentration of  $1 \times 10^6$  cells per milliliter, and 10 ng ml<sup>-1</sup> of human M-CSF (PeproTech) was added to the medium. Medium was changed every other day. From day 6 onward, 1  $\mu\text{g}$  ml<sup>-1</sup> of human IL-2 (PeproTech) was added to the medium for 24 hours before performing assays.

**Human thyroid epithelial cells.** Immortalized human thyroid epiCs were purchased from InSCREENex (INS-CI-1017) and cultured in the media provided from the manufacturer (INS-ME-1017, InSCREENex). The cells were maintained in culture and passaged using TrypLE 1:3 every 3–4 days.

**Human pancreatic beta cells.** Human iPSC-derived pancreatic beta cells were purchased from TakaraBio (ChiPSC22, Y10106) and cultured in Cellartis hPS Beta Cell Media Kit (Takara Bio, Y10108). Cells were plated in 12-well plates according to the manufacturer's protocol. Some cells were transduced with CD64t lentiviral particles (Gentarget).

**Human CAR T cells.** Human anti-CD19 CAR T cells were generated from human PBMCs using lentiviral particles carrying a transgene for the CD19 scFv-4-1BB-CD3 $\zeta$  construct (ProMab, PM-CAR1002-V). PBMCs were stimulated with IL-2 overnight and seeded in 96-well U-bottom plates at a density of  $10^5$  cells per well containing protamine sulfate and 0.1  $\mu\text{g}$  ml<sup>-1</sup> of IL-2 (PeproTech). Lentiviruses were added to the wells

at an MOI of 20. Some wells were transduced additionally with CD64t lentiviral particles at an MOI of 20 (Gentarget). Spinfection was carried out at 1,800 r.p.m. for 30 minutes at  $25^\circ\text{C}$ . After that, the cells were returned to a humidified 5%  $\text{CO}_2$  incubator overnight. Medium was changed after 2 days, and cells were seeded at a density of  $10^5$  per milliliter in T cell media (OpTmizer, Thermo Fisher Scientific). CD3/CD28 beads (Thermo Fisher Scientific) were used for T cell expansion. Cells were sorted for CAR<sup>+</sup> and CAR<sup>+</sup>/CD64t<sup>+</sup> populations on a BD FACSAria Fusion and used for further assays.

**Transduction and sorting of human cells.** In a pre-coated 12-well plate, human iECs, thyroid epiCs or beta cells were plated at a density of  $5 \times 10^4$  in cell-specific media and then incubated overnight at  $37^\circ\text{C}$  in 5%  $\text{CO}_2$ . The next day, cells were incubated overnight at  $37^\circ\text{C}$  in 5%  $\text{CO}_2$  with lentiviral particles carrying a transgene for human CD52 (NM\_001803, Gentarget, custom product), human CD64 (NM\_000566, Origene, RC207487L2V), human TPO (NM\_000547, Gentarget, custom product) or a truncated form of human CD64 (CD64t, ATGTGGTCTTGACAACTCTGCTCCTTTGGGTTCCAGTTGATGGGCAAGTGGACACACAAAAGGCAGTGATCACTTTGCAGCCTCCATGGGTCAGCGTGTTC-CAAGAGGAAACCGTAACCTTGCACTGTGAGGTGCTCCATCTGCCTGGGAGCAGCTTACACAGTGGTTTCTCAATGGCACAGCCACTCAGACTCGACCCCCAGCTACAGAATCACCTCTGCCAGTGTCAATGACAGTGGTGAATACAGGTGCCAGAGAGGTCTCTCAGGGCGAAGTGACC-CATACAGCTGGAATCCACAGAGGGTGGCTACTACTGCAGGTCTC-CAGCAGAGTCTTACCGAAGGAGAACCCTCTGGCCTTGAGGTGTCACTGGTGGAAAGGATAAGCTGGGTGACAATGTGCTTTACTATCGAAATG-GCAAAGCCTTTAAGTTTTCACCTGGAATTC:TAACCTCACCATTCT-GAAAACCAACATAAGTCACAATGGCACCTACCATTGCTCAGGCATGG-GAAAGCATCGCTACACATCAGCAGGAATATCTGTCACTGTGAAGAGC-TATTTCCAGCTCCAGTGTGAATGCATCTGTGACATCCCCTCCTG-GAGGGGAATCTGTACCCTGAGCTGTGAACAAAGTGTCTTGGCAG-GCCGCTGGTTTGGAGCTTACTTCTCCTTCTACTGAGGAGCAAGAC-CCTGCGAGGCAGGAACACATCCTCTGAATACAAATACTAAGTGTGA-GAAGAGAACTCTGGTTTACTGTTGCGAGGCTGCCACAGAGGATG-GAAATGTCTTAAGCGCAGCCCTGAGTTGGAGCTTCAAGTGTCTTGGC-CCTCAGTACCAACTCCTGTCTGGTTTCTATGCTCTTTCTATGCGCAG-TGGGAATAATGTTTTAGTGAACACTGTTCTCTGGGTGACAAATATAG, Gentarget, custom product) at an MOI of 4. Polybrene (8  $\mu\text{g}$  ml<sup>-1</sup>, Millipore) was added to the media, and the plate was centrifuged at 800g for 30 minutes before overnight incubation. Cell populations were sorted on a FACSAria (BD Biosciences) using APC-conjugated anti-human CD52 antibody (clone HI86, BioLegend, 316008, concentration 0.005 mg ml<sup>-1</sup>), BV421-labeled anti-human CD64 antibody (clone 10.1, BD Biosciences, 562872, concentration 0.01 mg ml<sup>-1</sup>), PE-conjugated anti-human TPO antibody (clone MoAb47, Santa Cruz Biotechnology, sc-58432, concentration 0.01 mg ml<sup>-1</sup>) or FITC-conjugated anti-FMC63 scFv (clone Y45, Acro Biosystems, FM3-FY45, dilution 1:50).

**CD64 knockdown in macrophages.** Human peripheral blood macrophages were purchased from STEMCELL Technologies (70042) and seeded in 12-well plates at a density of  $1 \times 10^5$  cells per well in RPMI-1640 media (Gibco) supplemented with 10% FCS HI (Sigma Aldrich). The next day, lentiviral particles with shRNA for human CD64 (custom order, Gentarget) were added to the media at an MOI 20, and 1  $\mu\text{g}$  ml<sup>-1</sup> of protamine sulfate was added. After 72 hours, the macrophages were harvested and sorted for CD64 deficiency using a BV421 mouse anti-human CD64 antibody (clone 10.1, 562872, BD Biosciences, concentration 0.01 mg ml<sup>-1</sup>) and the isotype-matched control mouse IgG1k antibody (clone MOPC-21, 400157, BioLegend, concentration 0.01 mg ml<sup>-1</sup>) on a FACSAria flow cytometer (BD Biosciences).

**FcyRIIb expression in HIP iECs.** A six-well plate was coated with gelatin, and  $1 \times 10^5$  HIP iECs<sup>CD52</sup> per well were seeded in 2.5 ml of EC media and incubated for 24 hours at  $37^\circ\text{C}$  in 5%  $\text{CO}_2$ . The next day, 1 ml of fresh



EC media was added to the wells, and human FcγRIIB lentiviral particles (custom order, Gentarget) were added to the media at an MOI of 20, and 1 μg ml<sup>-1</sup> of protamine sulfate was also added. After 24 hours, 1 ml of EC media was added to the cells, and, after subsequent 48 hours, a complete media change was performed. The cells were harvested and stained for FcγRIIB expression using an APC mouse anti-human CD32B/C antibody (clone SI8005H, 398304, BioLegend, concentration 0.0025 mg ml<sup>-1</sup>) together with the isotype-matched control APC mouse IgG1k antibody (clone MOPC-21, 555751, BD Biosciences, concentration 0.0025 mg ml<sup>-1</sup>). The FcγRIIB<sup>+</sup> cells were sorted on a FACSAria flow cytometer (BD Biosciences).

**Flow cytometry analysis.** Human iPSCs were grown in six-well plates in medium containing 100 ng ml<sup>-1</sup> of IFN-γ and 100 ng ml<sup>-1</sup> of TNFα for 48 hours. Cells were harvested and labeled with APC-conjugated anti-HLA A,B,C antibody (clone G46\_2.6, BD Biosciences, 562006, concentration 0.05 mg ml<sup>-1</sup>) for HLA class I detection or APC-conjugated IgG1 isotype-matched control antibody (clone MOPC-21, BD Biosciences, 555751, concentration 0.05 mg ml<sup>-1</sup>). For HLA class II detection, cell were labeled with Alexa Fluor 647-labeled anti-HLA-DR,DP,DQ antibody (clone Tu39, BD Biosciences, 563591, concentration 0.01 mg ml<sup>-1</sup>) or Alexa Fluor 647-labeled IgG2a isotype-matched control antibody (clone G155-178, BD Biosciences, 557715, concentration 0.01 mg ml<sup>-1</sup>). PerCP-Cy5.5-conjugated anti-CD47 (clone B6H12, BD Biosciences, 561261, concentration 0.01 mg ml<sup>-1</sup>) or PerCP-Cy5.5-conjugated IgG1 isotype-matched control antibody (clone MOPC-21, BD Biosciences, 552834, concentration 0.01 mg ml<sup>-1</sup>) were used for detection of CD47. For MICA detection, a humanized anti-MICA IgG1 (Creative Biolabs, TAB-0799CL, concentration 0.01 mg ml<sup>-1</sup>) with PE-labeled mouse anti-human IgG1F<sub>2</sub> secondary antibody (clone HP6001, SouthernBiotech, 9054-09, concentration 0.01 mg ml<sup>-1</sup>) was used. For SIRPα detection, an APC-labeled mouse anti-human SIRPα (clone 15-414, 372106, BioLegend, concentration 0.02 mg ml<sup>-1</sup>) with IgG2ak isotype-matched control antibody (557715, BD Biosciences, concentration 0.02 mg ml<sup>-1</sup>) was used. Surface expression of CD52, CD64/CD64t, TPO and anti-CD19 scFv was assessed using the antibodies listed above. To study competing CD52 binding, an APC-conjugated anti-CD52 mouse IgG2b was used (clone H1186, GTX80134, GeneTex).

To assess human CD64-F<sub>c</sub> binding, a humanized IgG1 anti-CD52 (alemtuzumab, ichorbio, ICH4002), a humanized IgG1 anti-TPO (clone B8, Creative Biolabs, FAMAB-0014JF) or humanized anti-SIRPα antibodies (clone KWAR23, IgG1, IgG2, IgG3 or IgG4, custom order, Creative Biolabs) and QDot655-labeled F(ab')<sub>2</sub>-goat anti-human IgG secondary antibody (Thermo Fisher Scientific, Q-11221MP, 0.002 mg ml<sup>-1</sup>) were used.

To assess alemtuzumab internalization, cells were incubated with 1 μg ml<sup>-1</sup> of Alexa Fluor 488-conjugated anti-CD52 (clone Hu116, FAB9889G, R&D Systems) for different time periods. Then, an anti-Alexa Fluor 488 quenching antibody (Invitrogen, A-11094) was used at 10 μg ml<sup>-1</sup> for 30 minutes. Flow cytometry of cells with and without the quenching antibody was done to assess total and intracellular fluorescence, respectively. Cells were analyzed on a LSR-Fortessa (BD Biosciences), and results were expressed as fold change to isotype-matched control Ig staining.

**XCelligence killing assays.** Real-time killing assays were performed on the XCelligence SP platform and MP platform (ACEA Biosciences). Special 96-well E-plates (ACEA Biosciences) coated with gelatin (Sigma-Aldrich) were used. A total of 4 × 10<sup>4</sup> human iECs, epiCs, beta cells, CART cells or macrophages were plated in 100 μl of medium. After the cell index reached 0.7, we added 4 × 10<sup>4</sup> human NK cells to ADCC assays or 50 μl of blood-type-compatible human serum to CDC assays. Patient serum samples were treated with DTT to eliminate blood type IgM antibodies before use. For NALM killing assays, 4 × 10<sup>4</sup> NALM cells were plated, and 4 × 10<sup>4</sup> CART cells were used as effector cells. The following antibodies were used and added after mixing with the NK cells

in 50 μl of medium or in the serum as indicated: humanized anti-CD52 IgG1 (alemtuzumab, ichorbio, ICH4002), humanized anti-MICA IgG1 (Creative Biolabs, TAB-0799CL), humanized anti-HLA-A2 IgG1 (clone 3PF12, Absolute Antibody, AB00947-10.0), humanized anti-Rh(D) IgG1 (clone FS, Creative Biolabs, FAMAB-0089WJ), humanized anti-TPO IgG1 (clone B8, Creative Biolabs, FAMAB-0014JF), humanized anti-CD3 IgG1 (Creative Biolabs, custom product) and humanized anti-CD19 scFv (FMC63) IgG1 (clone 136.20.1, Creative Biolabs, HPAB-0440-YJ-m/h). Different concentrations ranging from 0.0001 μg ml<sup>-1</sup> to 1 μg ml<sup>-1</sup> were used. As a negative control, cells were treated with 2% Triton X-100 in medium (data not shown). Data were standardized and analyzed with RTCA software (ACEA Biosciences).

**Ex vivo T cell priming.** Blood from an HLA-A2<sup>+</sup> donor was collected, and PBMCs were obtained after Ficoll separation. The PBMCs were primed by co-culturing 5 × 10<sup>5</sup> HLA-A2<sup>+</sup> wild-type iEC cells and 1 × 10<sup>6</sup> PBMCs in gelatin-coated flasks. The media, which consisted of a 1:1 mixture of EC medium and PBMC medium, was changed every 3 days. After 14 days, the cells in suspension were harvested and sorted using an APC mouse anti-human CD3 antibody (clone SP34-2, 557597, BD Biosciences, concentration 0.01 mg ml<sup>-1</sup>) together with the isotype-matched control APC mouse IgG1k antibody (clone MOPC-21, 550854, BD Biosciences, concentration 0.01 mg ml<sup>-1</sup>) and a BV421 mouse anti-human CD8 antibody (clone SK1, 34748, BioLegend, concentration 0.005 mg ml<sup>-1</sup>) together with the isotype-matched control mouse IgG1k antibody (clone MOPC-21, 400157, BioLegend, concentration 0.005 mg ml<sup>-1</sup>). The CD3<sup>+</sup>CD8<sup>+</sup> cells were sorted using a FACSAria flow cytometer (BD Biosciences) and used for real-time XCelligence killing assays with the anti-HLA-A2 IgG1 antibody, with or without prior treatment with anti-CD20 IgG1.

**Survival analysis of human iECs using BLI.** A total of 5 × 10<sup>4</sup> HIP iECs<sup>CD52</sup> or HIP iECs<sup>CD52,CD64</sup> were injected subcutaneously into NSG mice or humanized NSG-SGM3 mice mixed together with 1 million human NK cells with or without 1 mg of alemtuzumab. On the two subsequent days, 1-mg doses of alemtuzumab were injected subcutaneously into the vicinity of the cell transplants where indicated. Transplant experiments with human thyroid epiCs<sup>TPO</sup> and epiCs<sup>TPO,CD64t</sup> or human beta cells and beta cells<sup>CD64t</sup> were similarly performed in NSG mice with anti-TPO IgG1 or anti-HLA-A2 IgG1, respectively. All injected cells were Luc<sup>+</sup>. For imaging, D-luciferin firefly potassium salt (375 mg kg<sup>-1</sup>, Biosynth) was dissolved in PBS (pH 7.4, Gibco), and 250 μl was injected intraperitoneally in anesthetized mice. Animals were imaged in the AMIHT (Spectral Instruments). ROI bioluminescence was quantified in units of maximum p/s/cm<sup>2</sup>/sr. The maximum signal from an ROI was measured using Aura Imaging software (Spectral Instruments).

**In vivo cytotoxicity assay with adoptive transfer.** Five million DiO-labeled HIP iECs<sup>CD52</sup> and 5 million DiD-labeled HIP iECs<sup>CD52,CD64</sup> were mixed and injected intraperitoneally into NSG mice (Vybrant Multicolor Cell-Labeling Kit, Thermo Fisher Scientific). A total of 10<sup>8</sup> IL-2-stimulated human primary NK cells (STEM CELL Technologies) or 10<sup>8</sup> macrophages (differentiated from PBMCs) were also intraperitoneally injected. Human primary NK cells were pre-treated with human IL-2 (1 μg ml<sup>-1</sup>, PeproTech) for 12 hours before injection. After 48 hours, cells were collected from the peritoneum, and the ratio of both cell populations was assessed by flow cytometry (FACSAria, BD Biosciences).

**Thyroxine ELISA.** A 96-well plate was coated with gelatin, and 3 × 10<sup>4</sup> human thyroid epiCs<sup>TPO</sup> or epiCs<sup>TPO,CD64t</sup> per well were seeded in 100 μl of h7H media<sup>49</sup> and incubated for 24 hours at 37 °C in 5% CO<sub>2</sub>. The next day, the h7H media was changed and supplemented with 1 mU ml<sup>-1</sup> of native bovine thyroid-stimulating hormone (TSH) protein (TSH-1315B, Creative BioMart). Three wells per epiC group were also supplemented with 1 μg ml<sup>-1</sup> of anti-CD52 IgG1 (alemtuzumab, clone Campath-1H,

Bio-Rad). After 72 hours, the supernatant was collected, and the level of thyroxine was assessed using the thyroxine (T4) competitive ELISA kit (EIA T4C, Invitrogen) according to the manufacturer's instructions. Results are presented as change in optical density (OD) between groups with and without alemtuzumab.

**Insulin ELISA.** A 24-well plate was coated with gelatin, and  $5 \times 10^4$  iPSC-derived beta cells and beta cells<sup>CD64t</sup> (Y10108, Takara Bio) per well were seeded in 500  $\mu$ l of Cellartis hiPS beta cell media and incubated for 24 hours at 37 °C in 5% CO<sub>2</sub>. The next day, the Cellartis hiPS beta cell media was changed to RPMI-1640 without glucose (11879-020, Gibco) for 2 hours. After 2 hours, the media was changed to RPMI without glucose supplemented with 2 mM glucose (G7528, Sigma-Aldrich). Three wells per beta cell group were also supplemented with 1  $\mu$ g ml<sup>-1</sup> of anti-CD52 IgG1 (alemtuzumab, clone Campath-1H, MCA6101, Bio-Rad). After 20 minutes, the supernatant was collected, and the media was changed to RPMI without glucose supplemented with 20 mM glucose. Again, 1  $\mu$ g ml<sup>-1</sup> of alemtuzumab was added to three wells per group. After 20 minutes, the supernatant was collected, and the level of human insulin was determined using the human insulin ELISA kit (KAQ1251, Invitrogen) according to the manufacturer's instructions. Results are presented as change in OD between groups with and without alemtuzumab.

#### Statistics

All data are expressed as mean  $\pm$  s.d. Intergroup differences were appropriately assessed by either unpaired Student's *t*-test or one-way ANOVA with Bonferroni's post hoc test. To determine if the effect of anti-CD52 concentration on fluorescence intensity differed significantly by antibody type, linear regression was performed with mean fluorescence intensity as the dependent variable and an interaction term for antibody type (anti-CD52 versus anti-CD20) by ten-fold increase units of anti-CD52 concentration ( $\mu$ g ml<sup>-1</sup>). Hypothesis tests were two-sided, and the significance threshold was set to 0.05. To determine if the cell lines differed significantly in their capacity to internalize alemtuzumab, linear regression was performed with percentage of internalized alemtuzumab as the dependent variable and an interaction term for cell line (hiECs<sup>CD52</sup> versus hiECs<sup>CD52,CD64</sup>) by time after exposure to alemtuzumab. Exposure to alemtuzumab was treated as a continuous variable (1 = 10 minutes, 2 = 2 hours, 3 = 24 hours). Hypothesis tests were two-sided, and the significance threshold was set to 0.05. Statistical analyses were performed using SAS version 9.4.

#### Reporting summary

Further information on research design is available in the Nature Research Reporting Summary linked to this article.

#### Data availability

All data generated or analyzed during this study are included in this published article and its Supplementary Information files. No

pre-established data exclusion method was used. No clinical data were included. Supplementary Information is available in the online version of the paper.

#### References

49. Bravo, S. B. et al. Humanized medium (h7H) allows long-term primary follicular thyroid cultures from human normal thyroid, benign neoplasm, and cancer. *J. Clin. Endocrinol. Metab.* **98**, 2431–2441 (2013).

#### Acknowledgements

Special thanks to B. Nelson (Spectral Instruments) for technical support. Medical illustration was done by J. A. Klein of Mito Pop. Statistical support was expertly provided by A. Shui and the Biostatistics Core, which is funded by the UCSF Department of Surgery.

#### Author contributions

A.G. performed lentiviral transductions and cell sorting, immune killing assays and imaging studies. G.T. performed cell injections and imaging studies. R.R. provided transplant serum samples and gave technical support and conceptual advice. Z.Q. provided endocrine patient serum samples and gave technical support and conceptual advice. C.D. gave technical support and conceptual advice. S.S. established immune assays. T.D. designed the experiments, supervised the project and wrote the manuscript.

#### Competing interests

Sana Biotechnology, Inc. has an exclusive license on the HIP cell technology. S.S. is currently an employee of Sana Biotechnology, Inc. S.S. and T.D. own stock in Sana Biotechnology, Inc. Neither a reagent nor any funding from Sana Biotechnology, Inc. was used in this study. The University of California, San Francisco has filed patent applications that cover these inventions. Correspondence and requests for materials should be addressed to T.D. (tobias.deuse@ucsf.edu).

#### Additional information

**Supplementary information** The online version contains supplementary material available at <https://doi.org/10.1038/s41587-022-01540-7>.

**Correspondence and requests for materials** should be addressed to Tobias Deuse.

**Peer review information** *Nature Biotechnology* thanks the anonymous reviewers for their contribution to the peer review of this work.

**Reprints and permissions information** is available at [www.nature.com/reprints](http://www.nature.com/reprints).

## Supplementary Information

### Table of contents

**Supplementary Figure 1:** *Mouse Cd64 protects B6 iECs from MHC antibody-mediated killing.*

**Supplementary Figure 2:** *CD64 expression protects B6 HIP iECs<sup>CD52,CD64</sup> from non-MHC antibody killing in vitro and in vivo.*

**Supplementary Figure 3:** *CD64 expression binds IgG isotypes and protects human iECs from non-HLA antibody killing.*

**Supplementary Figure 4:** *CD64 expression protects human HIP iECs from rhesus blood type antibody killing.*

**Supplementary Figure 5:** *CD64 expression protects human HIP iECs<sup>CD52,CD64</sup> from non-HLA antibody NK cell and macrophage killing in vivo.*

**Supplementary Figure 6:** *CD64-knockdown macrophages have increased susceptibility for ADCC and CDC killing.*

**Supplementary Figure 7:** *The F<sub>c</sub> capture mechanism works despite the presence of competing antibodies and serum.*

**Supplementary Figure 8:** *High-affinity IgG F<sub>c</sub> receptor binding is necessary to establish antibody protection.*

**Supplementary Figure 9:** *Antibody protection depends on expression levels of CD64 and involves occupation of target antigens.*

**Supplementary Figure 10:** *Competitive anti-CD20 vs. anti-CD52 binding.*

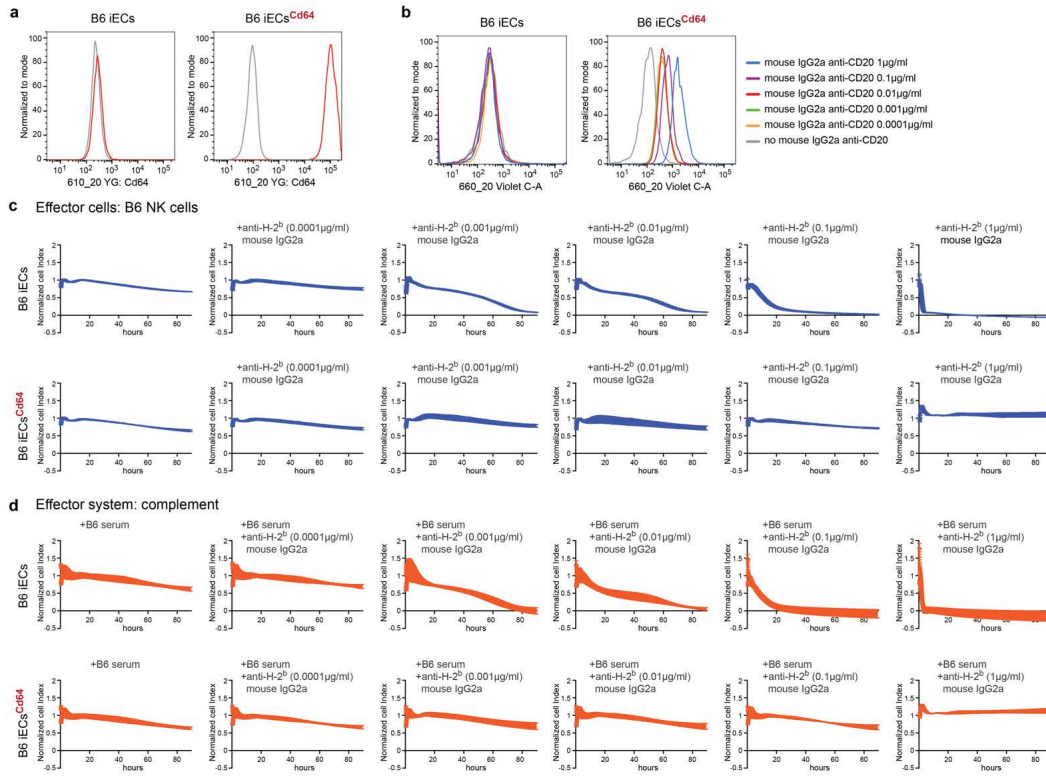
**Supplementary Figure 11:** *Competitive anti-CD20 vs. human IgG1 F<sub>c</sub> fragment.*

**Supplementary Figure 12:** *CD64 protects from CDC with competitive antibodies and from CD8<sup>+</sup> T cell ADCC.*

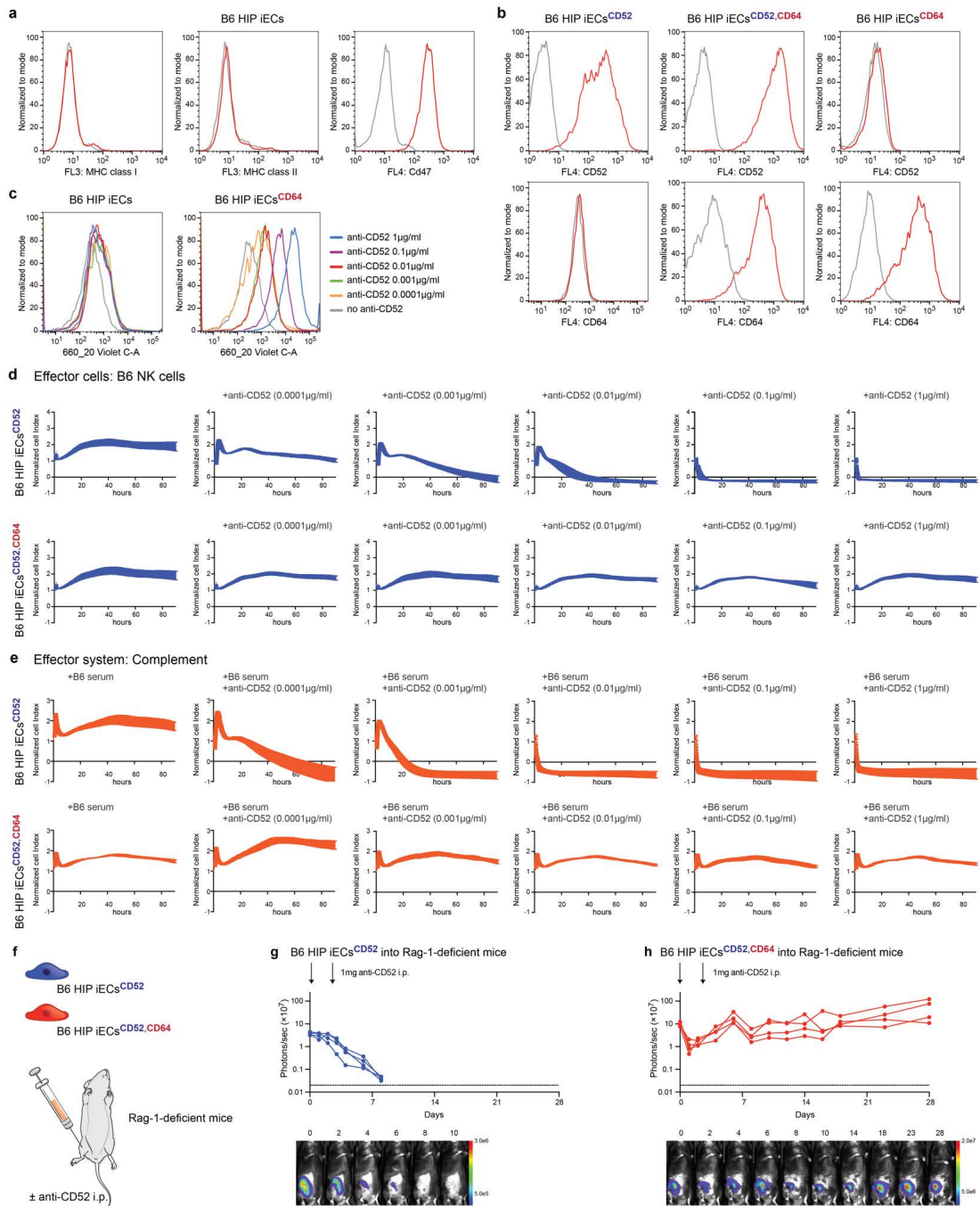
**Supplementary Figure 13:** *Truncated CD64 similarly protects from antibody-mediated killing.*

**Supplementary Figure 14:** *Characterization of human thyroid epiCs<sup>TPO,CD64t</sup>.*

**Supplementary Figure 15:** *Human beta cells<sup>CD64t</sup> are protected from antibody-mediated killing.*

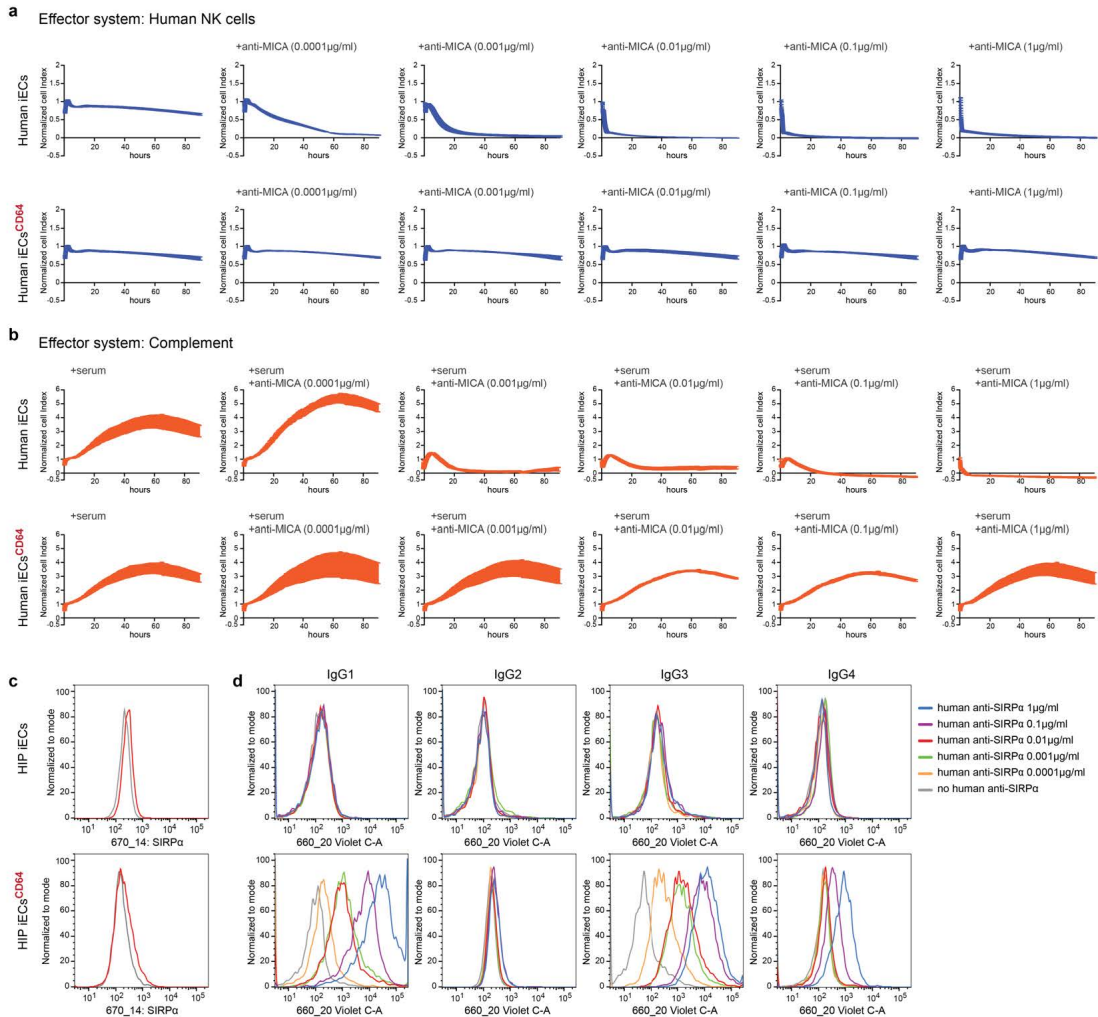


**Supplementary Figure 1: Mouse Cd64 protects B6 iECs from MHC antibody-mediated killing.** **a**, Flow cytometry histograms for Cd64 expression on B6 iECs and B6 iECs<sup>Cd64</sup> (representative graphs of two independent experiments). **b**, Flow cytometry histograms for the binding of free mouse IgG2a F<sub>c</sub> (anti-CD20, representative graph of two independent experiments). **c-d**, B6 iECs and B6 iECs<sup>Cd64</sup> were challenged in impedance NK cell ADCC (c) and CDC (d) assays with different concentrations of an anti-H-2<sup>b</sup> mouse IgG2a antibody (mean ± SD, three independent replicates per group and time point).

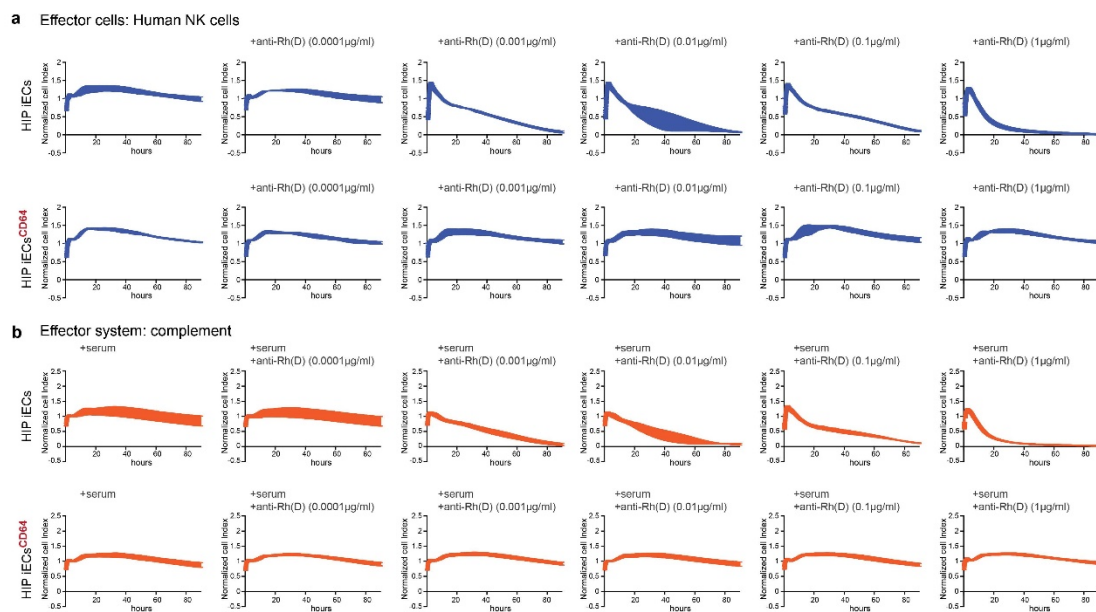


**Supplementary Figure 2: CD64 expression protects B6 HIP IECs<sup>CD52,CD64</sup> from non-MHC antibody killing *in vitro* and *in vivo*.** **a**, The HIP immune phenotype of MHC class I and II deficiency and Cd47 overexpression in

B6 HIP was confirmed in flow cytometry (representative graph of two independent experiments). **b**, Flow cytometry histograms for CD52 and CD64 expression on B6 HIP iECs<sup>CD52</sup>, B6 HIP iECs<sup>CD52,CD64</sup>, and B6 HIP iECs<sup>CD64</sup> (representative graphs of two independent experiments). **c**, Flow cytometry histograms for the binding of free IgG1 F<sub>c</sub> (anti-CD52, alemtuzumab, representative graph of two independent experiments). **d-e**, B6 HIP iECs<sup>CD52</sup> and B6 HIP iECs<sup>CD52,CD64</sup> were challenged in impedance NK cell ADCC (d) and CDC (e) assays with different concentrations of an anti-CD52 IgG1 antibody (mean ± SD, three independent replicates per group and time point). **f**, B6 HIP iECs<sup>CD52</sup> and B6 HIP iECs<sup>CD52,CD64</sup> were subcutaneously injected into Rag-1-deficient mice. Alemtuzumab (anti-CD52) was administered intraperitoneally on day 0 and 3 and cell survival was followed. **g-h**, B6 HIP iECs<sup>CD52</sup> (g) and B6 HIP iECs<sup>CD52,CD64</sup> (h) BLI signals were followed (all individual mice were plotted and BLI pictures of one representative mouse per group are shown).



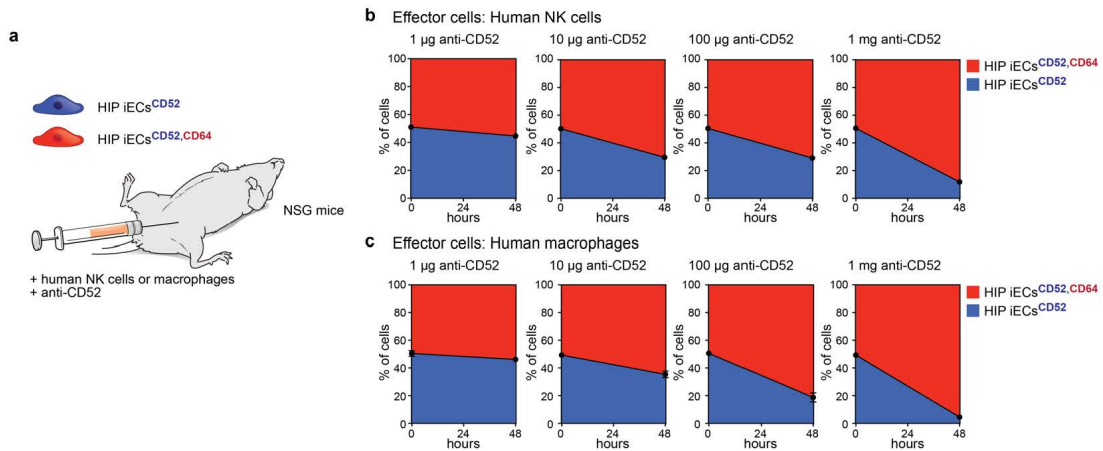
**Supplementary Figure 3: CD64 expression binds IgG isotypes and protects human iECs from non-HLA antibody killing.** **a-b**, Human iECs and iECs<sup>CD64</sup> were challenged in impedance NK cell ADCC (**a**) and CDC (**b**) assays with different concentrations of an anti-MICA IgG1 antibody (mean  $\pm$  SD, three independent replicates per group and time point). **c**, Flow cytometry histograms for SIRP $\alpha$  expression on HIP iECs and HIPIECs<sup>CD64</sup> (representative graphs of two independent experiments). **d**, Flow cytometry histograms for the binding of anti-SIRP $\alpha$  IgG1, IgG2, IgG3, and IgG4 (representative graph of two independent experiments).



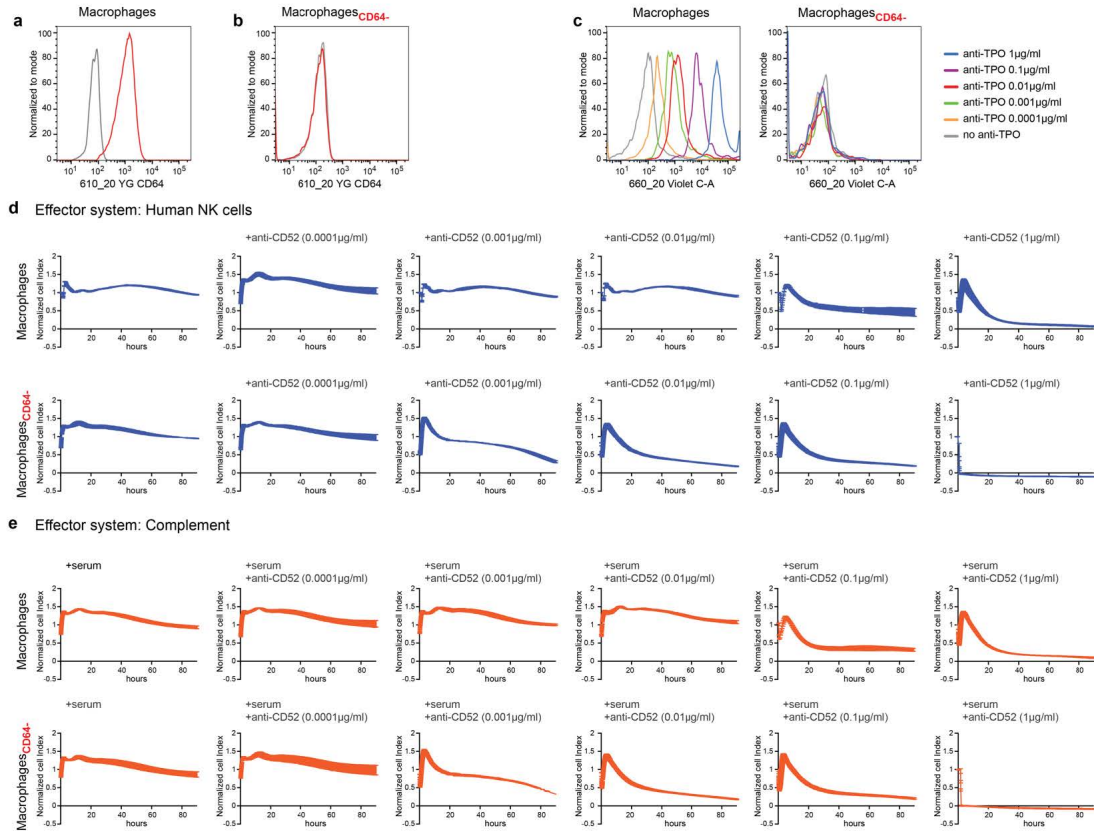
**Supplementary Figure 4: CD64 expression protects human HIP iECs from rhesus blood type antibody killing.**

**a-b,** Human HIP iECs and HIP iECs<sup>CD64</sup> were challenged in impedance NK cell ADCC (a) and CDC (b) assays with different concentrations of an anti-Rh(D) IgG1 antibody (mean ± SD, three independent replicates per group and time point).



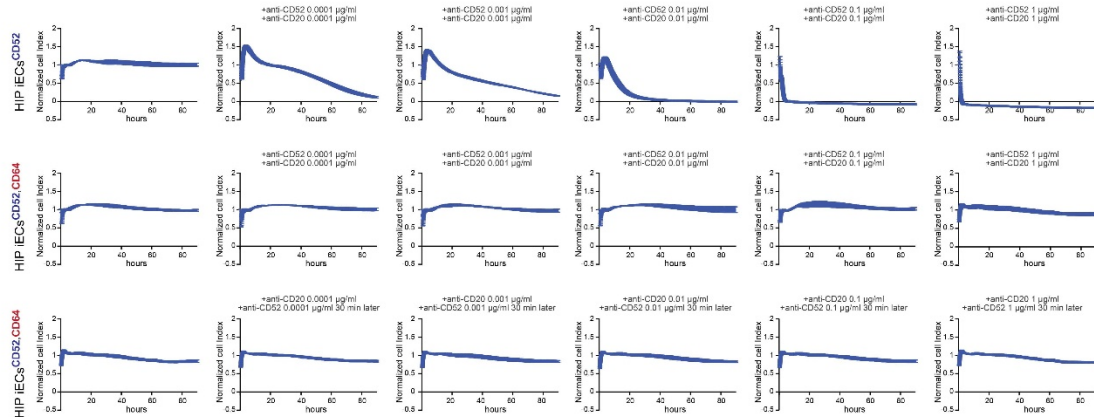


**Supplementary Figure 5: CD64 expression protects human HIP iECs<sup>CD52,CD64</sup> from non-HLA antibody NK cell and macrophage killing in vivo.** **a**, A 1:1 mixture of HIP iECs<sup>CD52</sup> and HIP iECs<sup>CD52,CD64</sup> was injected intraperitoneally into NSG mice together with allogeneic human NK cells or macrophages and alemtuzumab and was recovered 48 h later. **b-c**, The mixture was injected together with human NK cells (b) or macrophages (c) and the ratio of recovered cell populations is shown (mean ± SD, three independent replicates per group and time point).

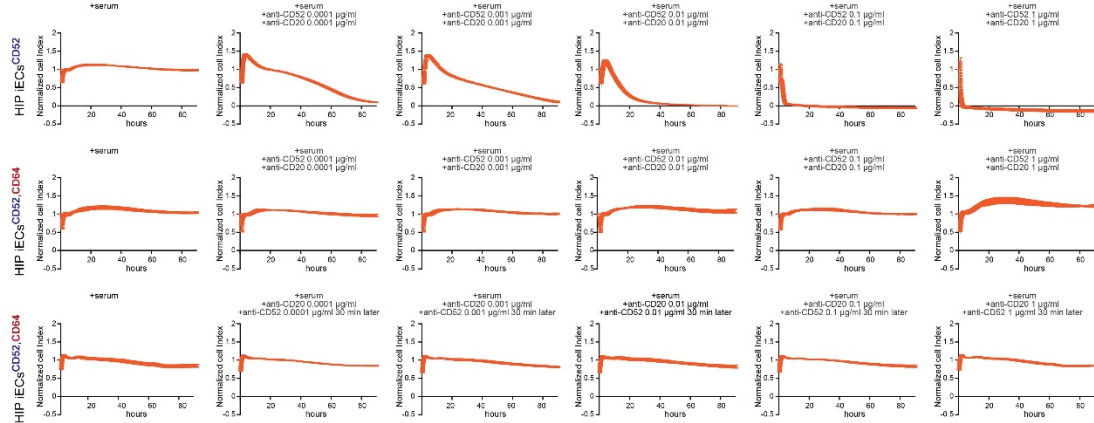


**Supplementary Figure 6: CD64-knockdown macrophages have increased susceptibility for ADCC and CDC killing.** **a-b**, Flow cytometry histograms for CD64 expression on human macrophages (a) and CD64-knockdown macrophages (b, macrophages<sub>CD64-</sub>) (representative graphs of two independent experiments). **c**, Flow cytometry histograms for the binding of free IgG1 F<sub>c</sub> (anti-TPO) on macrophages and macrophages<sub>CD64-</sub> (representative graph of two independent experiments). **d-e**, Macrophages and macrophages<sub>CD64-</sub> were challenged in impedance NK cell ADCC (d) and CDC (e) assays with different concentrations of the anti-CD52 IgG1 antibody alemtuzumab (mean ± SD, three independent replicates per group and time point).

**a Effector cells: Human NK cells**

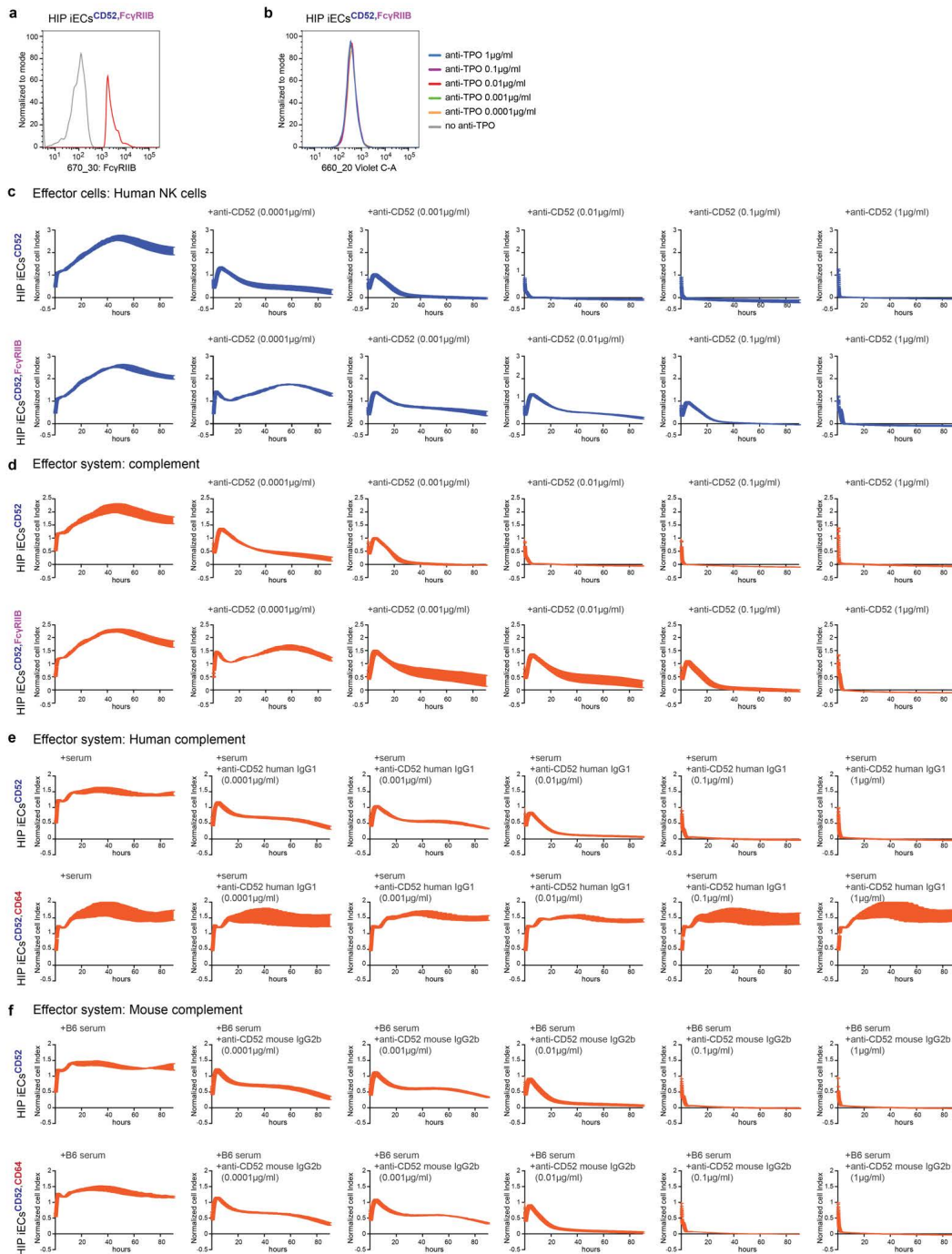


**b Effector system: Complement**



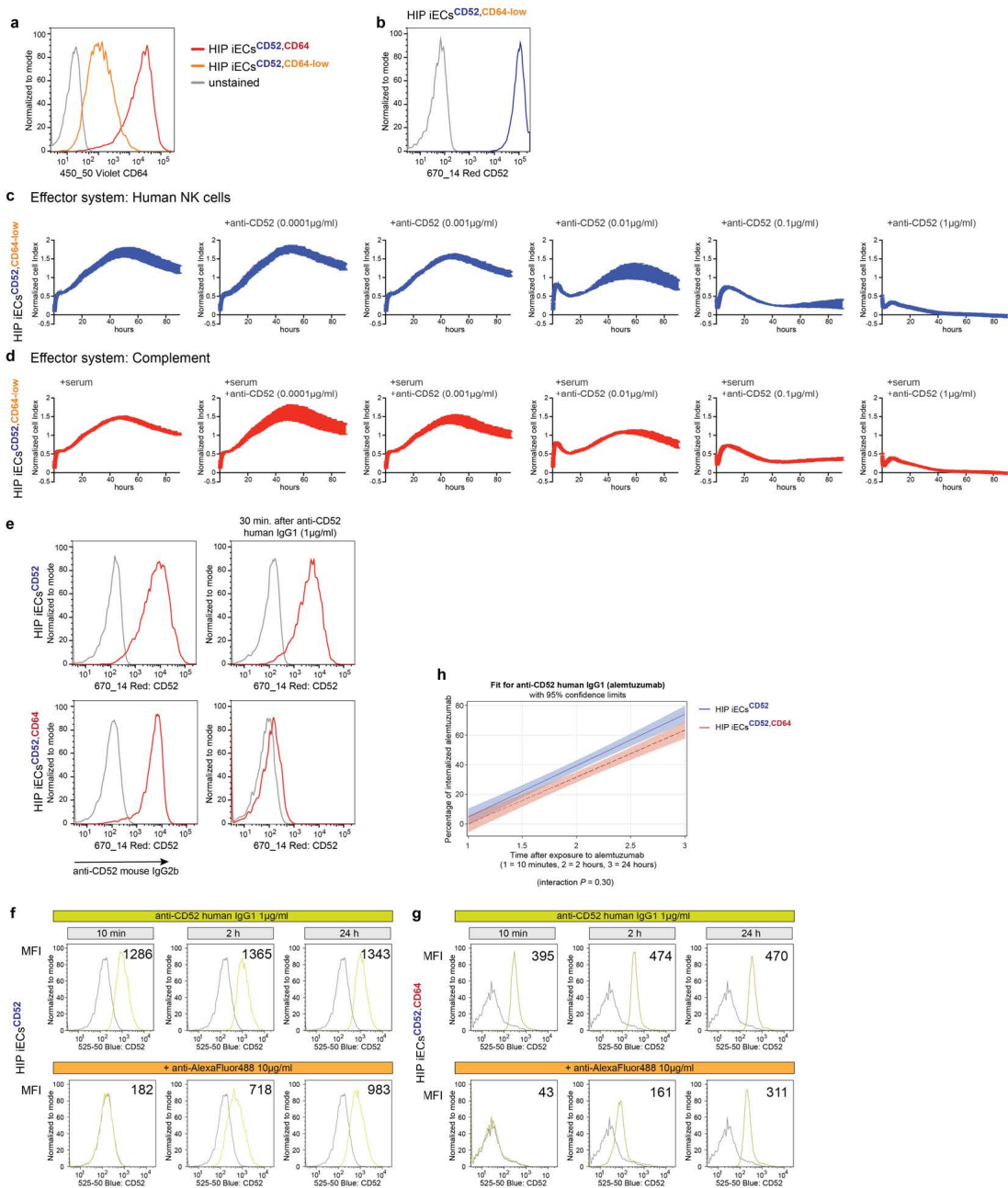
**Supplementary Figure 7: The  $F_c$  capture mechanism works despite the presence of competing antibodies**

and serum. **a-b**, Human HIP iECs<sup>CD52</sup> and HIP iECs<sup>CD52,CD64</sup> were challenged in impedance NK cell ADCC (a) and CDC (b) assays with different concentrations of two competing IgG1 antibodies (anti-CD52 and anti-CD20). In some experiments, anti-CD52 was added 30 min after anti-CD20 (mean  $\pm$  SD, three independent replicates per group and time point).



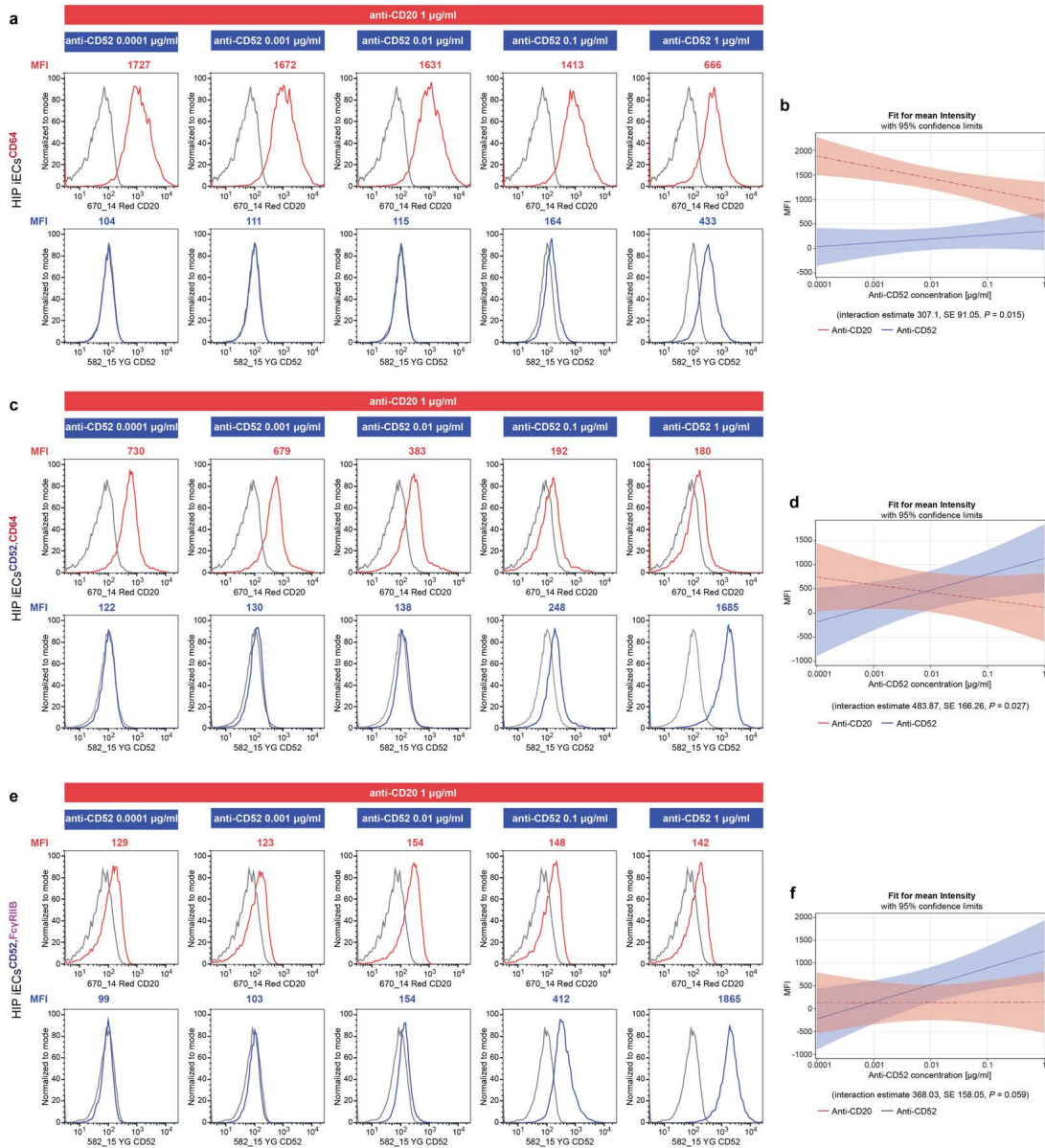
**Supplementary Figure 8: High-affinity IgG<sub>c</sub> receptor binding is necessary to establish antibody protection. a,**

Flow cytometry histogram for Fc $\gamma$ RIIB expression on human HIP iECs<sup>CD52,Fc $\gamma$ RIIB</sup> (representative graphs of two independent experiments). **b**, Flow cytometry histograms for the binding of free IgG1 F<sub>c</sub> (anti-TPO) on human HIP iECs<sup>CD52,Fc $\gamma$ RIIB</sup> (representative graph of two independent experiments). **c-d**, Human HIP iECs<sup>CD52</sup> and HIP iECs<sup>CD52,Fc $\gamma$ RIIB</sup> were challenged in impedance NK cell ADCC (c) and CDC (d) assays with the anti-CD52 IgG1 antibody alemtuzumab (mean  $\pm$  SD, three independent replicates per group and time point). **e-f**, Human HIP iECs<sup>CD52</sup> and HIP iECs<sup>CD52,CD64</sup> were challenged in impedance NK cell ADCC and CDC assays with complement-fixing human anti-CD52 IgG1 (e) or a mouse anti-human CD52 IgG2b (f) in different concentrations (mean  $\pm$  SD, three independent replicates per group and time point). The human IgG1 was used with human serum (e), the mouse IgG2b with mouse serum (f).



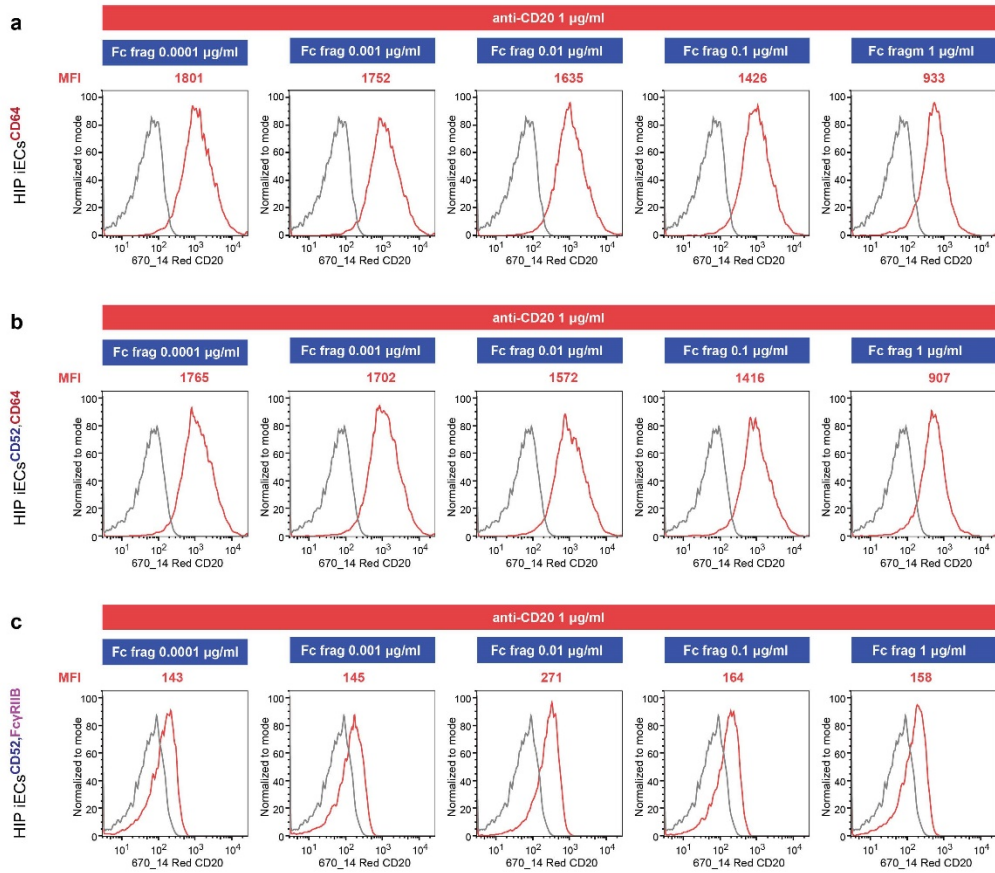
**Supplementary Figure 9: Antibody protection depends on expression levels of CD64 and involves occupation of target antigens. a**, Flow cytometry histograms for CD64 expression on HIP iEC<sup>CD52,CD64</sup> and HIP iEC<sup>CD52,CD64-low</sup> (representative graphs of two independent experiments). **b**, Flow cytometry histograms for CD52 expression

on HIP iEC<sup>CD52,CD64-low</sup> (representative graphs of two independent experiments). **c-d**, HIP iEC<sup>CD52,CD64-low</sup> were challenged in impedance NK cell ADCC (c) and CDC (d) assays with different concentrations of the anti-CD52 IgG1 antibody alemtuzumab (mean  $\pm$  SD, three independent replicates per group and time point). With increasing antibody concentrations, there was increasingly rapid target cell killing. **e**, Flow cytometry histograms for the binding of 1  $\mu$ g/ml anti-CD52 mouse IgG2b to HIP iEC<sup>CD52</sup> and HIP iEC<sup>CD52,CD64</sup> (representative graphs of two independent experiments) with and without prior incubation with 1  $\mu$ g/ml human anti-CD52 IgG1 (alemtuzumab). Only on HIP iEC<sup>CD52,CD64</sup>, pre-incubation with alemtuzumab mitigated the subsequent binding of the mouse IgG2b, which does not bind CD64 via F<sub>c</sub>. **f-h**, The internalization of CD52-bound alemtuzumab over time was assessed in HIP iEC<sup>CD52</sup> (f) and HIP iEC<sup>CD52,CD64</sup> (g). AlexaFluor488-conjugated anti-CD52 IgG1 was incubated for different time periods before the fluorochrome was quenched using an anti-AlexaFluor488 antibody. The remaining fluorescence is specific for the internalized fluorochrome fraction. Linear regression analysis showed that the percentage of internalized alemtuzumab over time did not differ significantly by cell line (interaction  $P = 0.30$ , h).

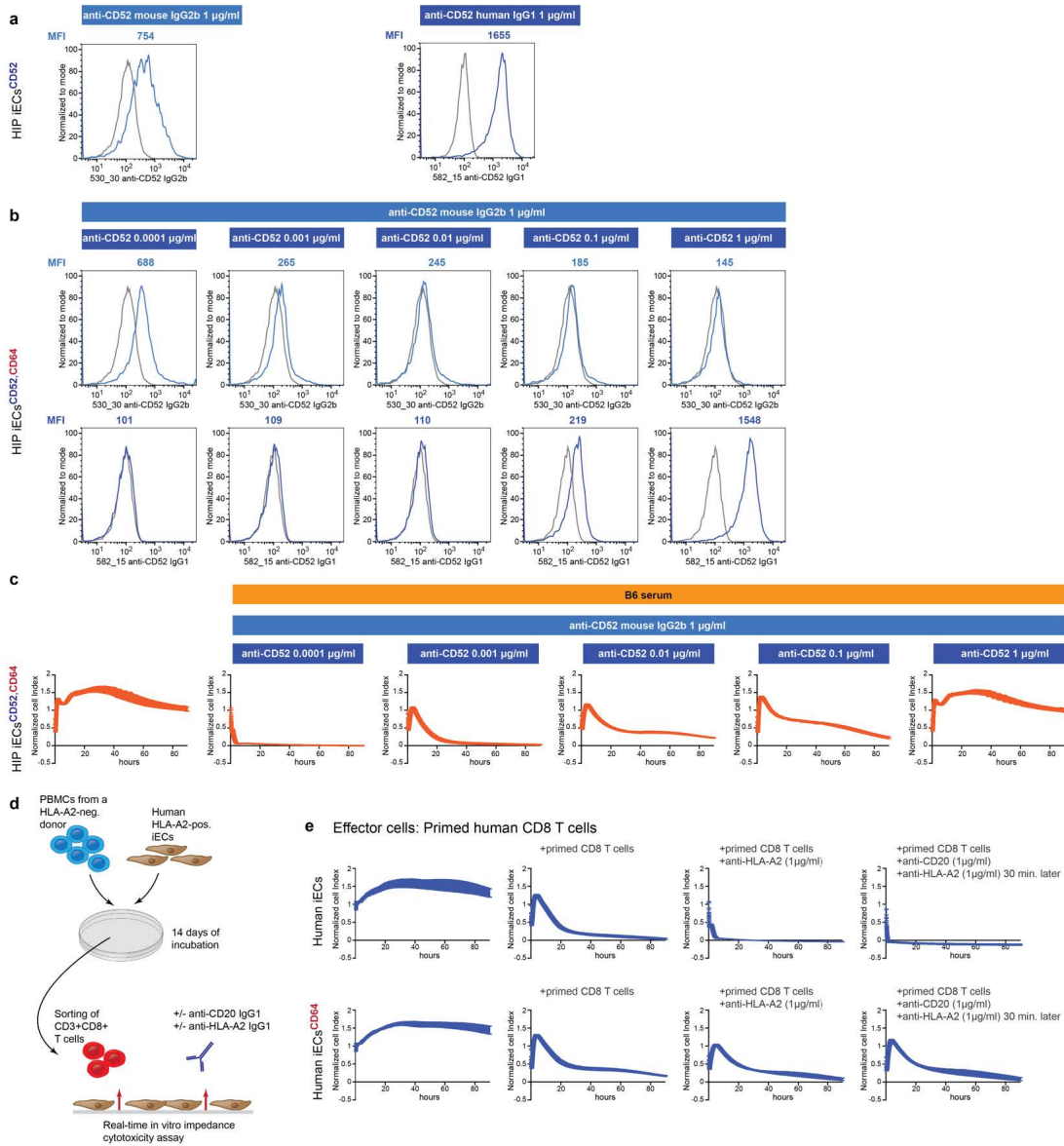


**Supplementary Figure 10: Competitive anti-CD20 vs. anti-CD52 binding.** Competitive binding of anti-CD52 and CD20 to HIP IECs<sup>CD64</sup> (a-b), HIP IECs<sup>CD52,CD64</sup> (c-d), and HIP IECs<sup>CD52,FcγRIIB</sup> (e-f) was determined by flow cytometry. Anti-CD20 was consistently used at 1 µg/ml while a range of anti-CD52 concentrations (0.0001 µg/ml to 1 µg/ml) was used (one representative histogram is shown). Linear regression plots for antibody interaction are shown (mean with 95% confidence limits, b, d, f).





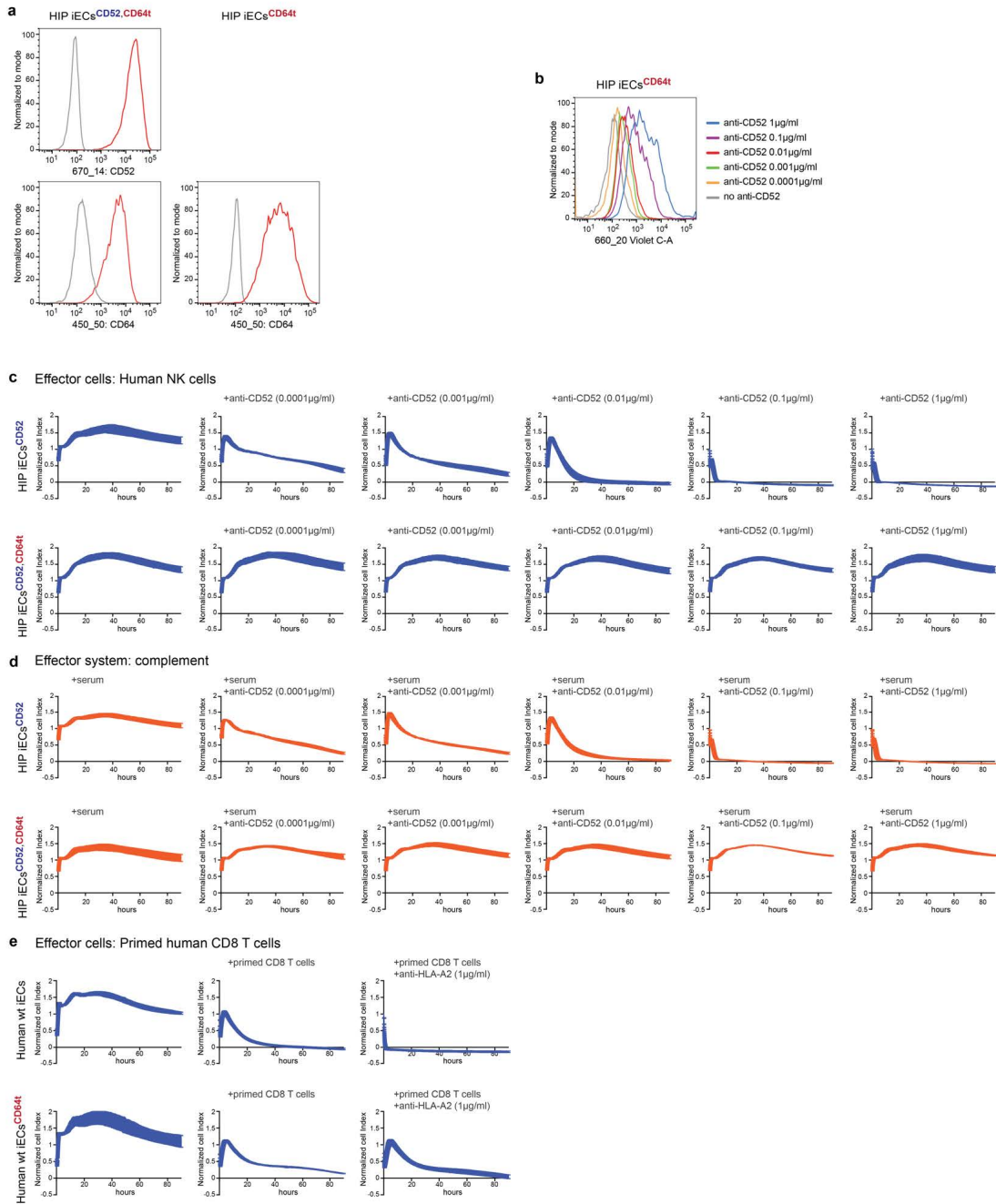
**Supplementary Figure 11: Competitive anti-CD20 vs. human IgG1 Fc fragment.** The binding of 1 µg/ml anti-CD20 to HIP iECs<sup>CD64</sup> (a), HIP iECs<sup>CD52,CD64</sup> (b), and HIP iECs<sup>CD52,Fc $\gamma$ RIIB</sup> (c) in the presence of human IgG1 Fc fragment (0.0001 µg/ml to 1 µg/ml) was assessed by flow cytometry (one representative histogram of two independent experiments).



**Supplementary Figure 12: CD64 protects from CDC with competitive antibodies and from CD8<sup>+</sup> T cell ADCC.**

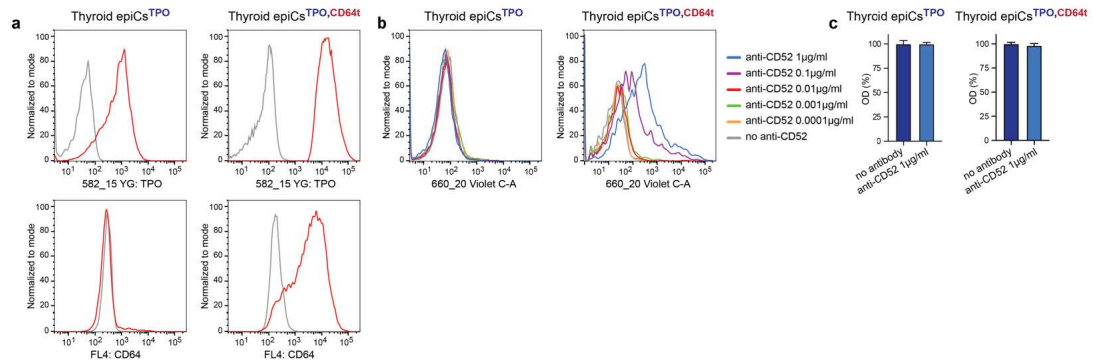
**a-b,** Flow cytometry histograms showing the binding of anti-CD52 mouse IgG2b (a) and anti-CD52 human IgG1 (b) to HIP iECs<sup>CD52</sup> (representative graph of two independent experiments). **b,** Competitive binding of anti-CD52 mouse IgG2b and anti-CD52 human IgG1 to HIP IECs<sup>CD52,CD64</sup> was determined by flow cytometry. Anti-CD52 mouse IgG2b was consistently used at 1  $\mu$ g/ml while anti-CD52 human IgG1 was used in a range of

concentrations (0.0001  $\mu\text{g/ml}$  to 1  $\mu\text{g/ml}$ , one representative histogram is shown). **c**, HIP iECs<sup>CD52,CD64</sup> were challenged in impedance CDC assays with complement-fixing anti-CD52 mouse IgG2b and human IgG1 in different concentrations (mean  $\pm$  SD, three independent replicates per group and time point). Mouse serum was used in the CDC assays). **d**, PBMCs from an HLA-A2-negative donor were incubated with HLA-A2-positive iECs for 14 days to prime T cells. CD8<sup>+</sup> T cells were sorted by flow cytometry and used for subsequent killing assays. **e**, *In vitro* impedance CD8<sup>+</sup> T cell killing assays of human iECs and iECs<sup>CD64</sup> were performed in the absence and presence of 1  $\mu\text{g/ml}$  anti-HLA-A2 IgG1, with or without previous incubation with a competing anti-CD20 IgG1 antibody (mean  $\pm$  SD, three independent replicates per group and time point).

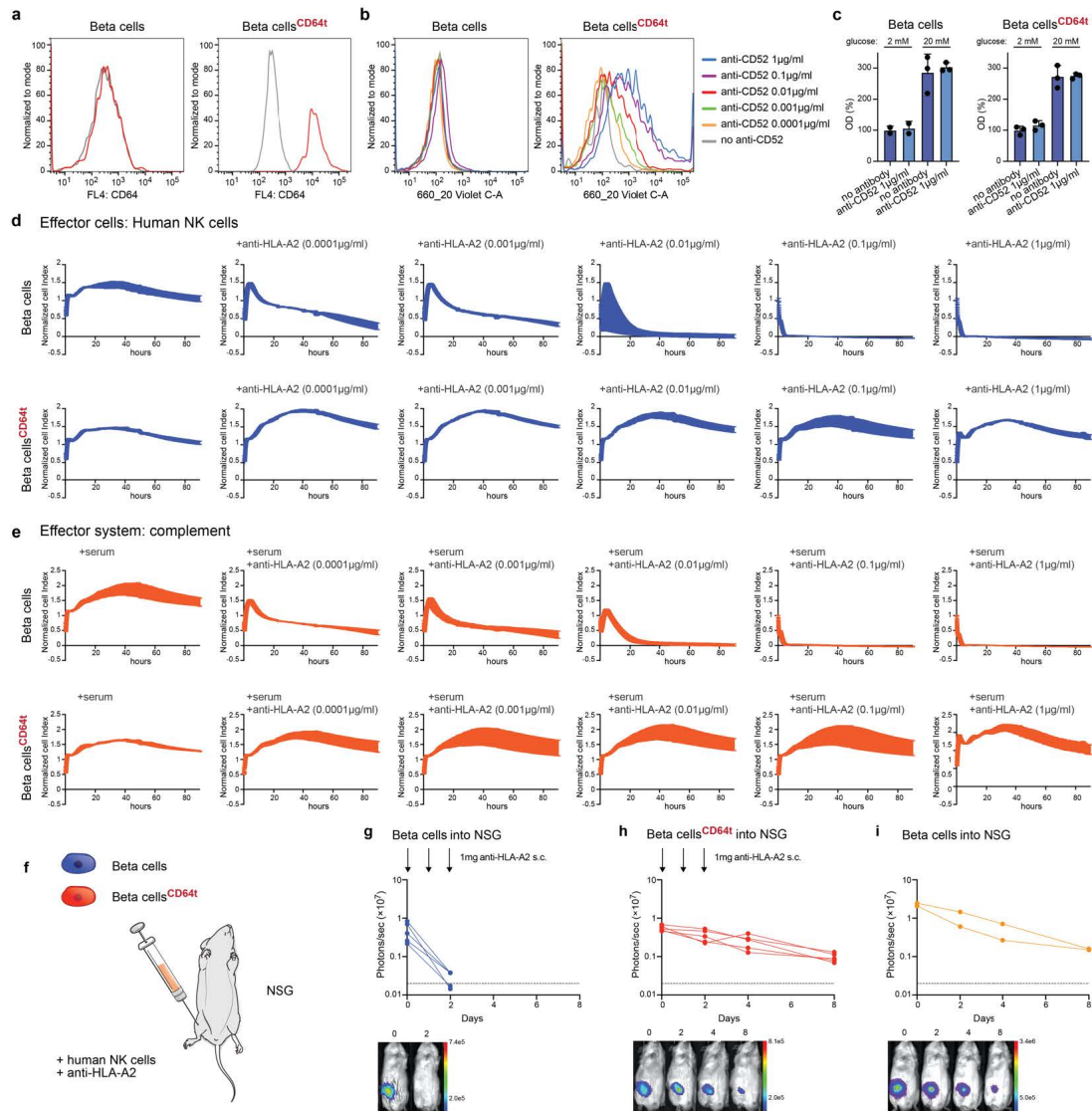


**Supplementary Figure 13: Truncated CD64 similarly protects from antibody-mediated killing. a, Flow**

cytometry histograms for CD52 and CD64t expression on HIP iEC<sup>CD52</sup> and HIP iEC<sup>CD52,CD64t</sup> (representative graphs of two independent experiments). **b**, Flow cytometry histograms for the binding of free IgG1 F<sub>c</sub> (anti-CD52, representative graph of two independent experiments). **c-d**, HIP iEC<sup>CD52</sup> and HIP iEC<sup>CD52,CD64t</sup> were challenged in impedance NK cell ADCC (c) and CDC (d) assays with different concentrations of the anti-CD52 IgG1 antibody alemtuzumab (mean ± SD, three independent replicates per group and time point). **e**, PBMCs from an HLA-A2-negative donor were incubated with HLA-A2-positive iECs for 14 days to prime T cells. CD8<sup>+</sup> T cells were sorted by flow cytometry and used for the killing assays. *In vitro* impedance CD8<sup>+</sup> T cell killing assays of human iECs and iECs<sup>CD64t</sup> were performed in the absence and presence of 1 μg/ml anti-HLA-A2 IgG1 (mean ± SD, three independent replicates per group and time point).



**Supplementary Figure 14: Characterization of human thyroid epiCs<sup>TPO,CD64t</sup>.** **a**, Flow cytometry histograms for TPO and CD64t expression on human thyroid epiCs<sup>TPO</sup> and epiCs<sup>TPO,CD64t</sup> (representative graphs of two independent experiments). **b**, Flow cytometry histograms for the binding of free IgG1 F<sub>c</sub> (alemtuzumab, representative graph of two independent experiments). **c**, Thyroxine production by epiCs<sup>TPO</sup> and epiCs<sup>TPO,CD64t</sup> was measured in the presence or absence of 1 µg/ml anti-CD52 IgG1 antibodies using an ELISA (mean ± SD, three independent replicates per group and time point).



**Supplementary Figure 15: Human beta cells<sup>CD64t</sup> are protected from antibody-mediated killing.** **a**, Flow cytometry histogram for CD64t expression on human beta cells<sup>CD64t</sup> (representative graph of two independent experiments). **b**, Flow cytometry histogram for the binding of free IgG1 F<sub>c</sub> (alemtuzumab, representative graph of two independent experiments). **c**, Glucose sensing and insulin production by human beta cells and beta cells<sup>CD64t</sup> was measured in the presence or absence of 1 µg/ml anti-CD52 IgG1 antibodies using an ELISA (mean ± SD, two or three independent replicates per group and time point). The assays were performed under

low (2 mM) and high (20 mM) glucose conditions. **d-e**, Human beta cells and beta cells<sup>CD64+</sup> were challenged in impedance NK cell ADCC (d) and CDC (e) assays with different concentrations of an anti-HLA-A2 IgG1 antibody (mean  $\pm$  SD, three independent replicates per group and time point). **f**,  $5 \times 10^4$  human beta cells or beta cells<sup>CD64+</sup> were injected subcutaneously into NSG mice with  $10^6$  human NK cells. Both groups received 3 subcutaneous 1 mg doses of anti-HLA-A2 IgG1 on days 0, 1, and 2. **g-h**, BLI signals of beta cells (g) and beta cells<sup>CD64+</sup> (h) were followed (all individual mice were plotted and BLI pictures of one representative mouse per group are shown). **i**,  $5 \times 10^4$  human beta cells were injected subcutaneously into NSG mice without NK cells and without antibodies (all individual mice were plotted and BLI pictures of one representative mouse are shown).



### 3 Discussion

There is a great disparity between organ demand and organ donations. Alongside with the unmet demand of organs for transplantation, the activation of the immune system of the recipient is a barrier to transplantation as many transplanted organs face rejection despite the use of strong immunosuppressive drugs.

A promising strategy to deal with this unmet demand could be through the use of cell therapy. Cell therapy is dedicated to the use of stem cells or progenitor cells to repair or replace damaged tissues or cells. For instance, ESCs are already used in various clinical trials to treat macular degeneration, spinal cord injury, type 1 diabetes, Parkinson disease and cancer (Trounson and McDonald 2015). However, ethical concerns regarding the origin of ESCs as well as concerns regarding their immunogenicity when allogeneically transplanted were raised. The discovery and routine generation of induced pluripotent stem cells (iPSCs) marked new possibilities for the cellular therapy field. iPSCs manufactured on an individual basis have many important applications such as understanding disease mechanisms and more efficient drug discovery and development (Rowe and Daley 2019). However, the use of autologous iPSCs for cell therapy requires long-term cell culture, reprogramming and gene editing which might lead to the expression of neoantigens and would therefore render the iPSCs and their derivatives immunogenic. Furthermore, relying only on autologous iPSCs would be highly time-consuming and would not be a viable option for patients suffering from acute diseases such as myocardial infarction.

In this work, we aimed at taking advantage of recent advances in genome editing (Jinek et al. 2012) to modify the iPSCs genome to reduce their immunogenicity in order to offer a strategy to help meet the unmet demand for organs. These edited cells or hypoimmunogenic cells would allow for successful allogeneic transplantation without the use of immunosuppressive drugs as well as faster and larger-scale manufacturing.

Specifically, this thesis entails the successful generation of mouse and human hypoimmunogenic iPSCs and their derivatives capable of evading all innate and adaptive immune responses in fully MHC-mismatched allogeneic recipients without the use of immunosuppressive drugs. The

obtained hypoimmunogenic iPSCs and their derivatives demonstrated long-term survival *in vivo* and resistance against antibody-mediated cytotoxicity.

We characterized the generated iPSCs on multiple levels. We assessed their ability to maintain pluripotency and to differentiate into various derivatives. Next, we validated cell survival *in vivo* in fully MHC-mismatched allogeneic mice. Furthermore, we challenged the iPSCs and their derivatives with the complete repertoire of immune cells and could show their successful protection against antibody-mediated cytotoxicity *in vivo* and *in vitro*. Lastly, disease-relevant cell types such as thyroid epithelial cells involved in Hashimoto's thyroiditis, pancreatic  $\beta$  cells involved in type 1 Diabetes Mellitus and antitumorigenic CAR T cells were engineered to be protected against antibody-mediated cytotoxicity, which was confirmed *in vitro* and *in vivo*. Thus, we successfully generated fully immune evasive iPSCs and their derivatives which have great potential to be used as cell therapeutics.

### 3.1 Generation of hypoimmunogenic stem cells and their derivatives

The concept of generating allogeneic cells able to engraft without triggering an immune response in the recipient is not new and it is best described during pregnancy. Pregnancy presents a unique situation as the fetus being only 50% identical to the mother is recognized by the maternal immune system, however does not get rejected (Arck and Hecher 2013). The mammals placenta is composed of various cell populations, among others the syncytiotrophoblasts are particularly interesting as they are forming a barrier between the fetus and maternal blood. To create a local immunosuppressive environment, the syncytiotrophoblasts do not express HLA-A and B and have a low expression of HLA-C molecules on their surface (Blaschitz, Hutter, and Dohr 2001), in addition they also do not express HLA class II molecules (Murphy, Choi, and Holtz 2004).

The first step towards the generation of hypoimmunogenic pluripotent stem cells was therefore to disrupt the expression of MHC class I molecules in C57BL/6 derived miPSCs. The most efficient way to target the surface expression of MHC class I molecules is to target their subunit  $\beta$ 2-microglobulin which confers them extracellular stability. CRISPR/Cas9 technology was used in combination with specifically designed guide RNAs targeting the gene of the subunit. The immunogenicity of the cells was determined after each genome editing step by *in vitro* and *in vivo* immunological assays.

miPSCs lacking MHC class I were less susceptible to CD8<sup>+</sup> T cell mediated killing as no interaction between their TCR and MHC was possible. Their survival in allogeneic mice increased from 0% to 60% as demonstrated by teratoma formation assays, while 100% of syngeneic unmodified miPSCs generated teratoma.

As a second step, the disruption of MHC class II molecules was achieved by disrupting the *Ciita* gene targeted by guide RNAs. *Ciita* is a gene that mediates transcription of MHC class II genes and promotes constitutive MHC class II expression on mammalian cells (Devaiah and Singer 2013). *B2m*<sup>-/-</sup> *Ciita*<sup>-/-</sup> miPSCs had an even better survival in allogeneic mice which increased from 60% to 91.7%. Engineered miPSCs did not induce activation of allogeneic CD8<sup>+</sup> and CD4<sup>+</sup> T cells and they were less susceptible to B cell mediated killing.

The absence of MHC class I and II molecules which typically are inhibitory ligands for macrophages and NK cells renders the edited cells susceptible to killing by these cells. Bone

marrow transplants from  $\beta 2$ -microglobulin knock-out mice to immunocompetent mice were rejected because the loss of normal cell-surface MHC class I expression triggered NK cell activation (Bix et al. 1991). The need to express immunomodulatory molecules on the surface of edited cells is therefore essential. Immunomodulatory molecules can include among others HLA-G, HLA-E, CD47, CD247 (also known as PD-L1) and CTLA4-Ig.

We selected CD47 given its function of phagocytosis inhibition its overexpression on a variety of malignant cells as an immune evasive strategy (Jaiswal et al. 2009).

*Cd47* was overexpressed in *B2m<sup>-/-</sup> Ciita<sup>-/-</sup>* miPSCs by lentiviral transduction. The survival of the cells *in vivo* was assessed by transplanting unmodified miPSCs or hypoimmunogenic miPSCs (*B2m<sup>-/-</sup> Ciita<sup>-/-</sup> Cd47<sup>tg</sup>*) in syngeneic C57BL/6 mice and in allogeneic BALB/c mice. 100% of syngeneic C57BL/6 mice that received the unmodified miPSCs generated teratoma suggesting survival and no teratoma was observed upon allogeneic transplantation in BALB/c mice. The failed teratoma growth of the grafted cells was also demonstrated by strong immune responses measured *in vitro*. When hypoimmunogenic miPSCs were allogeneically transplanted, 100% of them developed teratoma. No significant *in vitro* post-transplant immune responses were detected. The engrafted hypoimmunogenic miPSCs demonstrated long-term survival in allogeneic mice.

Further contribution of Cd47 to the edited miPSCs was assessed by injection of the cells in the peritoneum of syngeneic C57BL/6 mice. The peritoneum is rich in macrophages (Heel and Hall 1996) and the survival of the hypoimmunogenic cells was confirmed to be dependent upon the presence of Cd47. No immune response in NK cell toxicity assays was observed provided that *Cd47* was overexpressed.

The unmodified miPSCs and hypoimmunogenic miPSCs were differentiated into three mesodermal-derived cell lineages: mouse induced endothelial cells (miECs), smooth muscle cells (miSMCs) and cardiomyocytes (miCMs). Upon differentiation the expression of MHC class I and II were determined in each cell type. Not surprisingly, between the three lineages miECs WT displayed the highest upregulation of both MHC class I and II molecules upon IFN- $\gamma$  induction. Endothelial cells upregulate MHC class I and II molecules in the presence of IFN- $\gamma$  and can function as antigen presenting cells (Lapierre, Fiers, and Pober 1988). The absence of MHC class

I and II molecules on the hypoinmunogenic miECs was confirmed as well as the overexpression of *Cd47* with *in vitro* experiments.

The immunogenicity of the miPSC derivatives was assessed by *in vivo* assays. Unmodified miPSC-derived cells and hypoinmunogenic miPSC-derived cells were transplanted in either syngeneic C57BL/6 mice or allogeneic BALB/c mice. Unmodified cell grafts did not show any immune response when injected in syngeneic mice, however strong immune responses were observed in allogeneic mice. Hypoinmunogenic grafts did not cause any detectable immune response in both syngeneic and allogeneic mice. 100% of the hypoinmunogenic miPSC-derived cell grafts independently from the cell type survived long-term in allogeneic mice while unmodified miPSC-derived cells were rapidly cleared.

The triple editing of miPSCs and their derivatives led to 100% long-term survival of the cells without significant immune response in allogeneic mice.

Human iPSCs were similarly modified. First, *B2M* and *CIITA* were disrupted by CRISPR/Cas9 technology. Second, human surface protein CD47 was ectopically expressed through lentiviral transduction. This resulted in the generation of hiPS (*B2M*<sup>-/-</sup> *CIITA*<sup>-/-</sup> *CD47*<sup>tg</sup>) cells. The absence of HLA class I and II and the presence of CD47 were confirmed by *in vitro* experiments.

To assess the *in vivo* immunogenicity of the hiPSCs humanized allogeneic CD34<sup>+</sup> HSC-engrafted NSG-SGM3 mice were used. A strong immune response was measured in mice receiving unmodified hiPSCs, whereas in the hypoinmunogenic group no significant immune response was observed.

In order to use hypoinmunogenic cells as potential cell therapeutics, hiPSCs were differentiated into hiECs and hiCMs. The hypoinmunogenic hiPSC derivatives did not display any immune responses and 100% of the grafts survived in allogeneic humanized mice. To test hypoinmunogenicity of the hiPSC derivatives in another *in vivo* model, hypoinmunogenic hiECs were transplanted into Bone Marrow-Liver-Thymus (BLT) mice. BLT mice are humanized mice which received implantation of human fetal liver and thymic tissues under the kidney capsule. Thymic tissue allows for T cells selection upon binding of TCR to MHC class I and II. In four out of five mice long-term survival of the hypoinmunogenic hiECs was achieved, one mouse rejected

the engrafted cells, however further *in vitro* analyses showed no significant immune activation, potentially ruling it out as the cause for the rejection.

Overall, this study presents a new strategy to generate a universal source of iPSCs and their derivatives showing long-term survival of engrafted cells in allogeneic recipients without the use of immunosuppressive drugs.

### 3.1.1 Alternative strategies for the generation of hypoimmunogenic cells

Developing strategies to reduce the immunogenicity of cell therapeutics has been one of the main focuses of researchers in the field of regenerative medicine. Various approaches have been developed such as HLA matching and gene editing. HLA matching has been attempted by some groups through HLA typing and generation of large iPSC libraries that could match most individuals in certain populations (Solomon, Pitossi, and Rao 2015; Turner et al. 2013). While this is a clever approach, it would require many screened iPSC lines and would not be feasible for most of the countries as other populations have very heterogeneous HLA (Nakatsuji, Nakajima, and Tokunaga 2008; Pappas et al. 2015). Additionally, generating big iPSC banks is associated with high costs and labor.

Gene editing provides a cheaper, faster and more scalable alternative to HLA banking and recently many researchers have developed strategies to generate non-immunogenic hPSCs. Three different approaches are used to engineer allogeneic cells into hypoimmunogenic ones: knockout of B2M, generation of HLA-homozygous cells and knock-in of immunomodulatory molecules discovered in analyses of placental cells or cancer cell immune evasive mechanisms.

#### 3.1.1.1 Generation of hypoimmunogenic cells by B2M knockout

Beta-2-microglobulin is a protein required for the stability of HLA class I molecules to the cells surface and loss of B2M leads to HLA class I null cells. While the knockout of HLA class I molecules suppresses the activation of the adaptive immune system, it triggers innate immune cells activation and leads to rapid clearance of the cells in allogeneic recipients.

Xu et al. knocked out in hiPSCs HLA-A and -B and retained one matched HLA-C allele to counteract the activation of NK cells (Xu et al. 2019) and T cells *in vitro* and *in vivo*. The authors show similar *in vitro* T cell evasion results when comparing B2M<sup>-/-</sup> and HLA-A/-B<sup>-/-</sup> hiPSCs-derived CD43<sup>+</sup> blood cells. *In vivo* data in NRG mice (lacking T, B and NK cells) demonstrate survival of modified hiPSC-derived CD43<sup>+</sup> blood cells when adding either primed CD8<sup>+</sup> T cells or NK cells. To further reduce the immunogenicity of the modified hiPSCs, HLA class II knockout was also performed. Appropriate suppression of NK cell activity could pose issues in some

individuals as their inhibition is dependent on specific HLA alleles, for instance retained HLA-E can suppress NK cells that express NKG2A, KIR2DL1, 2, 3, and 4, however it does not protect them against other NK cell populations. Furthermore, minor histocompatibility antigens could still be presented from retained HLA-C molecules and engrafted cells could be eliminated by CD8<sup>+</sup> T cells or antibody-mediated rejection (**Figure 3**).

Mattapally et al. edited hiPSCs to generate cells lacking HLA class I and II by knockout of B2M and CIITA. Cardiomyocytes were differentiated from hiPSCs and only low levels of T cell activation were observed. The retention of HLA-E and -G allowed for the suppression of NK cell killing (Mattapally et al. 2018).

Gornalusse et al. knocked out B2M in hPSCs to prevent the activation of allogeneic CD8<sup>+</sup> T cells, and knocked in exogenous HLA-E to avoid the lysis by NKG2A<sup>+</sup> NK cells through missing-self response (Gornalusse et al. 2017). *In vitro* and *in vivo* data suggest that the loss of B2M lead to CD8<sup>+</sup> T cell evasion and the knock in of HLA-E protected the target cells against NKG2A<sup>+</sup> NK cells. This approach, however, is not conferring protection against KIR2D<sup>+</sup> NK cells or macrophages, which are known contributors to rejection of transplanted cells. The retained expression of HLA class II molecules could be immunogenic when differentiating hPSCs into antigen presenting cells such as endothelial cells.

Han et al. knocked out HLA-A/B/C, HLA class II and overexpressed HLA-G, PD-L1 and CD47 (Han et al. 2019). Significantly reduced T cell activation but not a complete loss was observed. These observations might suggest a role for retained HLA molecules in the presentation of antigens to T cells and their activation. After transplantation an inflammatory milieu is created and allografts are exposed to various cytokines, such as interferons which are known to promote expression of HLA class I and II (Seliger, Ruiz-Cabello, and Garrido 2008). Long-term survival of the allografts could be jeopardized by the presence of HLA molecules, therefore *in vivo* validation in humanized mice could have been insightful to study the engraftment of engineered cells long-term (**Figure 3**). It has to be noted that no humanized mouse model is currently fully recapitulating the human immune response to an allogeneic graft.



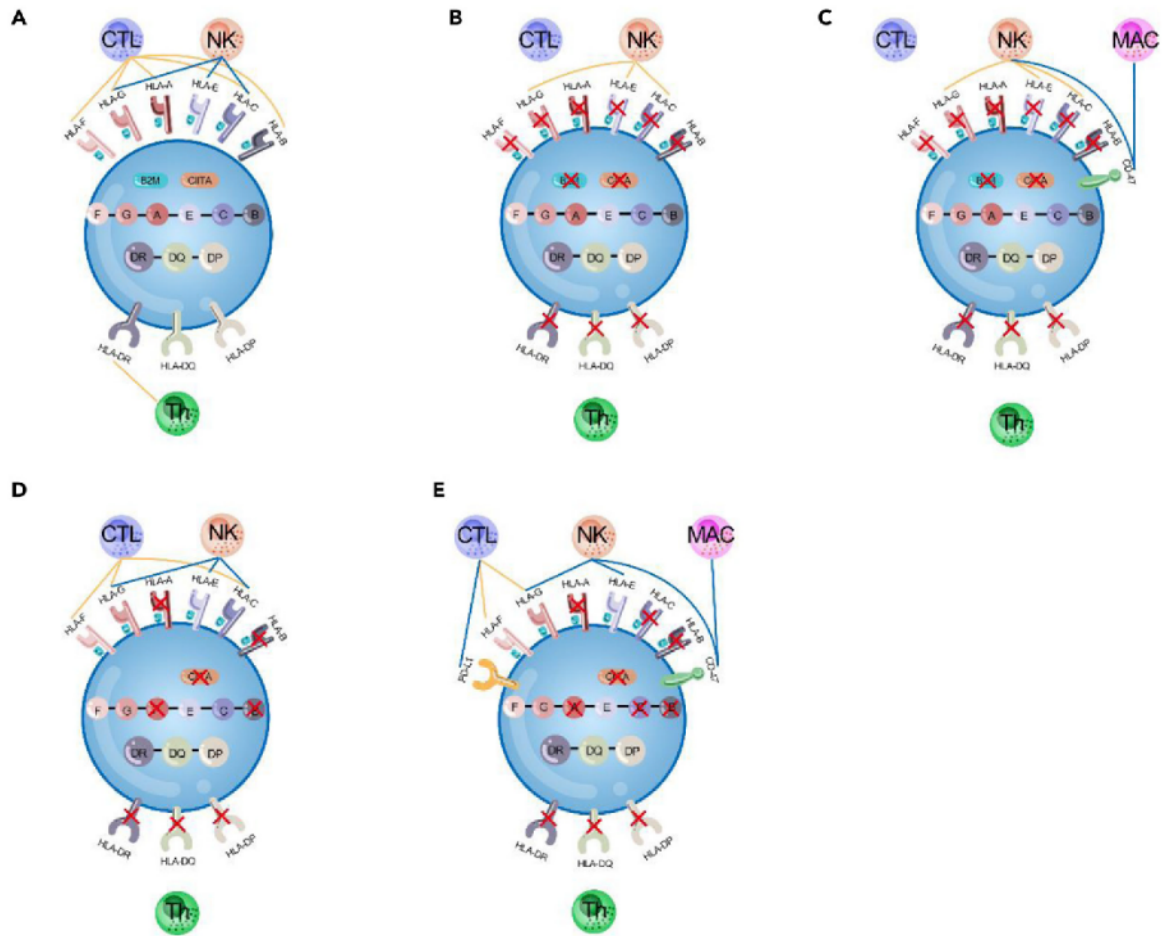


**Figure 3:** Schematic representation of the gene editing strategies to generate hypoimmunogenic cells.

- A) T cells are activated by allogeneic HLA molecules. HLA class I molecules suppress NK cell activity.
- B) Loss of HLA class I by *B2M* knockout and class II molecules by *CITA* knockout. T cell activity is suppressed, but NK cells are activated by loss of HLA class I.
- C) Loss of HLA class I and II and knock-in of CD47 to protect allogeneic cells from macrophages and NK cells.
- D) Loss of HLA-A and HLA-B but not HLA-C, HLA-E and HLA-G suppress NK cells activation.
- E) Loss of HLA-A/-B/-C and HLA class II molecules. Knock-in of CD47 and PD-L1 and retained expression of HLA-G evade T cells, macrophages and NK cells activation. (Zhao et al. 2020).

### 3.1.1.2 Generation of hypoimmunogenic cells by retaining homozygous HLA

Torikai and colleagues knocked out HLA-A molecules from hESCs and primary T cells while forcing the expression of non-classical HLA class I molecules such as HLA-E and/or HLA-G to protect the cells from NK cell lysis (Torikai et al. 2013). HLA-E is a ligand for the NK inhibitory

receptor CD94/NKG2A found on most NK cells (Lee et al. 1998) and can therefore protect the cells against NKG2A positive NK cells. HLA-E is however also a ligand for NKG2C on NK cells which triggers their activation (Watzl 2018). As expected, *in vitro* assays showed that HLA restricted CD8<sup>+</sup> T cells did not eliminate the engineered T cells or the hESCs. NK cells activation and lysis of the target cells was also prevented. While these are important findings, expression of one or more recipient's matched HLA alleles (HLA-A, B, or C) could prevent the elimination of target cells only by a subset of NK cells as well as only from CD8<sup>+</sup> T cells. This approach would need further *in vivo* model validation such as humanized mouse, which might reveal that the mismatch of HLA-B and C molecules would contribute to graft rejection.

### **3.1.1.3 Generation of hypoinmunogenic cells by knock-in of immunomodulatory molecules**

Rong et al. demonstrated the survival of hESC and hESC-derived fibroblasts and cardiomyocytes in allogeneic humanized mice through the forced expression of two immunosuppressive molecules. Cytotoxic T lymphocyte antigen 4-Ig (CTLA4-Ig) and PD-L1. CTLA4-Ig is a soluble fusion protein that competes for the binding of co-stimulatory molecules on T cells. PD-L1 expression leads to the activation of T cell inhibitory pathway. No T cell cytotoxicity was observed. *In vivo* data in humanized mice model suggest protection against T cell mediated rejection when both immunomodulatory molecules were expressed. Furthermore, analysis of T cell infiltration in teratoma of hESC CTLA4-Ig/PD-L1 knock-in cells revealed that the amount of T cells was reduced compared to control hESC derived teratoma (Rong et al. 2014). CTLA4-Ig is a ligand for CTLA-4 receptor ubiquitously expressed on regulatory T cells (Treg) which are important for transplant tolerance (Salomon et al. 2000) and the overexpression of CTLA4-Ig might compromise their functions (Bluestone, St Clair, and Turka 2006).

Another group (Harding et al. 2019) bypassed the deletion of HLA class I and II in mouse ESCs and their derivatives by introducing eight immunomodulatory genes. *Ccl21*, *Pd11*, *Fasl*, *Serp1nb9*, *H2-M3*, *Cd47*, *Cd200*, and *Mfge8* were exogenously expressed using CRISPR/Cas9 technology. Edited mESCs demonstrated survival in allogeneic mice, however the number of insertions required could increase the risk of oncogenic mutations in the cells.

Overall, these approaches modified or eliminated a combination of HLA class I and II molecules, however the presence of HLA molecules or other antigens in an allogeneic host could trigger an HLA or non-HLA directed antibody-mediated immune response and lead to hyperacute rejection of the cells (Iniotaki-Theodoraki 2001; Masson et al. 2007).

### **3.2 Generation of hypimmune cell therapeutics to treat cardiovascular and pulmonary diseases**

Cell therapy could be a promising strategy to treat worldwide spread diseases such as cardiovascular and pulmonary disorders. The generation of hypimmune cell therapeutics could potentially serve as a solution to treat acute cardiovascular and pulmonary diseases without the use of immunosuppressants.

The generation of hypimmune murine cell therapeutics was described above, briefly C57BL/6 derived mouse iPSCs were edited by knockout of B2m and Ciita genes by CRISPR-Cas9 technology to generate cells depleted of MHC Class I and Class II molecules. The cells were further edited by lentiviral expression of immune checkpoint molecule Cd47. The hypimmune murine iPSCs were then differentiated into cardiomyocytes (iCMs) and endothelial cells (iECs), these cell therapeutics and their treatment potential were investigated. A disease that currently lacks good treatment is Critical limb ischemia (CLI), a disease consisting in the obstruction of the arteries which leads to limb amputation in about 30% of the patients, and 25% of patients will die rapidly. Firstly, a model to recapitulate CLI in mice is performing ligation and excision of femoral artery, second step was to provide treatment with hypimmune iECs to affected BALB/c mice. One group of mice did not receive any treatment the other two groups received multiple injections of allogeneic unmodified B6 (allo iECs) or allogeneic hypimmune B6 iECs (alloHIP iECs) which were previously lentivirally transduced with the Firefly Luciferase gene (FLuc<sup>+</sup>). The survival of the cells was tracked *in vivo* for 28 days using bioluminescence imaging (BLI). All the allo iECs grafts were rejected within 15 days due to immune rejection, in contrast to alloHIP iECs which survived. The perfusion of the affected legs was measured using doppler imaging, which showed an increase in leg perfusion only in the alloHIP iECs group. Not only the leg perfusion was improved, but half of the mice receiving alloHIP iECs did not show gangrenous lesions and the

other half had less severe lesions compared to the other two groups. The recovered grafts were analyzed by immunofluorescence imaging revealing FLuc<sup>+</sup> cells being incorporated as part of the formed blood vessels in all alloHIP iEC recipients, whereas no FLuc<sup>+</sup> cells were detected in the recipients of allo iECs. The alloHIP iECs detected were also VE-cadherin<sup>+</sup> which is a marker for ECs. In conclusion, alloHIP iECs survive in allogeneic mice, integrating to form blood vessels and while improving leg perfusion they also improved the state of gangrenous lesions allowing for better limb preservation.

Another common acute disorder affecting the lungs, among other organs, is caused by the deficiency in the protein Alpha1-antitrypsin (A1AT) encoded by the SERPINA1 gene. Mouse model of A1AT deficiency is generated by knockout of *Serpina1a-e* genes, in order to trigger lung emphysema in the mice, mice need to be administered lipopolysaccharide (LPS). Lung emphysema develops as the lack of circulating A1AT cannot inhibit the activity of neutrophil elastase (NE) which damages the lungs. Hypoimmune iECs could be used as a source of A1AT to restore its levels in a mouse model of A1AT deficiency, therefore B6 and B6HIP iECs were manipulated to secrete A1AT by lentiviral transduction of *Serpina1e* gene (B6<sup>S1e</sup> and B6HIP<sup>S1e</sup>). Additionally, the cells were engineered to express H-2K<sup>d</sup>, a major histocompatibility molecule of allogeneic BALB/c mice, this step was necessary because the genetic background of *Serpina*<sup>-/-</sup> mice was syngeneic (B6). To generate more immunogenic cells, a BALB/c-variant of *Co3* protein which is a minor histocompatibility antigen (miHA) of mitochondrial DNA mismatched to B6 mice was lentivirally overexpressed in the cells. The transgenic <sup>e</sup>allo<sup>S1e</sup> and <sup>e</sup>alloHIP<sup>S1e</sup> iECs secreted levels of A1AT and the total amount of cells required to secrete physiological levels of A1AT was assessed. Cells were injected subcutaneously and i.p. in *Serpina*<sup>-/-</sup> mice before induction of emphysema by LPS. Two control groups consisted in *Serpina*<sup>-/-</sup> mice that did not receive cell injection and healthy B6. In both untreated *Serpina*<sup>-/-</sup> mice and mice in the group that received <sup>e</sup>allo<sup>S1e</sup> iECs no A1AT levels in the serum were detected. Mice treated with <sup>e</sup>alloHIP<sup>S1e</sup> iECs had levels of A1AT restored and the cells survived in the mice. Cell survival was assessed by BLI and the only group of grafted cells surviving was the <sup>e</sup>alloHIP<sup>S1e</sup> iECs recipients.

FlexiVent performed on day 14 revealed that untreated *Serpina*<sup>-/-</sup> B6 mice developed lung emphysema demonstrating that the model was sound. The <sup>e</sup>allo<sup>S1e</sup> iECs were rapidly rejected and did not prevent the development of lung emphysema, similarly to untreated *Serpina*<sup>-/-</sup> B6. The

group of mice which received  $\epsilon$ alloHIP<sup>S1e</sup> iECs showed prevention of lung emphysema similarly to healthy B6 mice. Histological analysis was performed and revealed structural damage in the lung of affected animals, except in the group of mice which received  $\epsilon$ alloHIP<sup>S1e</sup> iECs. To conclude, the use of hypoimmune iECs engineered to secrete A1AT in an allogeneic mouse model of A1AT deficiency showed prevention of lung emphysema.

The last translational application investigated was the use of HIP iECs to treat myocardial infarction in allogeneic mice. Cryoinjury-induced myocardial infarction which allows for precise and reproducible induction of myocardial infarction (Wang et al. 2019) was performed on BALB/c mice. After infarction injections of either allo iECs or alloHIP iECs into the affected area (both FLuc<sup>+</sup>). Similarly to previous results, allo iECs grafts were rejected within 15 days, but not alloHIP iECs which survived and showed some degree of proliferation. The mice underwent pressure–volume loop (PV loop) measurements to assess various heart function parameters. alloHIP iECs injection was the only treatment which provided benefit to some heart functions. After 28 days follow-up, histological analysis was performed on the recovered hearts and immunofluorescence staining revealed alloHIP iECs positive for FLuc in the injection sites, but no FLuc<sup>+</sup> allo iECs could be observed in the group that received those cells.

Because endothelial cells are contractile cells, a 1:1 mixture of allo iECs and iCMs or alloHIP iECs and iCMs was injected with the goal of improving the muscle functions of the infarcted hearts. As expected, an immune response leading to rejection within 14 days to allo iEC and iCM grafts was observed, which was not detectable in recipients receiving alloHIP iECs and iCMs cell mixture, surviving in allogeneic BALB/c. PV loop measurements assessed a significant increase of several cardiac functions in the group receiving the alloHIP cell mixture compared to allo iECs and iCMs. Histological sections of the hearts of the alloHIP group showed engrafted FLuc<sup>+</sup> cells, but not for the allo iECs iCMs graft cells. These data show the ability of alloHIP cells to improve some heart function parameters in allogeneic mice with myocardial infarction.

Overall, three major acute diseases were investigated in allogeneic mice and the therapeutic potential of hypoimmune cells was assessed. Current treatments for patients suffering from CLI reveals some good results with autologous CD34<sup>+</sup> or CD133<sup>+</sup> stem cells rigato (Rigato, Monami, and Fadini 2017), but alternatives that are not causing an immune response are needed. The amputation of the limb occurs in approximately 30% of the patients, which was observed also in

the mice. Treatment with alloHIP iECs increased limb preservation in mice, limb perfusion and *in vivo* imaging revealed survival of grafted alloHIP iECs without the use of immunosuppression. FLuc<sup>+</sup> graft cells were recovered and found to be integrated in the endothelial layer of vessels.

Another very prevalent disorder is chronic obstructive pulmonary disease and A1AT deficiency is a genetic mutation (Lomas and Silverman 2001) in the SERPINA1 gene. The deficiency of A1AT causes the lack of NE inhibition in the lung leading to damage of the lung structures (Greene et al. 2016). Currently patients do not have many treatment options and most of the treatments such as the infusion of pooled human A1AT are extremely expensive and patients need to receive the infusion weekly (Wewers et al. 1987). Using a *Serpina*<sup>-/-</sup> mouse model, the disease could be recapitulated. Administration of <sup>e</sup>alloHIP<sup>S1e</sup> iECs led to a normal production level of A1AT in the serum of the mice and prevented deterioration of lung function which occurred in the other two groups. Performing histological and FlexiVent analysis the study shows that <sup>e</sup>alloHIP<sup>S1e</sup> iECs secrete enough A1AT in order to replace physiological plasma levels and prevent lung emphysema.

Myocardial infarction and heart failure are major leading causes of death in the United States (Writing Group et al. 2016) and worldwide. This study, similarly to clinical trial endpoints, focused on the assessment of hemodynamic improvement (Fernandez-Aviles et al. 2018). AlloHIP cell therapeutics survived and engrafted in the areas where they were injected and the administration of alloHIP iECs showed an increase in cardiomyocyte survival, which potentially could suggest a survival-promoting effect of cardiomyocytes via paracrine (Narmoneva et al. 2004), potential cytokine release (Deuse et al. 2009) or exosomes release (Gao et al. 2020). This study shows the potential of universal “off-the-shelf” therapeutics in allogeneic recipients which could replace autologous cells currently used in clinical trials (Quyyumi et al. 2017). Mixture of alloHIP iECs and iCMs led to improvements in hemodynamic parameters compared to allo iECs and iCMs, also alloHIP iECs and iCMs showed survival and engraftment similarly to previously analyzed alloHIP iECs. Cardiomyocytes did not seem to add contractile functions to infarcted hearts when compared to alloHIP iECs only group. A possible explanation could be that the amount of cardiomyocytes injected was not sufficient to achieve this specific function. The use of xenogeneic (van Laake et al. 2007; Romagnuolo et al. 2019; Liu, Chen, et al. 2018) or allogeneic (Shiba et al. 2016; Mauritz et al. 2011) iCMs led to an improvement in cardiac function after transplantation, however the

cells were transplanted using immunosuppressive drugs to avoid graft rejection. Hypoimmune “off-the-shelf” cell therapeutics survived in allogeneic mice without the use of immunosuppression and without triggering an immune response, demonstrating the potential of a universal source of cardiomyocytes and endothelial cells that could be used to treat major disorders. In general, universal cell therapeutics could be used as a source of less expensive alternatives for regenerative medicine approaches to diseases requiring the use of allogeneic cells.

### **3.3 Generation of hypoimmunogenic stem cells and their derivatives resistant to antibody-mediated killing**

Antibody-mediated rejection (AMR) is a common issue in organ transplantation, especially in solid organ transplantations. AMR is usually characterized by tissue injury and the presence of circulating donor specific antibodies (DSAs) directed against the vascular endothelium of the graft. These antibodies are either present in the recipient beforehand or generated by the recipient *de novo* after transplantation despite the use of strong immunosuppressive drugs.

Despite efforts made in order to generate universal “off-the-shelf” by loss of HLA molecules, (Deuse, Hu, Gravina, et al. 2019; Xu et al. 2019; Han et al. 2019), the cells remain susceptible to antibody-mediated killing directed against non-HLA epitopes (Zhang et al. 2011), cell-specific autoantigens like angiotensin II type 1-receptor or anti-endothelial cell antibodies (AECAs) (Dragun et al. 2005; Delville et al. 2019; Sun et al. 2011), xenogeneic (Klee 2000) and synthetic (Choe et al. 2021) constructs or immunogenic byproducts of viral genome editing processes (Lamers et al. 2011). Besides transplantation, antibody-mediated cytotoxicity is also a hallmark of autoimmune diseases as the presence of autoantibodies mediates the destruction of the target cells. Evidence of antibody-mediated cytotoxicity is emerging also in the cancer therapy field where chimeric antigen receptor (CAR) T cells are rapidly cleared from the patient’s body by antibodies directed against them (Hege et al. 2017) especially when targeting non-B cell tumors.

In antibody dependent cellular cytotoxicity, immunoglobulins bind the epitope via the F<sub>ab</sub> domains and subsequently have the F<sub>c</sub> domain exposed which can trigger the activation of effector cells through FcRs. The forced expression of the FcR CD64 combined with the hypoimmunogenic edits

allowed the generation of fully immune evasive cell lines, which can improve the survival and persistence of cell therapeutics.

miEC derived from unmodified C57BL/6 miPSCs were modified to express mouse Cd64 and the free mouse IgG2a binding capacity of Cd64 was tested in various immune assays with a different range of MHC or non-MHC antibodies and concentrations. To then test the efficacy of the fully immune evasive cells model *in vitro* and *in vivo*, C57BL/6 hypoinmunogenic miEC ( $B2m^{-/-} Ciita^{-/-} Cd47^{tg}$ ) were transduced to express human CD64 and human CD52. Alemtuzumab binds its epitope CD52 and is a highly cytotoxic humanized IgG1 non-HLA directed antibody used for treatment of various B cell malignancies, hematopoietic disorders, and autoimmune diseases. *In vitro* immune assays demonstrated the resistance of the target cells to ADCC and CDC only when CD64 was expressed. To test the model *in vivo* syngeneic C57BL/6 Rag-1 mice lacking B and T cells but having functional NK cells were used. Mice receiving hypoinmunogenic miEC<sup>CD52</sup> rapidly rejected the grafted cells after multiple doses of Alemtuzumab, whereas C57BL/6 Rag-1 mice receiving hypoinmunogenic miEC<sup>CD52CD64</sup> did not reject the grafted cells.

To test this concept in human cells, hiEC derived from unmodified or hypoinmunogenic hiPSCs ( $B2M^{-/-} CIITA^{-/-} CD47^{tg}$ ) were modified to express CD64 and the free IgG binding capacity of CD64 was tested in multiple immune assays with a different range of HLA or non-HLA antibodies and concentrations. Unmodified hiEC and hiEC<sup>CD64</sup> were transduced to express CD52 using a lentiviral delivery approach. Immune assays demonstrated that while hiEC<sup>CD52</sup> were quickly killed via ADCC and CDC in an Alemtuzumab dose-dependent manner, 100% of the hiEC<sup>CD52CD64</sup> survived independently of antibody concentration. Similar results were obtained using the serum of two transplant recipients with high DSAs (anti-HLA-A2) and clinical signs of AMR. hiEC and hiEC<sup>CD64</sup> (previously typed and HLA-A2 positive) were incubated with the serum of the patients. While hiEC underwent rapid killing by CDC, hiEC<sup>CD64</sup> remained unaffected.

Hypoinmunogenic hiEC cells were transduced to express either CD52 or CD52 and CD64. *In vitro* data suggest that exposing the hypoinmunogenic hiEC<sup>CD52</sup> and hiEC<sup>CD52CD64</sup> cells to the whole repertoire of immune cells did not cause cytotoxicity until Alemtuzumab was added. The hypoinmunogenic hiEC<sup>CD52</sup> were quickly killed in contrast to hypoinmunogenic hiEC<sup>CD52CD64</sup> that were not affected. The long-term survival of hiEC<sup>CD52CD64</sup> after Alemtuzumab administration also was tested and validated *in vivo* by transplanting hypoinmunogenic hiEC<sup>CD52</sup> and



hiEC<sup>CD52CD64</sup> together with human NK cells in allogeneic humanized NSG-SGM3 mice engrafted with CD34<sup>+</sup> hematopoietic stem cells.

To further verify the essential protective role of CD64, hiEC<sup>CD52CD64</sup> were incubated with a human IgG1 or a mouse IgG2b anti-CD52 antibody, the latter does not bind to CD64. Human or mouse complement were used as effector system. hiEC<sup>CD52CD64</sup> were resistant against human anti-CD52 IgG1 but susceptible against mouse anti-CD52 IgG2b.

The IgG protection conferred by high expression of CD64 on hiEC<sup>CD64</sup> was broken when the expression on the target cells of CD64 was significantly reduced. Low expression of CD64 failed to protect the target cells against higher cytotoxic antibody concentrations.

To better understand the mechanism of action of CD64, *in vitro* assays revealed the binding mechanisms of antibodies when competing for the binding to CD64. Upon administration of two human IgG antibodies, the one finding an epitope on the target cell had a higher affinity to CD64 compared to the one lacking its epitope. The protection conferred by CD64 against the more cytotoxic antibody was not broken by the competitor.

Ensuring safety of cell products intended for use in translational applications is crucial, therefore the truncated form of CD64 (CD64t) which lacks any intracellular domain was used. CD64t was used to transduce human thyroid epithelial cells, beta cells and CAR T cells to protect them against autoantibodies. Human thyroid epithelial cells are present in the thyroid and are targeted by cytotoxic autoantibodies in most of the patients with Hashimoto's thyroiditis (Doullay et al. 1991; Rapoport and McLachlan 2001).

Beta cells are cells present in the pancreas and mainly targeted by T cells in patients with Type 1 diabetes (T1D), although antibodies are also present in T1D patients and accelerate their destruction.

CAR T cells are widely used in cancer therapy and studies have observed an antibody response against the CAR especially when CAR T cells are directed against solid tumors and not B cells.

These cell types gained protection against an array of autoantibodies (HLA and non-HLA directed) by forced expression of CD64t as demonstrated in various *in vitro* and *in vivo* immune assays in

allogeneic humanized NSG-SGM3 mice engrafted with CD34<sup>+</sup> hematopoietic stem cells. Importantly, CD64t expression did not compromise their cellular functions.

Overall, the ectopic expression of non-immunogenic FcγR1 in universal off-the-shelf hypoinmunogenic cells provided antibody resistance against anti-HLA and non-HLA antibodies demonstrated by various *in vitro* immune assays as well as *in vivo* assays. Ectopic expression of CD64 or CD64t was assessed in various translationally relevant cell types. These findings suggest that the regenerative impact of current cell therapeutics could be further improved by adding an additional layer of protection to the cells against antibody-mediated cytotoxicity. This could benefit especially treatment of diseases where lingering autoantibodies could jeopardize the persistence of cell therapeutics.

### **3.3.1 Strategies for the generation of cell therapeutics resistant to antibody-mediated cytotoxicity**

In transplantation various attempts have been made to improve successful organ transplants in patients with high DSA counts. Different antibodies have been generated to block key players in antibody-mediated rejection and many are currently being tested in Phase III clinical trials. Among those are Rituximab (anti-CD20; NCT03994783), Tocilizumab (anti-IL6; NCT04561986) and Eculizumab (anti-C5; NCT02013037).

Recently, IgG-degrading enzyme derived from the bacteria *Streptococcus pyogenes* (IdeS) has been used on patients with high pre-existing DSAs prior to HLA mismatched kidney transplant (Lonze et al. 2018) showing a reduction of IgG HLA levels in 24 out of 25 patients (Jordan et al. 2017). IdeS is a protease that can cleave all four classes of polyclonal human IgG at a specific amino acid position in their F<sub>c</sub> region. Without the F<sub>c</sub> region, FcRs on immune cells cannot interact with it anymore preventing ADCC and CDC activity. This study seems promising however it does not include long-term graft acceptance data and the small sample of patients included in the study is not guaranteeing the prevention of future rejection.

The activity of IdeS might be utilized not only in transplantation but also for other purposes, for instance as protection of CAR T cells against allogeneic antibody immune response. It has been

reported that components of the CAR might induce immunogenicity, particularly the mouse-derived single-chain variable fragments (Gorovits and Koren 2019). In fact, there is evidence in clinical trials that CAR T cell long-term persistence is challenged by host IgG antibodies directed against the CAR proteins (Hege et al. 2017; Wagner et al. 2021). Some patients suffering from B cell malignancies do not achieve complete remission, and might require re-infusion of CAR T cells. In these patients, anti-CAR antibodies have been detected and their presence has been linked to a reduced number of CAR T cells (Wagner et al. 2021).

Peraro and colleagues utilized the activity of IdeS to protect CAR T cells against allogeneic antibody immune response. CAR T cells were engineered to express both membrane-bound and secreted IdeS constructs. IdeS cleaved all the IgGs in proximity of the CAR T cells and F<sub>ab</sub> regions of IgGs remained bound to their epitope creating a physical shield preventing new attacks from additional IgGs while preserving CAR T cell function (Peraro et al. 2021). The depletion of IgGs was validated *in vitro* against human anti-HLA antibodies and both *in vitro* and *in vivo* in immunodeficient mice against human anti-CAR antibodies. The persistence of IdeS could be challenged by pre-formed IgG antibodies against IdeS. The presence of pre-formed IgG antibodies could be due to earlier *Streptococcus pyogenes* infections which are prevalent in the healthy population with an estimated 3/100000 cases in some regions (Reglinski et al. 2015). However, this could be prevented by the IdeS membrane bound or secreted enzyme which would be acting locally and could potentially protect itself against host anti-IdeS IgGs (Winstedt et al. 2015).

The current cellular therapies of autoimmune diseases such as T1D include the use of non-HLA matched hESCs derived islet cells (Butler and Gale 2022). Strategies have been developed to maximize the success of cell therapies. The encapsulation of islet cells using semipermeable biomaterials is a way to protect them against immune responses, however antibodies against the hESCs have been observed (Duvivier-Kali et al. 2004).

### 3.4 Risks

Genetic manipulation of iPSCs such as the knockout of *B2M* and *CIITA* might raise concerns regarding the safety of these cell therapeutics. Evidence suggests that B2m knock out mice are depleted of CD8<sup>+</sup> T cells but are generally healthy (Koller et al. 2010). In humans, HLA class I or

II deficiencies are so called rare primary immunodeficiencies (PID). HLA class I deficiency is caused by mutations of the proteins transporter associated with antigen processing (TAP) 1, TAP2 and tapasin. Deficiencies in HLA class II molecules are caused by the mutations in regulatory factors controlling the transcription of their genes. These are RFX containing ankyrin repeats (RFXANK), RFX5, and RFX-associated protein (RFXAP). The patients lacking HLA I or II do not seem to have a propensity to develop tumors and their antiviral immunity is intact (Hanna and Etzioni 2014). However, the elimination of HLA expression on cell surface affects peptide presentation to immune cells and this might be concerning if cells would get virally infected or become malignant. Viral clearance is mediated by the presentation of viral protein fragments from HLA class I and II on the infected cells to the appropriate immune cells. The immune system is then activated and eliminates the infected cells. While the efficacy of the immune system promoting viral clearance could be jeopardized by cells lacking HLA I and II molecules, a study has shown that even though the cells lost HLA proteins, other non-HLA dependent mechanisms promoted the viral clearance (Hou et al. 1992).

Generating cells with multiple genomic edits and their *ex vivo* culture could lead to potential oncogenic mutations. p53 is an essential antitumorigenic protein encoded by the gene *TP53*. p53 arrests the cell cycle in cells when DNA is damaged. If cells contain excessive and irreparable DNA damages, p53 triggers apoptosis before the cells become tumorigenic. Increases in point mutation rates in the *TP53* gene have been observed in correlation with time of hiPSCs culture by selecting for cells harboring p53 mutations (Merkle et al. 2017).

Tumorigenic transformations could occur in hypoimmunogenic cells and according to evidence in other species, loss of MHC in malignant cells can lead to the spreading of tumor cells even across allogeneic barriers. The Tasmanian devil population is threatened by devil facial tumor disease that can be transmitted through biting (Caldwell et al. 2018). Another example of transmissible tumor cells is the canine transmissible venereal tumor occurring in dogs and can be transmitted by contact with areas affected by the tumor (Welsh 2011). Currently there is no evidence for transmission of human cancer cells between human beings, however it is essential to ensure the safety of hypoimmunogenic cells before and after transplantation for oncogenic transformations when intended to be used for clinical applications (Merkle et al. 2017).

A possible solution to the problem concerning safety against oncogenic mutations or contamination of undifferentiated hiPSCs in hiPSC-derived cells, would be the integration of suicide genes (He et al. 2017). Suicide genes could be introduced in hypoimmunogenic cells under appropriate stem cell loci which would lead to their inactivation as soon as the stem cells are committed to differentiate. Two strategies are mainly used in hiPSC-based therapies, the use of herpes simplex virus thymidine kinase (HSV-TK) and the inducible caspase-9 (iC9) (Zarogoulidis et al. 2013). Targeted HSV-TK transduced hiPS-derived cells are able to convert a non-toxic pro-drug called ganciclovir (GCV) to ganciclovir triphosphate, which is toxic and blocks DNA replication (Moolten 1986). This is an effective strategy to eliminate rapidly dividing cells from slowly dividing or non-dividing cells, for instance neurons and gliomas (Nanda et al. 2001).

The inducible caspase-9 suicide gene encodes a human caspase-9 protein fused with a FK506-binding protein. Caspase-9 is a protein expressed in mammalian cells and requires activation to induce apoptosis. The activation is induced by a non-toxic dimerizer drug (AP20187) (Clackson et al. 1998) and the dimerization of iC9 results in rapid cell death. iC9 could be inserted under a stem cell gene promoter and transcribed whenever the gene is transcribed.

The forced overexpression of the protein CD47 on the surface of the hypoimmunogenic cells leads to an intracellular signaling cascade when bound to its ligands. Two of its own known ligands are SIRP $\alpha$  (Jiang, Lagenaur, and Narayanan 1999) and secreted thrombospondin-1 (TSP-1). Intracellular signaling upon TSP-1 binding has not been completely elucidated. Binding of CD47 by its ligands is associated with different signaling pathways such as angiogenesis, cell proliferation and differentiation, controlling cardiovascular homeostasis and immune regulation (Ishikawa-Sekigami et al. 2006; Soto-Pantoja, Kaur, and Roberts 2015; Yi et al. 2015).

Similarly, the ectopic expression of CD64 when IgG-bound or F $_c$  fragment-bound could potentially lead to an intracellular signaling cascade that could alter the cell functions. In monocytes, CD64 consists of the receptor associated with a  $\gamma$ -chain signaling subunit. The cytoplasmic domain of the  $\gamma$ -chain includes immunoreceptor tyrosine activation motifs (ITAMs). Following receptor binding by immune complexes activation, the ITAMs activate a series of signaling cascades via Proto-oncogene tyrosine-protein kinase (SRC) family kinases and spleen tyrosine kinase (SYK) (Daeron 1997; Nimmerjahn and Ravetch 2008). Downstream signaling results in antibody-CD64 complex to be internalized and recycled (Harrison et al. 1994) as well as

ADCC, phagocytosis and cytokine release (Nimmerjahn and Ravetch 2008). Studies show that the deletion of the cytosolic tail of CD64 prevents endocytosis and phagocytosis (Edberg et al. 1999). Therefore, the use of truncated alternatives would not cause any intracellular signaling and would mitigate potential risk of downstream signaling.

### **3.5 Future directions**

The work in this PhD thesis demonstrated that genetic engineering of mouse and human iPSCs and their derivatives has allowed them to successfully overcome allogeneic barriers of the immune system. This was demonstrated by survival *in vitro* and *in vivo* in various allogeneic models and settings. The addition of Cd64/CD64 allowed hypoimmunogenic cells to evade all humoral responses which is especially relevant to ensure graft survival when treating disorders characterized by the presence of autoantibodies such as autoimmune disorders.

Overall, this work demonstrated the effectiveness of fully immune evasive hypoimmunogenic cells and their potential for clinical regenerative applications. Such applications might include myocardial infarction which is an acute condition requiring a supply of cells that can be ready to be engrafted or improvement of current CAR T cell therapies to potentially reduce re-infusions in pre-sensitized patients.

## 4 References

- Araki, R., M. Uda, Y. Hoki, M. Sunayama, M. Nakamura, S. Ando, M. Sugiura, H. Ideno, A. Shimada, A. Nifuji, and M. Abe. 2013. 'Negligible immunogenicity of terminally differentiated cells derived from induced pluripotent or embryonic stem cells', *Nature*, 494: 100-4.
- Arck, P. C., and K. Hecher. 2013. 'Fetomaternal immune cross-talk and its consequences for maternal and offspring's health', *Nat Med*, 19: 548-56.
- Bibeau, F., E. Lopez-Crapez, F. Di Fiore, S. Thezenas, M. Ychou, F. Blanchard, A. Lamy, F. Penault-Llorca, T. Frebourg, P. Michel, J. C. Sabourin, and F. Boissiere-Michot. 2009. 'Impact of Fc{gamma}RIIa-Fc{gamma}RIIIa polymorphisms and KRAS mutations on the clinical outcome of patients with metastatic colorectal cancer treated with cetuximab plus irinotecan', *J Clin Oncol*, 27: 1122-9.
- Bix, M., N. S. Liao, M. Zijlstra, J. Loring, R. Jaenisch, and D. Raulet. 1991. 'Rejection of class I MHC-deficient haemopoietic cells by irradiated MHC-matched mice', *Nature*, 349: 329-31.
- Blaschitz, A., H. Hutter, and G. Dohr. 2001. 'HLA Class I protein expression in the human placenta', *Early Pregnancy*, 5: 67-9.
- Bluestone, J. A., E. W. St Clair, and L. A. Turka. 2006. 'CTLA4Ig: bridging the basic immunology with clinical application', *Immunity*, 24: 233-8.
- Bohmig, G. A., M. Exner, A. Habicht, M. Schillinger, U. Lang, J. Kletzmayer, M. D. Saemann, W. H. Horl, B. Watschinger, and H. Regele. 2002. 'Capillary C4d deposition in kidney allografts: a specific marker of alloantibody-dependent graft injury', *J Am Soc Nephrol*, 13: 1091-99.
- Butler, P. C., and E. A. Gale. 2022. 'Reversing type 1 diabetes with stem cell-derived islets: a step closer to the dream?', *J Clin Invest*, 132.
- Caldwell, A., R. Coleby, C. Tovar, M. R. Stammnitz, Y. M. Kwon, R. S. Owen, M. Tringides, E. P. Murchison, K. Skjodt, G. J. Thomas, J. Kaufman, T. Elliott, G. M. Woods, and H. V. Siddle. 2018. 'The newly-arisen Devil facial tumour disease 2 (DFT2) reveals a mechanism for the emergence of a contagious cancer', *Elife*, 7.
- Campos, E. F., H. Tedesco-Silva, P. G. Machado, M. Franco, J. O. Medina-Pestana, and M. Gerbase-DeLima. 2006. 'Post-transplant anti-HLA class II antibodies as risk factor for late kidney allograft failure', *Am J Transplant*, 6: 2316-20.
- Cartron, G., L. Dacheux, G. Salles, P. Solal-Celigny, P. Bardos, P. Colombat, and H. Watier. 2002. 'Therapeutic activity of humanized anti-CD20 monoclonal antibody and polymorphism in IgG Fc receptor FcgammaRIIIa gene', *Blood*, 99: 754-8.
- Chen, C. C., E. Pouliquen, A. Broisat, F. Andreatta, M. Racape, P. Bruneval, L. Kessler, M. Ahmadi, S. Bacot, C. Saison-Delaplace, M. Marcaud, J. D. Van Huyen, A. Loupy, J. Villard, S. Demuylder-Mischler, T. Berney, E. Morelon, M. K. Tsai, M. N. Kolopp-Sarda, A. Koenig, V. Mathias, S. Ducreux, C. Ghezzi, V. Dubois, A. Nicoletti, T. Defrance, and O. Thaunat. 2018. 'Endothelial chimerism and vascular sequestration protect pancreatic islet grafts from antibody-mediated rejection', *J Clin Invest*, 128: 219-32.
- Choe, J. H., P. B. Watchmaker, M. S. Simic, R. D. Gilbert, A. W. Li, N. A. Krasnow, K. M. Downey, W. Yu, D. A. Carrera, A. Celli, J. Cho, J. D. Briones, J. M. Duecker, Y. E. Goresky, R. Dannenfels, L. Cardarelli, O. Troyanskaya, S. S. Sidhu, K. T. Roybal, H. Okada, and W. A.

- Lim. 2021. 'SynNotch-CAR T cells overcome challenges of specificity, heterogeneity, and persistence in treating glioblastoma', *Sci Transl Med*, 13.
- Clackson, T., W. Yang, L. W. Rozamus, M. Hatada, J. F. Amara, C. T. Rollins, L. F. Stevenson, S. R. Magari, S. A. Wood, N. L. Courage, X. Lu, F. Cerasoli, Jr., M. Gilman, and D. A. Holt. 1998. 'Redesigning an FKBP-ligand interface to generate chemical dimerizers with novel specificity', *Proc Natl Acad Sci U S A*, 95: 10437-42.
- Clynes, R. A., T. L. Towers, L. G. Presta, and J. V. Ravetch. 2000. 'Inhibitory Fc receptors modulate in vivo cytotoxicity against tumor targets', *Nat Med*, 6: 443-6.
- Cockrell, A. S., and T. Kafri. 2007. 'Gene delivery by lentivirus vectors', *Mol Biotechnol*, 36: 184-204.
- Colvin, R. B., A. H. Cohen, C. Saiontz, S. Bonsib, M. Buick, B. Burke, S. Carter, T. Cavallo, M. Haas, A. Lindblad, J. C. Manivel, C. C. Nast, D. Salomon, C. Weaver, and M. Weiss. 1997. 'Evaluation of pathologic criteria for acute renal allograft rejection: reproducibility, sensitivity, and clinical correlation', *J Am Soc Nephrol*, 8: 1930-41.
- Cong, L., F. A. Ran, D. Cox, S. Lin, R. Barretto, N. Habib, P. D. Hsu, X. Wu, W. Jiang, L. A. Marraffini, and F. Zhang. 2013. 'Multiplex genome engineering using CRISPR/Cas systems', *Science*, 339: 819-23.
- Cooper, M. A., T. A. Fehniger, and M. A. Caligiuri. 2001. 'The biology of human natural killer-cell subsets', *Trends Immunol*, 22: 633-40.
- Daeron, M. 1997. 'Fc receptor biology', *Annu Rev Immunol*, 15: 203-34.
- Dausset, J. 1958. '[Iso-leuko-antibodies]', *Acta Haematol*, 20: 156-66.
- de Almeida, P. E., E. H. Meyer, N. G. Kooreman, S. Diecke, D. Dey, V. Sanchez-Freire, S. Hu, A. Ebert, J. Odegaard, N. M. Mordwinkin, T. P. Brouwer, D. Lo, D. T. Montoro, M. T. Longaker, R. S. Negrin, and J. C. Wu. 2014. 'Transplanted terminally differentiated induced pluripotent stem cells are accepted by immune mechanisms similar to self-tolerance', *Nat Commun*, 5: 3903.
- Delville, M., B. Lamarthee, S. Pagie, S. B. See, M. Rabant, C. Burger, P. Gatault, M. Giral, O. Thauinat, N. Arzouk, A. Hertig, M. Hazzan, M. Matignon, C. Mariat, S. Caillard, N. Kamar, J. Sayegh, P. F. Westeel, C. Garrouste, M. Ladriere, V. Vuiblet, J. Rivalan, P. Merville, D. Bertrand, A. Le Moine, J. P. Duong Van Huyen, A. Cesbron, N. Cagnard, O. Alibeu, S. C. Satchell, C. Legendre, E. Zorn, J. L. Taupin, B. Charreau, and D. Anglicheau. 2019. 'Early Acute Microvascular Kidney Transplant Rejection in the Absence of Anti-HLA Antibodies Is Associated with Preformed IgG Antibodies against Diverse Glomerular Endothelial Cell Antigens', *J Am Soc Nephrol*, 30: 692-709.
- Deuse, T., X. Hu, S. Agbor-Enoh, M. Koch, M. H. Spitzer, A. Gravina, M. Alawi, A. Marishta, B. Peters, Z. Kosaloglu-Yalcin, Y. Yang, R. Rajalingam, D. Wang, B. Nashan, R. Kieffmann, H. Reichenspurner, H. Valantine, I. L. Weissman, and S. Schrepfer. 2019. 'De novo mutations in mitochondrial DNA of iPSCs produce immunogenic neoepitopes in mice and humans', *Nat Biotechnol*, 37: 1137-44.
- Deuse, T., X. Hu, A. Gravina, D. Wang, G. Tediashvili, C. De, W. O. Thayer, A. Wahl, J. V. Garcia, H. Reichenspurner, M. M. Davis, L. L. Lanier, and S. Schrepfer. 2019. 'Hypoimmunogenic derivatives of induced pluripotent stem cells evade immune rejection in fully immunocompetent allogeneic recipients', *Nat Biotechnol*, 37: 252-58.
- Deuse, T., C. Peter, P. W. Fedak, T. Doyle, H. Reichenspurner, W. H. Zimmermann, T. Eschenhagen, W. Stein, J. C. Wu, R. C. Robbins, and S. Schrepfer. 2009. 'Hepatocyte growth factor or vascular endothelial growth factor gene transfer maximizes mesenchymal stem cell-based myocardial salvage after acute myocardial infarction', *Circulation*, 120: S247-54.
- Devaiah, B. N., and D. S. Singer. 2013. 'CIITA and Its Dual Roles in MHC Gene Transcription', *Front Immunol*, 4: 476.
- Doullay, F., J. Ruf, J. L. Codaccioni, and P. Carayon. 1991. 'Prevalence of autoantibodies to thyroperoxidase in patients with various thyroid and autoimmune diseases', *Autoimmunity*, 9: 237-44.



- Dragun, D., D. N. Muller, J. H. Brasen, L. Fritsche, M. Nieminen-Kelha, R. Dechend, U. Kintscher, B. Rudolph, J. Hoebeke, D. Eckert, I. Mazak, R. Plehm, C. Schonemann, T. Unger, K. Budde, H. H. Neumayer, F. C. Luft, and G. Wallukat. 2005. 'Angiotensin II type 1-receptor activating antibodies in renal-allograft rejection', *N Engl J Med*, 352: 558-69.
- Drukker, M., G. Katz, A. Urbach, M. Schuldiner, G. Markel, J. Itskovitz-Eldor, B. Reubinoff, O. Mandelboim, and N. Benvenisty. 2002. 'Characterization of the expression of MHC proteins in human embryonic stem cells', *Proc Natl Acad Sci U S A*, 99: 9864-9.
- Duvivier-Kali, V. F., A. Omer, M. D. Lopez-Avalos, J. J. O'Neil, and G. C. Weir. 2004. 'Survival of microencapsulated adult pig islets in mice in spite of an antibody response', *Am J Transplant*, 4: 1991-2000.
- Edberg, J. C., A. M. Yee, D. S. Rakshit, D. J. Chang, J. A. Gokhale, Z. K. Indik, A. D. Schreiber, and R. P. Kimberly. 1999. 'The cytoplasmic domain of human FcγRIa alters the functional properties of the FcγRI.γ-chain receptor complex', *J Biol Chem*, 274: 30328-33.
- Edgar, L., T. Pu, B. Porter, J. M. Aziz, C. La Pointe, A. Asthana, and G. Orlando. 2020. 'Regenerative medicine, organ bioengineering and transplantation', *Br J Surg*, 107: 793-800.
- Evans, M. J., and M. H. Kaufman. 1981. 'Establishment in culture of pluripotential cells from mouse embryos', *Nature*, 292: 154-6.
- Everly, M. J. 2013. 'Incidence and hazards of alloantibodies in renal transplantation', *Clin Transpl*: 313-7.
- Farkash, E. A., and R. B. Colvin. 2012. 'Diagnostic challenges in chronic antibody-mediated rejection', *Nat Rev Nephrol*, 8: 255-7.
- Fearon, D. T., and R. M. Locksley. 1996. 'The instructive role of innate immunity in the acquired immune response', *Science*, 272: 50-3.
- Fernandez-Aviles, F., R. Sanz-Ruiz, A. M. Climent, L. Badimon, R. Bolli, D. Charron, V. Fuster, S. Janssens, J. Kastrop, H. S. Kim, T. F. Luscher, J. F. Martin, P. Menasche, F. J. Pinto, R. D. Simari, G. W. Stone, A. Terzic, J. T. Willerson, J. C. Wu, and Tactics Writing Group. 2018. 'Global Overview of the Transnational Alliance for Regenerative Therapies in Cardiovascular Syndromes (TACTICS) Recommendations: A Comprehensive Series of Challenges and Priorities of Cardiovascular Regenerative Medicine', *Circ Res*, 122: 199-201.
- Feucht, H. E., H. Schneeberger, G. Hillebrand, K. Burkhardt, M. Weiss, G. Riethmuller, W. Land, and E. Albert. 1993. 'Capillary deposition of C4d complement fragment and early renal graft loss', *Kidney Int*, 43: 1333-8.
- Gabriel, C., D. Furst, I. Fae, S. Wenda, C. Zollkofer, J. Mytilineos, and G. F. Fischer. 2014. 'HLA typing by next-generation sequencing - getting closer to reality', *Tissue Antigens*, 83: 65-75.
- Gao, L., L. Wang, Y. Wei, P. Krishnamurthy, G. P. Walcott, P. Menasche, and J. Zhang. 2020. 'Exosomes secreted by hiPSC-derived cardiac cells improve recovery from myocardial infarction in swine', *Sci Transl Med*, 12.
- Gaston, R. S., J. M. Cecka, B. L. Kasiske, A. M. Fieberg, R. Leduc, F. C. Cosio, S. Gourishankar, J. Grande, P. Halloran, L. Hunsicker, R. Mannon, D. Rush, and A. J. Matas. 2010. 'Evidence for antibody-mediated injury as a major determinant of late kidney allograft failure', *Transplantation*, 90: 68-74.
- Gornalusse, G. G., R. K. Hirata, S. E. Funk, L. Riolobos, V. S. Lopes, G. Manske, D. Prunkard, A. G. Colunga, L. A. Hanafi, D. O. Clegg, C. Turtle, and D. W. Russell. 2017. 'HLA-E-expressing pluripotent stem cells escape allogeneic responses and lysis by NK cells', *Nat Biotechnol*, 35: 765-72.
- Gorovits, B., and E. Koren. 2019. 'Immunogenicity of Chimeric Antigen Receptor T-Cell Therapeutics', *BioDrugs*, 33: 275-84.
- Guha, P., J. W. Morgan, G. Mostoslavsky, N. P. Rodrigues, and A. S. Boyd. 2013. 'Lack of immune response to differentiated cells derived from syngeneic induced pluripotent stem cells', *Cell Stem Cell*, 12: 407-12.
- Hall, B. M. 1991. 'Cells mediating allograft rejection', *Transplantation*, 51: 1141-51.

- Han, X., M. Wang, S. Duan, P. J. Franco, J. H. Kenty, P. Hedrick, Y. Xia, A. Allen, L. M. R. Ferreira, J. L. Strominger, D. A. Melton, T. B. Meissner, and C. A. Cowan. 2019. 'Generation of hypoinmunogenic human pluripotent stem cells', *Proc Natl Acad Sci U S A*, 116: 10441-46.
- Hanna, S., and A. Etzioni. 2014. 'MHC class I and II deficiencies', *J Allergy Clin Immunol*, 134: 269-75.
- Harrison, P. T., W. Davis, J. C. Norman, A. R. Hockaday, and J. M. Allen. 1994. 'Binding of monomeric immunoglobulin G triggers Fc gamma RI-mediated endocytosis', *J Biol Chem*, 269: 24396-402.
- He, J., Z. Rong, X. Fu, and Y. Xu. 2017. 'A Safety Checkpoint to Eliminate Cancer Risk of the Immune Evasive Cells Derived from Human Embryonic Stem Cells', *Stem Cells*, 35: 1154-61.
- Heel, K. A., and J. C. Hall. 1996. 'Peritoneal defences and peritoneum-associated lymphoid tissue', *Br J Surg*, 83: 1031-6.
- Hege, K. M., E. K. Bergsland, G. A. Fisher, J. J. Nemunaitis, R. S. Warren, J. G. McArthur, A. A. Lin, J. Schlom, C. H. June, and S. A. Sherwin. 2017. 'Safety, tumor trafficking and immunogenicity of chimeric antigen receptor (CAR)-T cells specific for TAG-72 in colorectal cancer', *J Immunother Cancer*, 5: 22.
- Hou, S., P. C. Doherty, M. Zijlstra, R. Jaenisch, and J. M. Katz. 1992. 'Delayed clearance of Sendai virus in mice lacking class I MHC-restricted CD8+ T cells', *J Immunol*, 149: 1319-25.
- Huston, D. P. 1997. 'The biology of the immune system', *JAMA*, 278: 1804-14.
- Iniotaki-Theodoraki, A. 2001. 'The role of HLA class I and class II antibodies in renal transplantation', *Nephrol Dial Transplant*, 16 Suppl 6: 150-2.
- Ishikawa-Sekigami, T., Y. Kaneko, Y. Saito, Y. Murata, H. Okazawa, H. Ohnishi, P. A. Oldenborg, Y. Nojima, and T. Matozaki. 2006. 'Enhanced phagocytosis of CD47-deficient red blood cells by splenic macrophages requires SHPS-1', *Biochem Biophys Res Commun*, 343: 1197-200.
- Ishino, Y., H. Shinagawa, K. Makino, M. Amemura, and A. Nakata. 1987. 'Nucleotide sequence of the iap gene, responsible for alkaline phosphatase isozyme conversion in Escherichia coli, and identification of the gene product', *J Bacteriol*, 169: 5429-33.
- Jaiswal, S., C. H. Jamieson, W. W. Pang, C. Y. Park, M. P. Chao, R. Majeti, D. Traver, N. van Rooijen, and I. L. Weissman. 2009. 'CD47 is upregulated on circulating hematopoietic stem cells and leukemia cells to avoid phagocytosis', *Cell*, 138: 271-85.
- Jiang, P., C. F. Lagenaur, and V. Narayanan. 1999. 'Integrin-associated protein is a ligand for the P84 neural adhesion molecule', *J Biol Chem*, 274: 559-62.
- Jinek, M., K. Chylinski, I. Fonfara, M. Hauer, J. A. Doudna, and E. Charpentier. 2012. 'A programmable dual-RNA-guided DNA endonuclease in adaptive bacterial immunity', *Science*, 337: 816-21.
- Jordan, S. C., T. Lorant, J. Choi, C. Kjellman, L. Winstedt, M. Bengtsson, X. Zhang, T. Eich, M. Toyoda, B. M. Eriksson, S. Ge, A. Peng, S. Jarnum, K. J. Wood, T. Lundgren, L. Wennberg, L. Backman, E. Larsson, R. Villicana, J. Kahwaji, S. Louie, A. Kang, M. Haas, C. Nast, A. Vo, and G. Tufveson. 2017. 'IgG Endopeptidase in Highly Sensitized Patients Undergoing Transplantation', *N Engl J Med*, 377: 442-53.
- Karre, K., G. O. Klein, R. Kiessling, G. Klein, and J. C. Roder. 1980. 'Low natural in vivo resistance to syngeneic leukaemias in natural killer-deficient mice', *Nature*, 284: 624-6.
- Ke, Q., C. J. Kroger, M. Clark, and R. M. Tisch. 2020. 'Evolving Antibody Therapies for the Treatment of Type 1 Diabetes', *Front Immunol*, 11: 624568.
- Klee, G. G. 2000. 'Human anti-mouse antibodies', *Arch Pathol Lab Med*, 124: 921-3.
- Klein, U., and R. Dalla-Favera. 2008. 'Germinal centres: role in B-cell physiology and malignancy', *Nat Rev Immunol*, 8: 22-33.
- Koller, B. H., P. Marrack, J. W. Kappler, and O. Smithies. 2010. 'Normal development of mice deficient in beta 2M, MHC class I proteins, and CD8+ T cells. 1990', *J Immunol*, 184: 4592-5.
- Kong, Y. C. 2007. 'Experimental autoimmune thyroiditis in the mouse', *Curr Protoc Immunol*, Chapter 15: Unit 15 7.
- Lachmann, N., P. I. Terasaki, K. Budde, L. Liefeldt, A. Kahl, P. Reinke, J. Pratschke, B. Rudolph, D. Schmidt, A. Salama, and C. Schonemann. 2009. 'Anti-human leukocyte antigen and donor-

- specific antibodies detected by luminex posttransplant serve as biomarkers for chronic rejection of renal allografts', *Transplantation*, 87: 1505-13.
- Lamers, C. H., R. Willemsen, P. van Elzakker, S. van Steenberg-Langeveld, M. Broertjes, J. Oosterwijk-Wakka, E. Oosterwijk, S. Sleijfer, R. Debets, and J. W. Gratama. 2011. 'Immune responses to transgene and retroviral vector in patients treated with ex vivo-engineered T cells', *Blood*, 117: 72-82.
- Lapierre, L. A., W. Fiers, and J. S. Pober. 1988. 'Three distinct classes of regulatory cytokines control endothelial cell MHC antigen expression. Interactions with immune gamma interferon differentiate the effects of tumor necrosis factor and lymphotoxin from those of leukocyte alpha and fibroblast beta interferons', *J Exp Med*, 167: 794-804.
- Lederer, S. R., B. Kluth-Pepper, H. Schneeberger, E. Albert, W. Land, and H. E. Feucht. 2001. 'Impact of humoral alloreactivity early after transplantation on the long-term survival of renal allografts', *Kidney Int*, 59: 334-41.
- Lee, N., M. Llano, M. Carretero, A. Ishitani, F. Navarro, M. Lopez-Botet, and D. E. Geraghty. 1998. 'HLA-E is a major ligand for the natural killer inhibitory receptor CD94/NKG2A', *Proc Natl Acad Sci U S A*, 95: 5199-204.
- Lefaucheur, C., D. Viglietti, C. Bentelejewski, J. P. Duong van Huyen, D. Vernerey, O. Aubert, J. Verine, X. Jouven, C. Legendre, D. Glotz, A. Loupy, and A. Zeevi. 2016. 'IgG Donor-Specific Anti-Human HLA Antibody Subclasses and Kidney Allograft Antibody-Mediated Injury', *J Am Soc Nephrol*, 27: 293-304.
- Li, H., Y. Yang, W. Hong, M. Huang, M. Wu, and X. Zhao. 2020. 'Applications of genome editing technology in the targeted therapy of human diseases: mechanisms, advances and prospects', *Signal Transduct Target Ther*, 5: 1.
- Liang, G., and Y. Zhang. 2013. 'Embryonic stem cell and induced pluripotent stem cell: an epigenetic perspective', *Cell Res*, 23: 49-69.
- Liu, Y. W., B. Chen, X. Yang, J. A. Fugate, F. A. Kalucki, A. Futakuchi-Tsuchida, L. Couture, K. W. Vogel, C. A. Astley, A. Baldessari, J. Ogle, C. W. Don, Z. L. Steinberg, S. P. Seslar, S. A. Tuck, H. Tsuchida, A. V. Naumova, S. K. Dupras, M. S. Lyu, J. Lee, D. W. Hailey, H. Reinecke, L. Pabon, B. H. Fryer, W. R. MacLellan, R. S. Thies, and C. E. Murry. 2018. 'Human embryonic stem cell-derived cardiomyocytes restore function in infarcted hearts of non-human primates', *Nat Biotechnol*, 36: 597-605.
- Liu, Y., H. W. Xu, L. Wang, S. Y. Li, C. J. Zhao, J. Hao, Q. Y. Li, T. T. Zhao, W. Wu, Y. Wang, Q. Zhou, C. Qian, L. Wang, and Z. Q. Yin. 2018. 'Human embryonic stem cell-derived retinal pigment epithelium transplants as a potential treatment for wet age-related macular degeneration', *Cell Discov*, 4: 50.
- Lomas, D. A., and E. K. Silverman. 2001. 'The genetics of chronic obstructive pulmonary disease', *Respir Res*, 2: 20-6.
- Lonze, B. E., V. S. Tatapudi, E. P. Weldon, E. S. Min, N. M. Ali, C. L. Deterville, B. E. Gelb, J. A. Benstein, N. N. Dagher, M. Wu, and R. A. Montgomery. 2018. 'IdeS (Imlifidase): A Novel Agent That Cleaves Human IgG and Permits Successful Kidney Transplantation Across High-strength Donor-specific Antibody', *Ann Surg*, 268: 488-96.
- Mandai, M., Y. Kurimoto, and M. Takahashi. 2017. 'Autologous Induced Stem-Cell-Derived Retinal Cells for Macular Degeneration', *N Engl J Med*, 377: 792-93.
- Marchal, G., J. Dausset, and J. Colombani. 1962. '[Frequency of anti-platelet iso-antibodies in polytransfused patients]', *Bibl Haematol*, 13: 319-23.
- Martin, G. R. 1981. 'Isolation of a pluripotent cell line from early mouse embryos cultured in medium conditioned by teratocarcinoma stem cells', *Proc Natl Acad Sci U S A*, 78: 7634-8.
- Masson, E., M. Stern, J. Chabod, C. Thevenin, F. Gonin, J. M. Rebibou, and P. Tiberghien. 2007. 'Hyperacute rejection after lung transplantation caused by undetected low-titer anti-HLA antibodies', *J Heart Lung Transplant*, 26: 642-5.

- Mattapally, S., K. M. Pawlik, V. G. Fast, E. Zumaquero, F. E. Lund, T. D. Randall, T. M. Townes, and J. Zhang. 2018. 'Human Leukocyte Antigen Class I and II Knockout Human Induced Pluripotent Stem Cell-Derived Cells: Universal Donor for Cell Therapy', *J Am Heart Assoc*, 7: e010239.
- Mauviyyedi, S., P. D. Pelle, S. Saidman, A. B. Collins, M. Pascual, N. E. Tolkoff-Rubin, W. W. Williams, A. B. Cosimi, E. E. Schneeberger, and R. B. Colvin. 2001. 'Chronic humoral rejection: identification of antibody-mediated chronic renal allograft rejection by C4d deposits in peritubular capillaries', *J Am Soc Nephrol*, 12: 574-82.
- Mauritz, C., A. Martens, S. V. Rojas, T. Schnick, C. Rathert, N. Schecker, S. Menke, S. Glage, R. Zweigerdt, A. Haverich, U. Martin, and I. Kutschka. 2011. 'Induced pluripotent stem cell (iPSC)-derived Flk-1 progenitor cells engraft, differentiate, and improve heart function in a mouse model of acute myocardial infarction', *Eur Heart J*, 32: 2634-41.
- Menasche, P., V. Vanneaux, A. Hagege, A. Bel, B. Cholley, A. Parouchev, I. Cacciapuoti, R. Al-Daccak, N. Benhamouda, H. Blons, O. Agbulut, L. Tosca, J. H. Trouvin, J. R. Fabreguettes, V. Bellamy, D. Charron, E. Tartour, G. Tachdjian, M. Desnos, and J. Larghero. 2018. 'Transplantation of Human Embryonic Stem Cell-Derived Cardiovascular Progenitors for Severe Ischemic Left Ventricular Dysfunction', *J Am Coll Cardiol*, 71: 429-38.
- Merkle, F. T., S. Ghosh, N. Kamitaki, J. Mitchell, Y. Avior, C. Mello, S. Kashin, S. Mekhoubad, D. Ilic, M. Charlton, G. Saphier, R. E. Handsaker, G. Genovese, S. Bar, N. Benvenisty, S. A. McCarroll, and K. Eggan. 2017. 'Human pluripotent stem cells recurrently acquire and expand dominant negative P53 mutations', *Nature*, 545: 229-33.
- Mizutani, K., P. Terasaki, A. Rosen, V. Esquenazi, J. Miller, R. N. Shih, R. Pei, M. Ozawa, and J. Lee. 2005. 'Serial ten-year follow-up of HLA and MICA antibody production prior to kidney graft failure', *Am J Transplant*, 5: 2265-72.
- Moeller, E. 1965. 'Contact-Induced Cytotoxicity by Lymphoid Cells Containing Foreign Isoantigens', *Science*, 147: 873-9.
- Mojica, F. J., C. Diez-Villasenor, E. Soria, and G. Juez. 2000. 'Biological significance of a family of regularly spaced repeats in the genomes of Archaea, Bacteria and mitochondria', *Mol Microbiol*, 36: 244-6.
- Moolten, F. L. 1986. 'Tumor chemosensitivity conferred by inserted herpes thymidine kinase genes: paradigm for a prospective cancer control strategy', *Cancer Res*, 46: 5276-81.
- Morizane, A., D. Doi, T. Kikuchi, K. Okita, A. Hotta, T. Kawasaki, T. Hayashi, H. Onoe, T. Shiina, S. Yamanaka, and J. Takahashi. 2013. 'Direct comparison of autologous and allogeneic transplantation of iPSC-derived neural cells in the brain of a non-human primate', *Stem Cell Reports*, 1: 283-92.
- Murphy, S. P., J. C. Choi, and R. Holtz. 2004. 'Regulation of major histocompatibility complex class II gene expression in trophoblast cells', *Reprod Biol Endocrinol*, 2: 52.
- Nakatsuji, N., F. Nakajima, and K. Tokunaga. 2008. 'HLA-haplotype banking and iPS cells', *Nat Biotechnol*, 26: 739-40.
- Nanda, D., R. Vogels, M. Havenga, C. J. Avezaat, A. Bout, and P. S. Smitt. 2001. 'Treatment of malignant gliomas with a replicating adenoviral vector expressing herpes simplex virus-thymidine kinase', *Cancer Res*, 61: 8743-50.
- Narmoneva, D. A., R. Vukmirovic, M. E. Davis, R. D. Kamm, and R. T. Lee. 2004. 'Endothelial cells promote cardiac myocyte survival and spatial reorganization: implications for cardiac regeneration', *Circulation*, 110: 962-8.
- Nimmerjahn, F., and J. V. Ravetch. 2008. 'Fcgamma receptors as regulators of immune responses', *Nat Rev Immunol*, 8: 34-47.
- Nussbaum, J., E. Minami, M. A. Laflamme, J. A. Virag, C. B. Ware, A. Masino, V. Muskheli, L. Pabon, H. Reinecke, and C. E. Murry. 2007. 'Transplantation of undifferentiated murine embryonic stem cells in the heart: teratoma formation and immune response', *FASEB J*, 21: 1345-57.
- Pappas, D. J., P. A. Gourraud, C. Le Gall, J. Laurent, A. Trounson, N. DeWitt, and S. Talib. 2015. 'Proceedings: human leukocyte antigen haplo-homozygous induced pluripotent stem cell

- haplobank modeled after the california population: evaluating matching in a multiethnic and admixed population', *Stem Cells Transl Med*, 4: 413-8.
- Peraro, L., C. M. Bourne, M. M. Dacek, E. Akalin, J. H. Park, E. L. Smith, and D. A. Scheinberg. 2021. 'Incorporation of bacterial immunoevasins to protect cell therapies from host antibody-mediated immune rejection', *Mol Ther*, 29: 3398-409.
- Quyyumi, A. A., A. Vasquez, D. J. Kereiakes, M. Klapholz, G. L. Schaer, A. Abdel-Latif, S. Frohwein, T. D. Henry, R. A. Schatz, N. Dib, C. Toma, C. J. Davidson, G. W. Barsness, D. M. Shavelle, M. Cohen, J. Poole, T. Moss, P. Hyde, A. M. Kanakaraj, V. Druker, A. Chung, C. Junge, R. A. Preti, R. L. Smith, D. J. Mazzo, A. Pecora, and D. W. Losordo. 2017. 'PreSERVE-AMI: A Randomized, Double-Blind, Placebo-Controlled Clinical Trial of Intracoronary Administration of Autologous CD34+ Cells in Patients With Left Ventricular Dysfunction Post STEMI', *Circ Res*, 120: 324-31.
- Rapoport, B., and S. M. McLachlan. 2001. 'Thyroid autoimmunity', *J Clin Invest*, 108: 1253-9.
- Raulet, D. H. 2004. 'Interplay of natural killer cells and their receptors with the adaptive immune response', *Nat Immunol*, 5: 996-1002.
- Reglinski, M., M. Gierula, N. N. Lynskey, R. J. Edwards, and S. Sriskandan. 2015. 'Identification of the *Streptococcus pyogenes* surface antigens recognised by pooled human immunoglobulin', *Sci Rep*, 5: 15825.
- Reth, M. 1992. 'Antigen receptors on B lymphocytes', *Annu Rev Immunol*, 10: 97-121.
- Rigato, M., M. Monami, and G. P. Fadini. 2017. 'Autologous Cell Therapy for Peripheral Arterial Disease: Systematic Review and Meta-Analysis of Randomized, Nonrandomized, and Noncontrolled Studies', *Circ Res*, 120: 1326-40.
- Roitt, I. M., D. Doniach, P. N. Campbell, and R. V. Hudson. 1956. 'Auto-antibodies in Hashimoto's disease (lymphadenoid goitre)', *Lancet*, 271: 820-1.
- Romagnuolo, R., H. Masoudpour, A. Porta-Sanchez, B. Qiang, J. Barry, A. Laskary, X. Qi, S. Masse, K. Magtibay, H. Kawajiri, J. Wu, T. Valdman Sadikov, J. Rothberg, K. M. Panchalingam, E. Titus, R. K. Li, P. W. Zandstra, G. A. Wright, K. Nanthakumar, N. R. Ghugre, G. Keller, and M. A. Laflamme. 2019. 'Human Embryonic Stem Cell-Derived Cardiomyocytes Regenerate the Infarcted Pig Heart but Induce Ventricular Tachyarrhythmias', *Stem Cell Reports*, 12: 967-81.
- Rong, Z., M. Wang, Z. Hu, M. Stradner, S. Zhu, H. Kong, H. Yi, A. Goldrath, Y. G. Yang, Y. Xu, and X. Fu. 2014. 'An effective approach to prevent immune rejection of human ESC-derived allografts', *Cell Stem Cell*, 14: 121-30.
- Rowe, R. G., and G. Q. Daley. 2019. 'Induced pluripotent stem cells in disease modelling and drug discovery', *Nat Rev Genet*, 20: 377-88.
- Sadegh-Nasseri, S., and A. Kim. 2015. 'Exogenous antigens bind MHC class II first, and are processed by cathepsins later', *Mol Immunol*, 68: 81-4.
- Salomon, B., D. J. Lenschow, L. Rhee, N. Ashourian, B. Singh, A. Sharpe, and J. A. Bluestone. 2000. 'B7/CD28 costimulation is essential for the homeostasis of the CD4+CD25+ immunoregulatory T cells that control autoimmune diabetes', *Immunity*, 12: 431-40.
- Schulz, T. C. 2015. 'Concise Review: Manufacturing of Pancreatic Endoderm Cells for Clinical Trials in Type 1 Diabetes', *Stem Cells Transl Med*, 4: 927-31.
- Seliger, B., F. Ruiz-Cabello, and F. Garrido. 2008. 'IFN inducibility of major histocompatibility antigens in tumors', *Adv Cancer Res*, 101: 249-76.
- Shiba, Y., T. Gomibuchi, T. Seto, Y. Wada, H. Ichimura, Y. Tanaka, T. Ogasawara, K. Okada, N. Shiba, K. Sakamoto, D. Ido, T. Shiina, M. Ohkura, J. Nakai, N. Uno, Y. Kazuki, M. Oshimura, I. Minami, and U. Ikeda. 2016. 'Allogeneic transplantation of iPS cell-derived cardiomyocytes regenerates primate hearts', *Nature*, 538: 388-91.
- Sinha, A. A., M. T. Lopez, and H. O. McDevitt. 1990. 'Autoimmune diseases: the failure of self tolerance', *Science*, 248: 1380-8.
- Snell, G. D. 1948. 'Methods for the study of histocompatibility genes', *J Genet*, 49: 87-108.

- Solomon, S., F. Pitossi, and M. S. Rao. 2015. 'Banking on iPSC--is it doable and is it worthwhile', *Stem Cell Rev Rep*, 11: 1-10.
- Soto-Pantoja, D. R., S. Kaur, and D. D. Roberts. 2015. 'CD47 signaling pathways controlling cellular differentiation and responses to stress', *Crit Rev Biochem Mol Biol*, 50: 212-30.
- Sun, Q., Z. Cheng, D. Cheng, J. Chen, S. Ji, J. Wen, C. Zheng, and Z. Liu. 2011. 'De novo development of circulating anti-endothelial cell antibodies rather than pre-existing antibodies is associated with post-transplant allograft rejection', *Kidney Int*, 79: 655-62.
- Takahashi, K., K. Tanabe, M. Ohnuki, M. Narita, T. Ichisaka, K. Tomoda, and S. Yamanaka. 2007. 'Induction of pluripotent stem cells from adult human fibroblasts by defined factors', *Cell*, 131: 861-72.
- Takahashi, K., and S. Yamanaka. 2006. 'Induction of pluripotent stem cells from mouse embryonic and adult fibroblast cultures by defined factors', *Cell*, 126: 663-76.
- Thomson, J. A., J. Itskovitz-Eldor, S. S. Shapiro, M. A. Waknitz, J. J. Swiergiel, V. S. Marshall, and J. M. Jones. 1998. 'Embryonic stem cell lines derived from human blastocysts', *Science*, 282: 1145-7.
- Tian, P., J. Wang, X. Shen, J. F. Rey, Q. Yuan, and Y. Yan. 2017. 'Fundamental CRISPR-Cas9 tools and current applications in microbial systems', *Synth Syst Biotechnol*, 2: 219-25.
- Tomazic, V., and N. R. Rose. 1976. 'Autoimmune murine thyroiditis. VIII. Role of different thyroid antigens in the induction of experimental autoimmune thyroiditis', *Immunology*, 30: 63-8.
- Torikai, H., A. Reik, F. Soldner, E. H. Warren, C. Yuen, Y. Zhou, D. L. Crossland, H. Huls, N. Littman, Z. Zhang, S. S. Tykodi, P. Kebriaei, D. A. Lee, J. C. Miller, E. J. Rebar, M. C. Holmes, R. Jaenisch, R. E. Champlin, P. D. Gregory, and L. J. Cooper. 2013. 'Toward eliminating HLA class I expression to generate universal cells from allogeneic donors', *Blood*, 122: 1341-9.
- Trounson, A., and C. McDonald. 2015. 'Stem Cell Therapies in Clinical Trials: Progress and Challenges', *Cell Stem Cell*, 17: 11-22.
- Turner, M., S. Leslie, N. G. Martin, M. Peschanski, M. Rao, C. J. Taylor, A. Trounson, D. Turner, S. Yamanaka, and I. Wilmut. 2013. 'Toward the development of a global induced pluripotent stem cell library', *Cell Stem Cell*, 13: 382-4.
- van Laake, L. W., R. Passier, J. Monshouwer-Kloots, A. J. Verkleij, D. J. Lips, C. Freund, K. den Ouden, D. Ward-van Oostwaard, J. Korving, L. G. Tertoolen, C. J. van Echteld, P. A. Doevendans, and C. L. Mummery. 2007. 'Human embryonic stem cell-derived cardiomyocytes survive and mature in the mouse heart and transiently improve function after myocardial infarction', *Stem Cell Res*, 1: 9-24.
- Vivier, E., E. Tomasello, M. Baratin, T. Walzer, and S. Ugolini. 2008. 'Functions of natural killer cells', *Nat Immunol*, 9: 503-10.
- Waggoner, S. N., M. Cornberg, L. K. Selin, and R. M. Welsh. 2011. 'Natural killer cells act as rheostats modulating antiviral T cells', *Nature*, 481: 394-8.
- Wagner, D. L., E. Fritsche, M. A. Pulsipher, N. Ahmed, M. Hamieh, M. Hegde, M. Ruella, B. Savoldo, N. N. Shah, C. J. Turtle, A. S. Wayne, and M. Abou-EI-Enein. 2021. 'Immunogenicity of CAR T cells in cancer therapy', *Nat Rev Clin Oncol*, 18: 379-93.
- Walport, M. J. 2001. 'Complement. First of two parts', *N Engl J Med*, 344: 1058-66.
- Wang, D., G. Tediashvili, X. Hu, A. Gravina, S. G. Marcus, H. Zhang, J. E. Olgin, T. Deuse, and S. Schrepfer. 2019. 'A Cryoinjury Model to Study Myocardial Infarction in the Mouse', *J Vis Exp*.
- Watzl, C. 2018. 'Adaptive responses of innate lymphocytes', *Nat Immunol*, 19: 426-27.
- Weih, F., and J. Caamano. 2003. 'Regulation of secondary lymphoid organ development by the nuclear factor-kappaB signal transduction pathway', *Immunol Rev*, 195: 91-105.
- Welsh, J. S. 2011. 'Contagious cancer', *Oncologist*, 16: 1-4.
- Weng, W. K., D. Czerwinski, J. Timmerman, F. J. Hsu, and R. Levy. 2004. 'Clinical outcome of lymphoma patients after idiotype vaccination is correlated with humoral immune response and immunoglobulin G Fc receptor genotype', *J Clin Oncol*, 22: 4717-24.

- Wewers, M. D., M. A. Casolaro, S. E. Sellers, S. C. Swayze, K. M. McPhaul, J. T. Wittes, and R. G. Crystal. 1987. 'Replacement therapy for alpha 1-antitrypsin deficiency associated with emphysema', *N Engl J Med*, 316: 1055-62.
- Wiebe, C., I. W. Gibson, T. D. Blydt-Hansen, M. Karpinski, J. Ho, L. J. Storsley, A. Goldberg, P. E. Birk, D. N. Rush, and P. W. Nickerson. 2012. 'Evolution and clinical pathologic correlations of de novo donor-specific HLA antibody post kidney transplant', *Am J Transplant*, 12: 1157-67.
- Wieczorek, M., E. T. Abualrous, J. Sticht, M. Alvaro-Benito, S. Stolzenberg, F. Noe, and C. Freund. 2017. 'Major Histocompatibility Complex (MHC) Class I and MHC Class II Proteins: Conformational Plasticity in Antigen Presentation', *Front Immunol*, 8: 292.
- Winstedt, L., S. Jarnum, E. A. Nordahl, A. Olsson, A. Runstrom, R. Bockermann, C. Karlsson, J. Malmstrom, G. S. Palmgren, U. Malmqvist, L. Bjorck, and C. Kjellman. 2015. 'Complete Removal of Extracellular IgG Antibodies in a Randomized Dose-Escalation Phase I Study with the Bacterial Enzyme IdeS--A Novel Therapeutic Opportunity', *PLoS One*, 10: e0132011.
- Writing Group, Members, D. Mozaffarian, E. J. Benjamin, A. S. Go, D. K. Arnett, M. J. Blaha, M. Cushman, S. R. Das, S. de Ferranti, J. P. Despres, H. J. Fullerton, V. J. Howard, M. D. Huffman, C. R. Isasi, M. C. Jimenez, S. E. Judd, B. M. Kissela, J. H. Lichtman, L. D. Lisabeth, S. Liu, R. H. Mackey, D. J. Magid, D. K. McGuire, E. R. Mohler, 3rd, C. S. Moy, P. Muntner, M. E. Mussolino, K. Nasir, R. W. Neumar, G. Nichol, L. Palaniappan, D. K. Pandey, M. J. Reeves, C. J. Rodriguez, W. Rosamond, P. D. Sorlie, J. Stein, A. Towfighi, T. N. Turan, S. S. Virani, D. Woo, R. W. Yeh, M. B. Turner, Committee American Heart Association Statistics, and Subcommittee Stroke Statistics. 2016. 'Heart Disease and Stroke Statistics-2016 Update: A Report From the American Heart Association', *Circulation*, 133: e38-360.
- Xiao, Z. X., J. S. Miller, and S. G. Zheng. 2021. 'An updated advance of autoantibodies in autoimmune diseases', *Autoimmun Rev*, 20: 102743.
- Xu, H., B. Wang, M. Ono, A. Kagita, K. Fujii, N. Sasakawa, T. Ueda, P. Gee, M. Nishikawa, M. Nomura, F. Kitaoka, T. Takahashi, K. Okita, Y. Yoshida, S. Kaneko, and A. Hotta. 2019. 'Targeted Disruption of HLA Genes via CRISPR-Cas9 Generates iPSCs with Enhanced Immune Compatibility', *Cell Stem Cell*, 24: 566-78 e7.
- Yi, T., J. Li, H. Chen, J. Wu, J. An, Y. Xu, Y. Hu, C. A. Lowell, and J. G. Cyster. 2015. 'Splenic Dendritic Cells Survey Red Blood Cells for Missing Self-CD47 to Trigger Adaptive Immune Responses', *Immunity*, 43: 764-75.
- Zarogoulidis, P., K. Darwiche, A. Sakkas, L. Yarmus, H. Huang, Q. Li, L. Freitag, K. Zarogoulidis, and M. Malecki. 2013. 'Suicide Gene Therapy for Cancer - Current Strategies', *J Genet Syndr Gene Ther*, 4.
- Zhang, Q., J. M. Cecka, D. W. Gjertson, P. Ge, M. L. Rose, J. K. Patel, A. Ardehali, J. A. Kobashigawa, M. C. Fishbein, and E. F. Reed. 2011. 'HLA and MICA: targets of antibody-mediated rejection in heart transplantation', *Transplantation*, 91: 1153-8.
- Zhao, T., Z. N. Zhang, Z. Rong, and Y. Xu. 2011. 'Immunogenicity of induced pluripotent stem cells', *Nature*, 474: 212-5.
- Zhao, W., A. Lei, L. Tian, X. Wang, C. Correia, T. Weiskittel, H. Li, A. Trounson, Q. Fu, K. Yao, and J. Zhang. 2020. 'Strategies for Genetically Engineering Hypoimmunogenic Universal Pluripotent Stem Cells', *iScience*, 23: 101162.
- Zou, Y., F. Mirbaha, A. Lazaro, Y. Zhang, B. Lavingia, and P. Stastny. 2002. 'MICA is a target for complement-dependent cytotoxicity with mouse monoclonal antibodies and human alloantibodies', *Hum Immunol*, 63: 30-9.
- Zou, Y., P. Stastny, C. Susal, B. Dohler, and G. Opelz. 2007. 'Antibodies against MICA antigens and kidney-transplant rejection', *N Engl J Med*, 357: 1293-300.
- Zwirner, N. W., C. Y. Marcos, F. Mirbaha, Y. Zou, and P. Stastny. 2000. 'Identification of MICA as a new polymorphic alloantigen recognized by antibodies in sera of organ transplant recipients', *Hum Immunol*, 61: 917-24.





# Authorship contributions



Martinistrasse 52  
Campus Forschung, N27  
D-20246 Hamburg  
Phone: (040)7410-58048  
Fax: (040)7410-59663  
[Sonja.schrepfer@ucsf.edu](mailto:Sonja.schrepfer@ucsf.edu)  
[www.tsi-lab.de](http://www.tsi-lab.de)  
[www.uhz.de](http://www.uhz.de)

March 26<sup>th</sup> 2023

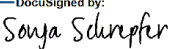
## Authorship contribution

Mrs. Alessia Gravina is submitting her cumulative dissertation entitled “Generation of fully immune evasive cell therapeutics” to obtain the Doctoral degree in Natural Sciences.

I hereby declare the contribution of Mrs. Alessia Gravina to the publication entitled “Hypoimmunogenic derivatives of induced pluripotent stem cells evade immune rejection in fully immunocompetent allogeneic recipients”. Her contribution consists of:

- Cell culture of human and murine endothelial cells, human and murine iPSCs, murine iPSC derived cardiomyocytes, and human and murine iPSC derived smooth muscle cells. The cell culture consisted of development and optimization of cell culture specific for the maintenance of those cultures, and freezing of the cells.
- Planning and execution of *in vivo* imaging studies to assess the survival of the differentiated transgenic cell lines in mouse models and data evaluation.
- Applicable methods section writing and manuscript proof-reading.

Sincerely,

DocuSigned by:  
  
51AFA650507949F  
Prof. Dr. Sonja Schrepfer



Martinistrasse 52  
Campus Forschung, N27  
D-20246 Hamburg  
Phone: (040)7410-58048  
Fax: (040)7410-59663  
[Sonja.schrepfer@ucsf.edu](mailto:Sonja.schrepfer@ucsf.edu)  
[www.tsi-lab.de](http://www.tsi-lab.de)  
[www.uhz.de](http://www.uhz.de)

March 26<sup>th</sup> 2023

## Authorship contribution

Mrs. Alessia Gravina is submitting her cumulative dissertation entitled “Generation of fully immune evasive cell therapeutics” to obtain the Doctoral degree in Natural Sciences.

I hereby declare the contribution of Mrs. Alessia Gravina to the publication entitled “Hypoimmune induced pluripotent stem cell-derived cell therapeutics treat cardiovascular and pulmonary diseases in immunocompetent allogeneic mice”. Her contribution consists of:

- Cell culture of murine endothelial cells, murine CMs, murine iPSCs. The cell culture consisted of development and optimization of cell culture specific for the maintenance of those cultures, and freezing of the cells.
- Planning, design, and execution of lentiviral transductions. Transductions were followed by cell sorting and flow cytometry analysis to purify and/or to evaluate the expression of the transgenes of the various cell lines.
- Planning and execution of *in vivo* studies and data evaluation.

- Manuscript preparation and manuscript proof-reading.

Sincerely,

DocuSigned by:  
*Sonja Schrepfer*  
51AFA850507949E  
Prof. Dr. Sonja Schrepfer



Martinistrasse 52  
Campus Forschung, N27  
D-20246 Hamburg  
Phone: (040)7410-58048  
Fax: (040)7410-59663  
[Sonja.schrepfer@ucsf.edu](mailto:Sonja.schrepfer@ucsf.edu)  
[www.tsi-lab.de](http://www.tsi-lab.de)  
[www.uhz.de](http://www.uhz.de)

March 26<sup>th</sup> 2023

## Authorship contribution

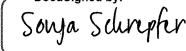
Mrs. Alessia Gravina is submitting her cumulative dissertation entitled “Generation of fully immune evasive cell therapeutics” to obtain the Doctoral degree in Natural Sciences.

I hereby declare the contribution of Mrs. Alessia Gravina to the publication entitled “Protection of cell therapeutics from antibody-mediated killing by CD64 overexpression”. Her contribution consists of:

- Cell culture of human and murine endothelial cells, human iPSCs, human PBMCs and T cells, human iPSC derived pancreatic beta cells, human thyroid epithelial cells, human macrophages, and human NK cells. The cell culture consisted of development and optimization of cell culture specific for the maintenance of those cultures, stimulation of the cells with cytokines when applicable, and freezing of the cells.
- Planning and execution of all lentiviral transductions including transduction of human and murine endothelial cells, transduction of human PBMCs, human iPSC derived pancreatic beta cells, human thyroid epithelial cells, and human macrophages. All the transductions were followed by cell sorting and flow cytometry analysis to purify and/or to evaluate the expression of the transgenes of the various cell lines.

- Execution of molecular biology and immune killing assays consisting of ELISAs, *in vitro* ADCC and CDC killing assays, execution of competitive antibody binding assays by flow cytometry analysis and data evaluation.
- Planning and execution of *in vivo* imaging studies to assess the survival of transgenic cell lines in various mouse models and data evaluation.
- Manuscript writing and manuscript proof-reading.

Sincerely,

DocuSigned by:  
  
51AEAB66507949F  
Prof. Dr. Sonja Schrepfer

## **Declaration on oath**

Hiermit bestätige ich, Alessia Gravina, dass die vorliegende Arbeit von mir selbständig verfasst wurde und ich keine anderen als die angegebenen Hilfsmittel – insbesondere keine im Quellenverzeichnis nicht benannten Internetquellen – benutzt habe und die Arbeit von mir vorher nicht einem anderen Prüfungsverfahren eingereicht wurde.

San Francisco, den 26.03.2023

A handwritten signature in black ink, consisting of a stylized 'A' followed by a cursive 'G' and a long horizontal flourish.

Alessia Gravina

## Acknowledgements

In this section I would like to thank the people that made my PhD years amazing by supporting and encouraging me.

Above all, I would like to thank my thesis advisor, Prof. Dr. Sonja Schrepfer who welcomed me in her lab in 2017 and allowed me to pursue my PhD at the University of Hamburg while working in San Francisco. She gave me the opportunity to be a part of several extremely exciting projects. Sonja, thank you so much for your help, trust and support during these PhD years.

I would like to thank Dr. Tobias Deuse for the great support and the supervision during the PhD years. I valued a lot the great discussions we had as well as the feedback given to me during the project.

I thank Prof. Dr. Dr. Andreas Guse for the time and work he has dedicated by being in my dissertation's committee as examiner.

I want to express my gratitude to Prof. Dr. Thomas Örtner and Prof. Dr. Tobias Lenz for representing the recording clerk and the head of the examination commission, respectively.

I thank the Parnassus Flow Cytometry Core for the help and support, it really felt like a second home for me with all the hours spent there.

I would like to express my gratitude to my colleagues Xiaomeng, Grigol, Annika, and Dong, who significantly contributed to the amazing lab environment and for their constant motivation and support. I could not have wished for a better team other than the one of the TSI Lab!

I want to thank my husband, Deniz, who has been always there for me during these 5 years and never stopped believing in me.

Finally, I thank my family for making all this possible. They have allowed me to follow my passion and supported me with patience and understanding.